

# Evaluation and Prediction of Bridge Pier and Contraction Scour of Cohesive River Sediments in Tennessee



**Tennessee Department of Transportation**



**Final Report**

September 30, 2018

Cover page photo: Highway SR205 Bridge crossing over the Big Creek in West Tennessee.  
*Photo by B. Mahalder June 2015*

## DISCLAIMER

This research was funded through the State Research and Planning (SPR) Program by the Tennessee Department of Transportation and the Federal Highway Administration under RES # 2013-36; Research Project Title: *Evaluation and Prediction of Bridge Pier and Construction Scour of Cohesive River Sediments in Tennessee.*

This document is disseminated under the sponsorship of the Tennessee Department of Transportation and the United States Department of Transportation in the interest of information exchange. The State of Tennessee and the United States Government assume no liability of its contents or use thereof.

The contents of this report reflect the views of the author(s) who are solely responsible for the facts and accuracy of the material presented. The contents do not necessarily reflect the official views of the Tennessee Department of Transportation or the United States Department of Transportation.

### Technical Report Documentation Page

1. Report No. RES#2013-36	2. Government Accession No.	3. Recipient's Catalog No.
4. Title and Subtitle  Evaluation and Prediction of Bridge Pier and Contraction Scour of Cohesive River Sediments in Tennessee	5. Report Date September 30, 2018	6. Performing Organization Code
	8. Performing Organization Report No.	
7. Author(s) John S. Schwartz and Angel M. Palomino	10. Work Unit No. (TRAIS)	
9. Performing Organization Name and Address University of Tennessee, Dept. of Civil & Environmental Engineering 851 Neyland Drive Knoxville, Tennessee 37996	11. Contract or Grant No. RES#2013-36	
	13. Type of Report and Period Covered Final Report June 1, 2013-August 31, 2018	
12. Sponsoring Agency Name and Address Tennessee Department of Transportation Long Range Planning Division James K. Polk Building, Suite 900 505 Deaderick Street Nashville, TN 37243-0334	14. Sponsoring Agency Code	
	15. Supplementary Notes	
16. Abstract <p>Approximately 450 scour critical bridges are maintained by Tennessee Department of Transportation (TDOT) across the state. Many of these bridges are located in river or stream beds and banks where cohesive soils are prevalent, particularly in western Tennessee. In the Hydraulic Engineering Circular No. 18 by the Federal Highway Administration, <i>Evaluating Scour at Bridges</i> (FHWA-HIF-12-003), existing HEC-18 equations for predicting scour depth at bridge piers and contractions in river beds for with non-cohesive, e.g., sand and gravel, tend to perform well. However, when cohesive sediments consisting of consolidated silts and clays commonly present on river beds, the HEC-18 equations tend to over-predict scour depth, although under-prediction also occurs as reported in published studies. The uncertainty of scour depth prediction can led to over design of bridge piers increasing construction costs, or under designed piers which may lead to bridge failure or future costly repairs. TDOT engineers identified that these equations need improvement and initiated the request for study in the state to better understand the variables that govern river bed scour in cohesive sediments near bridges. The objective of this research project is to enhance our understanding of river/stream bed scour and bank erosion behavior with cohesive sediments near bridges, and its relationships with <math>\tau_c</math> and <math>k_d</math> used in HEC-18 equations, including the time-dependent scour behavior and associated cohesive physical-geotechnical properties, and measurement of these erodibility parameters. In addition, this research focused on characterizing differences in physical-geotechnical properties of riverine cohesive sediments across the different physiographic provinces of Tennessee. The initial research investigated how field data collection and computational procedures for the in-situ mini-jet tester influenced <math>k_d</math> and <math>\tau_c</math> estimates. In order to meet the objectives, the following studies were completed: 1) statistical multivariate predictive equations were developed for <math>\tau_c</math> (and <math>k_d</math>) across the state's different physiographic provinces as a function of significant physical-geotechnical properties; 2) measured bridge scour data were correlated with cumulative effective stream power data from long-term river continuous flow records as a product of hydrological model simulations in order to test whether 'cumulative effective stream power' could be used as a predictive variable for scour depth in cohesive bed sediments; and 3) in a large open channel experimental flume around a physical model and test box consisting of a cylinder in natural cohesive soils, evolution of scour depths were measured for several multiple flow sequences to illustrate the scour time-dependency of cohesive sediments. This study identified that several factors were related to the erodibility parameters estimation for cohesive sediments: i) variability related to the device operation, ii) variability related to sediment source, iii) device dependent variability, and iv) soil heterogeneity among study sites. HEC-18</p>		

equations could be improved through more accurately measured  $\tau_c$  and  $k_d$  values using the mini-jet device and multiple-pressure setting procedures compared with a single pressure setting approach. A key finding of this study was that  $\tau_c$  and  $k_d$  were related to different physical-geochemical sediment properties, and unique to physiographic province representing different surficial geological formations. The physical-geochemical parameters found to be statistically relevant were moisture content (WC) and % finer particles passing a #200 sieve (Pass200) dominantly, but also cohesion (CC), dispersion ration (DR), liquid limit (LL), sodium adsorption ratio (SAR), and organic content (OC). Many different predictive models for the erodibility parameters have been developed in the United States, but were limited to one or only a few physical-geochemical parameters. Physical-geochemical parameters govern the time-dependent scour behavior in riverine cohesive sediment/soils. The time-dependent scour behavior correlated with cumulative effective stream power, a surrogate for shear stress duration over  $\tau_c$ , in addition to flow history. The open channel flume experiments also documented the importance of flow history on scour, in addition to the sediment bulk density (BD). In order to develop a more accurate predictive equation than reported in HEC-18, further research is required. Applying the finding from this study, recommendations proposed for future research include: 1) conduct more in-situ field tests with the mini-jet device to verify the  $\tau_c$  values among similar physiographic provinces, 2) implement a long-term field study at newly constructed bridge sites, and continuously and consistently monitor both flow and scour depths, and 3) conduct additional flume experiments incorporating more varied flow sequences and sediment types with measured physical-geochemical properties.

17. Key Words  <b>RIVER SCOUR; BRIDGES; COHESIVE SEDIMENTS, HEC-18 EQUATIONS</b>		18. Distribution Statement  No restriction. This document is available to the public from the sponsoring agency at the website <a href="https://www.tn.gov/">https://www.tn.gov/</a>	
19. Security Classif. (of this report) Unclassified	20. Security Classif. (of this page) Unclassified	21. No. of Pages 98	22. Price \$0.00

# Evaluation and Prediction of Bridge Pier and Contraction Scour of Cohesive River Sediments in Tennessee

*Submitted by:*

University of Tennessee, Knoxville  
*Department of Civil and Environmental Engineering*

John S. Schwartz, Ph.D., P.E.  
Angelica M. Palomino, Ph.D.  
Badal Mahalder, Ph.D.



*Prepared for:*

Tennessee Department of Transportation  
*Materials & Tests Division, Geotechnical Engineering Section*  
*Environmental Division, Ecology & Permits Office*

Jon Zirkle, P.E.  
Wesley Peck, P.E.



Final Report: September 30, 2018

# Table of Contents

	<u>Page</u>
Executive Summary .....	ix
Acknowledgements.....	xii
1.0 Introduction.....	1
1.1 Overview.....	1
1.2 Project Objectives .....	2
1.3 Scope of Work .....	2
1.4 Background Literature and Project Approach .....	3
2.0 Relationships Between Physical-Geochemical Soil Properties and Erodibility of Streambanks among Different Physiographic Provinces of Tennessee .....	7
2.1 Introduction.....	7
2.2 Review: Predictive Relationships for Soil Erodibility.....	8
2.3 Study Area .....	9
2.4 Methods.....	11
2.4.1 Data Collection .....	11
2.4.2 Laboratory Analysis .....	13
2.4.3 Parameters Prediction for Excess Shear Stress Equation .....	13
2.4.4 Multicollinearity in the Dataset .....	14
2.4.5 Cluster Analysis.....	14
2.4.6 Statistical Model Development for Variable Selection .....	14
2.5 Results.....	16
2.5.1 Soil Properties.....	16
2.5.2 Properties of the Cluster Groups .....	17
2.5.3 Statistical Correlation and Model Variable Selection.....	18
2.6 Discussion.....	22
2.6.1 Correlation Patterns of Significant Variables .....	25
2.6.2 Relationship of Critical Shear Stress with the Erodibility Coefficient .....	28
2.7 Conclusion .....	28
3.0 The Influence of Cumulative Effective Stream Power on Scour Depth Prediction Around Bridge Piers in Cohesive Earth Material .....	30
3.1 Introduction.....	30
3.2 Methods.....	32
3.2.1 Study Area .....	32
3.2.2 Erodibility Index Calculations .....	34
3.2.3 Hydrological Flow Simulations .....	35
3.2.4 Field Measurements of Stream Bank/Bed Soil Critical Shear Stress .....	36
3.2.5 Effective Stream Power Calculations .....	37
3.3 Results.....	38
3.3.1 Study Site Soil Properties .....	38
3.3.2 Case Study for Pond Creek Site on Temporal Scour Patterns .....	41
3.4 Discussion.....	41
3.5 Conclusion .....	46
4.0 Evolution of scour depths Around Cylinder in Natural Cohesive Soil from Multiple Flow Events .....	47
4.1 Introduction.....	47

4.2 Experimental Set-up and Procedures .....	48
4.2.1 Open Channel Flume Construction.....	48
4.2.2 Properties of Natural Cohesive Sediment .....	48
4.2.3 Flume Sediment Bed Preparation .....	48
4.2.4 Experimental Procedures .....	51
4.2.5 Available Equilibrium Scour Depth Prediction Equations for Cohesive Soil .....	52
4.3 Results and Discussion .....	54
4.3.1 Scour Depth Evolution.....	54
4.3.2 Influence of Multi-flow on Scour Propagation .....	56
4.3.3 Influence of Stress History on Scour Propagation.....	59
4.3.4 Comparison between Different Scour Depth Equations .....	60
4.4 Conclusion .....	63
5.0 Project Conclusions and Recommendations .....	64
5.1 Summary Conclusions .....	64
5.2 Limitations and Recommendations.....	65
References.....	67
Appendices.....	77

## List of Figures

	<u>Page</u>
Figure 1.1	Conceptual model of the sediment properties and processes that affect sediment erodibility (Grabowski et al., 2011). .....4
Figure 2.1	Study sites across different TDOT classified regions.....10
Figure 2.2	Map of physiographic provinces of Tennessee (Miller, 1974) with study sites shown as red triangles.....11
Figure 2.3	Relationship between critical shear stress and erodibility coefficient with erosion index (after Hanson and Simon, 2001). .....18
Figure 2.4	Four cluster groups using the “Ward” method and non-hierarchical “k-means” approach based on soil properties including critical shear stress. ....19
Figure 2.5	Measured and predicted critical shear stress (a) Cluster 1, (b) Cluster 2, (c) Cluster 3, and (d) Cluster 4 (using transformed data). .....23
Figure 3.1	Erosion in cohesive soils: a) around bridge piers in Crooked Creek, Shelby County, TN, b) undercutting at the bottom of creek in Coal Creek, Tipton County, TN .....31
Figure 3.2	Study watersheds showing locations of bridge sites in western Tennessee .....34
Figure 3.3	Simulated flow for gaged watershed (Stokes Creek): a) model calibration, b) model validation.....36
Figure 3.4	Example flow simulation for Pond Creek in Dyer County, West Tennessee, and the flow threshold at critical shear stress. ....37
Figure 3.5	Relationship between critical stream power and erodibility index. Where probability of erosion was calculated using the Wibowo et al. (2005) proposed probabilistic approach using logistic regression method. ....39
Figure 3.6	Relationship between cumulative effective stream power and scour depth measurement. Circled data points represent measurements at the Crooked Creek site. ....40
Figure 3.7	Relationship between relative scour depth and the number of flow events above the critical flow for the studied stream sites. Solid circles = regular scour data points, diamonds = scour data before 2004 with longer duration flow events; and squares = scour data after 2004 with short duration flow events. ....41
Figure 3.8	Long-term scour depth data and the number of flow events above critical flow at the bridge pier for Pond Creek showing three different scour rates over a 20-year period. ....42
Figure 3.9	Protective wooden logs at the vicinity of the pier in Crooked Creek. ....45
Figure 4.1	Detail of the flume: a) plan view, and b) long section of the flume (not to scale). ....49
Figure 4.2	a) Prepared sediment bed with the Plexiglas circular pier, b) placement of underwater camera during experiments for periodic scour depth measurement. ..50
Figure 4.3	Velocity distribution with depth: a) low flow (run no. 3), b) medium flow (run no. 4), and b) high flow (run no. 5). ....52
Figure 4.4	Scour hole development for: a) run 16, $V = 80.68$ cm/s, $WC = 37.45\%$ , b) run 14, $V = 80.10$ cm/s, $WC = 38.12\%$ , c) run 10, $V = 90.26$ cm/s, $WC = 31.25\%$ , and d) run 9, $V = 102.40$ cm/s, $WC = 31.25\%$ . ....55
Figure 4.5	Scour hole development and the soil removal erosion pattern at the wake zone of the pier: run 14, $V = 80.10$ cm/s, $WC = 38.12\%$ .....56

**List of Figures** *continued...*

	<u>Page</u>
Figure 4.6 The evolution of maximum scour depth: a) for High-Medium-Low (H-M-L) flow sequence at 270° and 90° of the pier, b) for Low-Medium-High (L-M-H) flow sequence at 90° and 45° of the pier. ....	58
Figure 4.7 The evolution of maximum scour depth: (a) for High-High-High (H-H-H) flow sequence at 270° and 90° of the pier, b) for Low-Low-Low (L-L-L) flow sequence at 90° and 270° of the pier.....	59
Figure 4.8 Observed and predicted scour depths after each experimental run .....	62

## List of Tables

	<u>Page</u>
Table 2.1 Study sites with identifying information on location, geological formation and rock characteristics (Miller, 1974), and watershed drainage area (km <sup>2</sup> ).....	12
Table 2.2 Soil tests and method standards used to characterize soil properties.....	13
Table 2.3 Statistical description of the measured variables for the dataset consisting of 128 soil samples among the different Tennessee physiographic provinces.....	15
Table 2.4 Degree of dispersion for the tested soils according to the US Army Corps of Engineers (USACE, 1970) classification criteria.....	17
Table 2.5 Multiple regression models for prediction of critical shear stress ( $\tau_c$ ) based on soil properties. Models included all possible regression (APR), McHenry algorithm (MHA), least angle regression (LAR), and stepwise multiple linear regression (STR). R <sup>2</sup> , p-value, and PRESS statistics are shown for each model....	20
Table 2.6 Coefficient p-values for individual variables and corresponding correlation sign among the predictive models for each cluster representing a unique physiographic province and surficial geology.....	24
Table 2.7 Predictive models in each cluster for erodibility coefficient ( $k_d$ ) as a function of critical shear stress ( $\tau_c$ ) for the entire dataset, and individually for the four identified data clusters.....	24
Table 3.1 Study sites characters including the watershed and highway bridge .....	33
Table 3.2 Statistical error calculation and validation targets .....	36
Table 3.3 Soil properties, erodibility index parameters, critical shear stress and critical stream power per unit width of channel, and channel slope for the nine study sites.....	39
Table 4.1 Properties of Crooked Creek sediment.....	50
Table 4.2 Experimental conditions in the open channel flume. ....	51
Table 4.3 Scour depth development around circular pier for different flow and soil condition .....	57
Table 4.4 Comparison of observed and predicted scour .....	61

## Appendices

- Appendix A:** *Published Journal Article:* Mahalder, B., J.S. Schwartz, A.M. Palomino, and J. Zirkle. 2018. Estimating erodibility parameters for streambanks with cohesive soils using the mini jet test device: A comparison of field and computational methods. *Water*, 10, 304. ....78
- Appendix B:** *Journal Article Manuscript:* Mahalder, B., J.S. Schwartz, A.N. Papanicolaou, A.M. Palomino, and J. Zirkle. 2018. Comparison of erodibility parameters for cohesive streambank soils between an in-situ jet test device and laboratory conduit flume. *Journal of Hydraulics Engineering* (prepared for submission). ....98

## List of Acronyms

ADV	Acoustic Doppler Velocimeter
BD	Bulk Density ( $\text{g}/\text{cm}^3$ );
CA	Clay Activity
CC	Cohesion
CLA	Non-hierarchical Cluster Analysis
Con	Consistency
$D_{50}$	Median Particle Size
DD	Dry Density of the Soil
DR	Dispersion Ratio
EC	Electrical Conductivity
$F_{\text{clay}}$	Clay Fraction
FHWA	Federal Highway Administration
HEC-18	Hydraulic Engineering Circular No. 18
$I_a$	Erosion Resistance
$K$	Erodibility Index (Annadale)
KIF	Potassium Intensity Factor
LI	Liquidity Index
LL	Liquid Limit
LOI	Loss on Ignition Analysis
MANOVA	Multiple Analysis of Variance
MPS	Multiple Pressure Setting
NRCS	National Resource Conservation Service
OC	Organic Content
Pass200	Sediment Passing #200 Sieve
PL	Plastic Limit
PRESS	Predicted Residual Error Sum of Squares Statistic
$Q$	Flow Discharge
$n$	Porosity
SAR	Sodium Adsorption Ratio
$S$	Channel Slope
SG	Specific Gravity
TDOT	Tennessee Department of Transportation
TRB	Transportation Research Board
TVA	Tennessee Valley Authority
USGS	United States Geological Survey
UTK	University of Tennessee, Knoxville
$V_c$	Critical Flow Velocity
WC	Water Content
$y_s$	Maximum Scour Depth
$\varepsilon_T$	Erosion Rate ( $\text{cm}\cdot\text{s}^{-1}$ )
$k_d$	Erodibility Coefficient ( $\text{cm}^3\cdot\text{N}^{-1}\cdot\text{s}^{-1}$ )
$\sigma_g$	Geometric Standard Deviation
$\Omega_c$	Critical Stream Power ( $\text{W}/\text{m}^2$ )
$\tau_b$	Bed shear stress
$\tau_c$	Critical shear stress

## Executive Summary

### Evaluation and Prediction of Bridge Pier and Contraction Scour of Cohesive River Sediments in Tennessee

Approximately 450 scour critical bridges are maintained by Tennessee Department of Transportation (TDOT) across the state. Many of these bridges are located in river or stream beds and banks where cohesive soils are prevalent, particularly in western Tennessee. In the Hydraulic Engineering Circular No. 18 by the Federal Highway Administration, *Evaluating Scour at Bridges* (FWHA-HIF-12-003), existing HEC-18 equations for predicting scour depth at bridge piers and contractions in river beds for with non-cohesive, e.g., sand and gravel, tend to perform well. However, when cohesive sediments consisting of consolidated silts and clays commonly present on river beds, the HEC-18 equations tend to over-predict scour depth, although under-prediction also occurs as reported in published studies. The uncertainty of scour depth prediction can led to over design of bridge piers increasing construction costs, or under designed piers which may lead to bridge failure or future costly repairs. TDOT engineers identified that these equations need improvement and initiated the request for study in the state to better understand the variables that govern river bed scour in cohesive sediments near bridges.

The HEC-18 equations for scour depth in cohesive sediments fundamental rely on the excess shear stress equation, expressed as:  $\varepsilon_T = k_d(\tau_b - \tau_c)^m$ , where  $\varepsilon_T$  is the erosion rate ( $\text{cm}\cdot\text{s}^{-1}$ ),  $k_d$  ( $\text{cm}^3\cdot\text{N}^{-1}\cdot\text{s}^{-1}$ ),  $\tau_c$  (Pa) is the critical shear stress consisting of a sediment's property of cohesion,  $\tau_b$  is the hydraulic boundary shear stress (Pa), and  $m$  is an empirical exponent. Detachment of cohesive sediment from river beds and banks is more complex than non-cohesive sediments because scour is function of physical-geochemical properties forming cohesive bonds between silt-clay particles, and erodibility is time-dependent where sediment mass fatigues and aggregates detach after a variable number of passing flood events. Many physical-geotechnical properties can influence  $k_d$  and  $\tau_c$  including: water content, unit weight or bulk density, plasticity, clay mineral type and content, cation exchange capacity, inter-particle forces, water and sediment temperature, which properties vary depending on regional river geomorphology. Reaching a maximum scour depth at a bridge site may take many years depending on the frequency and duration of flood events, and the cohesive strength of the bed sediment. With the HEC-18 equations dependent on  $k_d$  and  $\tau_c$ , measurement of these key parameters can also lead to uncertainty in scour prediction. The common measurement device for these parameters is the in-situ jet tester. Further research is needed to better understand how the measurement device and computational procedures can influence  $k_d$  and  $\tau_c$  estimates. Therefore, improving scour prediction in cohesive sediments must consider geochemical properties, the time-dependent behavior of erodibility per hydraulic interactions, and the field measurement of  $k_d$  and  $\tau_c$ .

The objective of this research project is to enhance our understanding of river/stream bed scour and bank erosion behavior with cohesive sediments near bridges, and its relationships with  $\tau_c$  and  $k_d$  used in HEC-18 equations, including the time-dependent scour behavior and associated cohesive physical-geotechnical properties, and measurement of these erodibility parameters. In addition, this research focused on characterizing differences in physical-geotechnical properties of riverine cohesive sediments across the different physiographic provinces of Tennessee. The initial research investigated how field data collection and computational procedures for the in-situ mini-jet tester influenced  $k_d$  and  $\tau_c$  estimates. In order to meet the objectives, the following studies were completed: 1) statistical multivariate predictive equations were developed for  $\tau_c$  (and  $k_d$ ) across the state's different physiographic provinces as a function of significant physical-

geotechnical properties; 2) measured bridge scour data were correlated with cumulative effective stream power data from long-term river continuous flow records as a product of hydrological model simulations in order to test whether ‘cumulative effective stream power’ could be used as a predictive variable for scour depth in cohesive bed sediments; and 3) in a large open channel experimental flume around a physical model and test box consisting of a cylinder in natural cohesive soils, evolution of scour depths were measured for several multiple flow sequences to illustrate the scour time-dependency of cohesive sediments.

Initial investigation on the use of the in-situ mini jet device to estimate for  $\tau_c$  and  $k_d$  examined field set-up procedures including the selected device pressure setting, time frequency for scour hole depth measurements, and the data computational procedures. It was observed that set-up procedures can greatly influence for  $\tau_c$  and  $k_d$  estimates at a river/stream site. A new field and computational procedure was developed applying multiple pressures during a test rather than a single pressure device setting, and using a shear stress  $\tau$  (Pa) versus pressure (Pa) plot to obtain a  $\tau_c$  value. The new procedure was published in the journal *Water* (2018) 10(3), 304; and the article titled *Estimating Erodibility Parameters for Streambanks with Cohesive Soils using the Mini-jet Test Device: A Comparison of Field and Computational Methods*. Further investigation of this new multiple pressure setting (MPS) procedure included comparing field results for  $\tau_c$  and  $k_d$  to a laboratory conduit flume. Each device measures these parameters under a unique set of hydraulic conditions, such as a normally-directed jet onto the in-situ sediment surface and applied dispersion principles for a submerged fluid jet to estimate shear stress. In contrast to a disturbed-sediment sample removed from the field and placed in a flume subjected to direct hydraulic boundary shear stresses. Comparison between the new MPS procedure with the mini jet device and sediment samples in a conduit flume resulted in similar estimates for  $\tau_c$  ( $R^2 = 0.58$ ) suggesting that the MPS jet test procedure better represented applied boundary shear stresses than using a single pressure setting. However,  $k_d$  estimates were substantially less for the conduit flume. Based on observation, it appears not all eroded sediment mass is accounted for during test collections. A manuscript of this work titled *Comparison of Erodibility Parameters for Cohesive Streambank Soils Between an In-situ Jet Test Device and Laboratory Conduit Flume.*, has been submitted for publication and is under review in the *Journal of Hydraulic Engineering*.

Statistical multivariate predictive equations were developed for  $\tau_c$  (and  $k_d$ ) across the state’s different physiographic provinces as a function of significant geotechnical properties. Using the in-situ mini jet device, field data were collected from 21 streams, and  $\tau_c$  and  $k_d$  were estimated using the MPS procedure. Sediment/soil samples were collected at each site and analyzed for 27 physical/ geotechnical parameters. Applying multivariate cluster analysis unique relationships for  $\tau_c$  based on significant physical/geotechnical parameters were found among four Tennessee physiographic provinces. They were: Ridge and Valley, West Highland Rim, Central Basin, and Coastal Plain bordering the Mississippi River Valley in the loess depositional area. Per statistical cluster, predictive models for  $\tau_c$  were developed by multivariate regression. The final variable set of soil properties with statistically significant model coefficients included 16 variables. Although, moisture content (WC) and % finer particles passing a #200 sieve (Pass200) dominated as variables in the  $\tau_c$  predictive models on among three of the four provinces. The properties: cohesion (CC), dispersion ration (DR), liquid limit (LL), sodium adsorption ratio (SAR), and organic content (OC) were also found to be dominant variables within the predictive models among the four provinces. It is interesting to note that  $D_{50}$  is the least significant variable in predicting  $\tau_c$  in cohesive soils. The relationship between  $\tau_c$  and  $k_d$  were significantly correlated ( $p < 0.001$ ), which is consistent with other studies. Within the entire dataset  $\tau_c$  ranged from 0.08 to 26.82 Pa with a mean of 5.17 Pa, and  $k_d$  ranged from 0.56 to 24.4  $\text{cm}^3 \text{N}^{-1} \text{s}^{-1}$  with a mean of

$3.51 \text{ cm}^3 \text{ N}^{-1} \text{ s}^{-1}$ . The key findings from this study suggests that no one soil property, or a common group of a select few properties will form a universal equation for predicting  $\tau_c$  and  $k_d$ . Relationships between the erodibility parameters and physical-geochemical sediment properties appear to be dependent on regional surficial geology. With the developed regional predictive models for  $\tau_c$  and  $k_d$  from this study, erodibility parameters can be obtained by sediment/soil samples and laboratory analyses rather than time-consuming field data collection using the in-situ jet device. TDOT engineers can use these model estimates of  $\tau_c$  and  $k_d$  for use in the HEC-18 equations on order to compute a maximum scour depth near a bridge pier or bridge contraction. Estimates can also be used in bank erosion models such as the USDA Bank Stability and Toe Erosion Model (BSTEM) for prediction channel cross-sectional adjustments.

Through an extensive hydrological modeling effort for rivers with TDOT-collected long-term bridge pier scour data, hydrological flow history was modeled using HEC-HMS and long-term climate data from the Tennessee Valley Authority. Continuous flow simulations for nine bridge sites were converted to cumulative effective stream power. Cumulative effective stream power is the cumulative duration of stream power over  $\tau_c$ , as determined from the field studies measuring it by the mini-jet device. The fundamental question researched was whether the variable cumulative effective stream power correlated with scour depth at bridge piers, and could this variable be used as a surrogate parameter to estimate if and when maximum scour depth is achieved. Combining the field tests and hydrologic flow simulation, it was identified that cumulative effective stream power correlated well with the observed bridge pier scour data. Scour depth development in cohesive soils appeared to be dependent on the effective shear stress duration rather than number of flow events above the  $\tau_c$  values. The influence of flow history on scour rate propagation in cohesive earth material from multiple flow events was also observed. In addition, the Erodibility Index ( $K$ ), a surrogate measure to scour resistance of earth (rock) material was significantly correlated to critical stream power ( $R^2 = 0.61$ ,  $p = 0.017$ ). Data from this study showed a clear deviation from published empirical relationship for soils with a  $K < 0.1$ . This finding implied that direct in-situ measurements of erodibility parameters are necessary for the critical stream power calculation rather using an empirical relationship. In summary, it was identified that shear stress duration, the number of flow events above  $\tau_c$ , and bridge age substantially affected the observed scour depths around bridge piers.

An experiment using a large open channel flume with a bed test chamber compacted with natural cohesive sediments and a vertically-position cylinder was conducted to examine scour behavior around a cylinder representing a modeled bridge pier. This unique study design, compared with other published studies, was that field-collected natural cohesive sediments and variable flows were used to mimic more “natural” conditions. Study findings suggested that scour commenced at the sides of the cylinder and maximum scour depth also occurred at sides irrespective of flow velocity and soil bulk density (BD). It was also observed that shallow water condition (since  $h/D < 2.0$ ) influenced the lateral and transverse scour-hole propagation at the downstream side of the cylinder compared with the sides and upstream of the cylinder. Scour propagation under multi-flow conditions showed that depending on the BD conditions, almost similar maximum scour depths were observed for both the Low-Medium-High (L-M-H) and High-Medium-Low (H-M-L) flow sequences. It was also observed that at higher BD conditions ( $1.81\text{-}2.04 \text{ gm/cm}^3$ ) scour depths initiated after 3 to 12 hours of sustained flow, which supported the hypothesis that memory effect could have influence on scour propagation in cohesive soils. The effect of multiple-flow sequences on scour depth propagation and the stress history (memory effect) were studied. Results from these experiments demonstrated that the flow sequence significantly influenced final scour depths per experimental run. Finally, HEC-18 equations were

observed to over-predict equilibrium depths on field-collected cohesive sediments with higher BD (1.81-20.4 gm/cm<sup>3</sup>). However, at lower BD sediments (1.51-186 gm/cm<sup>3</sup>) the observed experimental scour depths were comparable to the depths predicted by the HEC-18 equation. This finding suggested the HEC-18 equation for equilibrium scour depth in cohesive sediment may have been developed using lower BD sediments from commercially obtained materials, nonetheless, it suggests BD needs to be considered for equation improvement. Overall, findings from this research expand the body of knowledge on improving our understanding of erosion behavior and associated processes in cohesive sediment in stream beds.

In the project study, erosion behavior in riverine cohesive sediments was investigated through intensive field tests and data analyses, and laboratory flume experiments. It was identified that several factors were related to the erodibility parameters estimation for cohesive sediments: i) variability related to the device operation, ii) variability related to sediment source, iii) device dependent variability, and iv) soil heterogeneity among study sites. HEC-18 equations could be improved through more accurately measured  $\tau_c$  and  $k_d$  values using the mini-jet device and MPS procedures compared with a single pressure setting approach. A key finding of this study was that  $\tau_c$  and  $k_d$  were related to different physical-geochemical sediment properties, and unique to physiographic province representing different surficial geological formations. The physical-geochemical parameters found to be statistically relevant were WC and Pass200 dominantly, but also CC, DR, LL, SAR, and OC. Many different predictive models for the erodibility parameters have been developed in the United States, but were limited to one or only a few physical-geochemical parameters. Physical-geochemical parameters govern the time-dependent scour behavior in riverine cohesive sediment/soils. The time-dependent scour behavior correlated with cumulative effective stream power, a surrogate for shear stress duration over  $\tau_c$ , in addition to flow history. The open channel flume experiments also documented the importance of flow history on scour, in addition to the sediment BD. In order to develop a more accurate predictive equation than reported in HEC-18, further research is required. Applying the finding from this study, recommendations proposed for future research include: 1) conduct more in-situ field tests with the mini-jet device to verify the  $\tau_c$  values among similar physiographic provinces, 2) implement a long-term field study at newly constructed bridge sites, and continuously and consistently monitor both flow and scour depths, and 3) conduct additional flume experiments incorporating more varied flow sequences and sediment types with measured physical-geochemical properties.

Badal Mahadler was the full time research graduate student on the project. He graduated on May 2018 with PhD degree. His dissertation is titled: *Evaluation and Prediction of Cohesive Soil Erosion Parameters among Varying Soil Properties and Testing Procedures: Implications for River Bed Scour at Bridge Piers*.

## Acknowledgments

Research was funded by the Tennessee Department of Transportation (TDOT), Research group, Grant #: RES#2013-36 through the University of Tennessee Center for Transportation Research. Review of the research products and serving on Badal Mahalder's doctoral committee were Dr. Thanos Papanicolaou and Dr. Daniel Yoder at the University of Tennessee (UTK), and Dr. Tess Thompson at Virginia Tech. Support for fieldwork and laboratory from others included many: Jordan Hicks, Zachariah Seiden, Bijoy Halder, Adrian Gonzalez, Cyrus Jedari, Robert Woockman, Brandy Manka, Payton Smith, Alex Hollman, Maxwell Carter, Alan Jolly, Michael Walton, and Mollika Roy. Ms. Nancy Roberts help with the use of the soil analysis lab

equipment in the UTK Geotechnical Laboratory. Within the UTK Department of Civil and Environmental Engineering Mr. Andy Baker and Mr. Larry Roberts provided tireless help for the outdoor flume construction, and other equipment manufacturing and maintenance.

# 1.0 Introduction

## 1.1 Overview

In the Hydraulic Engineering Circular No. 18 (HEC-18, 5<sup>th</sup> edition, 2012) by the Federal Highway Administration, existing equations for predicting scour depth at bridge piers and contractions in river beds with non-cohesive, i.e. coarse-grained, sediments tend to perform well. However, when cohesive (fine-grained) sediments are present, the HEC-18 equations tend to over-predict scour near bridge piers in rivers. A recent study by the South Carolina Department of Transportation (SCDOT) and the US Geological Survey (USGS) found HEC-18 scour equations in cohesive sediments over-predicted scour depth for 84% of bridge sites surveyed, and over-predicted depths in a range from 0.1 to 13.4 ft (Benedict, 2009). In this same study, under-prediction did occur at 16% of the surveyed sites, which were a function of local bed sediment and geological conditions with high hydraulic resistance properties. Other USGS studies reported similar variability in model prediction of scour of cohesive river sediments, both bed and bank due to cohesive soil properties and the complex nature of scour behavior during flood events. Further study is warranted to improve our understanding of cohesive soil scour behavior with emphasis on this behavior adjacent to river bridge infrastructure.

Approximately 450 scour critical bridges are maintained by Tennessee Department of Transportation (TDOT) across the state. Many of these bridges are located in river or stream beds in which cohesive soils are prevalent, particularly in western Tennessee. Lack of predictive capability of the maximum scour depth in cohesive sediments of river beds remains an engineering problem for TDOT bridge engineers. Scour prediction is necessary in order to identify bridges in danger of foundation instability and failure; and conversely, in river bed conditions of high hydraulic resistance bridge piers and abutments may be overdesigned, increasing project construction costs. Overall, improved prediction of scour for riverine sediments in Tennessee can assist in more cost effective and safe bridge design across the state.

Scour of cohesive sediments (i.e., silts, clays) differs from that of non-cohesive sediments (i.e., sand, gravel) in that scour is a time-dependent variable requiring an estimate of erodibility rates (Hanson and Simon, 2001; TRB, 2004). Maximum scour depth often occurs after a multitude of passing floods, and in many cases over a long period of time. Erodibility is a function of many sediment geotechnical properties (e.g., unit weight, plasticity, clay mineral type and content, cation exchange capacity, inter-particle forces, water and sediment temperature, etc.), and which can vary depending on the regional riverine conditions. Because of the many potential properties influencing site erodibility, available predictive relationships for erosion rates and maximum scour depth have not been fully developed and applicable across different regions. In addition, the measurement of cohesive soil properties can be conducted by different devices, which have produced highly varying outcomes on measures of erodibility parameters used in the excess shear stress equation for scour prediction (Daly et al., 2015a, b).

According to the HEC-18 user's manual, cohesive sediment  $\tau_c$  and erodibility can be obtained by *in situ* field methods using a mini-jet tester, which UTK has several units available for use. Scour or erosion rates are expressed by the excess shear stress equation as:  $\varepsilon_T = k_d(\tau_b - \tau_c)^m$ , where  $\varepsilon_T$  is the erosion rate ( $\text{cm}\cdot\text{s}^{-1}$ ),  $k_d$  ( $\text{cm}^3\cdot\text{N}^{-1}\cdot\text{s}^{-1}$ ),  $\tau_c$  (Pa),  $\tau_b$  is the hydraulic boundary shear stress (Pa), and  $m$  is an empirical exponent (Hanson, 1990; Hanson and Simon, 2001). Research has shown that maximum scour depth adjacent an instream structure (i.e., bridge piers) requires bed erosion from multiple floods, a typical way of assessing it is with cumulative

shear stress duration over a critical shear stress ( $\tau_c$ ) for erosion to initiate. Cumulative stream power over  $\tau_c$  has also been used by others therefore dependent on hydrological history of the location. Scour development in cohesive soils on river beds near structures is a complex physical process at multiple scales. An identified research need is to better understand the how the different geotechnical properties of riverine cohesive soils and the hydrological dynamics play a role on scour near instream bridge pier structures.

## 1.2 Study Objective

The objective of this research is to enhance our understanding of stream bed scour and bank erosion with cohesive soils near bridge piers and its relationships with critical shear stress ( $\tau_c$ ) and the erodibility coefficient ( $k_d$ ) used in the excess shear stress equation for predicting erosion rates ( $\varepsilon_T$ ), including the time-dependent scour behavior and associated cohesive soil properties, and measurement of these erodibility parameters. This research was conducted specific to river and stream beds across the different and highly variable physiographic provinces in Tennessee.

## 1.3 Scope of Work

The scope of work as defined in the original proposal, the study compared measured scour depths at selected bridge sites with flood histories and cumulative shear stress (stream power), geotechnical characteristics of the bed sediment/soil properties, and channel geomorphic conditions; the following five tasks were completed to address this study objective.

- Task 1. Compile historic bridge information for the selected bridge sites.
- Task 2. Conduct a hydrologic analysis and develop cumulative shear stress and stream power duration curves, as well as summarize site flood-return frequencies.
- Task 3. Survey scour patterns at piers and contractions in the field at selected bridge sites, classify bed/bank sediment/soils, measure *in situ*  $\tau_c$  and erodibility with the submerged jet tester, determine selected geotechnical properties of sampled cohesive materials.
- Task 4. Conduct a statistical analysis correlating measured scour depth with hydrological analysis data gathered from Task 2 and measured geotechnical properties obtained from Task 3.
- Task 5. Depending on findings from Tasks 1-4. Attempt to develop preliminary predictive relationships for scour depths.

In order to support this study's analysis, fundamental studies included characterizing cohesive soil properties and erodibility rates across Tennessee among different physiographic regions, and comparing different field measurement protocols for cohesive soil erodibility. An additional task was added in Study Year 3 of the project in order to further develop our understanding of scour in cohesive soils at bridge piers consisting of building a large outdoor open channel flume and interior a physical model of bridge piers in a cohesive soil bed, and recording scour over time under different flow scenarios replicating varying hydrograph events.

Task 6 consists of generating a final project report, which is here within. The final report chapters follow the project tasks as listed above:

Chapter 2: Relationships between physical-geochemical soil properties and erodibility of streambanks among different physiographic provinces of Tennessee.

Chapter 3: The influence of cumulative effective stream power on scour depth prediction around bridge piers in cohesive earth material.

Chapter 4: Evolution of scour depths around cylinder in natural cohesive soil from multiple flow events.

Chapter 2 summarizes the research work of Task 3. It has been published in the journal *Earth Surface Processes and Landforms* (2018) Vol. 43(2), Pgs. 401-416. Because field accurate field measurements of cohesive soils in the riverine environment was a key element of this research, two supporting efforts were also completed related to the precision of the submerged jet tester. The two separate research studies were as follows:

1. Estimating erodibility parameters for streambanks with cohesive soils using the mini-jet test device: a comparison of field and computational methods. This research has been published in *Water* (2018) 10(3), 304; and for reference is in Appendix A.
2. Comparison of erodibility parameters for cohesive streambank soils between an in-situ jet test device and laboratory conduit flume. This research has been prepared for publication in the *Journal of Hydraulic Engineering*, and for reference is in Appendix B.

Chapter 3 summarizes the research work of Tasks 1 through 5 where scour at existing TDOT bridge piers were related to the measured cohesive soil properties (specifically Task 3) and the hydrological history summarized into units of cumulative effective stream power. The research for this chapter was fundamental investigating the question whether cumulative effective stream power is directly related to scour depth at bridge piers.

Chapter 4 summarizes the research on scour progression from flows at the physical model of bridge piers in cohesive soil bed from in an outdoor open channel flume. This research was fundamental observing scour of “natural” cohesive soils over a range of flow scenarios and what are the driving forces associated with scour adjacent to a vertically-positioned cylinder. The goal was to attempt to improve the predictive equations for scour in cohesive soil at bridge piers.

Scour behavior in riverine cohesive soils is complex and this research adds to the body of knowledge on this subject. Background on cohesive soil erosion is summarized in the next section (1.4) to provide the context for the project approach and research conducted.

## **1.4 Background Literature and Project Approach**

Due to expanding urban development civil infrastructure demands, there is a need to improve on engineering design and construction of transportation system components, including roadways and bridges. Bridge structures in riverine open channels have the potential to impact hydrological, ecological, and hydraulic elements of the aquatic environment. In particular, constructed structures in rivers influence sediment morphodynamics and structure stability. Structures may be prone to catastrophic failure if the design is not completed considering this dynamic sediment erosion processes. On the other hand, a balance must be reached to economically construct the needed infrastructure relying on technological development and refinement of the existing techniques. Natural geomorphic processes and erosion of cohesive riverbed sediment and bank soils is complex. The inter-dependent and inter-relational behavior of these complex environmental systems results in system of self-adjustments regulated by many controlling factors engineering design could be prohibitively expensive when the exact nature of the sediment transport around structures is not completely understood. Therefore, the nature of sediment movement, which is also known as erosion, is the foremost important factor to be

investigated prior to starting any sustainable and economically viable engineering design. However, predicting the erosional behavior is not a straightforward task as it is an intriguing phenomenon resulting from the interaction between the flow dynamics around the structures and the erosive resistance of the river boundary material.

It is well known that sediment detachment and its transport process significantly affect the evolution of river morphology. For non-cohesive sediments, sediment detachment or initiation of movement and the transport behavior due to in-stream hydraulics, known as bed load and suspended load are reasonably well understood. However, particle/aggregate detachment or initiation in cohesive material is yet to be understood completely and is an ongoing research area. The importance of understanding this process in cohesive soils is necessary for solving numerous engineering problems. Successful implementation and sustainability of some engineering projects, such as: embankment stability, navigation, bank erosion, local and contraction scour around bridge piers and abutments on cohesive soils are also heavily dependent on the understanding of the detachment process of cohesive soils.

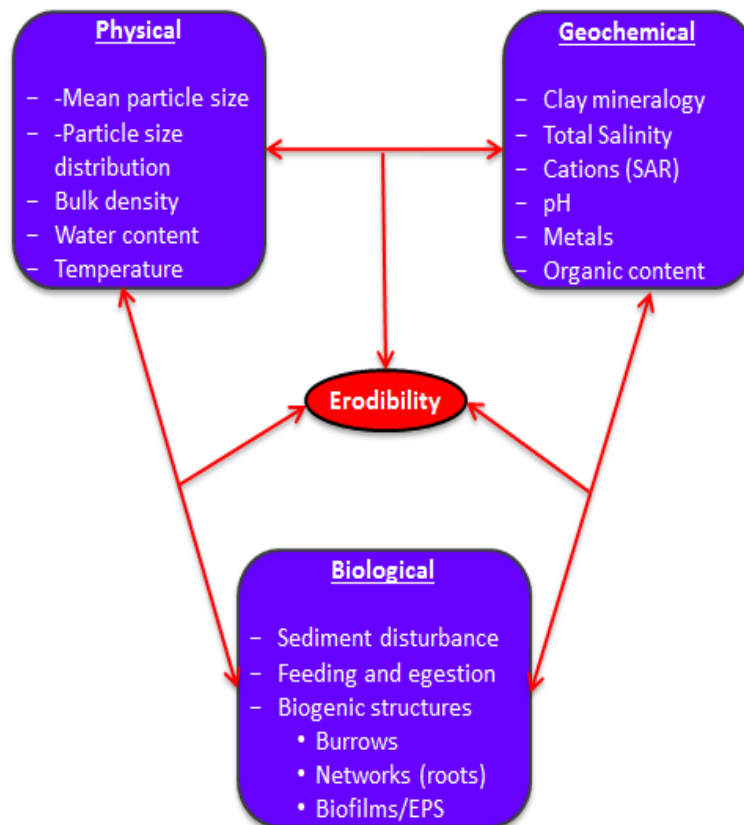


Figure 1.1. Conceptual model of the sediment properties and processes that affect sediment erodibility (Grabowski et al., 2011).

*Issues with critical shear stress measurement in cohesive soil.* Inter-particle attraction forces play a critical role in the erosion behavior of cohesive sediments. These inter-particle attraction forces are dependent on soil physical, geochemical and biological properties, consequently, the erodibility of cohesive sediments (Figure 1.1). Therefore, cohesive soil erodibility is a function of sediment geotechnical, geochemical and biological properties (e.g., unit weight, plasticity,

clay mineral type and content, cation exchange capacity, inter-particle forces, water and sediment temperature, sodium adsorption ratio (SAR), pH, organic content, biogenic structures, etc.). Yet, there remains a lack of reliable predictive relationships between erodibility and these soil properties.

*Scour depth prediction and consequences.* Soil is grossly classified into coarse grained (non-cohesive) and fine grained (cohesive). In water body, structures such as bridges and culverts foundations are constructed on different soils to a certain depth based on equilibrium scour depth prediction using the available equations. Current practice for equilibrium scour depth calculation is to use the Hydraulic Engineering Circular No. 18 (HEC-18, 5th edition, 2012) equations developed by the Federal Highway Administration for bridge piers and contractions in river beds in non-cohesive, i.e. coarse-grained sediments. There are approximately 610,749 bridges in the United States and about 500,000 of them are over water (National Bridge Inventory, 2017). During the last 30 years, about 1000 bridges have failed and about 60% of those failures are due to scour (Shirole and Holt, 1991; Cook, 2014). The average cost for flood damage repair of highways on the federal aid system is \$50 million per year (Lagasse et al., 1995). Therefore, efficient bridge design is necessary for avoiding any catastrophic bridge failure but must also remain cost effective to reduce construction costs. Recently, a study conducted by the SCDOT and USGS found HEC-18 equations over-predicted scour depth in cohesive sediments for 84% of bridge sites surveyed, with over-predicted depths ranging from 0.1 to 13.4 ft (Benedict and Caldwell, 2009). The study also showed 16% of the surveyed sites under-predicted the scour depth, which were a function of local bed sediment and geological conditions with high hydraulic resistance properties.

*Equilibrium scour behavior for cohesive soil.* The behavior of cohesive soil erosion around bridge piers and abutments is different compared to non-cohesive soils, and there is no widely accepted approach for erosion prediction for cohesive sediments. During a large storm event, the peak flood velocity may last for a few hours or days and is likely sufficient for maximum scour generation for non-cohesive soils. This the major difference between non-cohesive soils and cohesive soils erosion properties (TRB, 2004). Hence, knowing the peak flow or peak flow velocity is necessary for maximum or equilibrium scour depth calculations in non-cohesive soils. On the other hand, in cohesive soils, scour and erosion rate can be 1000 times slower than in non-cohesive soils. In cohesive soils, a few days may generate only a small fraction of the maximum scour depth, and so is termed a time dependent phenomena (Briaud et al., 2001).

*Geochemical properties of cohesive soil.* Based on a review of the existing literature, resistance to scour and scouring rates of cohesive sediments are controlled by a number of interacting and interrelated factors such as cohesion, water stability, density, specific gravity, mechanical composition, structure and texture, fissuring, plastic properties, mineralogical composition and saturation with cations, chemical composition and salinity, piping properties, moisture before exposure to flow, total moisture capacity, permeability, vegetal cover and species of plants, meteorological conditions, chemical composition of water and its turbidity, in-plane and cross-sectional geometry of the channel, roughness of the channel, flow depth, turbulence characteristics (scale intensity, frequency), etc. (Dunn, 1959; Smerdon and Beasley, 1959; Lyle and Smerdon, 1965; Alizadeh, 1974; Raudkivi, 1990; Wynn, 2004; Julian and Torres, 2006; Mostafa et al., 2008; Thoman and Niezgodna, 2008; Grabowski et al., 2011).

The abundance of these factors explains the inadequate description of scour processes in cohesive soils. However, some of these parameters are correlated. Nonetheless, the number of soil and environmental parameters affecting the repulsive forces, attractive forces and the

inherent van der Waals forces are more significant in cohesive (clay minerals) soils than in granular materials where the submerged gravitation force and the packing and orientation of the particles could be sufficient to predict the incipient erosion. Therefore, scour prediction formulas for cohesive soils are inconsistent and not widely acceptable compared to granular materials. Studies related to cohesive soil erosion either concentrates on a particular soil, pore water conditions, or highlighted the influence of sample type such as natural field samples (both remolded and undisturbed), pure cohesive materials mixed with granular materials. In those studies, the main goals were to attain the desired test conditions for flume or other laboratory tests. Some in-situ experiments were also conducted by several researchers to capture the environmental variability.

*Experimentation of cohesive soil erosion.* Laboratory experiments are often preferred over field measurements due to the ability to control the study design. However, in-situ results are more realistic as the complex compositional structure of natural cohesive sediments may not be accurately replicated in laboratory experiments (Paterson and Black, 1999). On contrary, samples used in laboratory experiments may not adequately represent the field condition as sediment properties may be altered significantly during transportation from the field to the laboratory (Black and Paterson, 1997). This may result in an erroneous estimation of erosion threshold parameters. Nevertheless, laboratory determination of erosion threshold and scour potential are needed when experiments cannot be performed in the field. It is also understood that experiments such as local scour and contraction scour of bridge structure studies are difficult or impossible to conduct in the field. Therefore, the in-situ measurement of critical erodibility parameters, and the use of those predicted parameters in laboratory experiments could be useful alternative for scour prediction around structures in cohesive sediments. It was also identified that variability associated with operational procedures and data analyses methods for the popular in-situ devices.

Scour phenomenon around bridge piers has been studied by numerous investigators. Shen et al. (1969) described the scour phenomena as: i) clear-water scour (no sediment transport from upstream flow), and ii) live-bed scour (sediment supply from upstream flow). Few studies have been conducted in cohesive soil to study the local scour around bridge piers (Hosny, 1995; Briaud et al., 1999; Ansari et al., 2002; Li, 2002; Mostafa, 2003; Oh, 2009; Debnath and Chaudhuri, 2010a,b). Experimental study of local pier scour in cohesive soil is difficult due to the complex erosion characteristics of fine-grained soils and the difficulty in scaling their properties. Therefore, the erosion rate prediction or the critical erodibility parameters prediction may vary widely for different soils and geological locations/origins as soil properties are widely varying in natural environments. It has been also identified from the literature that commercially available clay materials were extensively used in pervious scour studies using constant flow velocity during experiment. In natural streams flow hydrograph is not constant, so the influence of flow sequence on scour propagation should be investigated.

## 2.0 Relationships between Physical-Geochemical Soil Properties and Erodibility of Streambanks among Different Physiographic Provinces of Tennessee

### 2.1 Introduction

Erosion of cohesive soils in fluvial environments has been extensively studied in order to better predict streambank scour and failure as well as equilibrium scour depth on the channel bed near bridge piers and other civil infrastructures. In addition, erosion is studied to estimate model parameters for stream restoration design and excessive sediment yields to streams that can cause biological impairment (Arulanandan et al., 1980; Berlamont et al., 1993; McNeil et al., 1996; Molinas et al., 1999; Papanicolaou, 2001; Black et al., 2002; Mostafa, 2003; Wynn, 2004; Julian and Torres, 2006; Clark and Wynn, 2007; Mostafa et al., 2008; Thoman and Niezgoda, 2008; Wynn et al., 2008; Oh, 2009; Debnath and Chaudhuri, 2010; Karmaker and Dutta, 2011; Daly et al., 2015a; Schwartz et al., 2015). Within these studies, the excess shear stress equation has been predominantly used to predict erosion rates, which equation is expressed as:

$$\varepsilon_T = k_d (\tau_b - \tau_c)^m \quad (2.1)$$

where,  $\varepsilon_T$  is the erosion rate ( $\text{cm s}^{-1}$ ),  $k_d$  is the erodibility coefficient ( $\text{cm}^3 \text{N}^{-1} \text{s}^{-1}$ ),  $\tau_b$  is the average hydraulic boundary shear stress (Pa),  $\tau_c$  is the critical shear stress (Pa), and  $m$  is an empirical exponent (Arulanandan et al., 1980; Hanson, 1990a,b; Hanson and Simon, 2001; Sanford and Maa, 2001). Use of this equation requires measurement of  $k_d$  and  $\tau_c$ , where  $m$  is generally assumed equal to unity. To achieve these measurements in situ, the jet test device by Hanson (1990b) has been widely applied in erosion studies (Hanson and Simon, 2001; Hanson and Cook, 2004; Simon et al., 2010; Al-Madhhachi et al., 2013a) though other devices have been developed and used. Estimates for  $k_d$  and  $\tau_c$  can vary widely, for example  $\tau_c$  has been reported from near 0 to 400 Pa (Dunn, 1959; Hanson and Simon, 2001; Wynn and Mostaghimi, 2006; Debnath et al., 2007; Mostafa et al., 2008; Thoman and Niezgoda, 2008; Daly et al., 2015a,b). Parameter variability depends on many factors including the measurement approach; the soil physical and geochemical properties; bank conditions related to subaerial processes, root density, and percent cover of riparian vegetation; and spatial variability of boundary shear stress along the bank and bed (Kamphuis and Hall, 1983; Allen et al., 1999; Briaud et al., 1999; Wynn, 2004; Julian and Torres, 2006; Wynn and Mostaghimi, 2006; Thoman and Niezgoda, 2008; Wynn et al., 2008; Grabowski et al., 2011). Though many factors may affect estimates of  $k_d$  and  $\tau_c$ , a more comprehensive understanding is needed specifically on how physical and geochemical properties influence predictability of erosion utilizing the excess shear stress equation.

There have been several studies identifying various physical and geochemical properties that influence estimates of  $k_d$  and  $\tau_c$ , the results of which are not consistent. Properties that have been found to influence erodibility include: percent clay, organic matter, dispersion ratio, water content, clay activity, pore water pH, sodium adsorption ratio (SAR), soil bulk density, and plasticity index (Arunlanandan et al., 1980; Briaud et al., 2001; Wynn, 2004; Julian and Torres, 2006; Thoman and Niezgoda, 2008; Grabowski et al., 2011). Several of these properties appear to be due to inter-particle forces of cohesive soils and their control of detachment rates (Johnson et al., 1994; Droppo et al., 2008). Soil classification schemes characterizing physical properties have been applied to better predict  $k_d$  and  $\tau_c$  with some success (Smerdon and Beasley, 1961; Allen et al., 1999; Clark and Wynn, 2007; Utley and Wynn, 2008). However, these studies were

based on measured data from a single physiographic province and surficial geology (Hanson and Simon, 2001; Clark and Wynn, 2007; Thoman and Niezgodna, 2008; Daly et al., 2015a). In addition, estimates of the erodibility parameters were generally derived from a limited number of soil properties and/or study site samples (Dunn, 1959; Kamphuis and Hall, 1983; Allen et al., 1999; Thoman and Niezgodna, 2008; Daly et al., 2016). A review of published equations for cohesive soil erodibility, presented below, suggests that the erodibility parameters governed by the surficial geology within a given physiographic province.

The objectives of this study were to develop predictive relationships for erodibility parameters for use with the excess shear stress equation, investigate which physical-geochemical properties govern erodibility of cohesive soils, and determine whether governing properties vary among different surficial geologies. We hypothesized that the erodibility parameters  $k_d$  and  $\tau_c$  are largely dependent on mineralogy and soil cohesion, which are a function of surficial geology and soil genesis (Mitchell and Soga, 2005). This study applied jet tests to collect field-based  $k_d$  and  $\tau_c$  data across diverse physiographic provinces within the state of Tennessee, USA.

## 2.2 Review: Predictive Relationships for Soil Erodibility

The erodibility parameters  $k_d$  and  $\tau_c$  are dependent on soil physical, geochemical and biological parameters (Grabowski et al., 2011). In several studies, researchers have developed relationships between erodibility parameters and different soil properties. Most relationships have included multiple regression models for prediction of  $\tau_c$ , and power functions between the erodibility parameters  $k_d$  and  $\tau_c$ .

One of the earliest equation developments for predicting erodibility parameters was based on a laboratory flume study conducted by Smerdon and Beasley (1961). They suggested relationships for  $\tau_c$  (Pa) are related to the median grain size in mm ( $D_{50}$  or  $d_{50}$ ) and clay percentage ( $F_{clay}$ ) according to:

$$\tau_c = 3.54 \times 10^{-28.1d_{50}} \quad (2.2)$$

$$\tau_c = 0.493 \times 10^{0.0182F_{clay}} \quad (2.3)$$

In cohesive soils, the relationship between  $k_d$  and  $\tau_c$  is typically reported as an inverse power law. Hanson and Simon (2001) proposed an inverse relationship of  $k_d$  with  $\tau_c$  based on 83 jet tests conducted in the western United States (US). In their dataset, they showed 64% variation, which was recently incorporated into the Bank Stability and Toe Erosion Model (BSTEM) for estimating  $k_d$  and  $\tau_c$ :

$$k_d = 0.2\tau_c^{-0.5} \quad (2.4)$$

This relationship was later modified by Simon et al. (2011) by conducting hundreds of jet tests across the US in different streams:

$$k_d = 1.62\tau_c^{-0.838} \quad (2.5)$$

Similar to these relationships, Daly et al. (2015a) developed another set of relationships based on different solution techniques using an in-situ jet test device. Their proposed relationships were developed based on jet test data from 13 sites, and all of the tests were conducted in the same geological region, the Illinois River basin in Oklahoma:

$$k_d = 4.62\tau_c^{-0.207} \quad (2.6)$$

$$k_d = 84.32\tau_c^{-1.17} \quad (2.7)$$

Equation 2.6 was based on the Blaisdell et al. (1981) solution method with  $R^2$  value of 0.08, and subsequently Equation 2.7 was developed based on scour depth principle (Daly et al., 2013) with  $R^2$  value of 0.47. The above reported studies were limited in that they were either investigated only a few soil physical properties (mean grain size, water content, and plasticity index) or focused on individual watersheds.

Julian and Torres (2006) also conducted a similar type of study, where they found that silt-clay (SC) content was the only governing soil property for the  $\tau_c$  rating curve. The  $\tau_c$  was maximum at 100% SC and minimum at 0% SC, and their proposed relationship was derived as a third-order polynomial equation:

$$\tau_c = 0.1 + 0.1779 \cdot (SC\%) + 0.0028 \cdot (SC\%)^2 - 2.34e^{-5(SC\%)^3} \quad (2.8)$$

In southwest Virginia, correlation between cohesive soil parameters and  $\tau_c$  was developed based on data from 25 sites with a total of 140 jet tests (Wynn and Mostaghimi, 2006). They reported that soil bulk density, potassium intensity factor, soil/water pH, and water temperature were the most significant properties with  $R^2 = 0.569$ . To note, the stream banks considered in this study were mostly covered with vegetation. It is well known that vegetation cover and root systems in the soil can significantly affect the  $\tau_c$  compared to vegetation-free cohesive soils (Simon and Collison, 2002).

Thoman and Niezgoda (2008) conducted a comparable study in northeast Wyoming on five different creeks with a total of 25 observations. They found that activity of clay (CA), dry density of soil (DD), specific gravity (SG), pH, and water content (WC) of soil were significant soil parameters affecting cohesive soil  $\tau_c$ , and reported  $\tau_c$  range was between 0.11 Pa to 15.35 Pa. Their relationship from this geological region was developed as:

$$\tau_c = 77.28 + 2.20 \cdot (CA) + 0.26 \cdot (DD) - 13.49 \cdot (SG) - 6.4 \cdot (pH) + 0.12 \cdot (WC) \quad (2.9)$$

Regazzoni and Marot (2011) proposed a new way for expressing the cohesive soil erodibility expressed as erosion resistance ( $I_\alpha$ ). They developed multivariate relationships for dispersive and non-dispersive cohesive soils, respectively, as follows:

$$I_\alpha = -1.36 + 8.96\Delta_{wL} + 2.68c + 2.08S_r \quad (2.10)$$

$$I_\alpha = -2.31 + 0.69\Delta_{wL} + 1.41c + 6.07S_r \quad (2.11)$$

where,  $c = \rho_d / \rho_s$ ;  $\rho_d$  dry density and  $\rho_s$  solid density of soil;  $\Delta_{wL}$  clay water content,  $\Delta_{wL} = LL - w_{clay}$ ,  $w_{clay} = WC / F_{clay}$ ,  $w_{clay}$  clay water content,  $WC$  soil water content,  $F_{clay}$  clay fraction of the soil and  $S_r$  is the saturation ratio. Their study was conducted on remolded soils in a controlled laboratory environment using a jet test device. The sample size was 11 and 27 for dispersive and non-dispersive soils, respectively.

### 2.3 Study Area

In this study, 21 streams were selected across Tennessee, USA. The geology of Tennessee is very diverse. TDOT is grouped into four management units (Regions I, II, III, and IV) and

generally overlay with defined physiographic provinces and similar geologies (Figure 2.1). Identifying the geological formation of Tennessee (Safford, 1869; Miller, 1974) it is evident that these TDOT regions overlap. Therefore, instead of identifying the studied sites following the TDOT regions, the study sites were grouped based on the similarities of the respective physiographic provinces and geological formations (Figure 2.2).

The geology of Tennessee is divided into eight major physiographic provinces (Figure 2.1). The topography of Tennessee also ranges between the Appalachian Mountains in the east to Mississippi River bottoms in the west (Miller, 1974). Among these eight major physiographic provinces, in situ erodibility tests were conducted among four provinces and compared for differences in erodibility properties. The detail descriptions of these physiographic provinces are presented below (Figure 2.2, Table 2.1):

- 1) The Valley and Ridge physiographic province, characterized by elongate ridges and valleys, represents the remnants of an ancient fold-and-thrust belt formed during Alleghany orogeny. Erosion, beginning the Mesozoic Era, has resulted in the modern-day topography where more erosion-resistant rock (e.g., sandstone and shale) forms ridges and less resistant rock (e.g., limestone, dolomite, siltstone) forms the valleys (Miller, 1974).
- 2) The Highland Rim physiographic province, which is divided by the Central Basin physiographic province into two subregions: Eastern and Western Highland Rims. The Eastern Rim is marked by a dissected escarpment composed of Paleozoic carbonate rock and the Western Rim is marked with rolling hill topography created by differential erosion of Mississippian sandstone, shale, and limestone. This physiographic province also consists of karst terrain in Mississippian, Devonian, Silurian, Ordovician, and Cambrian limestones.
- 3) The Central Basin province was formed from the erosion of the Nashville Dome, which exposed less resistant underlying limestones forming a topography with rolling hills consisting of limestone, shale, dolomite, siltstone, and claystone.
- 4) Within the western area of Tennessee, a relatively flat and low elevation landscape is identified as the Coastal Plain physiographic province. It is divided into the West Tennessee Uplands and the West Tennessee Plain subregions. This physiographic province was formed during the Mesozoic and the Cenozoic Eras with predominantly sand, silt, clay, gravel and loess surficial materials (Safford, 1869; Miller, 1974).

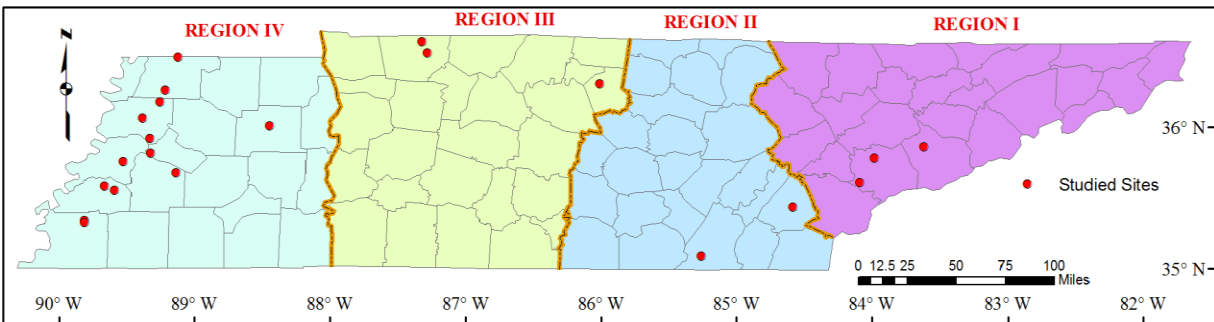


Figure 2.1. Study sites across different TDOT management regions.

In this study, five stream sites were selected from the eastern region of Tennessee in the Valley and Ridge physiographic province. Three sites each were selected from the West Highland Rim and the Central Basin from the middle region of Tennessee. The majority of the selected sites were from the western region of Tennessee, which stream bed and banks dominantly had cohesive (silt/clay) type soils. Selected sites from west Tennessee were: (i) West Tennessee Plain (11 sites), and (ii) West Tennessee Uplands (one site), areas of the Coastal Plain physiographic province. Table 2.1 lists the study sites and their location, study site physiographic province, drainage area, and geological formation and rock characteristics.

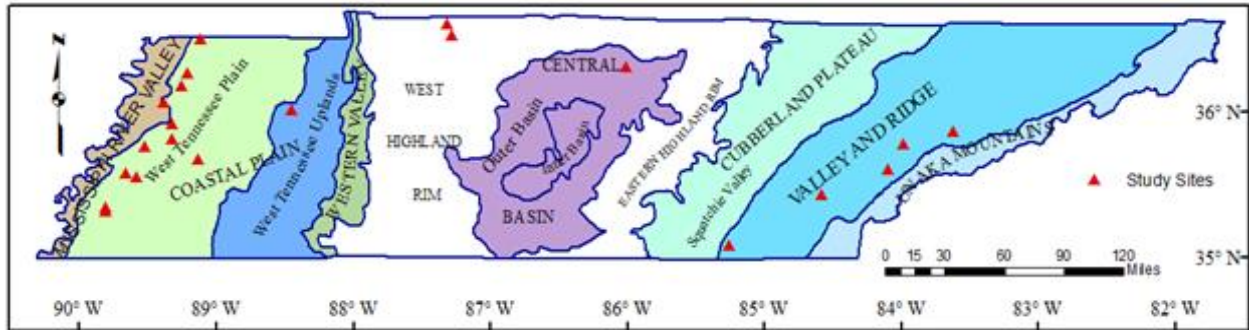


Figure 2.2. Map of physiographic provinces of Tennessee (Miller, 1974) with study sites shown as red triangles.

## 2.4 Methods

### 2.4.1 Data Collection

In this study, in-situ jet test data and soil samples were collected from the selected streams (Table 2.1). Data were collected from the five sites in east Tennessee from July 2014 to April 2015, and the remaining sixteen sites from May 2015 to August 2015. Soil natural moisture content prior to in-situ testing was relatively similar as fieldwork was not conducted within 24 hours after precipitation. Test locations were also visually free from pebbles or rocks, vegetation, and root systems. Test data were collected from six locations for each stream study site, approximated at higher, middle, and lower bank positions. In a few cases, rocks or vegetation prevented testing along all vertical positions, or both banks. In two streams (Lewis Creek and Pond Creek), 11 jet tests were conducted at bank failure locations to compare whether there were soil property differences between the failed material and the exposed bank surface.

Prior to each test, the soil surface was cleaned gently using a shovel and the bottom ring of the jet test device was inserted into the soil using uniform pressure to minimize surface disturbances. The jet test device was then operated following the procedures outlined by Hanson and Cook (2004) and Al-Madhhachi et al. (2013a,b) but with modification as discussed in detail by Mahalder et al. (2018) and presented in Appendix B. A constant head at each pressure was maintained using a pump that delivered stream water powered by a 2000 W portable generator. Before starting any test, the soil WC, electrical conductivity (EC), and soil temperature (T) were measured using a Decagon 5TE probe (Decagon Device Inc., Washington, US). This probe was factory calibrated and rechecked for WC and temperature in the laboratory before field use. Accuracy for WC readings were  $\pm 3\%$ ,  $\pm 10\%$  for EC readings, and  $\pm 1^\circ\text{C}$  for temperature measurements. Water pH was measured using a portable Orion 250 A+ pH meter (Thermo Elect-

Table 2.1. Study sites with identifying information on location, geological formation and rock characteristics (Miller, 1974), and watershed drainage area (km<sup>2</sup>).

Creek Name	County	Physiographic Province	Geological Formation and Rock Characteristics		Latitude	Longitude	Watershed Area (km <sup>2</sup> )
Pistol Creek	Blount	Valley and Ridge	Ordovician and Cambrian System • Knox Group • Chilhowee Group Conasauga Group	Shale, dolomite, limestone, sandstone, conglomerate, quartzite, arkose, greywacke, and siltstone	35.781954	-83.984316	77.67
Nine Mile Creek					35.609316	-84.093183	117.25
Gist Creek	Sevier				35.8613667	-83.619066	26.89
South Chickamauga Creek	Hamilton				35.0873194	-85.260766	1204.76
Oostanaula Creek	McMinn				35.4325810	-84.585825	149.66
Spring Creek	Montgomery	Western Highland Rim	Mississippian and Pennsylvanian System	Limestone, sandstone, shale, siltstone, and dolomite	36.604722	-87.318056	195.34
Red River					36.526111	-87.279444	1344.16
Peyton Creek	Smith	Central Basin			36.308889	-86.007778	128.85
Beaver Creek	Carrol	West Tennessee Uplands (sub-region)			36.013041	-88.445056	58.39
Lewis Creek					36.064388	-89.379583	66.95
Pond Creek	Dyer				35.921027	-89.325277	139.96
Reeds Creek					36.179666	-89.25400	134.10
Mud Creek	Haywood	West Tennessee Plain (sub-region)	Cretaceous in age Neogene and Quaternary System Deposit from both marine and non-marine sand, silt and clay with sand dominant	Sand, silt, clay, gravel and loess	35.678261	-89.132721	64.60
Cane Creek	Lauderdale				35.759750	-89.522583	87.60
North Reelfoot Creek	Obion				36.495533	-89.118099	9.02
Richland Creek					36.262007	-89.212328	45.28
Big Creek	Shelby				35.342108	-89.806569	83.29
Crooked Creek					35.323894	-89.807139	44.63
Coal Creek	Town				35.552611	-89.585556	19.00
Town Creek		35.581445	-89.657422	29.15			
Black Creek	Crockett				35.815902	-89.320778	151.22

ron Corporation, Massachusetts, US) with an accuracy of  $\pm 0.2$  pH units. Prior to each measurement, the pH probe was calibrated using the auto-calibration mode with two buffer solutions (4.01 and 7.00 pH solutions). After completing each test, two core samples near the test location were collected using a 5.08 cm dia. cylindrical stainless steel coring instrument. These core samples were used to measure bulk density (BD), WC and unconfined compression (UC) strength. The core cylinders were immediately end capped and sealed in an air-tight plastic bag to minimize moisture loss.

The sealed samples were then stored in a cooler. Approximately 1.4 kg of soil was also collected per test site from inside the jet device’s bottom ring for laboratory analyses of other soil physical and geochemical properties (Table 2.2). After completing the fieldwork, a GIS base map was prepared for the studied watersheds including: a digital elevation model (DEM) from the USGS, topographic data, and Natural Resources Conservation Service (NRCS) Soil Survey Geographic (SSURGO) data. For all the study sites, the SSURGO soil database was used for identifying the soil horizons and source of parent materials.

#### 2.4.2 Laboratory Analysis

The collected cores and soil samples from each test location were used for determining mechanical, physical, and geochemical properties. The core samples were extruded and analyzed for BD (ASTM D2937) and WC (ASTM D7263). Extruded cylindrical samples were then trimmed and subjected to UC tests using a triaxial testing device (Loadframe 1, GEOTAC) (ASTM D2166). Soil samples collected from each test location for measuring soil physical and geochemical properties were air dried and ground. A summary of the performed tests and corresponding protocols are presented in Table 2.2.

#### 2.4.3 Parameters Prediction for Excess Shear Stress Equation

The erodibility parameter  $\tau_c$  and  $k_d$  were calculated by the Blaisdell et al. (1981) approach with modification as discussed by Mahalder et al. (2018) and presented in Appendix B. These two parameters were correlated utilizing the 128 soil samples, and compared with Simon et al. (2011) developed equations to validate the existing model for this dataset. Tested soils were also classified based on the erodibility index described by Hanson and Simon (2001).

Table 2.2. Soil tests and method standards used to characterize soil properties.

<b>Test</b>	<b>Measurement Method</b>
Liquid Limit	BS1377
Plastic Limit	ASTM D4318
Median Grain Size ( $D_{50}$ )	ASTM D422
Specific Gravity of soil	ASTM D854
Dispersion Ratio	ASTM D4221
Specific Surface	Modified European Spot Method (Santamarina et al., 2002)
Organic Content	LOI method (USDA 2011)
Saturated paste preparation	USDA 2011
Extract from saturated paste	Centrifuging and vacuum filtration (0.45 $\mu\text{m}$ filter)
Soil pore water pH	Direct measurement from the soil extract
Pore water electric conductivity	Direct measurement from the soil extract
Cations ( $\text{Na}^+$ , $\text{K}^+$ , $\text{Ca}^{2+}$ , $\text{Mg}^{2+}$ )	IC Analysis on soil paste extract
USCS Classification	ASTM D2487

#### 2.4.4 Multicollinearity in the Dataset

Multicollinearity is the existence of near-linear relationships among the independent variables violating basic assumptions for regression analyses. It may also create inaccurate regression coefficients estimation and inflation of the standard errors of the regression coefficients, deflate the partial t-tests for the regression coefficients, compute false, nonsignificant p-values, and/or reduce model predictability (Statistical software package NCSS v.9.0 Tutorial). Working with comprehensive datasets for soil properties substantially increases the possibility of multicollinearity due to various tests measuring similar characteristics. However, in this study, multicollinearity was minimized by removing co-varying variables from the original dataset. For example, the variable DD was calculated from the measured BD and WC, which caused multicollinearity. Plasticity index (PI) is calculated from liquid limit (LL) and plastic limit (PL), so this variable obviously showed strong collinearity. Porosity ( $n$ ) of soil is calculated from the void ratio ( $e$ ), which showed strong collinearity as well. The percent sand, silt, and clay content was calculated from the grain size distribution curve; therefore, these variables have a significant linear relationship. Hence, the variable selection process using regression may encounter division by zero or by a very small quantity causing biased results (NCSS v.9.0 Tutorial). Thus, DD,  $e$ , PI and sand% variables were omitted during the variable selection procedure.

Multicollinearity among the independent variables was also checked by following Belsley et al. (1980) criteria in NCSS, and a cluster analysis (as described below) was used to assess selected variables within data clusters. Using statistical software package SPSS v.23.0, the variable inflation factor (VIF) for individual variables and Durbin-Watson coefficient value for each model were calculated for each data cluster. Results of these analyses showed that the VIF for each variable in each cluster was less than 10 (O'Brian, 2007), and the Durbin-Watson values were between 1.67 and 2.23. Therefore, possible multicollinearity issues for this dataset were addressed in a systematic manner.

#### 2.4.5 Cluster Analysis

A two-stage non-parametric and non-hierarchical cluster analysis (CLA) was used to identify statistically significant cluster groupings of sites based on similar soil properties and results assessed for similarity in surficial geology. CLA was performed in statistical software package SAS v.9.4 where the non-parametric clustering method “Ward” and non-hierarchical “k-means” approaches were used. The pattern of the individual observation classified into a particular cluster, based on the corresponding probability value was also validated by the two-stage CLA using both SAS v.9.4 and NCSS v.9.0. The non-hierarchical clustering method identified the misclassification of observations in any cluster and reassigned them into the appropriate cluster from individual observation probabilities.

#### 2.4.6 Statistical Model Development for Variable Selection

Multiple regression equations were developed for the entire dataset and unique site groupings from the cluster analysis as described above. Different variable selection algorithms are available for the multivariate statistical data analysis because each may generate different regression models with significant predictor variables based on data type. Four different variable selection algorithms were used for this study and the role of those algorithms was evaluated for variable selection on erodibility parameters prediction. Variable transformations were performed when necessary to convert values within similar orders of magnitude (Table 2.3).

Table 2.3. Statistical description of the measured variables for the dataset consisting of 128 soil samples among the different Tennessee physiographic provinces.

<b>Variables</b>	<b>Range</b>	<b>Min</b>	<b>Max</b>	<b>Mean</b>	<b>Std. Deviation</b>	<b>Data Transformation Technique Used</b>
Critical Shear Stress (Pa)	26.72	0.08	26.8	5.17	3.81	SQRT
$k_d$ (cm <sup>3</sup> /N-s)	23.84	0.56	24.4	3.51	4.11	SQRT
Water Content, WC (%)	24.76	17.6	42.36	29.03	5.16	Decimal
Bulk Density, BD (g/cm <sup>3</sup> )	0.60	1.52	2.12	1.88	0.11	None
Dry Density, DD (g/cm <sup>3</sup> )	0.78	0.98	1.76	1.45	0.14	None
Median Grain Size, D <sub>50</sub> (μm)	36.3	3.7	40.0	15.52	6.71	Log
Dispersion Ratio (DR)	0.48	0.15	0.63	0.36	0.10	None
Specific Gravity (SG)	0.21	2.49	2.7	2.62	0.04	None
Cohesion, CC (psi)	14.42	1.24	15.65	5.12	2.78	Log
Strain, Str (%)	20.45	2.45	22.9	10.82	4.48	Decimal
Void Ratio (e)	1.11	0.50	1.61	0.82	0.18	None
Porosity (n)	0.38	0.24	0.61	0.44	0.06	None
Liquid Limit (LL)	18.9	23.6	42.5	31.66	4.15	Decimal
Plastic Limit (PL)	13.89	16.76	30.65	22.74	3.21	Decimal
Plasticity Index (PI)	17.23	3.44	20.66	8.93	3.63	Decimal
Organic Content (OC) (%)	7.17	1.48	8.65	3.28	1.55	Decimal
Sodium Adsorption Ratio (SAR)	25.19	0.32	25.51	4.67	5.21	SQRT
Potassium Intensity Factor (KIF)	1.23	0.02	1.25	0.19	0.2	None
Passing # 200 sieve (%)	39.0	60.0	99.0	89.9	8.35	Decimal
Geometric Standard Deviation ( $\sigma_g$ )	25.25	2.04	27.29	10.46	6.16	Log
Sand (%)	48.0	2.0	50.0	12.48	9.83	Decimal
Silt (%)	50.0	30.0	80.0	63.37	11.41	Decimal
Clay (%)	33.0	10.0	43.0	24.15	7.48	Decimal
pH	3.29	4.83	8.12	7.0	0.64	Log
Specific Surface, SS (m <sup>2</sup> /g)	141.29	12.84	154.14	50.35	22.82	Log
T (°C)	17.7	16.8	34.5	26.63	4.02	Log
Clay Activity (CA)	0.41	0.20	0.61	0.37	0.07	None
Electric Conductivity, EC (μS/cm)	684.93	7.07	692.0	263.42	187.17	Log
Consistency (Con)	3.95	-2.07	1.88	0.15	0.63	None

Transformations aided in reducing the dataset skewness. In order to identify the dominant independent variables related to erodibility, a systematic approach to the statistical analyses followed these steps:

- 1) all possible regression (APR) analyses were performed for significant variables selection due to the large number of independent variables; the possible number of outliers in the dataset were also identified using NCSS v.9.0 for decision making prior to conducting the variable selection analyses;
- 2) the variables found to be significant from the APR were compared with the McHenry algorithm (MHA) variable selection technique, the least angle regression (LAR) (Efron et al., 2004) analysis, and stepwise multiple linear regression (STR) method; the LAR analysis was conducted using a Matlab routine developed by Chen (2012), and the APR, MHA and STR analyses were conducted using NCSS v.9.0;
- 3) the selected variables found to be significant using these variable selection procedures were used for a multiple regression equation for developing a prediction model for  $\tau_c$  prediction;
- 4) the corresponding p-value of the individual variables were examined from the analysis; the variable(s) with coefficient p-value greater than 0.05 were omitted from the model; depending on the resulting change in the  $R^2$  value, the predictive model was either kept intact or modified by excluding the non-significant variable(s); and
- 5) the residual distribution patterns were checked for normality in NCSS v.9.0; VIF and Durbin-Watson values were also checked using SPSS v.23.0.

PRESS statistics were computed for each regression model developed using SPSS v.23.0. PRESS statistic, or predicted residual sum of squares is the sum of the squared deleted residuals, which is a cross-validation technique approach for the performance analysis of a predictive model.

## 2.5 Results

### 2.5.1 Soil Properties

As classified by the USDA (Foth, 1990), the soil samples consisted of a variety of soil textures including: loam, clay-loam, silty-clay, silty-loam and silty-clay-loam, but were predominantly silty-loam and silty-clay-loam. Atterberg limit tests indicated the presence of cohesiveness in the soil samples since the PI values were between 3.40 and 20.70 (Table 2.3). The LL and PL values were between 23.6% and 42.5%, and 16.80% and 30.70%, respectively. Some of the soil samples had a low PI, even though the material met the criteria for cohesive soils (minimum clay content of 5%-10% by weight) as defined by Raudkivi (1990) and Mitchell and Soga (2005). Soil BD ranged from 1.52 g cm<sup>-3</sup> to 2.12 g cm<sup>-3</sup> and D<sub>50</sub> was between 3.7 μm and 40 μm. The size geometric standard deviation ( $\sigma_g$ ) of the tested soils ranged between 2.04 and 27.29 with a mean of 10.46, indicating widely varying grain sizes. The range of soil cohesion (CC) was between 8.55 kPa and 107.90 kPa, and organic content (OC) ranged between 1.48% and 8.65%. The soil dispersion ratio (DR) ranged from 0.15 to 0.63. The dispersive behavior of clay was classified and identified according to the US Army Corps of Engineers (USACE, 1970) classification criteria as presented in Table 2.4. The majority of the soil samples were either non-dispersive or in the intermediate range. Results also suggested the studied soils

Table 2.4. Degree of dispersion for the tested soils according to the US Army Corps of Engineers (USACE, 1970) classification criteria.

Percent Dispersion	Count	Degree of Dispersion
< 35%	66	Non-dispersive
35-50%	51	Intermediate
> 50%	11	Dispersive

were mostly inactive (Skempton, 1953) based on a maximum CA value of 0.61 and specific surface (SS) values of  $12.8 \text{ m}^2 \text{ g}^{-1}$  to  $154.1 \text{ m}^2 \text{ g}^{-1}$ . Some of the tested soils (43 observations) had a negative consistency value, which was thought to be influenced by the presence of organic matter and/or possibly precipitation events before conducting the field tests.

The physiochemical properties of the soil samples in bank failure locations were not found statistically different from the in-situ bank material ( $p = 0.58$ ). However, erodibility parameters  $\tau_c$  and  $k_d$  were found different for the failed bank materials compared to the in-situ bank material ( $p = 0.002, 0.030$ , respectively).

The  $\tau_c$  and  $k_d$  values were calculated by the methods developed in the Mahalder et al. 2018b (Appendix A), in which values for  $\tau_c$  ranged from 0.08 Pa to 26.82 Pa with a mean of 5.17 Pa and standard deviation of 3.81 Pa (Table 2.4). The  $k_d$  ranged between 0.56 and  $24.4 \text{ cm}^3 \text{ N}^{-1} \text{ s}^{-1}$ , with a mean of  $3.51 \text{ cm}^3 \text{ N}^{-1} \text{ s}^{-1}$  and standard deviation of 4.11. The  $\tau_c$  and  $k_d$  values were strongly correlated as shown in Figure 2.3 ( $R^2 = 0.78$ ;  $p < 0.001$ ). The erodibility index of the tested soil was also plotted on the same figure. Results showed the tested soils were very erodible to erodible based on the Hanson and Simon (2001) classification scheme.

### 2.5.2 Properties of the Cluster Groups

In order to observe whether soil properties were distinct among Tennessee physiographic providences, CLA was performed using complete dataset (Table 2.3). Four cluster groups were significantly identified using CLA (Figure 2.4). It is important to note that these clusters highlight the important association with different surficial geologies among the physiographic provinces. In Cluster 1, 32 observations were found and a majority of the observations (25) were from the Valley and Ridge physiographic province. Cluster 2 was formed with 30 observations from two border counties (Dyer and Obion) of the West Tennessee Plain, subregion of Coastal Plain (Table 2.1). In Cluster 3, observations were assigned from six counties (Carroll, Crockett, Haywood, Obion, Shelby, and Town) of West Tennessee in the Coastal Plain physiographic province with 49 observations. The remaining 17 observations were classified into Cluster 4 from the West Highland Rim and Central Basin physiographic provinces. The results of the CLA indicated that  $\tau_c$  was dependent on a comprehensive set of soil physical and geochemical properties that appear to be inherently related to the associated surficial geology (Table 2.1). Acceptability of the cluster data was verified by applying MANOVA tests using SPSS v.23.0. Results showed the significance level of Pillai's Trace value as 0.0001, so the groups were significantly different ( $p < 0.05$ ).

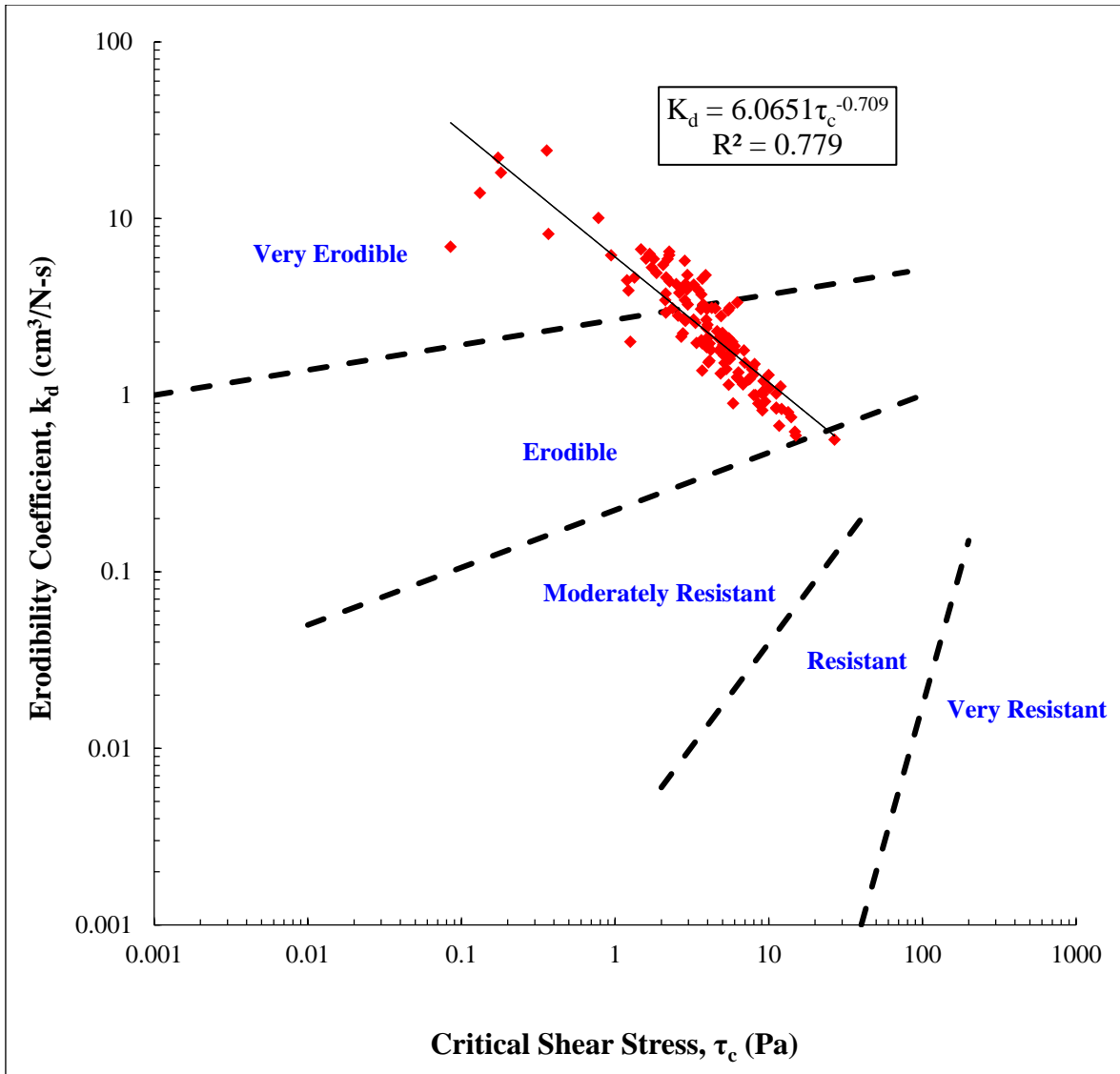


Figure 2.3. Relationship between critical shear stress and erodibility coefficient with erosion index (after Hanson and Simon, 2001).

### 2.5.3 Statistical Correlation and Model Variable Selection

Development of statistical models for predicting  $\tau_c$  as a function of significant independent variables was completed using APR, MHA, LAR, and STR methods. These analyses were performed on the complete transformed dataset (Table 2.3), and separately on the four clusters identified in Figure 2.4 and as described above. The normality and independence assumptions were met for each significant regression variable from visual assessments of residual plots.

Predictive statistical models as presented in Table 2.5 showed statistically significant selected variables using the above mentioned methods and corresponding regression p-values. Changes in  $R^2$  value and adjusted  $R^2$  value were also examined by omitting variables with coefficient-p value  $> 0.05$  in order to obtain the best-fit model. As stated earlier, four different statistical techniques were used for significant variable selection. Based on PRESS statistics

value and nature of the dataset, predictive statistical model using LAR method was adopted for variable selection for the entire dataset of 128 observations. Among these suite of regression models, three variables: CC, DR, and SAR were common (Table 2.5). However, in the best predictive multiple regression model, seven variables: BD, CC, DR, OC, SAR and  $\sigma_g$  were found statistically significant (adjusted  $R^2 = 0.29$ ;  $p < 0.001$ ):

$$\tau_c = -3.798 + 1.784 * BD + 1.082 * CC + 1.45 * DR + 12.292 * OC + 0.18 * SAR + 0.53 * \sigma_g \quad (2.12)$$

Variables selected in the model showed high significance (coefficient  $p < 0.05$ ) except  $\sigma_g$  (coefficient  $p = 0.078$ ). Though, the inclusion of  $\sigma_g$  increased the correlation of the model. The plot of the predicted versus observed  $\tau_c$  and the residuals plot showed variation from the normal probability distribution patterns. Statistical data analysis also showed models using the entire

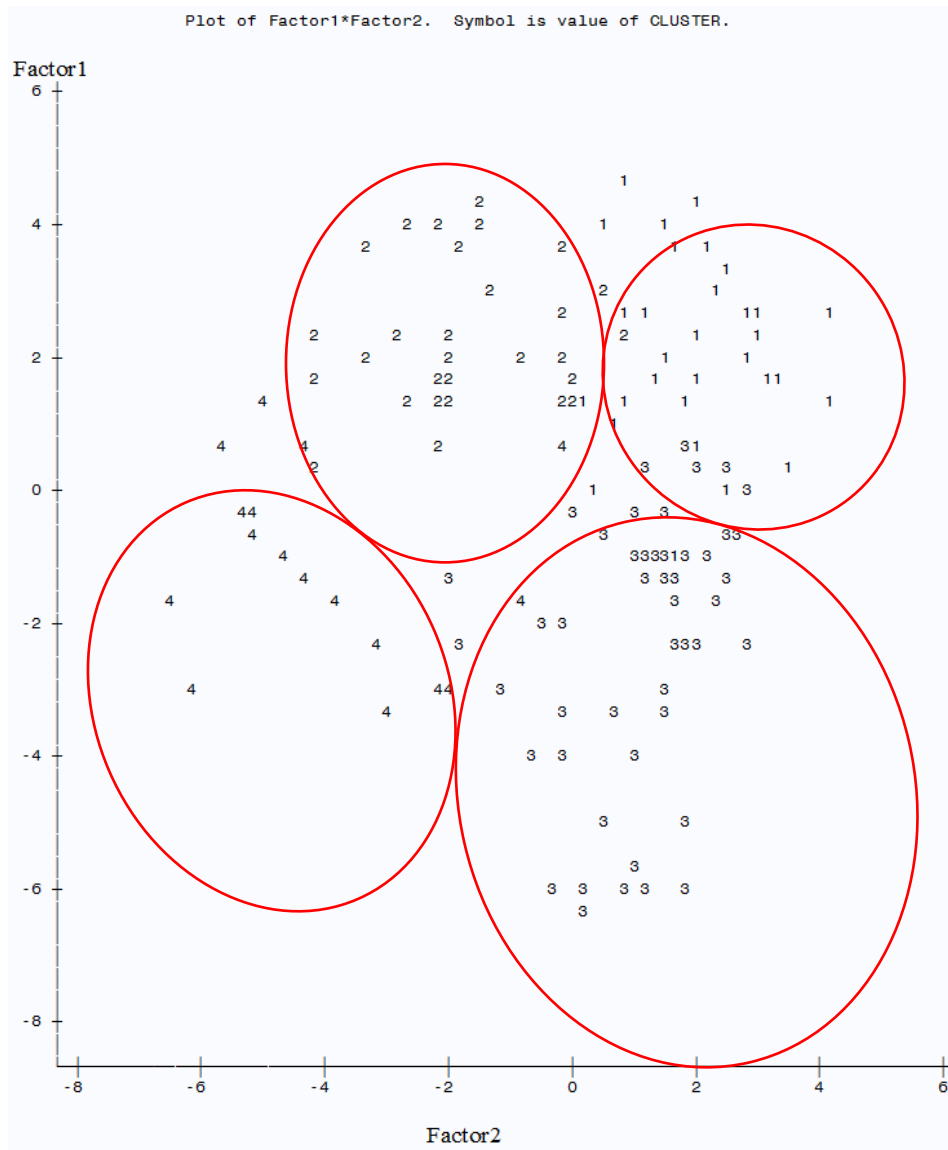


Figure 2.4. Four cluster groups using the “Ward” method and non-hierarchical “k-means” approach based on soil properties including critical shear stress.

Table 2.5. Multiple regression models for prediction of critical shear stress ( $\tau_c$ ) based on soil properties. Models included all possible regression (APR), McHenry algorithm (MHA), least angle regression (LAR), and stepwise multiple linear regression (STR).  $R^2$ , p-value, and PRESS statistics are shown for each model.

Data type	Predicting Model	Method	N	$R^2$	p-value	PRESS
All data	$\tau_c = -4.853 + 2.519 * BD + 1.171 * CC + 1.183 * DR + 20.242 * OC + 0.189 * SAR$	APR	128	0.21	0.0001	57.38
	$\tau_c = -4.20 + 1.304 * CC - 0.733 * D_{50} + 2.13 * DR + 0.154 * SAR + 1.06 * \sigma_g + 2.424 * T + 2.72 * WC$	MHA	128	0.30	0.0001	56.06
	$\tau_c = -3.798 + 1.784 * BD + 1.082 * CC + 1.45 * DR + 12.292 * OC + 0.18 * SAR + 0.53 * \sigma_g$	LAR	128	0.29	0.0001	56.38
	$\tau_c = -2.533 + 1.063 * CC - 0.619 * D_{50} + 2.06 * DR + 0.15 * SAR + 0.93 * \sigma_g + 1.93 * T$	STR	128	0.28	0.0001	57.12
Cluster 1	$\tau_c = -1.927 + 1.348 * CC + 1.921 * Clay - 0.568 * Con + 2.032 * DR - 1.926 * KIF + 5.151 * LL + 0.562 * \sigma_g$	APR	32	0.72	0.0001	5.44
	$\tau_c = -1.927 + 1.348 * CC + 1.921 * Clay - 0.568 * Con + 2.032 * DR - 1.926 * KIF + 5.151 * LL + 0.562 * \sigma_g$	MHA	32	0.72	0.0001	5.44
	$\tau_c = -0.97 + 0.98 * CC + 2.77 * Clay + 2.06 * DR - 1.956 * KIF + 4.146 * WC$	LAR	32	0.61	0.0001	6.16
	$\tau_c = -1.916 + 1.334 * CC + 2.267 * Clay + 1.79 * DR - 1.78 * KIF + 0.265 * SAR + 0.573 * \sigma_g + 3.93 * WC$	STR	32	0.67	0.0001	6.17
Cluster 2	$\tau_c = 3.94 + 2.76 * CC - 2.335 * D_{50} - 2.72 * Pass200 + 0.24 * SAR - 1.49 * SS + 6.13 * Str + 8.1 * WC$	APR	30	0.45	0.0033	11.30
	$\tau_c = 3.94 + 2.76 * CC - 2.335 * D_{50} - 2.72 * Pass200 + 0.24 * SAR - 1.49 * SS + 6.13 * Str + 8.1 * WC$	MHA	30	0.45	0.0033	11.30
	$\tau_c = 6.644 + 2.492 * CC - 1.70 * D_{50} + 1.362 * DR - 4.12 * Pass200 - 6.06 * pH + 0.343 * SAR + 10.48 * WC$	LAR	30	0.44	0.0045	11.63
	$\tau_c = 5.352 + 1.676 * CC - 5.682 * pH$	STR	30	0.42	0.0002	10.00
Cluster 3	$\tau_c = -33.802 + 14.161 * BD + 5.643 * CA - 18.84 * LL + 69.1 * OC + 8.545 * Pass200 - 3.49 * pH + 21.0 * WC$	APR	49	0.54	0.0001	19.12
	$\tau_c = -27.63 + 10.96 * BD - 0.812 * Con + 1.13 * DR - 0.433 * EC + 49.33 * OC + 7.97 * Pass200 + 0.605 * SS$	MHA	49	0.48	0.0001	22.86
	$\tau_c = -10.42 + 5.035 * BD + 0.261 * CC - 1.272 * D_{50} + 1.86 * DR + 1.06 * KIF + 2.614 * Pass200 + 0.665 * SS$	LAR	49	0.38	0.0002	26.09
	$\tau_c = -30.03 + 12.29 * BD - 0.769 * Con + 57.516 * OC + 8.042 * Pass200$	STR	49	0.46	0.0001	20.65
Cluster 4	$\tau_c = -7.698 + 14.161 * CA - 12.678 * n - 21.39 * OC + 9.38 * Pass200 - 0.548 * SAR + 12.90 * WC$	APR	17	0.80	0.0005	2.32
	$\tau_c = 25.318 - 0.374 * DR + 2.316 * KIF + 44.394 * LL - 59.53 * PL - 0.68 * SAR - 9.32 * SG + 10.03 * Str$	MHA	17	0.65	0.0117	5.95
	$\tau_c = 8.77 + 1.223 * CC + 8.8 * DR + 4.3 * EC + 3.955 * KIF - 9.61 * n + 13.99 * Pass200 - 20.466 * T$	LAR	17	0.74	0.0032	6.07
	$\tau_c = 0.904 + 4.56 * DR$	STR	17	0.18	0.0489	7.06

$\tau_{c(actual)} = (\tau_c)^2$ , Critical Shear Stress; BD = Bulk Density ( $\text{g}/\text{cm}^3$ ); CC =  $\log(\text{CC}_{actual})$ , Cohesion; DR = Dispersion Ratio; OC = Organic Content;  $\sigma_g$  = Geometric Standard Deviation;  $D_{50} = \log(D_{50(actual)})$ , Sediment Diameter ( $\mu\text{m}$ ); SAR = SQRT ( $\text{SAR}_{actual}$ ), Sodium Adsorption Ratio; T =  $\log(T)$ , Water Temperature ( $^{\circ}\text{C}$ ); WC = Water Content; Clay = Clay Content in the soil; Con = Soil Consistency (PI/Clay Content); KIF = Potassium Intensity Factor; LL = Liquid Limit; Pass200 = Sediment Passing 200 Sieve; SS =  $\log(\text{SS}_{actual})$ , Specific Surface ( $\text{m}^2/\text{g}$ ); Str = Strain Rate from UC Test; CA = Clay Activity; n = Porosity; PL = Plastic Limit; SG = Specific Gravity of Soil.

dataset differed from the models when developed individually per data from each cluster representing different physiographic provinces (Figure 2.4). Those models are described below.

Of the 32 observations classified into Cluster 1, the soil samples consisted mostly of non-dispersive inactive clay materials. The majority of the observations were from the Valley and Ridge physiographic province consisting of geological formations comprised of shales, limestone, and sandstone (Table 2.1). Though seven observations were also grouped into Cluster 1 from western Tennessee with calcareous type soils composed of fine siliceous loam with the presence of lime concretions. Calcium was thought to be the key geochemical property governing the statistical similarity with observations from the Valley and Ridge physiographic province. APR, MHA and STR methods identified seven significant variables for predicting  $\tau_c$ . APR and MHA methods predicted models were found to have the best correlation (adjusted  $R^2 = 0.72$ ; Table 2.5):

$$\begin{aligned} \tau_c = & -1.927 + 1.348 * CC + 1.921 * Clay - 0.568 * Con + 2.032 * DR \\ & - 1.926 * KIF + 5.151 * LL + 0.562 * \sigma_g \end{aligned} \quad (2.13)$$

The inclusion of  $\sigma_g$  increased the correlation most significantly though the coefficient  $p = 0.083$ . DR was identified the second most significant variable.

In Cluster 2, 30 observations were grouped from two counties (Dyer and Obion County) from the West Tennessee Plain, a sub-region of the Coastal Plains physiographic province. Grain size distribution curve for these soils showed sand, silt, and clay in the soil formation with no gravel. This cluster group showed a higher number of outliers (30% observations) compared to other clusters. The LAR model resulted in the best-fit model after variable selection with adjusted  $R^2 = 0.44$  (Table 2.5):

$$\begin{aligned} \tau_c = & 6.644 + 2.492 * CC - 1.70 * D_{50} + 1.362 * DR - 4.12 * Pass200 \\ & - 6.06 * pH + 0.343 * SAR + 10.48 * WC \end{aligned} \quad (2.14)$$

WC explained most variance in this dataset as it significantly affected the  $R^2$  value. Pass200 and pH were the second and third most significant variables, respectively, to predict  $\tau_c$ .

Within Cluster 3, 49 observations were from the West Tennessee Plain and the West Tennessee Uplands (sub-regions of the Coastal Plain physiographic province). Similar to Cluster 2, in this cluster no gravel material was found from the grain size distribution curves. The overall soil characteristics were found as laminated sands and clays, with well-marked beds of bluff loams with beds of clay with poor drainage. In this cluster, three observations were identified as outliers due to the presence of dispersive clay. APR, MHA and LAR methods identified seven significant variables for the model. Based on the coefficient  $p$ -value of individual variables and significance of the correlation, APR method generated the best-fit model with (adjusted  $R^2 = 0.55$ ;  $p < 0.001$ ) (Table 2.5):

$$\begin{aligned} \tau_c = & -33.802 + 14.161 * BD + 5.643 * CA - 18.84 * LL + 69.1 * OC + \\ & 8.545 * Pass200 - 3.49 * pH + 21.0 * WC \end{aligned} \quad (2.15)$$

In this model, the Pass200 variable explained most variance in this dataset as the inclusion of this variable increased the correlation and WC was the second most significant variable.

Within Cluster 4, 17 observations were from Middle Tennessee covering the Western Highland Rim and the Central Basin physiographic provinces. The geologic rock at study sites in

this cluster included limestone, siltstone, sandstone and sandy shales, and interstratified with layers of chert. In this region, soil samples consisted of a higher percentage of coarse silt (wider grain size distribution curve in the silt range was observed) compared to other clusters and the average PI value was less than the other three clusters. In Cluster 4, the APR variable selection method generated the best-fit model for  $\tau_c$  (adjusted  $R^2 = 0.80$ ; Table 2.5):

$$\tau_c = -7.698 + 14.61 * CA - 12.678 * n - 21.39 * OC + 9.38 * Pass200 - 0.548 * SAR + 12.90 * WC \quad (2.16)$$

The variable OC with coefficient  $p = 0.083$  significantly increased the model's correlation. WC and CA were the two other most significant variables.

PRESS statistic values for each predicted models using different variable selection algorithms are also presented in Table 2.5. It is expected that the PRESS statistics would be lower for a better predictive model, which was found analogous with the reported best predictive models as developed per multivariate regression analyses. However, in Cluster 2, the PRESS statistic value for the selected predictive model was found to be slightly higher compared to other predictive models.

Using these four predictive models, unique for each cluster, the correlation between measured  $\tau_c$  and predicted  $\tau_c$  for different clusters are presented in Figure 2.5. In summary, 16 soil physiochemical parameters were identified as significant among the developed predictive models for  $\tau_c$ . Four variable selection algorithms were used in this study to identify significant soil physiochemical parameters to predict  $\tau_c$  in the four cluster groups. However, based on the data characteristics, one algorithm was usually found to be the best predictive model. In this study, APR, MHA, and LAR predicted 3 to 5 common variables in the predictive models in each cluster group with similar correlation and adjusted  $R^2$  values (Table 2.5). Statistically, it was interesting to note that STR showed overall lower  $R^2$  and adjusted  $R^2$  values and different sets of variables compared to other three methods. Differences were observed in coefficient  $p$ -values for individual variables among the dominant models (Equations 2.13-2.16).

The coefficient  $p$ -values for individual variables and the correlation sign to  $\tau_c$  among the predictive models are presented in Table 2.6. WC and Pass200 were selected as a significant model variable among three clusters, and CC, DR, LL, SAR, and OC were selected for at least two of the four cluster models. In this study, no analyses were completed for  $k_d$  prediction rather, empirical equations were developed among the four clusters using the study's jet test data (Table 2.7). Highly significant relationships were developed for all clusters ( $p < 0.001$ ).

## 2.6 Discussion

The importance of developing predictive relationships for the erodibility parameters ( $k_d$  and  $\tau_c$ ) was highlighted in the background section summarizing the different empirical models developed from numerous published studies. Existing models for  $\tau_c$ , differed widely for various reasons, which included the set of physical-geochemical properties selected as independent variables. Few field studies used a more comprehensive variable dataset of soil properties, and the studies were generally conducted in a single geologic region. The primary interest of this study was to provide better insight into which physical-geochemical properties dominantly control soil erodibility, and knowing that these properties are derived from the parent soils material. The state of Tennessee with its many physiographic provinces and diverse geology

provided a unique US region to examine the differences in the erodibility parameters among different surficial geologies.

With an in situ testing apparatus, the mini-jet, results from this study provided evidence that different governing physical-geochemical soil properties dominate among different physiographic provinces. The key finding from our study suggests that a single universal equation for predicting erodibility parameters is highly unlikely, and predictive relationships need to be developed per province. A physiographic province consists of a distinct surficial

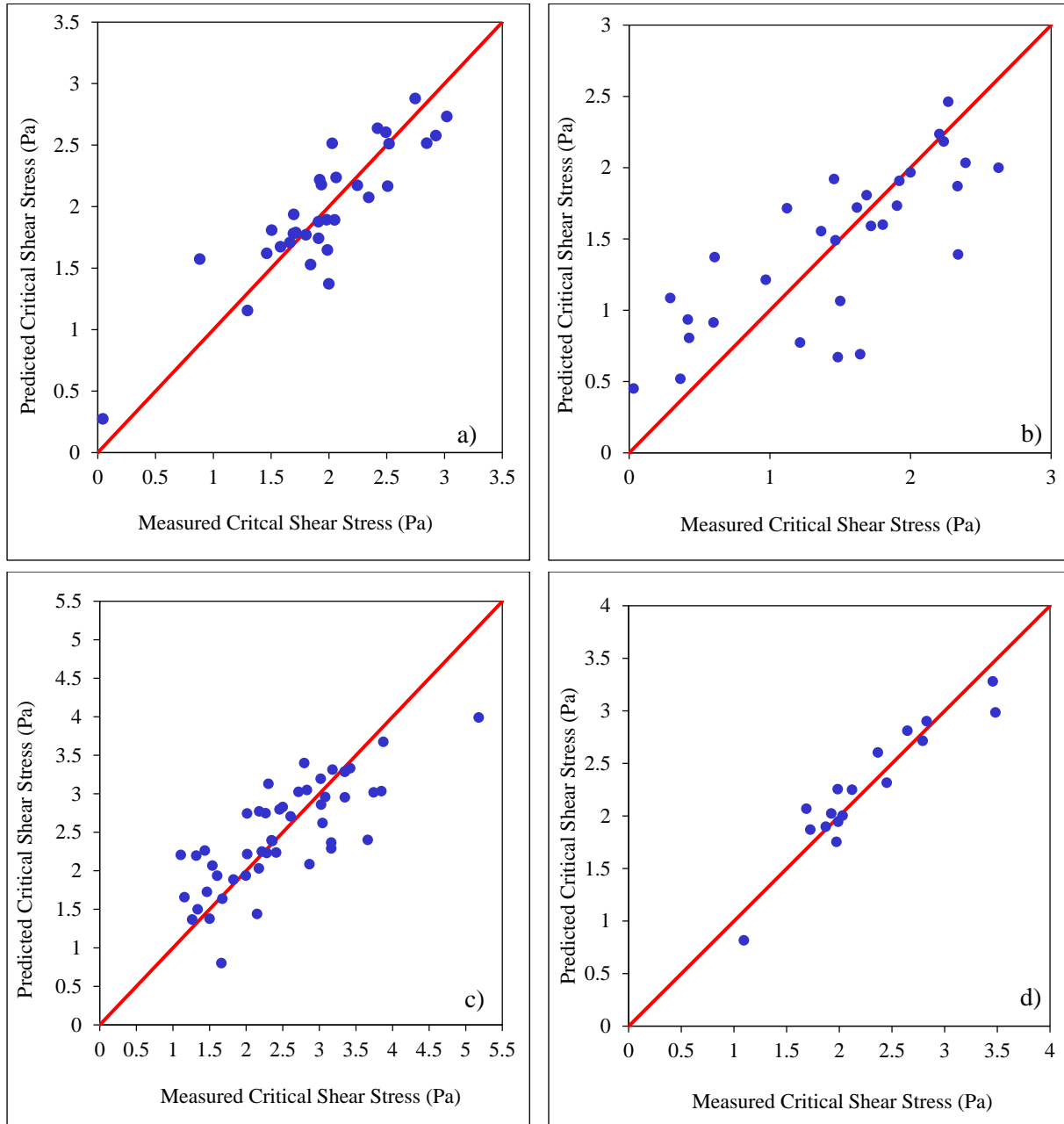


Figure 2.5. Measured and predicted critical shear stress (a) Cluster 1, (b) Cluster 2, (c) Cluster 3, and (d) Cluster 4 (using transformed data).

Table 2.6. Coefficient p-values for individual variables and corresponding correlation sign among the predictive models for each cluster representing a unique physiographic province and surficial geology.

<b>Name of Variables</b>	<b>Cluster 1 (Eq. 2.13)</b>	<b>Cluster 2 (Eq. 2.14)</b>	<b>Cluster 3 (Eq. 2.15)</b>	<b>Cluster 4 (Eq. 2.16)</b>
Passing # 200 sieve (Pass200)	-	(-) 0.215	(+) < 0.001	(+) < 0.001
Water Content (WC)	-	(+) 0.014	(+) < 0.001	(+) < 0.001
Cohesion (CC)	(+) < 0.001	(+) 0.026	-	-
Dispersion Ratio (DR)	(+) 0.014	(+) 0.025	-	-
Liquid Limit (LL)	(+) 0.008	-	(-) 0.003	-
pH	-	(-) 0.100	(-) 0.083	-
Sodium Adsorption Ratio (SAR)	-	(+) 0.010	-	(-) < 0.001
Clay Activity (CA)	-	-	(+) 0.026	(+) < 0.001
Organic Content (OC)	-	-	(+) < 0.001	(-) 0.083
Consistency (Con)	(-) < 0.001	-	-	-
Potassium Intensity Factor (KIF)	(-) < 0.001	-	-	-
Clay Content (Clay)	(+) 0.043	-	-	-
Geometric Standard Deviation ( $\sigma_g$ )	(+) 0.083	-	-	-
Bulk Density (BD)	-	-	(+) < 0.001	-
Median Grain Size ( $D_{50}$ )	-	(-) 0.018	-	-
Porosity (n)	-	-	-	(-) < 0.001

+/- Sign indicates the correlation to the  $\tau_c$

Table 2.7. Predictive models in each cluster for erodibility coefficient ( $k_d$ ) as a function of critical shear stress ( $\tau_c$ ) for the entire dataset, and individually for the four identified data clusters.

<b>Cluster</b>	<b>Empirical Equation</b>	<b>R<sup>2</sup> value</b>	<b>Model p-value</b>
Entire Data	$k_d = 6.065\tau_c^{-0.709}$	0.78	< 0.0001
1	$k_d = 8.708\tau_c^{-1.009}$	0.79	< 0.0001
2	$k_d = 5.561\tau_c^{-0.538}$	0.70	< 0.0001
3	$k_d = 7.822\tau_c^{-0.876}$	0.87	< 0.0001
4	$k_d = 9.524\tau_c^{-0.899}$	0.73	< 0.0001

geology, and climate and vegetation conditions that control soil genesis, and the existing physical-geochemical properties. The possible effect of geology on the empirical erodibility coefficient prediction models was also reported by Clark and Wynn (2007), but was not

researched among different physiographic provinces. Therefore, it was necessary to assess a comprehensive set of the soil properties because of the possibility of varying controlling properties per province. In addition, our approach to predictive model development utilized four separate logistic regression techniques to find the best-fit model where we found that statistical method did influence the results. Observing the differences in predictive models for  $\tau_c$ , our study compared a predictive model developed from the entire dataset to that of four statistically significant site groups that correlated with unique surficial geologies.

As reported earlier, in the four clusters, different soil physiochemical properties were controlling the  $\tau_c$  prediction equation consisting similar geology. In Cluster 1, as reported in the results section, seven observations were grouped from western Tennessee containing lime concretions. Miller (1991) reported that lime concretions in this area were not the carbonate rather a silicate precipitate or an infilling of silt, which deposited later. Soil horizons in Cluster 1 from the SSURGO soil database were identified as Hamlin (Hb), Dekoven (De), Etowah loam (Eo), Newark (Ne), Sequatchie loam (Sc), and Steadman (Su) from silty loam parent material originated from limestone, sandstone, and calcareous shale. In this cluster, since sand percentage was higher compared to other three clusters, dispersive nature of the soil with clay content influenced the  $\tau_c$  prediction equation (Equation 2.12).

Cluster 2 and Cluster 3 were formed from the same physiographic province. Soil horizons: Calloway (Ca), Collins (Cl), Waverly silt (Ws), and Waverly (Wv) were found in Cluster 2 and parent material type was silty alluvium. In Cluster 3, silty alluvium and loess parent material were present with Adler (Ad), Ca, Wolftever (Wo), and Wv soil horizons. Though similar in texture, material of Cluster 2 was generally softer and more friable than the underlying deposits, commonly breaking to fine crumbs between the fingers compared to Cluster 3 (William and Diehl, 1993). They also reported that the upper 5-20 feet in the region of Cluster 2 were deposited in the past few hundred years compared to the area of Cluster 3, which was formed during Quaternary period. William and Diehl (1993) also reported that the presence of water table influenced the cohesiveness of the soil. In this study it was identified that  $\tau_c$  values were lower in Cluster 2 compared to Cluster 3, which supported the findings of William and Diehl (1993) study. The presence of outliers in Cluster 2 also supported the hypothesis that the local soil deposition pattern and age of deposition influenced the formation of two distinct clusters from the same physiographic province.

In Cluster 4, soil horizons were found as Arrington (Ar), Atkins (At), Amanda (AmD2) from silty alluvium material originating from limestone and siltstone. In this cluster, since coarse silt with higher  $\sigma_g$  was observed the presence of OC and WC in the soil significantly affected the cohesion, consequently the  $\tau_c$  values (Equation 2.16). These findings supported the hypothesis that the clusters were formed based on geological formation, rock type, and the characteristics of parent material.

### 2.6.1 Correlation Pattern of Significant Variables

Six soil physiochemical parameters were identified as statistically significant to predicting  $\tau_c$  when using the entire dataset among four physiographic provinces (Equation 2.12; adjusted  $R^2 = 0.29$ ;  $p < 0.001$ ); included: BD, CC, DR, OC, SAR, and  $\sigma_g$ . All the significant variables showed a positive correlation with  $\tau_c$  and the adjusted  $R^2$  value was lower than individual predictive models for data groups clustered by physiographic province (Table 2.5). It is also important to note that the PRESS statistics values were much higher for the models developed with the

complete dataset compared to the clustered datasets. Therefore, this regression model with the complete dataset was considered to have a higher level of uncertainty comparatively with the models based on clustered datasets that aligned with similar geological and soil properties (Figure 2.4).

Statistical analyses in this study showed that Pass200 and WC (Table 2.6) were the most significant variables among the cluster groups to predict  $\tau_c$ , consistent with other findings (Hanson and Robinson, 1993; Allen et al., 1999; Briaud et al., 1999; van Ledden et al., 2004; Thoman and Niezgod, 2008). Briaud et al. (1999) reported that the percentage Passing #200 sieve has a positive correlation with  $\tau_c$ , which was found to be consistent with the findings in this study for Clusters 3 and 4 (Equations 2.15 and 2.16). However, in Cluster 2, a negative correlation with  $\tau_c$  was observed (Equation 2.14). The behavior of clay minerals likely affected the characteristics of the cohesive sediments; hence, a detailed clay mineralogical analysis would provide some insight to these results.

WC directly affects the mechanical properties of clay (Gillott, 1987; van Ledden et al., 2004; Grabowski et al., 2011) as well as the plastic deformation. Therefore, a positive correlation with  $\tau_c$  (Equations 2.14, 2.15 and 2.16) was expected, which is supported by several other researchers (Hanson and Robinson, 1993; van Ledden et al., 2004; Thoman and Niezgod, 2008). However, Allen et al. (1999), and Wynn and Mostaghimi (2006) reported a negative correlation between WC to  $\tau_c$  and reported that for non-plastic soils, WC significantly affect the erosion behavior. The inconsistency could be related to the presence of organic matter and root systems that significantly enhanced the stability of those studied soils and could have altered the behavior of granular material to resemble that of cohesive soil when water coats the granular particles.

The second most significant set of variables was found to be BD, CA, CC, DR, LL, OC, pH and SAR (Table 2.6). However, BD and CC were interrelated and these variables showed a positive correlation with  $\tau_c$  for the complete dataset and in the cluster groupings. Previous researchers have reported that soil erosion rates decreased with increasing BD (Hanson and Robinson, 1993; Allen et al., 1999; Wynn, 2004, Wynn and Mostaghimi, 2006 and Grabowski et al., 2011). Therefore, it is expected that an increase in BD or CC will significantly increase the  $\tau_c$  of the tested soils. In this study, results showed a positive correlation between DR and  $\tau_c$  (Equations 2.13 and 2.14), which was supported by other study results. Thoman and Niezgod (2008) found a similar relationship between DR and  $\tau_c$  in their study, and the tested soils of the study were also non-dispersive and unsaturated. Shaikh et al. (1988) and Lim (2006) reported similar findings though they did not propose any direct correlation with  $\tau_c$ . The positive correlation between DR and  $\tau_c$  identified from this study is also supported by the results as reported by Smerdon and Beasley (1959) and Lyle and Smerdon (1965).

In this study, the tested clay was found to be inactive, so, clay content dominated the ratio (CA = PI/clay content), which is used to define the clay activity for the studied soils (Skempton, 1953). Therefore, the increase in percent clay and the decrease of CA were found to be analogous for a specific clay type. Positive correlations between  $\tau_c$  and these two parameters (Clay and CA) were identified from this study (Equations 2.13, 2.15 and 2.16). The increase in clay content for these soils (since the tested soil was inactive) increased the probability that the clay would be more inactive. In addition, experimental results suggest that an increase in clay content increases the erosion threshold (increase in  $\tau_c$ ) due to the combination of hydrodynamic smoothing, clay/sand adhesion and clay cohesion (Lick et al., 2004; Grabowski et al., 2011). The

positive correlation between  $\tau_c$  and clay content is also supported by the field investigation of erosion resistance for different clay minerals (Dickhudt et al., 2011).

Inverse relationships between  $\tau_c$  and soil pore water pH were identified from the multiple linear regression equations for both Cluster 2 and 3 datasets (Equations 2.14 and 2.15). As the pH increases, the concentration of  $H^+$  ions decreases resulting in an increase in the double layer thickness. Consequently, a greater repulsive force was expected (Winterwerp and van Kesteren, 2004) and the  $\tau_c$  values reduced with increasing pH. The formation of surface crusting was also reported as another significant physical change on the soil surface due to increase in pH (Wischmeier and Mannering, 1969; Wynn, 2004). These negative correlations were also supported by other studies (Wynn, 2004; Wynn and Mostaghimi, 2006; Thoman and Niezgoda, 2008). However, the variable OC showed both positive and negative correlations with  $\tau_c$  (Equations 2.15 and 2.16). Depending on the nature of the organic matter and the pore water chemistry for different clay minerals, the erodibility may increase or decrease significantly (Morgan, 2005; Ravisangar et al., 2005). In this study, OC was measured by the LOI method (at 550°C) for air-dried samples, which did not differentiate between living or dead organisms, fecal material, and the extracellular organic compounds. However, for natural riverine environments, a positive correlation between OC and  $\tau_c$  has been reported as the inter-particle attraction forces are affected by the presence of organic matter in the natural soil (Gerbersdorf et al., 2007). Therefore, both positive and negative correlations may be observed, which was found in this study.

Similar to OC, both positive and negative correlations with  $\tau_c$  were observed in the predicting model (Equations 2.13 - 2.16) for LL and SAR. Clay mineralogy, the environment to which the soil is exposed, and pore water chemistry were found to be the defining parameters for  $\tau_c$  (Liou, 1970; Alizadeh, 1974; Arulanandan, 1975). A negative correlation between SAR and  $\tau_c$  were reported by Alizadeh (1974), Arulanandan (1975) and Lim (2006). According to the above-mentioned study results, as the SAR increased the repulsive forces increased, consequently influencing the erosion potential. Using different clay minerals and pore fluid conditions, Liou (1970) also reported a positive correlation between SAR and  $\tau_c$ . Therefore, identifying the mineral type and pore water chemistry are necessary to conclusively define the relationship between these two parameters. A similar explanation was also applicable to the LL, as the ratio of LL for Na-montmorillonite to Ca-montmorillonite clay is about 6 times (522% and 90% respectively; Shaikh et al., 1988). The presence of kaolinite or porcelain clay can reduce the LL value significantly. Henceforth, based on the clay mineralogy, both positive and negative correlations between LL and  $\tau_c$  were expected.

The contribution of four other variables, Con, KIF,  $D_{50}$  and  $\sigma_g$ , were found only once in the predicting models as shown in Table 2.6 (Equations 2.13 and 2.14). In the Cluster 1 dataset, the sand percentage was greater compared to the other three cluster groups. In this cluster, a positive correlation between  $\tau_c$  and  $\sigma_g$  was found, which is similar to Wynn and Mostaghimi's (2006) findings. The sediment size range is higher for a larger  $\sigma_g$  value, which reduces the possibility of interaction between hydraulic forces and larger particles as the smaller particles fill the open spaces in the soil array. Therefore, the soil entrainment rate is reduced or the  $\tau_c$  increases. The remaining three variables showed negative correlations with  $\tau_c$ . Fine natural sediment ( $D_{50} < 120 \mu m$ ) showed a significant negative correlation with  $\tau_c$  (Roberts et al., 1998), which was later supported by Thomsen and Gust (2000) in an estuarine environment. A similar result was also

found in this study. However, the  $D_{50}$  value was not found to be as significant to  $\tau_c$  prediction in cohesive soils compared to granular sediments.

Soil consistency, which is the state of the soil (liquid, semiliquid or solid), showed a negative correlation with  $\tau_c$ . Therefore, the change in state of the soil changes the BD and CC, which supported the negative correlation. A negative correlation between KIF and  $\tau_c$  was also found for the Cluster 1 data, which was in agreement with Wynn and Mostaghimi (2006). Soils with higher KIF values indicate the sources were primarily micas and illite. Therefore, soils with high KIF values were typically friable and eroded away easily. Consequently, a negative correlation was expected (Wynn and Mostaghimi, 2006).

Variable selection procedures appeared to be dependent on the properties of the dataset and the statistical procedures, influencing the resulting predictive models, which have led to the observed differences from other studies (e.g., Wynn, 2004; Wynn and Mostaghimi, 2006; Thoman and Niezgodna, 2008). This analysis also showed that the STR variable selection method was the least influential method as this method is dependent on the probability of including and omitting a variable from the model and the defining criteria (coefficient p-value; Akaike information criterion, AIC; or Bayesian information criterion, BIC). In this study, predictive models for  $\tau_c$  (Equations 2.13 - 2.16) for the four clusters showed 16 total variables as statistically significant (Table 2.6). Some variables were found positively correlated to  $\tau_c$ , and some variables were found negatively correlated. However, some variables were showed both positive and negative correlation to  $\tau_c$ .

### 2.6.2 Relationship of Critical Shear Stress with the Erodibility Coefficient

In this study, a strong inverse correlation between  $k_d$  and  $\tau_c$  was identified (Figure 2.3), which followed similar trends to those in other studies (Hanson and Simon, 2001; Wynn, 2004; Thoman and Niezgodna, 2008; Karmaker and Dutta, 2011; Simon et al., 2011; Layzell and Mandel, 2014; Daly et al., 2015a). The trend line of the entire dataset followed a power law relationship to estimate  $k_d$  as a function of  $\tau_c$  with an  $R^2$  value of 0.78 (Table 2.7). However, unique relationships were found for the four different data clusters that represent different physiographic provinces. In this study, the updated Simon et al. (2011) relationship was also evaluated to its prediction of  $k_d$  based on  $\tau_c$ . The Simon et al. (2011) model predicted lower  $k_d$  values for the same  $\tau_c$ , or a downward shift of the trend line compared to the results in this study. Therefore, use of these empirically derived models for the erodibility coefficient should be used with the understanding that geologic region in conjunction with soil geochemical properties and field testing protocols may play a significant role in their relationships. Knowing that predictive models for  $k_d$  and  $\tau_c$  may differ based on geologic and regional differences, these results can assist in improving outputs from bank erosion models that incorporate the excess shear stress equation (Equation 2.1), e.g., the BSTEM, Water Erosion Prediction Project (WEPP), Soil and Water Assessment Tool (SWAT), and Conservational Channel Evolution and Pollutant Transport Systems (CONCEPTS) (Langendoen, 2000; Abaci and Papanicolaou, 2009; NEH, 2011; Neitsch et al., 2011).

## 2.7 Conclusions

Unique relationships for the prediction of  $\tau_c$  were determined among four physiographic provinces in Tennessee associated with different surficial geologies. They were: Ridge and Valley, West Highland Rim, Central Basin, and Coastal Plain bordering the Mississippi River

Valley in the loess depositional area. Among these provinces, four data clusters were statistically identified through multivariate cluster analysis. Per regional cluster, predictive models were developed by multivariate regression utilizing a suite of 27 soil physical-geochemical properties, removing variables with multicollinearity. The final variable set of soil properties with statistically significant model coefficients included 16 variables. The key findings from this study suggests that no one soil property, or a common group of a select few properties will form a universal equation for predicting  $\tau_c$ . Controlling soil properties for  $\tau_c$  appear to be dependent on the overall soil composition based on the regional surficial geology, which determine the properties that will dominate.

Within the four physiographic regions, the soil properties WC and Pass200 were found to control  $\tau_c$  prediction among three of the four regions. The properties CC, DR, LL, SAR, and OC were also found to be dominant variables within the predictive models among the four provinces. It is interesting to observe that  $D_{50}$  is the least significant variable in predicting  $\tau_c$  in cohesive soils. The relationship between  $\tau_c$  and  $k_d$  were highly correlated, which is consistent with other studies. Within the entire dataset  $\tau_c$  ranged from 0.08 to 26.82 Pa with a mean of 5.17 Pa, and  $k_d$  ranged from 0.56 to 24.4  $\text{cm}^3 \text{N}^{-1} \text{s}^{-1}$  with a mean of 3.51  $\text{cm}^3 \text{N}^{-1} \text{s}^{-1}$ .

Overall, findings from this study identified dominant physiochemical variables that control erosion behavior of cohesive soils. With these findings, it suggests that individual equations need to be developed based on physiographic provinces. However, our findings also illustrated that statistical methodology appears to influence resulting predictive models, and likely also contributes to the diverse number of published predictive models for  $\tau_c$ . Further research through a study design specifically targeting the relationships among unique geologies, soil properties, and erosion behavior are necessary to better understand the significant variables, which were selected from the statistical models.

## 3.0 The Influence of Cumulative Effective Stream Power on Scour Depth Prediction around Bridge Piers in Cohesive Earth Material

### 3.1 Introduction

Among many factors resulting in bridge foundation failure, local scour at piers and abutment is the most critical (Shirole and Holt, 1991; Wardhana and Hadipriono, 2003; Cook et al., 2015). Local scour is caused when the instream structure diverts turbulent hydraulic forces towards the streambed and these forces exceed the erosive resistance of earthen bed material. There are approximately 500,000 bridges in the United States that span over waterbodies (FHWA, 2017). During the past 30 years more than 1,000 bridges have failed and about 50-60% of those failures were due to hydraulic forces and bed scour (Shirole and Holt, 1991; Wardhana and Hadipriono, 2003; Cook et al., 2015). In Tennessee, among 20,169 highway bridges about 989 bridges have been designated as scour critical, which is about 5% of the existing bridges (FHWA, 2017). Wu (2010) reported that older bridges constructed before 1960 are more susceptible to critical scour and failure. Though design and construction of riverine bridge piers and abutments have improved, maintenance and replacement is currently a national priority (ASCE Infrastructure Report Card, 2017). Better predictive equations for local scour at bridge piers further improve on cost-effective designs.

Design equations for equilibrium scour depth at bridge piers most commonly applied and based on granular-type alluvial material (Richardson and Davis, 2001). Equations incorporated into HEC-18, developed for non-cohesive sediments have been extensively used for scour depth prediction regardless of soil type. An equation for pier scour on cohesive sediment has been developed by the Federal Highway Administration (FHWA), expressed as:

$$y_s = 2.2K_1K_2D^{0.65} \left( \frac{2.6V - V_c}{\sqrt{g}} \right) \quad (3.1)$$

where,  $y_s$  is the maximum scour depth,  $K_1$  and  $K_2$  are the correction factor for pier shape and angle of attack, respectively,  $D$  is the pier diameter,  $V$  is the flow velocity,  $V_c$  is the critical flow velocity for scour initiation, and  $g$  is the gravitational acceleration. It has been reported that these equations can grossly under- and over-predict scour depth, which emphasizes the need for further research when the stream bed is composed of cohesive sediments (Benedict 2003, Brubaker et al. 2004, Pierce et al. 2011). Recently, a study conducted by the SCDOT and the USGS found HEC-18 equations over-predicted scour depth in cohesive sediments for 84% of bridge sites surveyed, with over-predicted depths ranging from 0.1 to 13.4 ft (Benedict and Caldwell, 2009). The study also showed 16% of the surveyed sites under-predicted the scour depth, which were a function of local bed sediment and geological conditions with high hydraulic resistance properties.

Erosion behavior of cohesive sediment is more complicated than non-cohesive soils due to chemical bonding forces of a consolidated mass, which leads to the uncertainty in scour prediction. The properties of cohesive sediment are analogous to a chemical gel, which erosion process is complex as both aggregates (clods) of materials and particles are detached from the sediment surface (Croad, 1981; Tan, 1983; Mehta et al., 1989; Annandale, 2006). Flow turbulence generated at the pier or other structures causes a positive pressure pulse acting on the sediment boundary enhancing pore pressure within the bed sediment. Over time the fixed chemical bonds between clay elements are broken down due to the repeated pressure fluctuations leading to clay aggregate removal known as the “plucking” phenomenon (Croad, 1981; Tan,

1983; Briaud et al., 2001; Annandale, 2006). The “plucking” erosion mode is common for both in consolidated cohesive sediments and rocks, though rocks also erode in other forms such as: dissolution, cavitation, and abrasion (Keaton, 2013). From field observations among sites in Tennessee, similarities of stream bed/bank erosion between rock and cohesive sediments were also identified (Figure 3.1).



Figure 3.1. Erosion in cohesive soils: a) around bridge piers in Crooked Creek, Shelby County, TN, b) undercutting at the bottom of creek in Coal Creek, Tipton County, TN.

Both in rocks and cohesive soils, the scour rate is slow and time dependent, and can take days to years to reach an equilibrium scour depth (Briaud et al., 1999; Ting et al., 2001; HEC-18, 2012). The time-dependent scour behavior of cohesive sediments identifies the necessity to consider the influence of long-term hydraulic history from multiple flow events over many years rather than considering a single flood event for maximum scour depth design as typically applied for non-cohesive sediments. This scour behavior with rock and cohesive boundary materials demonstrate the complexity associated with these types of material.

Annandale (1995) introduced the concept of stream power (erosion capacity of water) and erodibility index (erosion resistance for earth material) for bridge scour study. The concept of an erodibility index was first introduced by (Kirsten, 1982) and in the early 1990s number of researchers analyzed field and laboratory scour data for identifying relationship between stream power and erodibility index value (Annandale, 1995, 2006). This concept has been used for bridge foundation on rocks and head-cut erosion studies in spillways. In those studies, critical stream power has been calculated based on the functional relationship between erodibility index and stream power. Because cohesive soil erosion behavior is complex; the use of an empirical relationship for critical stream power calculations could be problematic. Furthermore, previous scour studies with cohesive sediment around bridge piers and abutments have not related critical stream power and duration history to pier scour development. The possible lack of published studies could be due to availability of long-term scour data, and the difficulty of measuring the critical shear stress ( $\tau_c$ ) of the soil/sediment near bridge sites. To date, no study has quantified the relationship between erodibility index and the effective cumulative stream power in cohesive sediments, only observed time-independent direct scour relations to stream power.

This study uniquely measured  $\tau_c$  and modeled long-term flow history to estimate cumulative effective stream power and its relation on pier scour depth on cohesive sediments. The objectives

were to: 1) examine whether bed scour rates are a function of erosive flood history quantified as effective cumulative stream power (sum of stream power duration over critical shear stress), and 2) determine whether an erosion index ( $K$ ) (*proposed by Annandale, 1995*) for cohesive soil erodibility correlates with critical stream power. The hypothesis is that bed scour on cohesive soils is a time-dependent function which can be associated with effective cumulative stream power. Other factors also affect scour rates such as the geophysical characteristics of the soil, bridge pier configuration, and channel geometry at and upstream of the structure. Secondly, this study provides some insight on the time-dependency scour behavior in terms of scour depth equilibrium at bridge piers.

## 3.2 Methods

### 3.2.1 Study Design

The study utilized bridge scour data collected at nine bridge sites on streams in western Tennessee where the bank/bed materials are predominantly composed of cohesive (silt/clay) soils (Figure 3.2). Long-term scour data around bridge piers and abutments were collected from the TDOT bridge inventory database (Table 3.1). Scour data were not available from the period immediately following bridge construction, except for the Pond Creek bridge site. The drainage basin size varied among the nine study sites ranging from 19 to 151 km<sup>2</sup>.

In order to compute the cumulative effective stream power and number of days exceeding  $\tau_c$ , each site required long-term hydrological modeling from the time of bridge construction completion through the dates in which bridge scour data were collected. Hydrological modeling estimated the flow record for each site applying climatic variable inputs. In addition to flow, stream power ( $\Omega$ ) and reach-scale hydraulic shear stress ( $\tau$ ) calculations required channel slope and cross-sectional geometry. The mini-jet tester, an in situ field device was used to estimate  $\tau_c$  of the streambed/bank cohesive soils near the bridge site (Mahalder et al. 2018a,b). Per site, the flow discharge ( $Q$ ) where  $\tau > \tau_c$  was used as the threshold  $Q$  to estimate effective stream power ( $\Omega_e$ ), in other words the critical stream power ( $\Omega_c$ ) that can scour the local cohesive soils. The cumulative effective stream power sums the  $\Omega$  over a unit time interval where  $\Omega_c > \Omega$ . Calculation of site  $K$ ,  $\tau_c$ ,  $\Omega_c$ , and effective cumulative stream power, and measured scour depths ( $\Delta y_s$ ) at bridge piers were used to examine the following relationships: 1)  $K$  vs  $\Omega_c$ ; 2)  $\Delta y_s$  vs cumulative effective stream power, and 3) number of days exceeding  $\Omega_c$  vs  $\Delta y_s/y_t$ , where  $y_t$  is the total measured scour depth.

In the TDOT bridge inventory dataset among these nine stream sites, Pond Creek site had scour data available from the beginning of bridge construction. These scour depth data over 20 years provided the information to observe the temporal variability of pier scour depth over the long-term flow history and estimate the equilibrium condition for scour depth. Qualitative assessment of scour behavior was conducted with the hydrological and scours data for this stream site. It also provided a context to evaluate the results relating  $\Delta y_s$  vs cumulative effective stream power suggesting which measurements represent equilibrium depths. Pond Creek is a 3<sup>rd</sup> order stream with contributing watershed area of 139.96 km<sup>2</sup> at the bridge site and the bankfull width is 31.27m, which is an undeveloped/rural ungaged watershed. In the watershed, 84.63% of the total area is agricultural land, 8.03% medium residential area, 4.75% water body, and 2.59% forest area. The bridge length is 35.50 m with two abutments and two piers both in the channel with flow and substantial scour at Pier#1 was observed.

Table 3.1. Study sites characters including the watershed and highway bridge.

Creek Name	County	Latitude	Longitude	Watershed Area (km <sup>2</sup> )	Bridge Construction Year	Highway No.	Bridge Pier type	Bridge Length (m)	No. of scour data points	Percent impervious	USGS data availability
Beaver Creek	Carroll	36.01304	-88.445056	151.23	1969	SR 77	Square Bent	106.70	6	1.53	1962-1994
Black Creek	Crockett	35.815902	-89.320778	70.12	1974	SR 88	Circular	78.30	10	1.13	N/A
Pond Creek	Dyer	35.921027	-89.325277	139.96	1990	0A 443	Round Nose	35.50	6	1.33	N/A
Mud Creek	Haywood	35.678261	-89.132721	64.60	1934	SR 076	Square Bent	95.40	5	1.24	N/A
Cane Creek	Lauderdale	35.75975	-89.522583	87.60	1982	SR 209	Rectangular	33.80	11	2.33	1957-1987
Richland Creek	Obion	36.262007	-89.212328	45.28	1980	SR 183	Round Nose	46.60	8	0.51	N/A
Big Creek		35.342108	-89.806569	83.29	1966	SR 205	Square Bent	51.20	8	3.17	N/A
Crooked Creek	Shelby	35.323894	-89.807139	44.63	1952	SR 14	Round Nose	65.20	6	1.37	N/A
Coal Creek	Tipton	35.5526	-89.585556	19.00	1986	SR54	Round Nose	43.00	5	0.95	N/A

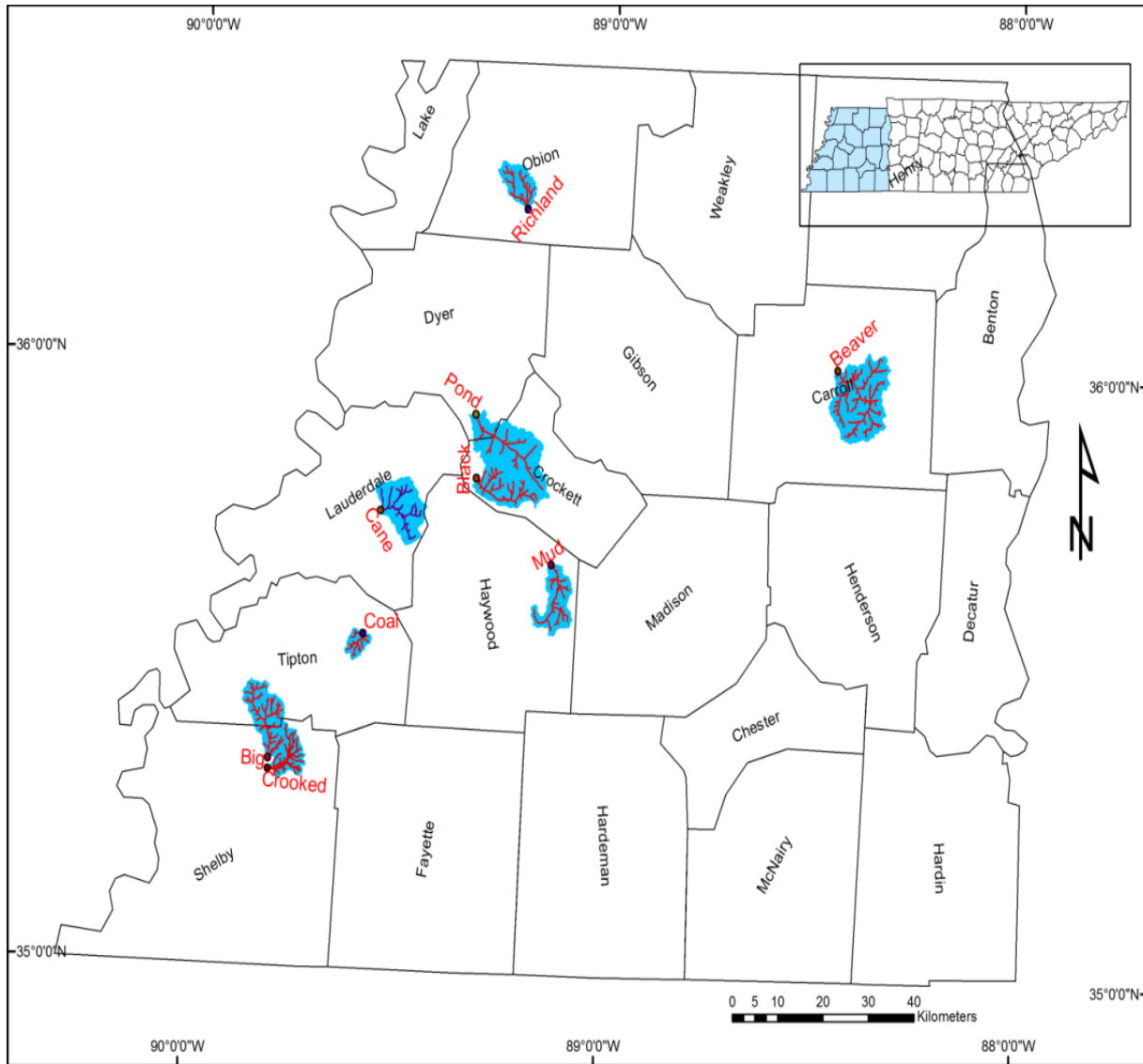


Figure 3.2. Study watersheds showing locations of bridge sites in western Tennessee.

### 3.2.2 Erodibility Index Calculations

The erodibility index  $K$  is a geomechanical property of earthen material, which is used to quantify the relative resistance of rock and other materials from the erosive capacity of flowing water (Annandale, 2006). Annandale (1995, 2006) reported an empirical relationship between stream power and erodibility index for soils with lower erodibility index values. The erodibility index is defined as follows:

$$K = M_s \cdot K_b \cdot K_d \cdot J_s \quad (3.2)$$

where,  $M_s$  is the mass strength number;  $K_b$  is the block size number;  $K_d$  is the discontinuity bond shear strength number; an  $J_s$  is the relative ground structure number.  $M_s$  for cohesive sediments can be calculated based on either the vane shear strength value or UCS values (Moore, 1997; Annandale, 2006). The equation for  $M_s$  is defined as follows.

$$M_s = 0.78(\text{UCS})^{1.09} \text{ for } \text{UCS} \leq 10 \text{ MPa, and } M_s = \text{UCS} \text{ for } \text{UCS} > 10 \text{ MPa} \quad (3.3)$$

The  $K_b$  value for intact cohesive soil is used as 1 and the  $K_d$  value is calculated using the drained residual friction angle ( $\phi$ ).

$$K_d = \tan \phi \quad (3.4)$$

$\phi$  can be calculated using the liquid limit ( $LL$ ) of tested cohesive soils and three ranges of clay size fraction (USDS-NRCS, 1997).

$$\text{For } \leq 20\% \text{ clay, } \phi = 169.58(LL)^{-0.4925} \quad (3.5)$$

$$\text{For } 25 - 45\% \text{ clay, } \phi = 329.56(LL)^{-0.7100} \quad (3.6)$$

$$\text{For } \geq 45\% \text{ clay, } \phi = 234.73(LL)^{-0.6655} \quad (3.7)$$

Cohesive soil material is considered intact (without structure), so  $J_s = 1$  (Moore, 1997; Annandale, 2006). In this study, all of these parameters were calculated based on the measured soil properties according to above mentioned guidelines.

### 3.2.3 Hydrological Flow Simulations

Daily flow data was necessary for stream power calculations, which were obtained from the USGS gage stations when data were available. Only two of the sites had limited USGS data. With most study streams being ungaged, hydrological flow simulations were required (Table 3.1). The hydrological model HEC-HMS 4.0 was used for the long-term daily flow simulation. Necessary supporting files for HEC-HMS 4.0 were generated using ArcGIS 10.1, where HEC-GeoHMS tool was used for watershed delineation. Long-term flow simulations required climatic variables inputs including: precipitation, air temperature, and evapotranspiration were collected from the NOAA website (<https://gis.ncdc.noaa.gov/>). DEM, land cover, percent impervious data were collected from USGS TNM 2.0 viewer (<https://viewer.nationalmap.gov/>) website. SSURGO soil database was collected from web soil survey of USDA (<https://websoilsurvey.sc.egov.usda.gov/>) for necessary watershed parameters calculation.

In the ungaged watersheds, parameters obtained from another hydrologically and geologically similar gaged watershed were used for the long-term flow simulations. Pond Creek is an ungaged watershed, which is hydrologically and geologically similar to the Stokes Creek watershed (USGS gage station 07029035) of Crockett County (Figure 3.3). From the available daily flow data, model was calibrated (data from January 1999 to December 31, 1999), and for model validation, data from January 1, 2000 to May 31, 2000 were used for Stokes Creek watershed. The yearlong data was used for model calibration to account the seasonal variation in the watershed for estimating different parameters used in HEC-HMS simulation for Pond Creek watershed. The calibrated results illustrated in Figure 3.2a were in good agreement with the observed and simulated daily flow data. However, two peaks: one in March 1999 and another one in June 1999 were not captured by this model. The differences in peaks were likely due to variations between precipitation station data and actual conditions in the watershed where summer storms can be quite localized. During the model validation, simulated daily flow events demonstrated good agreement with the observed data based on plot inspection (Figure 3.3b). The peak flows were captured very well with some deviation as some peaks over-estimated and under-estimated. Statistical errors were calculated for model validation. From the statistical error analysis (Table 3.2), it was found that the errors were in an acceptable range for a hydrological modeling similar to this type of watersheds as reported by Fleming and Neary (2004).

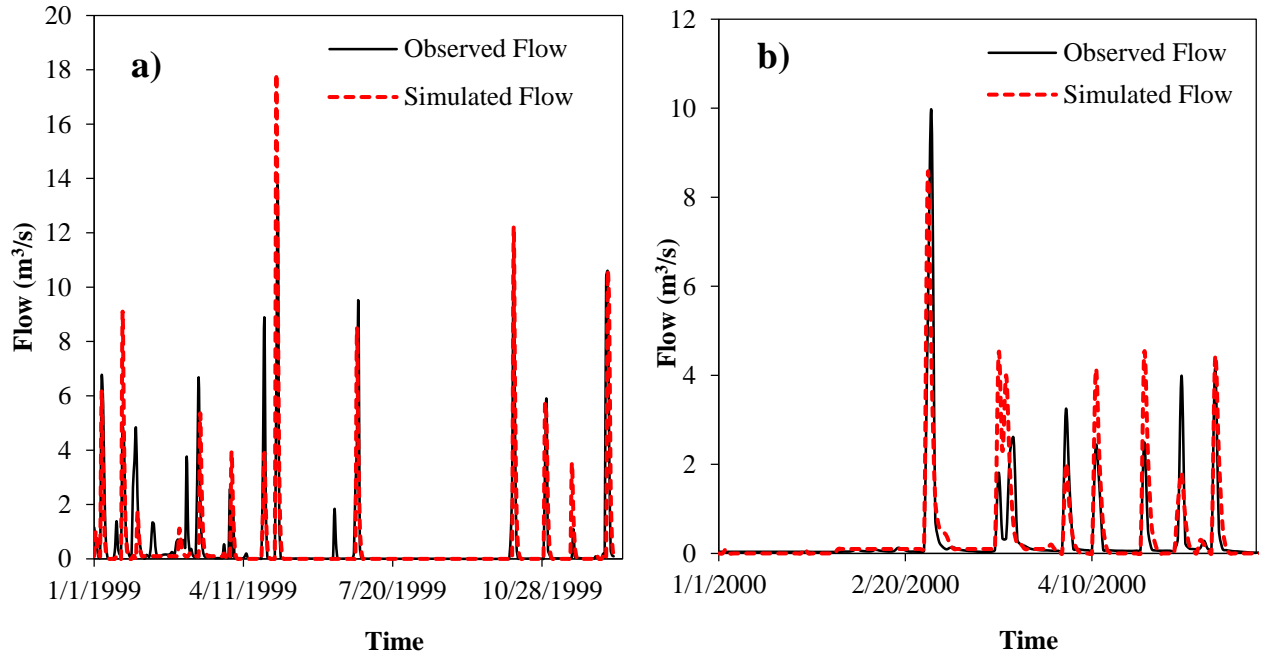


Figure 3.3. Simulated flow for gaged watershed (Stokes Creek): a) model calibration, b) model validation.

Table 3.2. Statistical error calculation and validation targets.

Error Type	Calibration	Validation
Mean Absolute Error $(1/n) \sum  Q_0 - Q_s $	1.25	2.53
Root mean square error $\sqrt{[\sum (Q_0 - Q_s)^2]/n}$	6.99	7.07
Average error in magnitude of peaks (%) $[(1/n) \sum  (Q_0 - Q_s)/Q_0 ] \times 100$	55.50	58.39

Finally, the necessary hydrological model input parameters from the Stokes Creek watershed were used for the ungaged Pond Creek watershed. Flood frequency analysis was also conducted using the simulated flow for the ungaged watershed using the Bulletin 17B method in HEC-SSP and compared with the TDOT regression equations by computing different peak flows. Figure 3.4 demonstrates a typical output from the HEC-HMS model using Pond Creek as the example. Similar procedures were followed for the other ungaged watersheds in this study.

### 3.2.4 Field Measurements of Stream Bank/Bed Soil Critical Shear Stress

In this study stream bank/bed  $\tau_c$  measurements of cohesive soils were obtained by the use an in-situ mini-jet test device (Simon et al., 2010; Al-Madhhachi et al., 2013). The mini-jet device was developed for measuring soil erodibility parameters in-situ, but it can also be used in the laboratory. For jet operation, a constant head is necessary, which was maintained using a pump that delivered stream water powered by a 2000 W portable generator. Field operational and

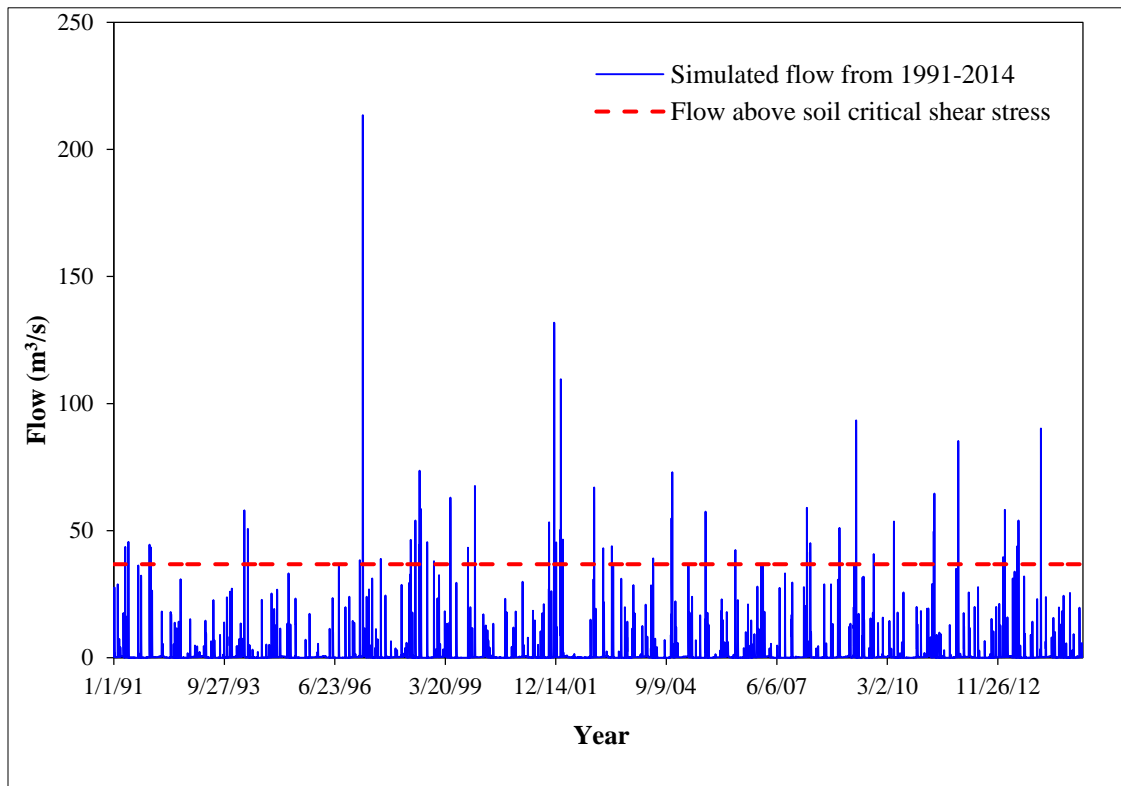


Figure 3.4. Example flow simulation for Pond Creek in Dyer County, West Tennessee, and the flow threshold at critical shear stress.

computational procedures for jet operation and data analyses are described in detail by Mahalder et al. (2018). Per stream sites, 4 to 5 jet tests were conducted around the bridge piers or at lower bank to find the average  $\tau_c$  for a stream from May 2015 to August 2015. After completing each test, two core soil samples near the test location were collected using a 5.08 cm dia. cylindrical stainless steel coring instrument. These core samples were used to measure bulk density (BD), water content (WC) and unconfined compression strength (UCS). The core cylinders were immediately end capped and sealed in an air-tight plastic bag to minimize moisture loss. Approximately 1.4 kg of soil was also collected per test site from inside the jet device's bottom ring for laboratory analyses of other soil physical properties: grain size distribution, LL, plastic limit (PL), plasticity index (PI), and organic content.

### 3.2.5 Effective Stream Power Calculations

Stream power defines the capability of a stream to transport sediments as bed load and fine sediments in suspension (Bagnold, 1960). Numerous researchers have used stream power ( $\Omega$ ) for sediment movement (Leopold et al., 1964; Hickin and Nanson, 1984; Sklar and Dietrich, 2004; Larsen et al., 2006) based on Bagnold (1960) theory, which is calculated from the stream flow data and channel slope. The excess stream power or  $\Omega_e$  is the difference between the stream power due to daily flow and  $\Omega_c$ , which can be calculated using the following equations.

$$\Omega = \rho g Q_n S \quad (3.8)$$

$$\Omega_c = \rho g Q_c S \quad (3.9)$$

$$\Omega_e = \Omega - \Omega_c \quad (3.10)$$

where,  $\Omega$  is the stream power per unit width of channel ( $\text{W/m}^2$ );  $\rho$  is the density of water ( $\text{kg/m}^3$ );  $g$  is the gravitational acceleration ( $\text{m/s}^2$ );  $Q_n$  is the daily discharge ( $\text{m}^3/\text{s}$ );  $Q_c$  is the threshold stream power per unit width of channel ( $\text{W/m}^2$ ) above which erosion will take place; and  $S$  is the channel slope ( $\text{m/m}$ ). In order to calculate the  $\Omega_e$ , threshold discharge for scour was calculated for each stream sites from the measured  $\tau_c$  values from jet tests, channel roughness data (Manning's  $n$ ) and the channel cross-sectional data by assuming uniform flow. In literature, a threshold hydraulic condition for scour is identified through numerous forms, e.g., critical flow velocity, critical shear stress for earth material, critical stream power, or bankfull/channel-forming discharge.

Stream cross-sectional data and scour data around the bridge foundations were collected from the TDOT bridge inventory database. Cumulative effective stream power was calculated based on the scour depth data measurement frequency found in the TDOT bridge inventory database for each stream sites. Flow data was also used for calculating the number of events above the threshold discharge. These data were used to observe the influence on scour pattern at different soil types and pattern of scour development around those bridge sites.

### 3.3 Results

#### 3.3.1 Study Site Soil Properties

Among the nine study sites, soil were predominantly silty-loam and silty-clay-loam, where LL values were between ~28-37%, BD ranged from  $1.79 \text{ g cm}^{-3}$  to  $2.06 \text{ g cm}^{-3}$  and  $D_{50}$  was between  $9.0 \text{ }\mu\text{m}$  and  $24 \text{ }\mu\text{m}$  (Table 3.3). The tested soil samples were characterized as cohesive since plasticity index values were  $>10\%$  and clay content was  $>10\%$  by weight (Raudkivi, 1990). However, the cohesion values showed a wide range in the dataset.

Measured  $\tau_c$  from in-situ jet test were used to calculate the threshold discharge or termed the effective flow per study stream sites, which are the flows that generate reach-scale shear stress ( $\tau$ ) over  $\tau_c$ . Measured  $\tau_c$  are in Table 3.3. The bridge at Mud Creek was the oldest studied bridges among data collected, though in 2010, major repair works have been conducted on this bridge sites. Average  $\tau_c$  values ranged between  $4.20\text{-}17.67 \text{ Pa}$  among these stream sites and the corresponding critical flow was between  $7.05\text{-}50.30 \text{ m}^3/\text{s}$ . The channel slope was mild around the bridge location and varied between  $0.000123 \text{ (m/m)}$  to  $0.000976 \text{ (m/m)}$ . Calculated  $\Omega_c$  varied between  $37.31 \text{ W/m}^2$  to  $482.84 \text{ W/m}^2$ . Contributing watersheds of the studied streams were undeveloped as percent impervious area among these watersheds was between  $0.51$  and  $3.17\%$ .

The relationship between  $K$  and  $\Omega_c$  was developed from the data analysis for these nine stream sites. A good functional correlation between critical stream power and erodibility index was observed ( $R^2 = 0.61$ ,  $p = 0.017$ ) with a power function (Figure 3.5). However, this observed power function deviated from the proposed relationship developed by Annandale (1995, 2006) for soil with erodibility  $K$  index value less than  $0.10$ . Wibowo et al. (2005) developed a probabilistic approach by logistic regression method to quantify the erosion probability based on the Annandale (1995, 2006) threshold line. Findings from this analysis showed that all the data for these studied stream sites were enclosed between the  $99\%$  probability and  $1\%$  probability lines (Figure 3.5).

Table 3.3. Soil properties, erodibility index parameters, critical shear stress and critical stream power per unit width of channel, and channel slope for the nine study sites.

Creek Name	BD (g/cm <sup>3</sup> )	D <sub>50</sub> (μm)	Cohesion (kPa)	Clay%	LL	Erodibility Index, K	Average critical shear stress, τ <sub>c</sub> (Pa)	Critical flow (m <sup>3</sup> /s)	Critical Stream Power (W/m <sup>2</sup> )	Average Channel Slope at bridge location (m/m)
Beaver Creek	2.06	13.00	88.08	28	27.80	0.082	10.15	50.30	443.12	0.000604
Black Creek	1.96	14.60	59.81	24	35.40	0.046	12.00	20.56	314.98	0.000976
Pond Creek	2.02	9.00	61.01	39	35.00	0.050	5.72	36.80	272.46	0.000694
Mud Creek	1.86	11.50	31.51	25	28.60	0.017	10.10	12.60	207.18	0.000123
Cane Creek	1.79	18.00	38.61	18	29.00	0.027	4.20	10.81	98.84	0.000932
Richland Creek	1.81	24.00	22.06	14	29.40	0.013	5.45	7.98	37.31	0.000261
Big Creek	2.01	15.80	67.05	22	27.80	0.073	14.80	16.97	160.32	0.000963
Crooked Creek	2.05	12.00	67.56	25	29.00	0.078	17.67	27.78	482.84	0.000285
Coal Creek	1.89	15.00	70.46	29	36.60	0.062	13.40	7.05	322.69	0.000970

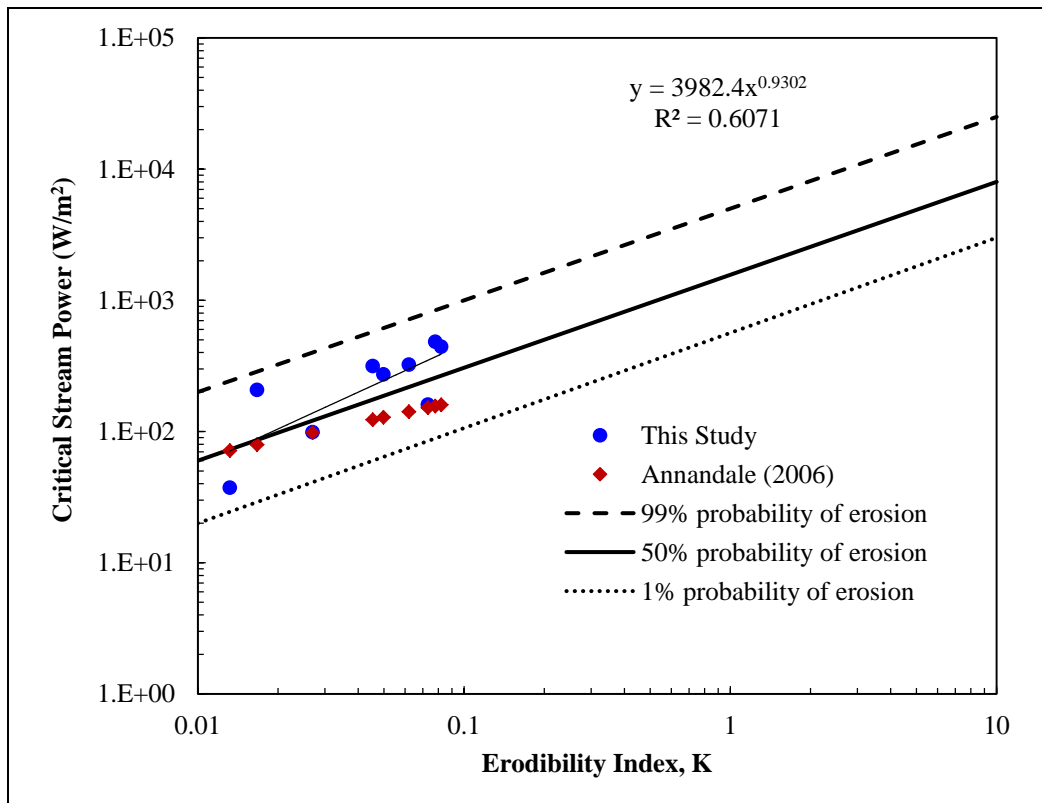


Figure 3.5. Relationship between critical stream power, and erodibility index. Where probability of erosion was calculated using the Wibowo et al. (2005) proposed probabilistic approach using logistic regression method.

The scour depths ( $\Delta y_s$ ) was computed and compared with the cumulative effective stream power for the specified duration in which bridge scour depth was measured (Figure 3.6). The pattern of this dataset shows that a good correlation exists between effective cumulative stream power and the depth of scour ( $R^2 = 0.56$ ,  $p < 0.001$ ). However, in some cases at lower cumulative stream power, very high erosion rate was observed. The influence of flow history on scour development among these studied streams sites over multiple years and flood events was also analyzed by examining the number of days above critical flow and a non-dimensional scour depth value  $\Delta y_s / y_t$  (Figure 3.7). This result showed three distinct areas (Area “A”, “B”, “C”) in the dataset, which were found dependent on the soil properties, number of continuous flow events above critical value, and the age of a bridge.

Analyzing the characteristics of the dataset in those zones, it was observed that in the enclosed area “A”, at lower number of flow events ( $< 20$  events) relative scour depths were higher compared with the enclosed area “B” on the same figure. Soil physical properties and erodibility data showed that both the  $\tau_c$  values (4.20-6.10 Pa) and the soil cohesion (22.06-38.61 kPa) values were low expect for Pond Creek where  $\tau_c$  was 5.72 Pa and cohesion was 61.01 kPa (Table 3.3). Area “C” in Figure 3.7 represents the more recent scour depths data, where both the short duration higher peak flow events and the longer duration moderate flow events were observed.

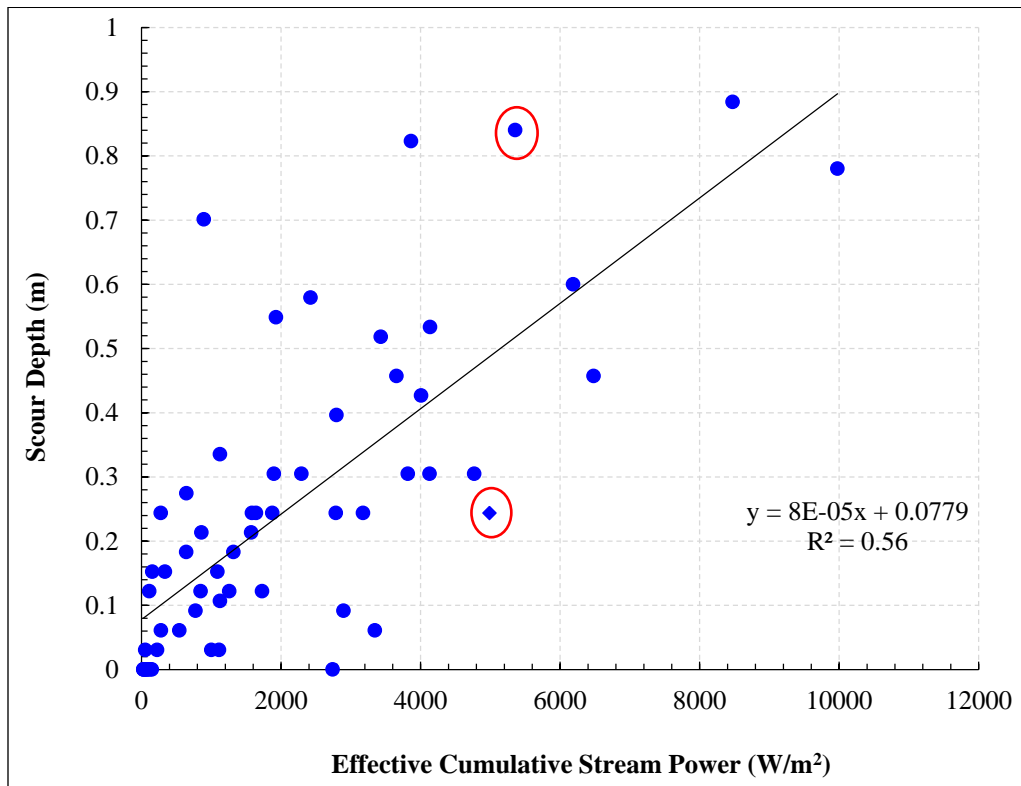


Figure 3.6. Relationship between cumulative effective stream power and scour depth measurement. Circled data points represent measurements at the Crooked Creek site.

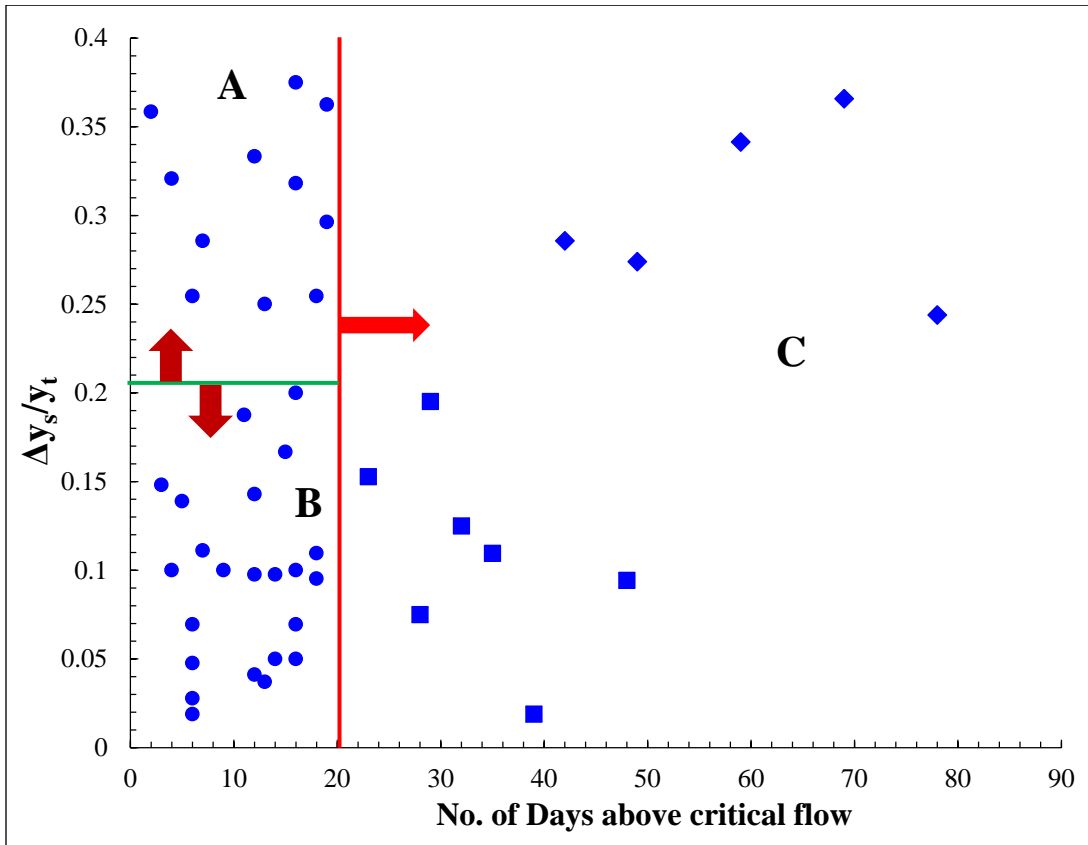


Figure 3.7. Relationship between relative scour depth and the number of flow events above the critical flow for the studied stream sites. Solid circles = regular scour data points, diamonds = scour data before 2004 with longer duration flow events; and squares = scour data after 2004 with short duration flow events.

### 3.3.2 Case Study for Pond Creek Site on Temporal Scour Patterns

At the Pond Creek bridge site, TDOT measured scour depths over 20 years showed some interesting trends with three different scour rates (Figure 3.8). Computing the critical flow from channel geometry and measured average  $\tau_c$  data, it was observed that both short duration high peak and continuous moderate flow events occurred between the year 1991 and 1999 (Figure 3.4), consequently very high scour rate (0.25 m/year) was observed (Figure 3.6, Zone-A). After the year 1999, scour rate receded (0.07 m/year) substantially (Zone-B). In the year 2000, no flow events were observed above the critical and possible deposition took place since elevated bed profile was observed (Figure 3.8, Zone-B). Number of flow events above the critical flow was plotted on the same graph (Figure 3.8). Analyzing the graph, it was found that even though several flow events were above critical, no significant scour rate was observed. Specifically, the erosion rate reduced dramatically after the year 2002.

### 3.4 Discussion

For equilibrium scour depth calculation, the erosive capacity of flowing water has been calculated by several methods including average flow velocity, shear stress, peak flow, and

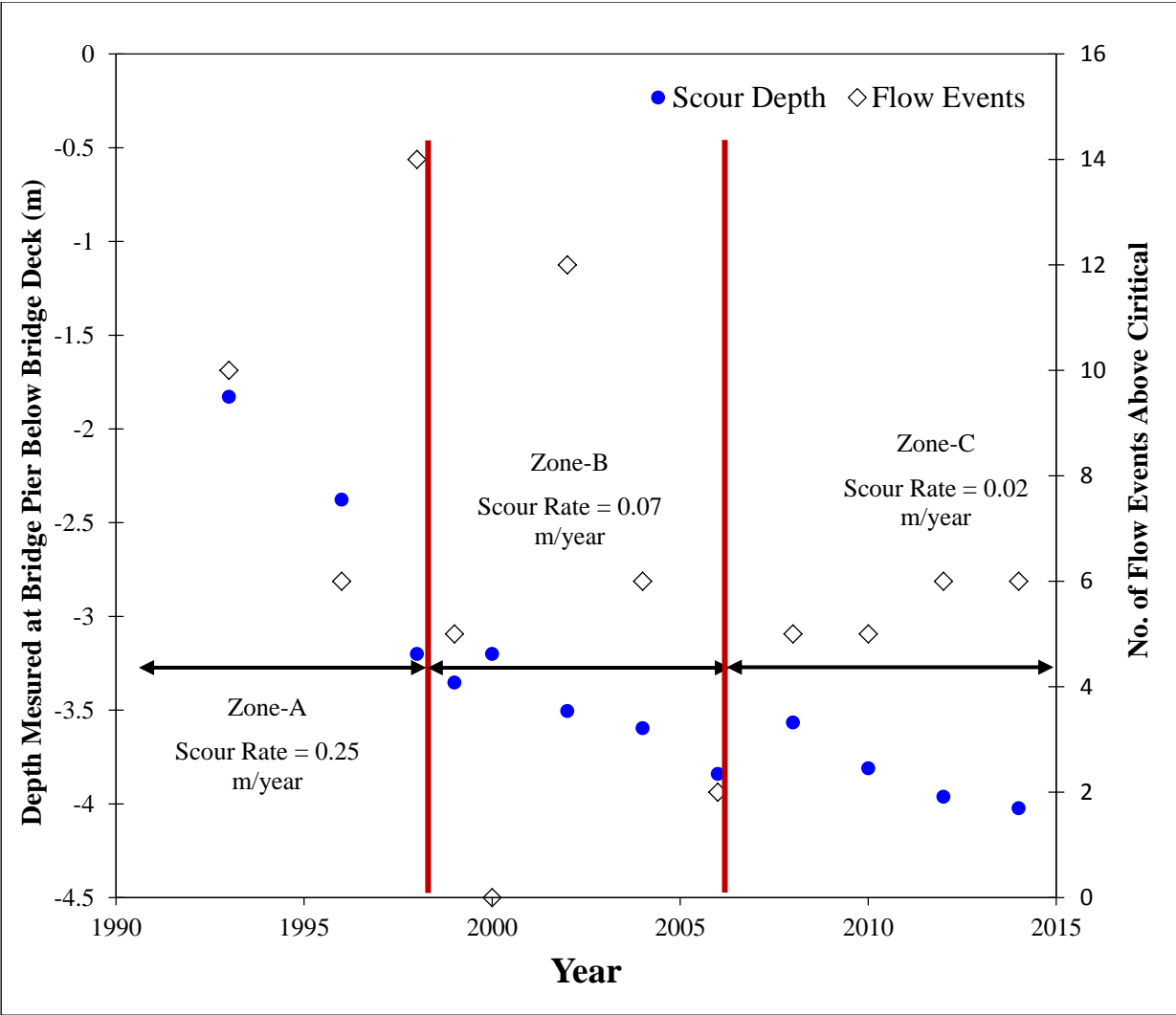


Figure 3.8. Long-term scour depth data and the number of flow events above critical flow at the bridge pier for Pond Creek showing three different scour rates over a 20-year period.

stream power. The FHWA developed three technical guidance for bridge foundation design; they are: HEC-18 (for developing scour evaluation program and (analyzing bridges for scour), HEC-20 (for analyzing the effect of stream instability on bridges), and HEC-23 (countermeasures for mitigating potential damage to bridges and highways at stream crossings). The FHWA applies risk-based approaches for bridge-scour assessment and design by considering the structural safety and reliability, and corresponding economic consequences of failure. In this approach, bridges are designed for 100-year flood and checked for the 500-year flood (HEC-18, 2012).

Pier scour in cohesive soils are slow and time dependent, where many factors influence scour development rates and equilibrium depth. The cumulative effect of long-term flow history from many flood events over many years is required to predict scour depth rates to reach equilibrium, rather than applying hydraulic loading from a single flood event (Kwak, 2000; Briaud et al., 2001; HEC-18, 2012; Keaton et al., 2012).

Numerous studies reported relationships between stream power and various forms of sediment detachment and transport (Bagnold, 1960; Yang, 1972; Yang, 1973; Chang, 1979; Annandale, 1995; van den Berg, 1995; Annandale, 2006). It has been reported that erosion behavior soil with high silt-clay content or cohesive sediments is dominated by subaerial processes or excess shear stress duration in the flow hydrograph (Costa and O'Connor, 1995; Julian and Torres, 2006). However, sediment encroachment and movement around bridge piers and abutments are fundamentally different from the fluvial erosion process. HEC-18 (2012) introduced an equation for predicting equilibrium scour depth in cohesive soils based on mean and critical flow velocity. This time-dependent phenomenon has been introduced in the scour prediction procedures based on a proposed method by Briaud et al. (2011). This proposed method was developed based on laboratory experiments with commercially available clay soil. However, it is understood that the complex interaction between soil physiochemical and biological properties is not easily possible to develop in the laboratory.

It is also understood that numerous number of flow events above critical might occur for natural streams. It was hypothesized that in cohesive soils, cumulative shear stress duration/cumulative stream power over a critical value for scour initiation could be valuable. Similarities exist between rock erosion and the cohesive soil erosion behavior, though orders of magnitude higher erosive capacity of flowing water is required for rock compared with the consolidated cohesive sediments. Therefore, possible deviations from the empirical relationship between  $K$  and  $\Omega_c$  for cohesive soils were also studied.

Annandale (1995, 2006) estimated the critical stream power/erosive power required for scour initiation based on a functional relationship with the  $K$  value. In this method, only three soil properties, USC, clay content and LL are necessary to calculate the  $K$  value. Based on published data from numerous studies, Annandale (1995, 2006) proposed a power relationship to predict  $\Omega_c$  for earth material when  $K$  value is less than 0.1 (Figure 3.5). Data from this study as calculated from the in-situ  $\tau_c$  measurement and the channel geometry showed a clear deviation from the Annandale (1995, 2006) proposed empirical relationship. Non-parametric Mann-Whitney U test also identified that the median values were statistically different ( $p = 0.024$ ). It is important to note that  $\Omega_c$  calculated from the in-situ measurement showed a good correlation with the  $K$  value (Figure 3.5). It was assumed that variation in these data could be related to simplified analysis procedures and fundamentally different inherent erosive resistance properties of the tested cohesive earth material. Wibowo et al. (2005) identified that a probabilistic approach better quantifies erosion behavior of highly variable earthen material based on Annandale (1995, 2006) study. Data from this study also fits well in between those proposed erosion probability lines of 99% and 1% as per the Wibowo et al. (2005) equation. It is hypothesized that the influence of erosion properties or prediction of  $\tau_c$  values for cohesive earth material could have significant influence on the threshold stream power calculation, consequently influenced the observed variation from the Annandale (1995, 2006) proposed relationship. Therefore, for calculating  $\Omega_c$ , the in-situ  $\tau_c$  measurement could be an alternative approach for cohesive sediment as developed in this study.

Effective stream power acting on soil surface is a surrogate measure for shear duration or excesses shear stress above critical value in erosion study where hydraulic loading is critical for maximum scour depth development. A total of 65 scour depth measurements at bridge piers were available from TDOT bridge inventory database among this study sites. Measured scour depth data over time were directly correlated with cumulative effective stream power among these

studied stream sites ( $R^2 = 0.56$ ,  $p < 0.001$ ) (Figure 3.6). In Figure 3.6 a few high scour depths were associated with lower cumulative stream power estimates. From field observations during the in-situ jet test operations, it was identified that in some streams a non-cohesive granular material layer blanketed cohesive soil layer at the stream bottom, and among the other cases stream beds were exposed with the cohesive sediment layer. It is hypothesized that during low flow events as sediment capacity of the flowing water receded, transported granular (non-cohesive) sediments were deposited on the streambed and presumably within the scour holes. Consequently, during short peaked flow events above the erosion threshold might have eroded those granular materials around bridge piers and a large jump in scour depth was observed (Figure 3.6). Further analyzing the daily flow data for each stream and the corresponding scour depth value, it was identified that multiple possible factors had significant influence on the observed scour depth pattern, not only the number of flow events flow duration over critical stress for erosion.

Several studies identified the influence of flow duration, flow magnitude and flow frequency on erosion behavior in different earth materials for both the bank erosion, fluvial erosion (channel incision) and localized scour around structures (Wolman, 1959; Costa and O'Connor, 1995; Julian and Torres, 2006; Keaton et al., 2012). Costa and O'Connor (1995) showed that short duration spikes with higher flow intensity might not generate sufficient erosive power for cohesive soils to be scoured compared with long duration medium intensity flood events. Similar observations were also reported by Julien and Torres (2006) for bank erosion estimation in cohesive sediments. In this study, it was identified that at lower cumulative effective stream powers ( $< 2000 \text{ W/m}^2$ ) generally produced lower scour depths with some exception as for Richland Creek and Mud Creek data (Figure 3.6). In those two stream beds, substantial amounts of granular material (sand and gravel) were observed on the top of cohesive sediment layer during field tests. Therefore, short duration flashy flow events could have removed the granular material from the vicinity of the pier and higher scour depths readings were recorded.

A major disparity among this study's dataset was observed when the cumulative effective stream power range was between  $2000\text{-}5200 \text{ W/m}^2$  (Figure 3.6). In this stream power range, both the flow and the soil physical properties influenced the erosional behavior. Specifically, with soils having higher  $K$  values per Beaver Creek, Big Creek, Coal Creek, and Crooked Creek data had lower scour depths and represent those data points below the regression line as shown in Figure 3.6. Among the other studied streams, higher scour depths were observed. For both of these cases, the influence of flow duration was also identified as the key controlling variable. Cumulative effective stream power above  $5200 \text{ W/m}^2$  displayed an interesting trend in the dataset. In this region, the longer flow duration above the critical  $\tau$  value could have influenced for the higher scour depths, since more continuous flow events were observed in the flow hydrograph except for Crooked Creek data (represented in a circle above the best fit line in Figure 3.6). In Crooked Creek, several wooden logs were found driven into the stream bed close to the pier foundation for protecting bank failure (Figure 3.9). It is hypothesized that the local turbulence due to wooden logs near the pier could have influenced the higher scour depth since after that measurement very low scour depth was observed (data points in a circle below the best fit line in Figure 3.6).

For investigation of the influence of shear stress duration above critical  $\tau$  threshold for erosion, relative scour depth values were plotted against the number of flow events above critical

flow using the simulated flow data (Figure 3.7). In this analysis, three distinct zones were identified. Higher relative scour depths were observed inside the enclosed area “A” compared with the enclosed area “B”. As expected, lower relative scour depths were observed for the stream sites with higher  $\tau_c$  and higher cohesion values at lower number of flow events above the critical flow (area “B” of Figure 3.7). However, in the area “C” in Figure 3.7, the influence of both the flow duration and the time of scour depth measurement were identified. It was observed that for higher relative scour depth data, several continuous flow events were observed during the scour depth measurement periods (diamond-shaped points, Figure 3.7), consequently higher relative scour depth values were observed. Conversely, short duration and isolated flow events above a critical value showed lower relative scour depths though the number of flow events was higher (square points in Figure 3.7). These observations were supported by other studies for fluvial erosion process of cohesive earthen material (Costa and O'Connor, 1995; Julien and Torres, 2006; NRCHP, 2012).

The combination of number of flow events and the influence of flow duration on scour rate propagation was observed from the Pond Creek data (Figure 3.8). Though cohesion for Pond Creek was high (61.01 kPa) at lower number of effective flow events, relatively higher scour depths were observed during the early age of the bridge. It is hypothesized that channel geomorphology was still adjusting from the local hydrodynamics at the vicinity of the bridge, consequently higher relative scour depths were observed. It was also observed that, scour depths reduced significantly after 1999, even though several continuous high to moderate daily flow events were observed. After 2006, scour rates was reduced significantly. The probable explanation could be the state of equilibrium might have been attained due to the repeated flood events above critical for this bridge site. Observing the evolution of scour depth around the pier of this these bridge and the corresponding flow events, an agreement with the previously stated hypothesis was established, where both the cumulative effective stream power and the number of flow events above critical flow had substantial influence on scour depth propagation in cohesive soils. Flow duration is also found significantly influencing the scour pattern as identified by other studies.



Figure 3.9. Protective wooden logs at the vicinity of the pier in Crooked Creek.

In this study, some limitations were identified to achieve an outcome of a predictive relationship between cumulative effective stream power and an equilibrium scour depth in cohesive sediment beds. They included a lack of channel cross-sectional data over time which could have influenced the critical flow calculation, since one cross-sectional data was used for the calculation by assuming uniform flow depth. Also scour data were collected by several TDOT operators without a standard operating procedure. Further research is needed to development predictive relationships through a well-designed and long-term field study initiated immediately following completion of a constructed bridge.

### 3.5 Conclusion

The influence of shear stress duration for scour prediction in cohesive earthen material around bridge piers was investigated in this study. Cumulative effective stream power is thought to be a surrogate measure to the shear stress duration over a  $\tau_c$  threshold for erosion. Using the in-situ measured  $\tau_c$  values and the recent measured channel geometry data, critical/threshold steam power was computed for the studied stream sites. Calculated erodibility  $K$  index values and the corresponding critical stream power estimates were significantly correlated ( $R^2 = 0.61$ ,  $p = 0.017$ ). Data from this study showed a clear deviation from the Annandale (1995, 2006) developed empirical relationship for soils with erodibility index value less than 0.1. Although these values were fitted in between the 99% and 1% erosion probability lines as suggested by Wibowo et al. (2005) using logistic regression approach. This finding supports the hypothesis that erosion behavior of cohesive sediments should be based on critical stream power calculation rather using an empirical relationship.

It was also hypothesized that the flow duration in association with the cumulative stream power over a scour depth measurement period could have significant impact on scour depth development. Collecting long-term scour depth data from the TODT bridge inventory for the selected nine stream sites this study was conducted. It appeared that cumulative effective stream power showed a reasonable correlation with the observed scour depths around different bridge piers among these stream sites with some localized and site specific variations ( $R^2 = 0.56$ ,  $p < 0.001$ ). Scour depth development in cohesive soils appeared to be dependent on the effective shear stress duration rather than number of flow events above the critical threshold values. The influence of flow history on scour rate propagation in cohesive earth material from multiple flow events was observed from the Pond Creek data where continuous scour depths were recorded from the time of bridge construction.

Overall, it appears that scour depth can be predicted by calculating the critical stream power from the  $\tau_c$  values and channel geometric data. Though, the erodibility index method for scour prediction is not a new concept, cautions should be taken for predicting the critical stream power from empirical relationships for cohesive soils. Findings from this study also suggest further research is needed to investigate the acceptability of effective stream power on the scour depth prediction in a detail continuous monitoring stream site or in a controlled laboratory environment.

## **4.0 Evolution of scour depths Around Cylinder in Natural Cohesive Soil from Multiple Flow Events**

### **4.1 Introduction**

Local scour around bridge piers are dependent on several factors including flow conditions, stream bed material, pier characteristics, and time of scour (Hosny, 1995; Melville and Chiew, 1999; Kwak, 2000; Devi and Barbhuiya, 2017). Many scour studies involving circular bridge piers in non-cohesive soils have been completed by numerous researchers to date. However, very few scour studies focusing on cohesive sediments have been conducted, likely due to the complex erosion behavior of cohesive sediments (Briaud et al., 1999; Molinas and Hosny 1999; Ting et al., 2001; Ansari et al. 2002; Debnath and Chaudhuri, 2010a,b; Debnath and Chaudhuri, 2012; Kothyari et al., 2014). Erosion of cohesive sediments and near bed particles initiate detachment when inter-particle bonds connecting aggregate, floc or individual particle breaks due to the applied stress from the flowing water (Debnath and Chaudhuri, 2010a). Reported scour studies in cohesive sediments have been conducted using the mixture of non-cohesive sediments with clay at different proportions. The presence of clay content (C) and antecedent moisture content (WC) have been reported the most critical parameters on equilibrium scour depths prediction (Molinas and Hosny, 1999; Ansari et al., 2002; Debnath and Chaudhuri, 2010a,b; Debnath and Chaudhuri, 2012).

Scour rates in cohesive soils are slow and represent a fatigue failure behavior compared to non-cohesive sediments represented by an incipient motion theoretical basis, where for cohesive soils it has been reported that it takes several days with multiple flow events for attaining equilibrium scour depths (Briaud et al., 2001; Ting et al., 2001). Several studies identified the influence of flow duration, flow magnitude and flow frequency on erosion behavior in different earth materials for both the bank erosion, fluvial erosion (channel incision) and localized scour around in-stream structures (Wolman, 1959; Costa and O'Connor, 1995; Julian and Torres, 2006; Keaton et al., 2012). These studies on cohesive sediments assumed constant flow velocities however they do not represent a natural stream/river flow hydrograph. The flow hydrograph for a stream shows three parts: a rising limb, a constant peak flow and a falling limb. Based on storm duration and the characteristics of the watershed, the constant peak flow duration may vary and recede afterwards. Therefore, a sequence of low-medium-high flow event sequences or vice versa is expected for a flow hydrograph over the life span of a bridge. It is these multiple flow events that will generate scour around the piers or abutments. Because the scour rate in cohesive soil is typically slow; it is hypothesized that the influence of stress history from multiple flow events could have significant influence on scour depth evolution around bridge piers.

Gudavalli (1997) conducted an experimental study on commercially available pure clay soils to observe the influence of multiple flow events on scour depth evolution around circular bridge piers and developed a conceptual model for ultimate scour depth predictions using two sets of experiments. Later, the method was modified by Briaud et al. (2001). However, in natural sediments, sand, silt, and clay are present at different proportions. In addition to the inherent attractive forces between the clay particles, the biological properties developed over time in the sediments also influence the cohesive characteristics of the cohesive sediments, consequently the erosive behavior (Black et al., 2002; Grabowski et al., 2011). It is nearly impossible to develop the biological parameters in the soil during the experimental period in the laboratory. Therefore, the objective of this study was to observe the evolution of scour depths around a cylinder from

multiple flow events in natural cohesive sediments. The influence of stress history or memory effect was studied using high-flow velocity conditions for laboratory flume experiments.

## 4.2 Experimental Set-up and Procedures

### 4.2.1 Open Channel Flume Construction

For this experimental study, a 12.20 m long, 1.22 m wide and 0.61 m deep outdoor flume was constructed at the University of Tennessee, Knoxville on the ETREC Plant Sciences Unit property (Figure 4.1). The sides and bottom of this flume were constructed with plywood material and a geo-liner was used as a water seal. A test section (1.22-m x 1.22-m x 0.3-m) was constructed 8.23 m downstream from the flume entrance (Figure 4.1). Water was pumped from a nearby slough using a 6-inch suction pump with a 0.13 m<sup>3</sup>/s maximum flow capacity (United Rental, Inc.). The desired flow velocity was maintained with the variable control system attached to the pump. The slope of the flume was kept constant at 0.85%.

### 4.2.2 Properties of Natural Cohesive Sediment

In this experimental study, natural cohesive sediments were used for each flow condition. The sediment samples were collected from Crooked Creek, Shelby County, Tennessee. The geological properties of this stream site are described in detail in Mahalder et al. (2018). In-situ WC and bulk density (BD) were 23.82% and 2.04 gm/cm<sup>3</sup>, respectively, which were measured for the undisturbed condition prior to collecting the soil sample. The details of other soil properties are reported in Table 4.1. The natural cohesive soil has approximately 72% silt and 25% clay. A standard proctor test was conducted on the collected soil after remolding, which showed that the maximum density was attained at a much lower WC than the field WC. Replicating the exact in-situ soil conditions (e.g., in-situ density at the in-situ WC) is difficult given the variations of physical properties between remolded and in-situ soils. Therefore, the test sediment beds were prepared by targeting the desired BD values measuring the corresponding WC values rather than compacting the soil to the optimum water content.

### 4.2.3 Flume Sediment Bed Preparation

Three different compaction efforts were applied to prepare the sediment beds for the experiments. For matching the field BD of the sediment bed, water was spread over the dry soil and covered for 24 hours hydrate the soil uniformly. The moist soil was then placed in the test chamber (box) and compacted in three approximately equal lifts. Each lift was compacted with a 25.4 cm x 25.4 cm cast iron tamper dropped manually ~30 cm above the lift surface. After compaction, a 16 kg roller was used to smooth out the surface and avoid any possible kneading in the soil for attaining desired BD. Two core samples were collected from each lift for WC and BD measurements using the standard method. A 101.6-mm diameter clear Plexiglass cylinder was inserted in the middle of the test section. Figure 4.2a shows the locations of vertical graduated tank tape strips glued to the inner surface of the cylinder at different circumference locations (counter-clockwise: 0° (front), 45°, 90° (right side), 135°, 180° (back), 270° (left side), 225°, and 315°) for periodic scour depth measurements.

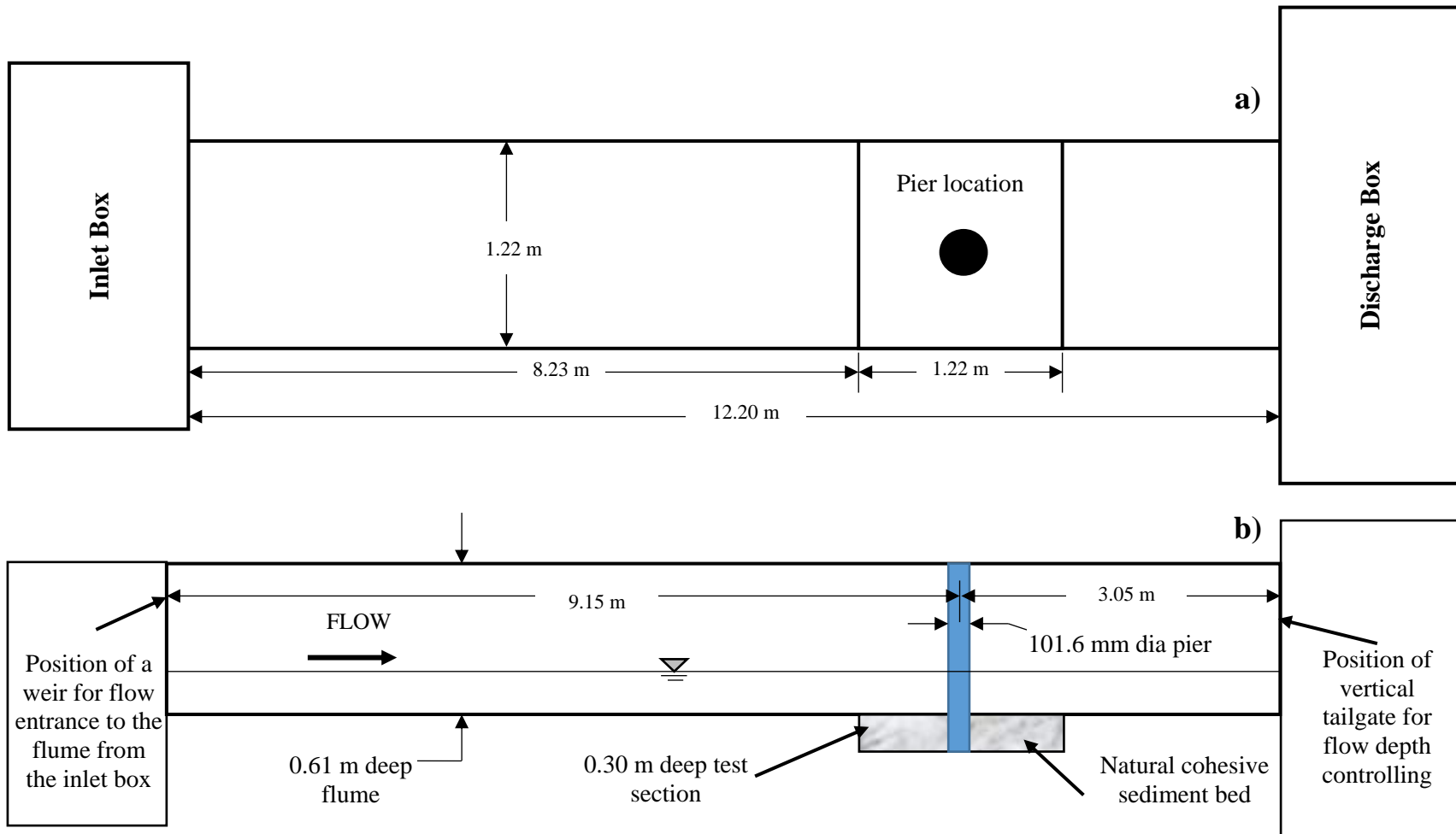


Figure 4.1. Detail of the flume: a) plan view, and b) long section of the flume (not to scale).

Experiments were also conducted on sediment beds with three other BD values:  $BD = 1.81-1.86 \text{ g/cm}^3$ ,  $BD = 1.69-1.71 \text{ g/cm}^3$  and  $BD = 1.52-1.56 \text{ g/cm}^3$ . For the first set of targeted BD values, the soil was mixed thoroughly by hand by adding water and then placing the moistened soil into the test section. The soil was then compacted using the tamper for attaining the desired BD. The low density sediment bed was prepared by adding more water to the soil and compacting by hand using a wooden board to achieve the target density. The sediment beds were compacted in three lifts.

Table 4.1. Properties of Crooked Creek sediment.

Soil Properties and Units	Value
Median grain size ( $\mu\text{m}$ )	12.00
Liquid limit, LL	29.00
Plastic limit, PL	18.95
Plasticity index, PI	10.05
In-situ moisture content	23.82
In-situ cohesion (kPa)	67.56
Sand %	3.00
Silt %	72.00
Clay %	25.00
Clay activity	0.41
Specific surface area ( $\text{m}^2/\text{g}$ )	46.49
Sodium adsorption ration (SAR)	5.34
Potassium intensity factor (KIF)	0.07
Field bulk density, BD ( $\text{gm/cm}^3$ )	2.04
Specific gravity	2.658
Geometric standard deviation ( $\sigma_g$ )	9.83

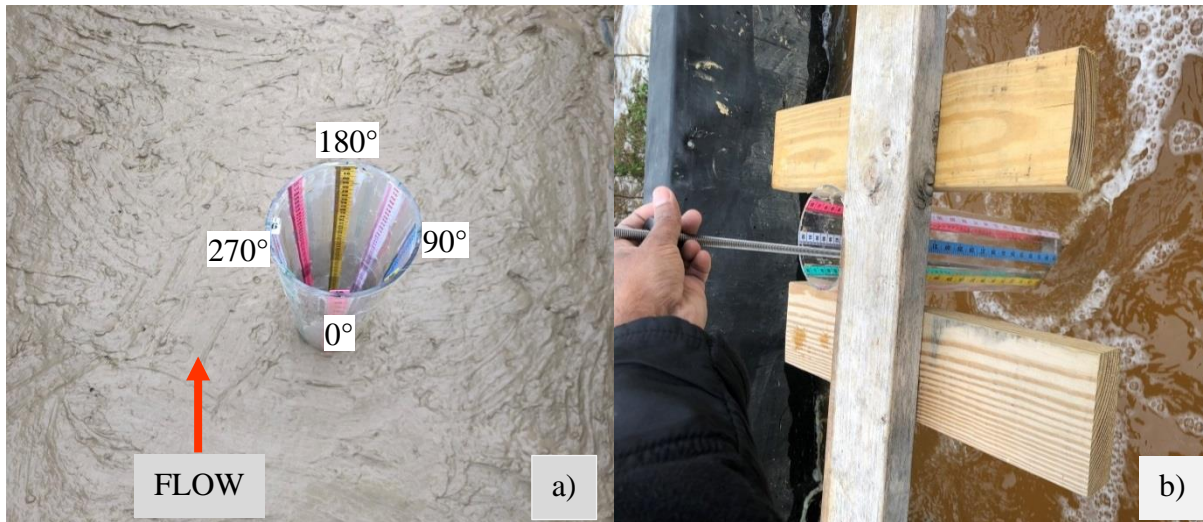


Figure 4.2. a) Prepared sediment bed with the Plexiglas circular pier, b) placement of underwater camera during experiments for periodic scour depth measurement.

After preparing the sediment bed, the critical shear stress ( $\tau_c$ ) was measured at two downstream locations using a mini-jet device following the procedure described in Mahalder et al. (2018). Soil shear strength was also measured using a hand-held vane shear instrument (E-286 Inspection Vane, Omnimetrix, Canada) at four to five locations (ASTM D2573). The top surface of the prepared sediment bed was levelled gently by hand using a trowel. The prepared sediment bed was then kept covered for 16-24 hours before starting a test. For each experimental set-up a fresh sediment bed was prepared following similar procedures (Table 4.2).

#### 4.2.4 Experimental Procedures

In this experiment, shallow water condition ( $h/D = 1.50$ ) was maintained for attaining higher velocities during experiments. During the trial run, it was identified that at least 70 cm/s depth average velocity was required for observing any scour depth over 12 hours. For attaining flow velocities higher than 70 cm/s, 15.25 cm water depth was maintained throughout the experiments at subcritical flow condition by controlling the tailgate height. Since the flume boundary was smooth, the mean velocity profile was approximated by the log law (Nezu and Nakagawa, 1993). A handheld SonTek/YSI ADV (Version 2.5) was used for velocity measurements at different points during the experiments. Depth average mean velocity was approximated by measuring the velocity using the handheld ADV at 0.2y and 0.8y depths and averaging the values (e.g., Ting et al., 2001; Debnath and Chaudhuri, 2012). Velocity distributions with depth for three different flow conditions are presented in Figure 4.3.

Table 4.2. Experimental conditions in the open channel flume.

<b>Experiment Set-up</b>	<b>Run No</b>	<b>Flow Condition</b>	<b>Flow velocity (cm/s)</b>	<b>Duration (Hours)</b>	<b>BD (gm/cm<sup>3</sup>)</b>	<b>WC</b>
<b>1</b>	1	Low	81.25	36	2.04	25.31
	2	High	102.20	36	2.03	25.31
<b>2</b>	3	Low	79.98	12	1.84	30.16
	4	Medium	89.41	12	1.84	30.16
	5	High	100.34	12	1.84	30.16
<b>3</b>	6	Low	80.40	12	1.71	37.86
	7	Medium	91.25	12	1.71	37.86
	8	High	100.60	12	1.71	37.86
<b>4</b>	9	High	102.40	12	1.86	31.25
	10	Medium	90.26	12	1.86	31.25
	11	Low	80.36	12	1.86	31.25
<b>5</b>	12	High	101.40	12	1.69	38.12
	13	Medium	89.52	12	1.69	38.12
	14	Low	80.10	12	1.69	38.12
<b>6</b>	15	Low	81.25	36	1.81	31.24
<b>7</b>	16	Low	80.68	36	1.56	37.45
<b>8</b>	17	High	99.89	36	1.83	30.65
<b>9</b>	18	High	100.26	36	1.52	37.90

Note: Approach flow depth,  $h = 15.25$  cm and cylinder diameter = 10.16 cm

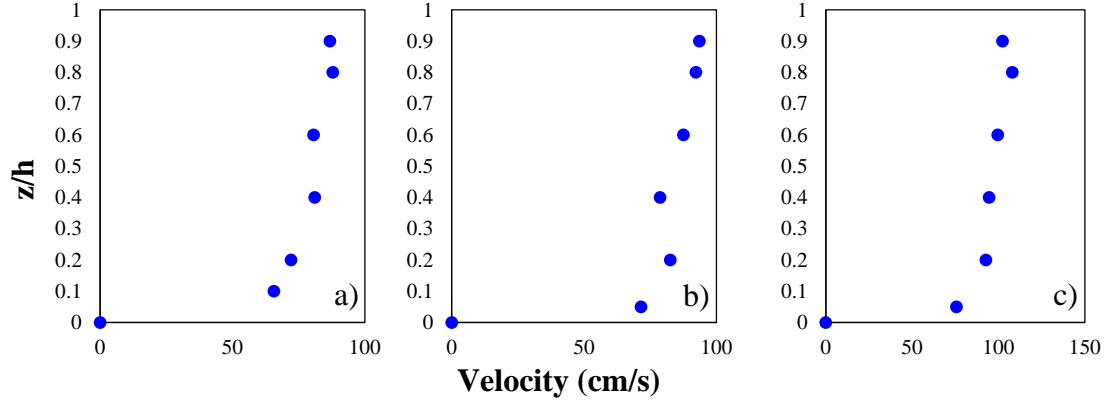


Figure 4.3. Velocity distribution with depth: a) low flow (run no. 3), b) medium flow (run no. 4), and c) high flow (run no. 5).

The goal of this experiment was to observe the scour depth evolution under multiple flow conditions using different flow stage sequences. During each experiment, flow depth was monitored throughout the experimental run using graduated tape attached to the sides at different locations of the flume. For the above mentioned BD conditions, four flow velocity sequences were used in this experimental study as presented in Table 4.2. A total of 18 experimental runs were conducted comprising nine different scenarios using natural cohesive soil. During each experiment, an underwater camera was used for taking periodic pictures and videos of scour depths on the graduated tapes attached inside the cylinder. After finishing each experimental run, the water was drained out from the scour hole and the detail measurements were conducted using a point gage mounted on the top of the flume.

#### 4.2.5. Available Equilibrium Scour Depth Prediction Equations for Cohesive Soil

Several equations are available for equilibrium scour depth prediction in cohesive soils. Those equations were developed with different flow and soil conditions using commercially available clay or mixture of clay-sand at different proportions. From those studies, it was identified the relative slowness in scouring processes compared with non-cohesive soils. Contradictory findings have been reported on equilibrium scour depths prediction. Some of those studies reported similar maximum scour depths for both non-cohesive and cohesive sediments under similar flow conditions, whereas some studies reported lower or even higher maximum scour depths for cohesive soils compared to non-cohesive soils.

Molinas and Hosny (1999) developed equations for estimating geometric dimensions of scour hole and maximum scour depths based on the observed scour volume using three sets of laboratory flume experiments. They proposed an equation for clay-sand mixture with less than 31% clay-silt proportions:

$$\frac{y_s}{D} = 18.92 \left( \frac{F_r^{2.08}}{(1+C)^{1.88}} \right) \quad (4.1)$$

where,  $y_s$  is the maximum scour depth,  $D$  is the pier diameter,  $C$  is the fraction of cohesive soil, and  $F_r$  is the Froude number, which should be in between 0.18-0.33.

Briaud et al. (1999) introduced a new method for scour prediction in cohesive soils by introducing the time dependent scour depth prediction using a hyperbolic equation. In this

method, maximum shear stress at pier was calculated and based on the value initial erosion rate is estimated from erosion function apparatus (EFA) tests. Later, a generalized curve was developed based on different soil types to predict the initial erosion rate for different maximum shear stress ( $\tau_{max}$ ) values at pier. The proposed equation for estimating  $\tau_{max}$  value is:

$$\tau_{max} = 0.094\rho V^2 \left( \frac{1}{\log R_p} - \frac{1}{10} \right) \quad (4.2)$$

where,  $\tau_{max}$  is the maximum shear stress at the pier.  $\rho$  is the density of water,  $V$  is the approach flow velocity, and  $R_p$  is the pier Reynolds number. The time-dependent scour depth was then calculated using the following formula:

$$y_t = \frac{t}{\frac{1}{z_i} + \frac{t}{y_s}} \quad (4.3)$$

where,  $t$  is the time of scour,  $z_i$  is the initial erosion rate calculated using the  $\tau_{max}$  value, and  $y_s$  is the maximum scour depth calculated using the following functional relationship with  $R_p$ :

$$y_s = 0.018R_p^{0.635} \quad (4.4)$$

This method is applicable for circular pier with deep water condition and constant flow velocity. Considering the flow variation in natural streams, this method was later modified by Briaud et al based on series of experiments.

Briaud et al (2001) modified the equation for incorporating the influence of shallow water effect, attack-angle effect, pier shape effect and pier spacing effect. The modified equations of maximum shear stress and maximum scour depth with the correction factors are as follows:

$$\tau_{max} = k_w k_{sp} k_{sh} k_a 0.094\rho V^2 \left( \frac{1}{\log \frac{Vb}{v}} - \frac{1}{10} \right) \quad (4.5)$$

$$y_s = k_w k_{sp} k_{sh} 0.018R_p^{0.635} \quad (4.6)$$

where,  $b$  is the projected pier width perpendicular the flow,  $k_w$ ,  $k_{sp}$  and  $k_a$  are the correction factors for shallow water, pier spacing and angle of attack, respectively.

$$k_w = \begin{cases} 0.85 \left( \frac{h}{b} \right)^{0.34} & \text{for } h/b < 1.62 \\ 1 & \text{for } h/b > 1.62 \end{cases} \quad (4.7)$$

Debnath and Chaudhuri (2010 a,b, 2012) conducted series of flume experiments on clay-sand mixed sediment at different WC and clay content condition. Based on the experimental data, Debnath and Chaudhuri (2010a) proposed regression equations to estimate the dimensionless maximum scour depth at circular pier founded in clay sand mixed bed:

$$\hat{y}_s = 2.05F_{rp}^{1.72} C^{-1.29} \hat{t}_s^{-0.37} \text{ for } WC = 20 - 23.22\% \text{ and } 20\% \leq C \leq 85\% \quad (4.8)$$

$$\hat{y}_s = 3.64F_{rp}^{0.22} C^{-1.01} \hat{t}_s^{-0.69} \text{ for } WC = 27.95 - 33.55\% \text{ and } 20\% \leq C \leq 50\% \quad (4.9)$$

$$\hat{y}_s = 20.52F_{rp}^{1.28} C^{0.19} \hat{t}_s^{-0.89} \text{ for } WC = 27.95 - 33.55\% \text{ and } 50\% \leq C \leq 100\% \quad (4.10)$$

$$\hat{y}_s = 3.32F_{rp}^{0.72} C^{-0.62} WC^{0.36} \hat{t}_s^{-0.29} \text{ for } WC = 33.60 - 45.92\% \text{ and } 20\% \leq C \leq 70\% \quad (4.11)$$

$$\hat{y}_s = 8F_{rp}^{0.61} C^{0.58} WC^{1.24} \hat{t}_s^{-0.19} \text{ for } WC = 33.60 - 45.92\% \text{ and } 70\% \leq C \leq 100\% \quad (4.12)$$

where.  $\hat{y}_s$  is the non-dimensional maximum scour depth ( $\hat{y}_s = \frac{y_s}{D}$ ),  $F_{rp}$  is the pier Froude number,  $C$  is the clay content,  $\hat{\tau}_s$  is the non-dimensional bed shear stress  $\hat{\tau}_s = \frac{\tau_s}{\rho V^2}$ , and  $\tau_s$  is the vane shear strength of the soil.

Briaud et al. (2011) updated the pier scour equation for cohesive material by incorporating the critical velocity for initiation of erosion, which was added to Hydraulic Engineering Circular No. 18 (HEC-18, 2012) and expressed as:

$$y_s = 2.2K_1K_2D^{0.65} \left( \frac{2.6V - V_c}{\sqrt{g}} \right) \quad (4.13)$$

where,  $y_s$  is the maximum scour depth,  $K_1$  and  $K_2$  are the correction factors for pier shape and angle of attack, respectively,  $D$  is the pier diameter,  $V$  is the flow velocity,  $V_c$  is the critical flow velocity for scour initiation, and  $g$  is the gravitational acceleration. However, for calculating the time dependent development of scour depth, Equation 4.3 should be used.

Equations for maximum scour depth prediction only were developed by Milonas and Hosny (1999) and Debnath and Chaudhuri (2010a). Briaud et al. (2001, 2011) equations considered the time dependent scour development in addition to the maximum scour depth prediction. In the later stage, a generalized curve developed by Briaud et al. (2011), which was used for estimating initial erosion rate ( $z_i$ ) based on soil type. However, they recommended applying to the EFA for developing erosion rate curve for a tested soil. In this study, the observed scour depths from each flow events were compared with the predicted scour depths using the hyperbolic time dependent scour formula developed by Briaud et al (1999). The HEC-18 equation was also used for maximum scour depth prediction with the experimental condition to observe the possible variations among these sets of equations.

## 4.3 Results and Discussion

### 4.3.1 Scour Depth Evolution

Periodic scour depths measurements around the cylinder showed that for each experimental run, scour initiated at the sides of the cylinder. It was also observed that maximum scour developed at the sides except for one scenario (experimental set #4), where maximum scour depth was observed between 45° and 90° of the cylinder (Table 4.3). Similar findings have been reported in the literature from other studies (Ting et al., 2001; Debnath and Chaudhuri, 2010a,b; Chaudhuri and Debnath, 2013). Since all of the experiments were conducted in shallow water depth, faster scour depth was expected (Briaud et al., 2001). Experimental results from this study also demonstrated that the progression of scour depths were dependent on the BD values. It was observed that in the wake zone (downstream side of the cylinder), the lateral and transverse extent of the scour hole was much higher compared with other sides of the cylinder (Figure 4.4). Further analyzing the scouring processes around the cylinder, it was identified that scouring initiated at the sides and gradually propagated either upstream or downstream directions for all cases. Overall, scour depths at the nose of the pier (0°) were higher compared with the scour depths at the wake zone (180°) for each experimental condition.

Ting et al. (2001) reported that at lower pier Reynold ( $R_d$ ) numbers the scour depth at downstream and upstream side of pier is similar, whereas for higher  $R_d$  numbers, downstream side scour depth is compared more with the upstream side. However, Debnath and Chaudhuri (2010a) reported that this hypothesis was not always valid. They argued that in addition to the  $R_d$

values,  $\tau_{max}$  (calculated using Equation 4.5) has strong influence on the scour depth propagation towards either the downstream or the upstream direction of cylinder.

In this experiment  $\tau_{max}$  values were significantly higher compared with Ting et al. (2001) study and  $R_d$  values were in between 66,265 to 98,087. The scour depths were found propagating more towards the downstream direction of the cylinder at all flow and BD conditions compared to upstream direction. This observation was clearly deviated from the hypothesis developed by Debnath and Chaudhuri (2010a) but followed the Ting et al. (2001) observations for scour hole propagation. However, higher scour depths were observed at the nose of the cylinder compared with back side of the cylinder. It was hypothesized that since the flow depth was shallow, the horse shoe vortex was not fully developed. The upstream turbulent flow was also forcing the vortex to move around the downstream side of the pier; consequently the soil layer was removed from a wider downstream area compared with other locations (Figure 4.5).

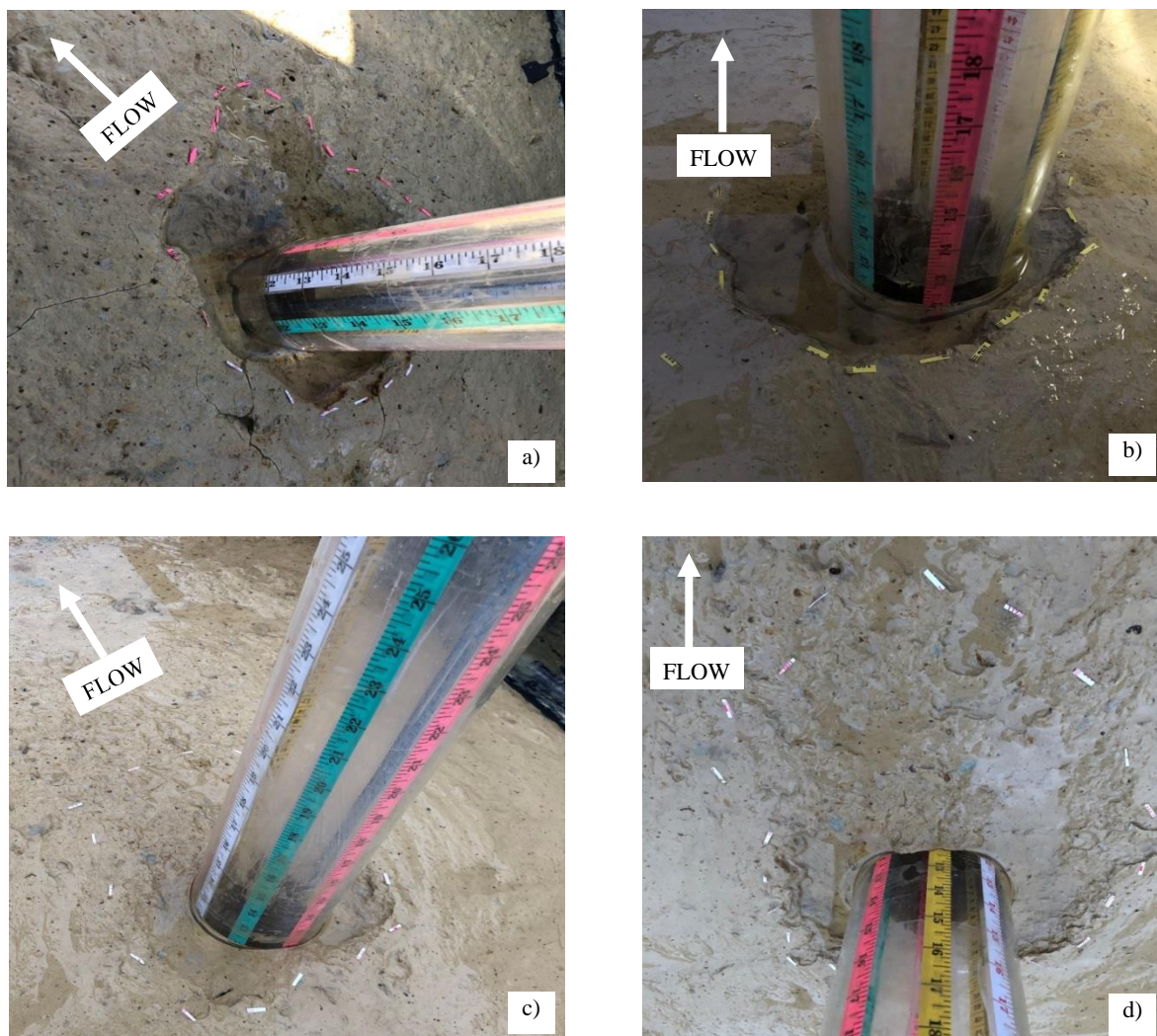


Figure 4.4. Scour hole development for: a) run 16,  $V = 80.68$  cm/s,  $WC = 37.45\%$ , b) run 14,  $V = 80.10$  cm/s,  $WC = 38.12\%$ , c) run 10,  $V = 90.26$  cm/s,  $WC = 31.25\%$ , and d) run 9,  $V = 102.40$  cm/s,  $WC = 31.25\%$ .



Figure 4.5. Scour hole development and the soil removal erosion pattern at the wake zone of the pier: run 14,  $V = 80.10$  cm/s,  $WC = 38.12\%$ .

It is important to note that the behavior of cohesive sediment likely influenced the scour propagation during the experiments. In this study, natural cohesive sediments were used and it was expected cohesion developed more rapidly in the test soils than if the commercially available completely-remolded clay soils were used.

Analyzing the scour depth data around the cylinder, it was observed that scour depths did not propagate at the same rate along the entire experiment duration (Table 4.3). Both down-cutting and widening in scour holes were observed with time rather than deepening at the same location. It was hypothesized that a pressure gradient and uneven shear stress distribution in the scour hole influenced scour-hole growth. The maximum scour hole developed at one side of the cylinder after initial flow condition influenced the scour propagations on the adjacent side of the cylinder during intermediate flow conditions. Higher scour depth readings were recorded at different attached graduated tape positions rather than in the same position as during deep scour-hole formation. This observation was identified as a dynamic process as for the next flow condition higher scour depth was recorded at the previous maximum scour depth position. It was also envisaged that if another set of flow sequences were applied, similar scenarios would be observed. However due to the some constrains, another set of flow sequences was not tested in this experiment, which has been suggested for future research to more fully understand the scour behavior in cohesive soils adjacent to bridge piers.

#### 4.3.2 Influence of Multi-flow on Scour Propagation

Similar to non-cohesive sediment, previous research on bridge scour has been conducted with a single flow event without considering a sequence of flow events. In nature during the design life of a bridge, it is expected that a bridge structure to experience multiple flow events above critical with different magnitudes, frequency and duration. It is expected that scour depth development could be affected by the sequence of different flow events. Briaud et al. (2001) studied and reported the significance of multi-flow events based on two laboratory experiments in commercially available clay material. They developed a hyperbolic equation for predicting the time dependent scour depth for different flow events as discussed in the previous section. In this study, two sequences of flow events were used: i) Low-Medium-High (L-M-H), and ii) High-

Medium-Low (H-M-L) on different soil BD conditions (Table 4.2). Results from this experimental study showed that flow sequence had notable influence on scour depth evolution for different soil BD conditions (Figure 4.6).

Table 4.3. Scour depth development around circular pier for different flow and soil condition.

Run No	Location of max scour depth		Observed scour depth around the sides of pier (cm)									Lateral extent of scour hole around the pier, $x_L$ (cm)							
	After each flow	End of test	0°	45°	90°	135°	180°	225°	270°	315°	0°	45°	90°	135°	180°	225°	270°	315°	
1	90°	90°	0.50	1.40	2.20	2.00	1.20	0.60	0.60	0.30	4.57	7.62	11.43	5.08	10.16	3.81	4.10	4.57	
2	90°	270°	0.50	2.90	3.10	3.00	1.10	1.50	1.00	1.60	3.60	7.25	9.80	10.26	17.00	12.25	5.60	6.25	
3	90°		0.20	0.60	0.70	0.40	0.40	0.60	0.60	0.40	2.60	2.51	2.60	3.50	6.60	3.60	2.40	3.20	
4	270°	90°	1.00	1.30	0.90	1.10	0.30	0.80	1.40	1.00	2.70	3.20	3.00	3.50	7.12	4.00	3.60	3.50	
5	90°		0.50	1.50	2.50	1.30	0.80	0.80	2.20	1.40	3.50	5.00	4.00	4.00	8.15	7.25	4.20	4.00	
6	45°		1.70	3.10	1.90	0.20	0.50	0.50	1.70	1.20	3.00	4.50	3.00	4.50	4.00	8.00	6.00	3.00	
7	270°	45°	0.40	0.70	0.90	1.30	0.50	1.00	1.50	0.90	3.00	4.50	6.00	8.00	14.00	9.00	7.00	5.50	
8	45°		0.70	2.90	1.50	1.20	0.30	1.50	1.00	1.00	4.50	5.00	6.50	11.00	17.00	13.00	8.00	8.00	
9	270°		1.30	1.50	2.00	1.80	1.50	1.50	3.00	2.00	1.50	2.00	3.00	9.00	12.00	4.00	3.00	2.00	
10	90°	270°	0.20	1.00	1.00	1.10	0.90	1.60	0.60	1.00	4.00	2.50	5.00	14.00	23.00	8.00	6.00	4.00	
11	270°		0.30	1.20	0.80	0.80	1.00	1.40	1.50	0.90	4.50	4.60	6.50	14.00	23.00	8.50	6.50	4.60	
12	270°		2.10	3.50	4.00	0.70	1.20	2.00	4.30	4.20	4.00	2.00	2.60	6.00	9.00	8.00	6.00	5.00	
13	90°	90°	0.20	0.70	1.10	1.00	0.30	1.00	1.00	1.00	5.00	2.00	3.50	11.00	11.00	9.00	7.00	6.00	
14	90°		1.00	0.50	2.20	1.50	0.70	1.00	0.70	0.50	5.00	3.00	6.00	12.00	12.00	12.00	8.00	6.00	
15	90° and 270°		1.10	2.10	3.20	1.20	1.50	2.10	3.20	2.20	3.50	6.20	8.00	10.80	11.30	8.60	6.20	5.00	
16	90°		2.60	5.80	6.40	3.90	2.70	5.30	4.80	4.80	6.00	10.00	8.50	14.00	9.00	4.50	5.00	4.00	
17	90° and 270°		2.00	3.70	5.30	4.10	2.60	3.00	5.30	3.40	6.00	5.50	11.50	18.50	13.00	12.00	8.00	5.00	
18	90°		4.50	6.80	9.00	8.00	1.40	5.20	6.60	4.80	6.50	9.00	14.00	11.00	7.00	5.00	5.50	5.00	

Note: Approach flow depth,  $h = 15.25$  cm and cylinder diameter,  $D = 10.16$  cm

Regardless of the flow sequence, similar scour depths at the end of experiment set were observed for the natural cohesive soil with BD 1.69-1.86 gm/cm<sup>3</sup>. It was observed that for the H-M-L flow sequence a large jump in the scour depth initially occurred (Figure 4.6a), then scour slowed during for medium flow condition, which was again increased for low flow condition. The scour rate for higher BD soil (1.86 gm/cm<sup>3</sup>) reduced substantially at the end of high flow events. For lower BD soil (1.69 gm/cm<sup>3</sup>), higher scour rate was observed at high flow and reduced significantly for medium flow, which was picked up again at lower flow events.

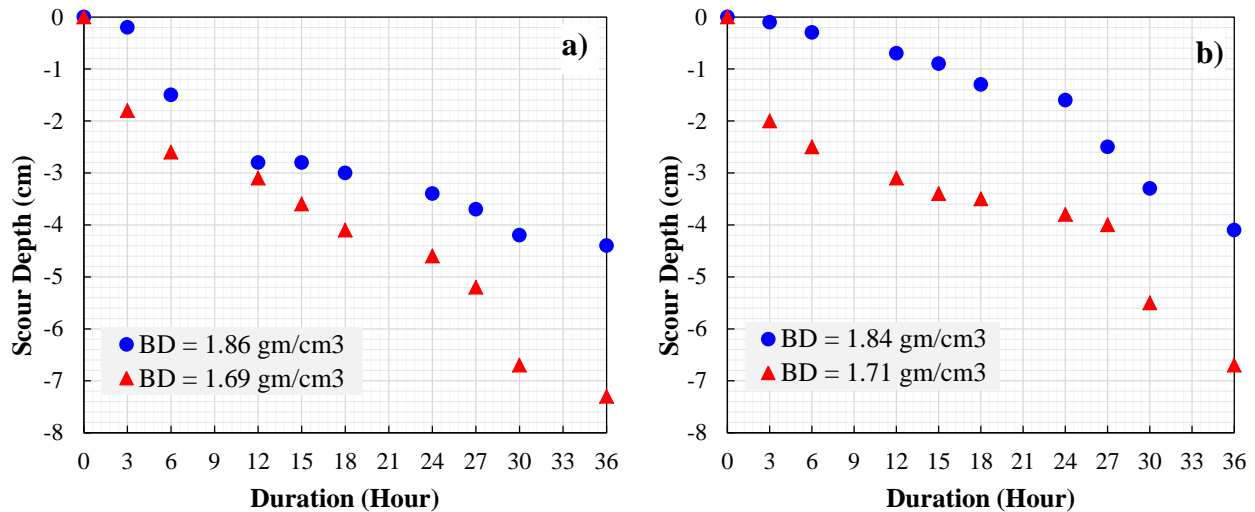


Figure 4.6. The evolution of maximum scour depth: a) for High-Medium-Low (H-M-L) flow sequence at 270° and 90° of the pier, b) for Low-Medium-High (L-M-H) flow sequence at 90° and 45° of the pier.

Scour depth progression over time was studied for very dense natural sediments (BD = 2.03-2.04 gm/cm<sup>3</sup>), medium density (BD = 1.81-1.83 gm/cm<sup>3</sup>) and low density (BD = 1.52-1.56 gm/cm<sup>3</sup>) sediments using low and high flow conditions (Figure 4.7). In this set of experiments, after each 12-hour period the experiment was stopped for scour-hole measurement without disturbing the soil surface and after measurement the experiment was restarted. Temporal scour depth measurements showed that for each soil density condition the scour rates were reduced after 24 hours except for low density soil at high flow conditions (Figure 4.7a).

In case of lower BD conditions (1.51-1.71 gm/cm<sup>3</sup>) scour depths initiated during each flow event condition. Analyzing the recorded videos during experiments, it was observed that for “soft” bed sediments, particle by particle and detachment of aggregates (or flocs) was prominent. As experimental time progressed and the scour holes deepened, the soil saturation played an influential part in removing soil aggregates from the scour hole at higher flow condition. Whereas at lower flow velocities, it was assumed that the erosive capacity of the flowing water was not high enough in the deeper scour hole as very few aggregates were removed per visual observation. Reduction of effective shear stress in the scour hole could have influenced the slower scour rate at low flow velocities. It was assumed that during the lower shear stress conditions more particles were eroded away since smoother scour holes were consequently observed. At high flow velocities the surface of scour hole was rough suggesting the possibility

of aggregate removal. Due to pump capacity, flow sequences (L-M-H and H-M-L) were not used for dense test soils since at low flow no scour was observed after 12 hours of run (Figure 4.7b).

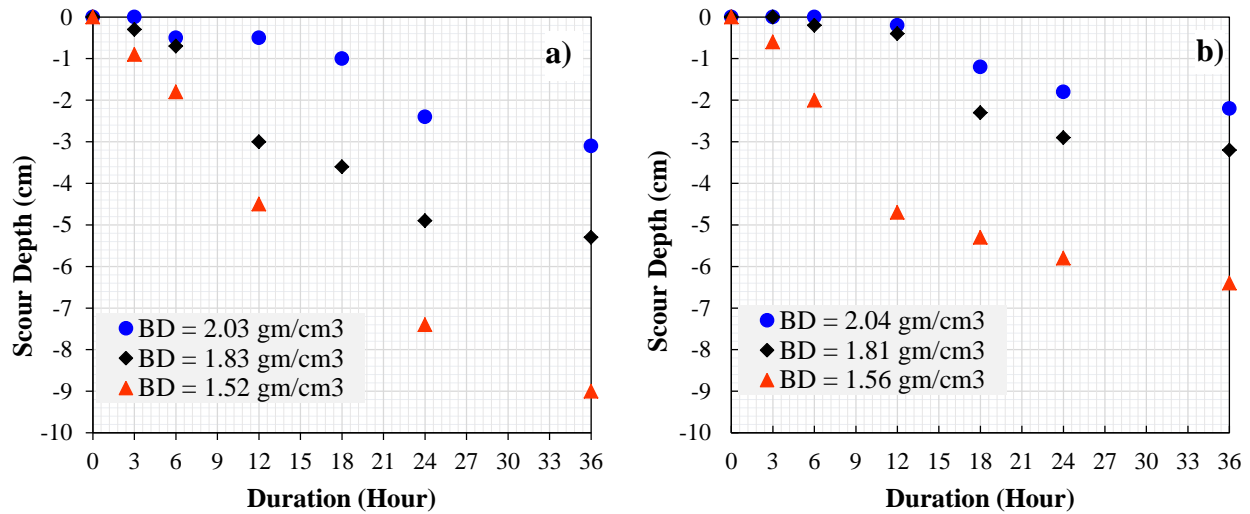


Figure 4.7. The evolution of maximum scour depth: (a) for High-High-High (H-H-H) flow sequence at 270° and 90° of the pier, b) for Low-Low-Low (L-L-L) flow sequence at 90° and 270° of the pier.

#### 4.3.3 Influence of Stress History on Scour Propagation

It has been reported that erosion behavior of soil with high silt-clay content or cohesive sediments is dominated by subaerial processes or excess shear stress duration in the flow hydrograph (Costa and O'Connor, 1995; Julian and Torres, 2006). Though the sediment encroachment and movement around bridge piers and abutments are fundamentally different from the fluvial erosion process, it was expected that the stress history could have influence on the scour propagation around bridge piers. It is interesting to note that the effect of stress history on scour development was observed from these experimental results since scour depths were not visible immediately after starting the experiment for higher BD conditions. Results from this study revealed that scour initiated immediately after starting an experiment for low BD soil, which is reported in the previous section. Soil with higher BD condition (1.81-2.04 gm/cm<sup>3</sup>) scour depth initiation time was found dependent on flow velocity. At lower flow velocity, scour depths were observed usually after 12 hours, whereas at high flow velocity scour depths were observed after 3-6 hours of experimental run.

It was also observed that after the initial scour depth formation, rate of scour slowed down for both the H-M-L and L-M-H flow sequences for each BD condition (from 12-24 hours in Figure 4.6). Scour rate increased significantly after that period regardless of flow condition, though at higher flow velocity sequence greater scour depths were observed for both BD conditions. It was hypothesized that at the end of initial flow condition, some intermediate equilibrium state was attained. During the intermediate flow events, the developed scour hole from the previous flow event was exposed to either higher or lower shear stresses. Previous stress history influenced the scour rate for this intermediate flow condition, though relatively lower scour rates were observed for each BD conditions. In the H-M-L flow sequence, since the

previous stress history was higher, a lower scour rate was observed compared with the L-M-H flow sequence. It was observed that at the end of intermediate flow velocity, scour rate increased again regardless of the flow condition for the last stage of the experiment. It was thought that since the scour hole was exposed to a certain shear stress history for a longer period of time, introduction of higher flow events could have influence the higher scour rate. In each case, both the shear duration and saturation during the experimental period could have influenced the scouring processes. It was also observed that the scour rate was not linear at any stage of the flow sequence.

The influence of repetitive action of shear force due to water velocity on the soil surface for both the low and high flow conditions were observed at field BD condition (2.03-2.04 gm/cm<sup>3</sup>). It was observed that at higher flow velocity, less time was required for aggregate entrainment around the cylinder compared with low flow velocity, where increased time was required. This observation revealed that greater exposure time was required to break inter-particle attractive forces between cohesive sediments at lower flow velocities and vice versa for higher flow velocities. However, soil with lower BD behaved more as non-cohesive sediment particle as scour initiated at the start of the experiment. Using completely remolded sediment could have influenced scour behavior at lower BD since higher WC played role in bed sediment detachment where shear strength was significantly reduced. Hotz and Kovacs (1981) found that clay soils behave as a liquid when thoroughly remolded at field same moisture content. Therefore, scour rate in remolded cohesive soils could be significantly different from the in-situ undisturbed consolidated cohesive soil.

#### 4.3.4 Comparison between Different Scour Depth Equations

Using the flow hydraulics around the cylinder and soil properties, maximum scour depths were estimated using equations from several published studies, including Molinas and Hosny (1999), Debnath and Chaudhuri (2010a), and Briaud et al. (2011), and compared with the HEC-18 equation (Table 4.4). It was observed that all of these equations estimated similar maximum scour depths as HEC-18 equation except the Molinas and Hosny (1999) equation. It is interesting to note that Debnath and Chaudhuri (2010a) estimated equilibrium scour depths were less when the soil shear strength was higher compared with other methods. In other methods, soil properties were not considered for developing maximum scour depth equation except Briaud et al. (2011) equation. Briaud et al. (2001, 2011) considered time-dependency and multi-flow conditions for scour depth estimation using a hyperbolic time dependent formula. Depending on the duration of experimental run and other flow properties, therefore, the scour depths were estimated at each experimental run and compared with the time dependent scour depth equation (Table 4.4).

Results showed that overall the Briaud et al. (2001, 2011) methods predicted higher scour depths reasonably well after each flow condition (Figure 4.8). Further analyzing the data, it was observed that at lower BD conditions (1.51-1.86 gm/cm<sup>3</sup>), the low flow sequence closely predicted the time dependent scour depths in both L-M-H and L-L-L flow sequences. This method using time dependent formula to predict scour depths was deviated mostly for the intermediate flow condition for higher soil BD values. A deviation was observed in this study for the H-M-L flow sequence, though in this sequence at low flow the predicted scour depths were similar between measured and equation prediction. At higher flow conditions, probably the less accurate erosion rates estimated from the generalized curve in Briaud et al. (2011) could have influenced the scour depth estimations (Equation 4.3).

Table 4.4. Comparison of observed and predicted scour depth.

Run No	$\tau_c$ (Pa)	$\tau_s$ (kPa)	Water Temp (°C)	Pier Reynolds No. ( $R_d$ )	Froude No. ( $Fr$ )	Observed max scour from this experiment after each flow (cm)	Total maximum scour after each experiment set (cm)	Estimated scour depth (cm)						
								Molinas and Hosny (1999)	Briaud et al. (2001)		Briaud et al. (2011)		Debnath and Chaudhuri, (2010a)	HEC-18
									After each flow	Max Scour	After each flow	Max Scour		
1	6.65	1.36	16.50	75429	0.743	2.20	2.20	64.16	9.65	23.97	9.77	21.19	13.08	20.61
2	6.52	1.40	17.80	98087	0.934	3.10	3.10	103.38	11.01	28.32	11.23	29.85	9.82	22.75
3	3.85	0.93	15.60	72521	0.731	1.00		62.09	2.15	23.38	2.17	22.93	17.31	20.47
4	3.85	0.93	12.60	74759	0.817	1.30	4.10	78.28	3.13	23.84	3.17	26.82	15.21	21.48
5	3.85	0.93	14.40	88127	0.917	2.50		99.51	4.89	26.46	5.04	31.34	13.31	22.57
6	2.35	0.62	16.50	74640	0.735	3.10		62.76	2.18	23.81	2.20	25.81	29.51	20.52
7	2.35	0.62	12.10	75245	0.834	1.50	6.70	81.67	3.13	23.93	3.22	30.29	30.04	21.67
8	2.35	0.62	10.90	80183	0.920	2.90		100.05	4.84	24.92	5.10	34.15	30.45	22.59
9	3.86	0.96	9.60	78614	0.936	3.00		103.81	4.83	24.61	5.06	32.17	12.72	22.77
10	3.86	0.96	10.20	70509	0.825	2.00	4.40	79.84	3.11	22.97	3.18	27.16	14.73	21.57
11	3.86	0.96	12.10	66265	0.735	1.40		62.70	2.16	22.08	2.17	23.07	16.85	20.51
12	2.10	0.65	14.40	89058	0.927	4.70		101.71	4.90	26.64	5.12	34.99	29.58	22.67
13	2.10	0.65	11.60	72785	0.818	1.30	7.30	78.48	3.12	23.43	3.22	30.09	30.11	21.49
14	2.10	0.65	13.40	68468	0.732	2.50		62.28	2.17	22.54	2.20	26.20	30.53	20.49
15	3.67	0.96	10.20	63470	0.743	2.50	2.50	64.15	5.39	21.48	5.53	23.75	16.63	20.61
16	2.05	0.48	13.40	68964	0.738	3.20	3.20	63.22	5.46	22.65	5.66	26.54	30.33	20.55
17	3.83	1.10	12.60	83522	0.913	5.30	5.30	98.58	9.92	25.58	10.66	31.19	11.91	22.53
18	2.28	0.48	10.60	79228	0.917	9.00	9.00	99.34	10.42	24.73	11.79	34.15	30.46	22.56

Note: Approach flow depth,  $h = 15.25$  cm and cylinder diameter,  $D = 10.16$  cm.

Soil consistency, which is also known as Liquidity Index (LI) is the relative ease to deform soil and dependent on the clay minerals and water content. LI is calculated based on field WC, LL, and PL. If  $LI < 0$ , soil will be brittle fracture if shredded, if  $LI = 0-1$ , is acts as plastic and if  $LI > 1$  it acts as viscous liquid. Soil with  $LI > 1$  is very sensitive to breakdown, though in undisturbed condition the soil is really strong (Hotz and Kovacs, 1981). Henceforth, the behavior of remolded soil could be drastically different from the undisturbed field sample used for scour study. For the natural soil used in this study, the LI value was 0.49, so the soil was classified as plastic. However at low BD conditions, the soil was completely remolded, and consequently affected the erosion behavior and observed higher erosion rates.

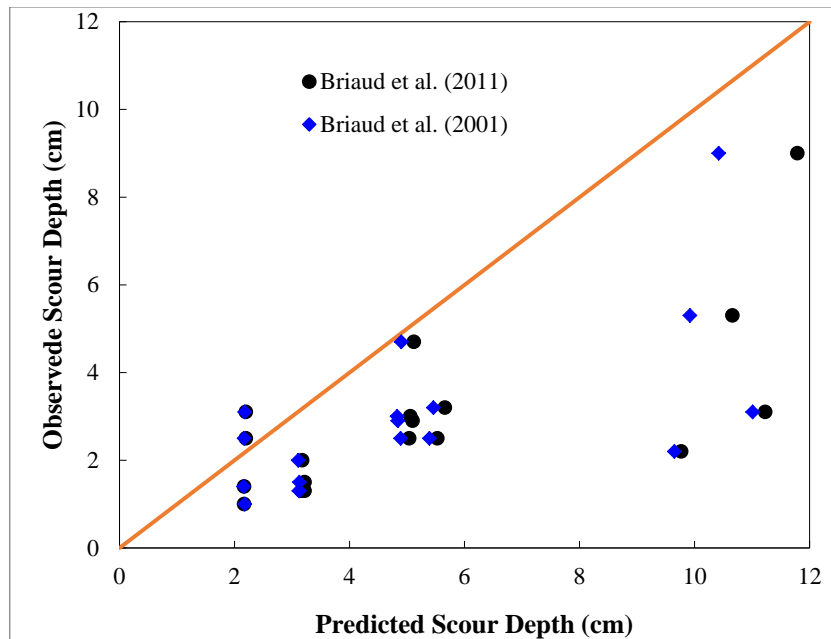


Figure 4.8. Observed and predicted scour depths after each experimental run.

To note, prior to collecting soil samples in-situ mini-jet tests were conducted to estimate average critical shear stress, which ranged between 8.68 to 10.76 Pa. Measured critical shear stresses of the prepared sediment in the test bed chambers (boxes) were measured as 6.52-6.65 Pa, which was comparable to field conditions. This measure also provided information to compare the influence of soil physical properties on scour in other published studies. Briaud et al. (1999, 2001, 2011) and Ting et al. (2001) identified the study design criteria and reported that soil should be tested in EFA for erosion rate measurement. In those studies, ultimate scour depth prediction equations were developed based on the commercially available clay soil, which was remolded completely. However, as we observed that the properties of field soil samples could be significantly different from those commercially available clay soils, consequently the erosion behavior could be different. Debnath and Chaudhuri (2010a) used field soil samples in their study, which was completely remolded and mixed with sand at different proportions at different WC conditions. They did not report any specific scour pattern from their experiments rather only

reported higher shear strength for the field sample. It was expected that variations in shear strength of soil, scour patterns should be different.

#### 4.4 Conclusions

This study reports new data on scour around a vertically-positioned cylinder in natural cohesive sediments under multi-flow conditions. The natural cohesive soil consists of 3% sand, 72% silt, and 25% clay. The influence of multi-flow events on scour evolution, the influence of previous stress history, and the time dependent scour developments were investigated. Contradictory findings have been reported in literature for local scour study around cylinders in cohesive beds, where either pure clay or mixture of clay-sand-gravel was used in those previous studies. Our study suggested that scour commenced at the lateral sides of the cylinder and maximum scour depth also occurred at sides irrespective of flow velocity and BD condition. For each flow and BD conditions both the  $\tau_{max}$  and  $R_d$  values were higher, and larger downstream direction scour propagations were observed. It was also observed that shallow water condition (since  $h/D < 2.0$ ) influenced the lateral and transverse scour-hole formation at the downstream side of the cylinder compared with the sides and upstream of the cylinder.

Scour propagation under multi-flow condition showed that depending on the soil BD conditions, almost similar maximum scour depths were observed for both the L-M-H and H-M-L flow sequence. The rate of scour rate was found dependent on initial flow and BD, where regardless of flow sequence scour rate was always slow at medium flow velocity. It was also observed that at higher BD condition ( $1.81\text{-}2.04 \text{ gm/cm}^3$ ) scour depths initiated after 3-12 hours of flow. Analyzing the time-dependent scour development, it was observed that the available equations over predicted the equilibrium depths. For the field BD condition, those equations were estimating substantially higher scour depths, compared with observed scour depths from this study. This finding identified that the predicted equilibrium depth for this natural cohesive sediment was not similar to the non-cohesive sediments, which was reported by previous studies. Further research through a similar study design specifically targeting more flow events are necessary to better understand the scour development in natural cohesive soils and development of equilibrium scour depth equation. In addition to suggesting a new equation to predict a maximum scour depth at bridge piers in cohesive sediments.

## 5.0 Project Conclusions and Future Recommendations

### 5.1 Summary Conclusions

Erosion behavior in riverine cohesive sediments was investigated through intensive field tests, scour measurements correlated with long-term hydrological modeling at existing bridge sites, and flume experiments. Multiple studies completed in this report support advancing our understanding of erosional processes with cohesive sediments, and support the improvement of the FHWA HEC-18 equations used to predict scour at bridge structures. Field tests were conducted using the mini-jet device developed by the USDA (Hanson and Simon, 2001; Simon et al. 2010; Al-Madhhachli et al. 2013a). Through our field investigations with the mini-jet device it was identified that several factors affected in situ estimations of erodibility parameters, which parameters are based on the excess shear stress equation for cohesive sediments and used in the HEC-18 equations: The factors include: i) device dependent variability, ii) variability related to the device operation in the field and site environmental conditions, iii) variability related to regional sediment characteristics, and iv) soil heterogeneity at some study sites. Scour depth data measured by TDOT staff at selected bridge piers were used to investigate whether the variable ‘cumulative effective stream power’ could be used in a predictive scour model. Long-term hydrological simulations using the HEC-HMS model were used, along with the  $\tau_c$  estimates from the mini-jet device field tests, to compute estimates of ‘cumulative effective stream power’ at the different bridge sites. Experimentation using a large open channel flume with a physical model of a bridge pier investigated local scour depth propagation around a cylinder, in which natural cohesive sediments were uniquely used rather than commercially-obtained and molded test sediments as reported in other studies. General conclusions from these studies, and detailed in Chapters 2 through 4 in this report are summarized as follow.

1. New field operational and computational procedures for the mini-jet device to estimate  $\tau_c$  and  $k_d$  values were developed applying multiple pressure settings (MPS) during a test rather than selecting a single pressure (SPS). Initial use of the device demonstrated variability in  $\tau_c$  and  $k_d$  values as a function of jet operational and data analyses procedures leading to development of the MPS method. The MPS method appears to better reflect fluvial erosion processes along a stream bed and bank, because it applies a more uniform shear stress throughout the jet test, effectively generating depth-averaged  $\tau_c$  and  $k_d$  value accounting for sediment layer differences in cohesion properties from the surficial soil layer into the river bed or bank. The MPS methodology also provided a better control on device field operations and data analysis, and  $\tau_c$  and  $k_d$  estimates are more reflective of riverbed scour near bridge piers.
2. Estimates of  $\tau_c$  and  $k_d$  using a SPS settling with the mini-jet device can be greatly affected by “loose” surficial sediment on the river bed or bank tending to under-estimate  $\tau_c$  and over-estimate  $k_d$ . A reduction factor ( $\alpha$ ) has been suggested by others to be incorporated in the excess shear stress equation for calculating erosion rate to address this issue. The MPS provides a more quantitative approach rather than applying an  $\alpha$  factor, which can only be obtained recursively.
3. Extensive in-situ mini-jet tests among several physiographic provinces with diverse geological formations across Tennessee revealed that no single soil physical-geochemical property, or a common group of properties were able to develop a universal equation for predicting  $\tau_c$  and  $k_d$ . Rather predictive equations for  $\tau_c$  and  $k_d$  were unique among the

Tennessee provinces studied. This finding is significant because it suggests predictive equations need to be developed for each physiographic provinces or geological region in the US to improve the accuracy of  $\tau_c$  and  $k_d$  estimations. In general, the soil physical-geochemical properties of water content (WC) and % finer sediment passing through a #200 sieve (Pass200) dominated as significant variable for  $\tau_c$  prediction. Other soil properties included: cohesion, dispersion ratio, liquid limit, sodium adsorption ratio, and organic content (CC, DR, LL, SAR, and OC) were also found to be dominant variables within the predictive models. To note,  $D_{50}$  was found the least significant variable in predicting  $\tau_c$  for cohesive soils.

4. Device dependent variability was studied for the erodibility parameters ( $\tau_c$  and  $k_d$ ) using a laboratory pressurized conduit flume and the in-situ mini-jet device: Each device has advantages and disadvantages. The laboratory flume requires a sediment sample to be collected from the field, transported, and placed into the flume where sample disturbance is inevitable. The pressured flume generates a velocity profile and hydraulic turbulence structure different than the jet device; however it applies a boundary shear stress more similar physically to what occurs in river flow. The mini-jet device is applied in situ to an undisturbed sample; however, the jet is applied normal to the sediment surface and relies on hydraulic diffusion principles to estimate  $\tau_c$ . In theory, the mini-jet MPS procedure more closely reflects the hydraulics to that in natural river flow and the horizontally-positioned sample in the laboratory flume than the SPS method. Experimental results for  $\tau_c$  estimates were similar between the mini-jet MPS procedure and the conduit flume, but not for  $\tau_c$  when a jet SPS was used. This suggests the above stated hypothesis could be correct and that the MPS procedure may better represent river hydraulics and applied boundary shear stresses. Experimental  $k_d$  estimates were not similar between the two devices, and qualitatively it was observed that  $k_d$  was under-predicts in the conduit flume because eroded sediment aggregates were not accounted for during the test runs.
5. In general, it was identified that  $k_d$  estimations were the most uncertain regardless of the device used, and variability in estimates were due to soil type and moisture content.
6. Continuous reach-scale estimates of shear stress ( $\tau$ ) from the HEC-HMS hydrological model, compared with a bridge site's  $\tau_c$  from the in-situ mini-jet tests provided estimates of a scour duration when the model  $\tau$  exceeded the site  $\tau_c$ . Durations of  $\tau$  estimates exceeding  $\tau_c$  were used, converted into units of stream power, and used to compute cumulative effective stream power. Long-term hydrological flow simulations for nine bridge sites allowed for a statistically correlation of 'cumulative effective stream power' with measured bed scour depth adjacent to the bridge pier. It was identified that cumulative effective stream power correlated with the observed bridge pier scour data suggesting that this variable is significant, and could be used to improve the predictive equation for equilibrium scour depth in cohesive sediments. Scour depth development appeared to be dependent on the effective shear stress duration rather than number of flow events above a  $\tau_c$  threshold. The influence of flow history on scour rate propagation in cohesive bed sediments from multiple flow events was also observed qualitatively.
7. The Erodibility Index ( $K$ ) developed by Annandale ((1995), a surrogate measure to scour resistance of earth materials primarily rock was significantly correlated with critical stream power ( $R^2 = 0.61$ ,  $p = 0.017$ ). For  $K$  values less than 0.1, data from this study deviated from the Annandale (2006) study, where in this study critical stream power was greater for a

specific K value. This finding implied that in-situ measurements of erodibility parameters are necessary for critical stream power calculations rather than relying on a common empirical relationship for all cohesive sediments.

8. Using a large open channel flume, experiments were conducted on field-collected riverine cohesive sediments around a cylinder (physical model of a pier) in a test bed chamber suppressed into the flume bottom and subjected to multi-flow conditions in attempt to mimic more natural scour phenomenon. Based on experimental observations, scour commenced on the sides of the cylinder, and maximum scour depth also occurred at the sides irrespective of flow velocity and BD condition. It was recorded that shallow water conditions (since  $h/D < 2.0$ ) influenced the lateral and transverse scour hole propagation on the downstream side of the cylinder compared with no scour on the sides and upstream of the cylinder
9. Experiments in the open channel flume under multi-flow condition resulted in scour propagation where scour depended on the soil BD conditions. It was observed that at higher BD test sediments ( $1.81\text{-}2.04 \text{ gm/cm}^3$ ) scour depths initiated after 3-12 hours of flow, in contrast to lower BD sediments which initiated earlier. This result suggests that the hypothesis of a memory effect as a function of BD could influence scour propagation in cohesive soils. Similar maximum scour depths were observed for both the low-medium-high (L-M-H) and high-medium-low (H-M-L) flow sequences.
10. Utilizing time-dependent scour data from the open channel flume experiments, HEC-18 equations over-predicted equilibrium depths on field-collected cohesive sediments with higher BD ( $1.81\text{-}20.4 \text{ gm/cm}^3$ ). However, at lower BD sediments ( $1.51\text{-}186 \text{ gm/cm}^3$ ) the observed experimental scour depths were comparable to the depths predicted by the HEC-18 equation. This finding suggested the HEC-18 equation for equilibrium scour depth in cohesive sediment may have been developed using lower BD sediments from commercially obtained materials, nonetheless, it suggests BD needs to be considered for equation improvement.

## 5.2 Limitations and Recommendations

Soil heterogeneity is common when working with natural undisturbed sediments among river beds and banks, consequently variability was expected in this research related to predicting erodibility for cohesive soils. As with most field-based environmental studies having sufficient data to statistically address measurement variability is important. Additional mini-jet test across Tennessee could improve the predictive  $\tau_c$  model developed in Chapter 2. In Chapter 3, the study comparing bridge scour data over time with modeled hydrological history lacked channel cross-sectional data surveyed over time, which likely influenced the critical stream power calculations. Also, scour data collected at bridge by TDOT operators using its bridge inspection manual, but measurements may have not been consistently applied over time in the field and across regions. A long-term study initiated at the time of new bridge construction collecting continuous flow and bed scour measurements would provide the data needed to improve the existing HEC-18 scour equations for cohesive sediment.

Due to resource and time constraints with the large open channel flume experiments, a limited numbers of flow sequences were conducted for the scour experiments. A statistically-valid predictive equation was not able to be developed with the limited data. However, valuable

results with the unique study design utilizing natural cohesive sediments, and evidence suggested that future studies should detail multiple experimental flow sequences and the physical-geochemical properties of the test sediment, particularly bulk density. It was hypothesized that scour of cohesive river beds at bridge piers may be influenced by bedload sediment transport over the bed sediment scour history. Further experiments should couple scour measurements with active bedload transport.

Overall, considering these two key limitations in this study, the following recommendations are proposed for future research.

1. Additional field tests with the mini-jet tester should be conducted to verify the critical shear stress predictive equations among the physiographic provinces in Tennessee.
2. A study should be implemented at several bridge sites with cohesive soils and consistently monitored continuously over time for both the scour depths and flow. Measurements should use specified measurement protocols and allied for the long-term (10-20 years). Scour prediction equations could be improved by such a field study since flume experiments do not always incorporate all the complex hydrodynamic variables that can occur in the natural riverine environment.
3. Additional experiments with the open channel flume should prepare homogenous sediment test beds using natural cohesive sediment, where the test sediments are consolidated to field conditions and placed in a controlled environment to develop cohesion strength from organic matter and soil otter sphere ion charges.
4. Open channel flume experiments should be extended by incorporating more flow sequences and soil types, where prepared sediment should be kept under same field condition for long time for attaining necessary cohesive strengths and consolidation. Test sediments should be characterized for key physical-geochemical properties including CC, DR, LL, SAR, OC, WC, Pass200, and BD. Based on those experiments, scour depth prediction equations could be improved for greater accuracy.

## References

- Abaci O, Papanicolaou AN. 2009. Long-term effects of management practices on water-driven soil erosion in an intense agricultural sub-watershed: Monitoring and modeling. *Hydrological Processes* 23: 2818-2837. DOI: 10.1002/hyp.7380.
- Alizadeh A. 1974. Amount and type of clay and pore fluid influences on the critical shear stress and swelling of cohesive sediments. Ph.D. Dissertation, University of California, Davis, CA, USA.
- Allen PM, Arnold J, Jakubowski E. 1999. Prediction of stream channel erosion potential. *Environ. Eng. Geosci.* 5(3): 339-351.
- Al-Madhhachi AT, Hanson GJ, Fox GA, Tyagi AK, Bulut R. 2013a. Measuring soil erodibility using a laboratory “mini” JET. *Trans. ASABE* 56(3): 901-910.
- Al-Madhhachi AT, Hanson GJ, Fox GA, Tyagi AK, Bulut R. 2013b. Deriving parameters of a fundamental detachment model for cohesive soils from flume and jet erosion tests. *Trans. ASABE* 56(2): 489-504.
- Ansari SA, Kothyari UC, Ranga Raju KG. 2002. Influence of cohesion on scour around bridge piers. *J. Hydraul. Research* 40 (6): 717-729.
- Arulanandan K; Gillogley E; Tully R. 1980. Development of a quantitative method to predict critical shear stress and rate of erosion of natural undisturbed cohesive soils. USACE, Waterways Experiment Station Technical Report, GL-80-5, Vicksburg, MS, USA
- Annandale GW. 1995. Erodibility. *Journal of Hydraulic Research* 33:471-94.
- Annandale GW. 2006. Scour technology: Mechanics and engineering practice. McGraw-Hill, New York, USA.
- Ansari SA, Kothyari UC, Ranga Raju KG. 2002. Influence of cohesion on scour around bridge piers. *J. Hydraul. Res.* 40(6): 717-729. DOI: DOI: 10.1080/00221680209499918.
- Arulanandan K. 1975. Fundamental aspects of erosion of cohesive sediments. *Journal of Hydraulics Division, ASCE* 101(HY5): 635-639, USA.
- Arulanandan K, Gillogley E, Tully R. 1980. Development of a quantitative method to predict critical shear stress and rate of erosion of natural undisturbed cohesive Soils. USACE, Waterways Experiment Station Technical Report GL-80-5, Vicksburg, MS, USA.
- ASTM. 2007. Standard test method for particle-size analysis of soils-ASTM Standard D422. ASTM International, West Conshohocken, PA, USA.
- ASTM. 2009. Standard test methods for laboratory determination of density (Unit Weight) of soil specimens-ASTM Standard D7263. ASTM International, West Conshohocken, PA, USA.
- ASTM. 2010. Standard test methods for liquid limit, plastic limit, and plasticity index of soils-ASTM Standard D4318. ASTM International, West Conshohocken, PA, USA.
- ASTM. 2010. Standard test method for density of soil in place by the drive-cylinder method-ASTM Standard D2937. ASTM International, West Conshohocken, PA, USA.
- ASTM. 2011. Standard practice for classification of soils for engineering purposes (Unified Soil Classification System) -ASTM Standard D2487. ASTM International, West Conshohocken, PA, USA.
- ASTM. 2011. Standard test method for dispersive characteristics of clay soil by double hydrometer-ASTM Standard D4221. ASTM International, West Conshohocken, PA, USA.
- ASTM. 2013. Standard test method for unconfined compressive strength of cohesive soil-ASTM Standard D2166. ASTM International, West Conshohocken, PA, USA.

- ASTM. 2014. Standard test methods for specific gravity of soil solids by water pycnometer- ASTM Standard D854. ASTM International, West Conshohocken, PA, USA.
- Bagnold RA. 1960. Sediment discharge and stream power: a preliminary announcement, U.S. Geological Survey
- Belsley DA, Kuh E, Welsch RE. 1980. Regression diagnostics: Identifying influential data sources and sources of collinearity, Wiley, New York.
- Benedict ST. 2003. Clear-water abutment and contraction scour in the Coastal Plain and Piedmont Provinces of South Carolina, 1996-99. U.S. Geological Survey, Water-Resources Investigations Report 03-4064, Reston, Virginia.
- Benedict ST, Caldwell AW. 2009. Development and evaluation of live-bed pier and contraction scour envelope curves in the coastal plain and piedmont provinces of South Carolina, USA. Geological Survey Scientific Investigations, Report 2009-5099.
- Berlamont JE, Ockenden MC, Toorman EA Winterwerp JC. 1993. The characterization of cohesive sediment properties. *Coastal Eng.* 21(1-3): 105-128.
- Black KS, Paterson DM. 1997. Measurement of the erosion potential of cohesive marine sediments: A Review of Current in situ Technology. *J. Marine Environ. Eng.* 4: 43-83.
- Black KS, Tolhurst TJ, Paterson DM, Hagerthey SE. 2002. Working with natural cohesive sediments. *J. Hydraul. Eng., ASCE* 128(1): 2-8.
- Blaisdell FW, Clayton LA, Hebaus CG. Ultimate dimension of local scour. *J. Hydraul. Division-ASCE* 107(3): 327-337.
- Blaisdell FW, Clayton LA, Hebaus CG. 1981. Ultimate dimension of local scour. *Journal of Hydraulics Division-ASCE* 107(3): 327-337.
- Bonelli S, Brivois O. 2008. The scaling law in the hole erosion test with a constant pressure drop. *International Journal for Numerical and Analytical Methods in Geomechanics* 32: 1573-1595. DOI: 10.1002/nag.683.
- Bonelli S, Golay F, Mercier F. 2012. Chapter 6 - On the modelling of interface erosion. *Erosion of Geomaterials Wiley/ISTE*: 187-222.
- Briaud J, Ting F, Chen HC, Gudavilli R, Kwak K, Philogene B, Han S, Perugu S, Wei G, Nurtjahyo P, Cao Y, Li Y. 2001. SRICOS: Prediction of scour rate at bridge piers. Report 2937-1, Texas Transportation Institute, The Texas A&M University, College Station, Texas, USA.
- Briaud JL, Ting FC, Chen H, Gudavalli R, Perugu S, Wei G. 1999. SRICOS: Prediction of scour rate in cohesive soils at bridge piers. *Journal of Geotechnical and Geoenvironmental Engineering* 125(4): 237-246.
- Briaud JL, Ting F, Chen HC, Gudavalli R, Kwak K, Philogene B, Han SW, Perugu S, Wei GS, Nurtjahyo P, Cao YW, Li Y. 1999. SRICOS: Prediction of scour rate at bridge piers, TTI Report no. 2937-1 to the Texas DOT, Texas A&M University, College Station, Texas, USA.
- Briaud JL, Ting FCK, Chen HC, Cao Y, Han SW, Kwak KW. 2001. Erosion function apparatus for scour rate prediction. *Geochem. J.* 127Z(2): 105-113. DOI: 10.1061/(ASCE)1090-0241(2001)127:2(105).
- Briaud J, Ting F, Chen H, Cao Y, Han S, Kwak K. 2001. Erosion function apparatus for scour rate predictions. *Journal of Geotechnical and Geoenvironmental Engineering* 127:105-113.
- Briaud JL, Chen HC, Kwak KW, Han SW, Ting FCK. 2001. Multiflood and multilayer method for scour rate prediction at bridge piers. *J. Geotech. Geoenviron. Eng.* 127(2): 114-125.

- Briaud JL, Chen HC, Chang KA, Oh SJ, Chen S, Wang J, Li Y, Kwak K, Nartjaho P, Gudaralli R, Wei W, Pergu S, Cao YW, Ting F. 2011. The SRICOS-EFA Method. Summary Report, Texas A&M University, TX, USA.
- Brubaker KL, Ghelardi V, Goodings D, Guy L, Pathak P. 2004. Estimation of long-term scour at Maryland Bridges Using EFA/SRICOS. Maryland Department of Transportation, Final Report, Project SP107B4E, University of Maryland, College Park, MD.
- BS, 1990. British standard methods of test for soils for civil engineering purposes-BS 1377-2. British Standards Institution, Milton Keynes.
- Chang HH. 1979. Minimum stream power and river channel patterns. *Journal of Hydrology* 41:303-327.
- Chaudhuri S, Debnath K. 2013. Observations on initiation of pier scour and equilibrium scour hole in cohesive sediments. *ISH J. Hydraulic Engineering* 19(1): 27-37. DOI: <http://dx.doi.org/10.1080/09715010.2012.749011>
- Chen X. 2012. Matlab code for the LARS algorithm. University of Illinois, Urbana-Champaign, Illinois. <https://publish.illinois.edu/xiaohuichen/code/lars/>
- Clark LA, Wynn TM. 2007. Methods for determining streambank critical shear stress and soil erodibility: Implications for erosion rate predictions. *Transactions of the ASABE* 50(1): 95-106. DOI: <http://dx.doi.org/10.13031/2013.22415>.
- Cook W. 2014. Bridge failure rates, consequences, and predictive trends. PhD Dissertation, Civil and Environmental Engineering, Utah State University, Logan, Utah, USA.
- Cook W, Barr PJ, Halling MW. 2015. Bridge failure rate. *Journal of Performance of Constructed Facilities* 29:04014080. DOI:10.1061/(asce)cf.1943-5509.0000571.
- Costa JE, O'Connor JE. 1995. Geomorphically effective floods. In *Natural and Anthropogenic Influences in Fluvial Geomorphology* 89:45-56.
- Craft T, Graham L, Launder B. 1993. Impinging jet studies for turbulence model assessment-II. An examination of the performance of four turbulence models. *Int. J. Heat Mass Transfer* 36(10): 2685-2697. DOI: [https://doi.org/10.1016/S0017-9310\(05\)80205-4](https://doi.org/10.1016/S0017-9310(05)80205-4)
- Croad RN. 198). Physics of erosion of cohesive soils. PhD Thesis, Department of Civil Engineering, University of Auckland, New Zealand.
- Daly ER, Fox GA, Al-Madhhachi AT, Miller RB 2013. A scour depth approach for deriving erodibility parameters from jet erosion tests. *Trans. ASABE* 56(6): 1343-1351.
- Daly ER, Fox GA, Al-Madhhachi AT, Storm DE. 2015a. Variability of fluvial erodibility parameters for streambanks on a watershed scale. *Geomorphology* 231: 281-291.
- Daly ER, Fox GA, Enlow HK, Storm DE, Hunt SL. 2015b. Site-scale variability of streambank fluvial erodibility parameters as measured with a jet erosion test. DOI: 10.1002/hyp.10547.
- Daly ER, Miller RB, Fox GA. 2015. Modelling streambank erosion and failure along protected and unprotected composite streambanks. *Advances in Water Resources, Special Issue on Fluvial Eco-Hydraulics and Morphodynamics: New Insights and Challenges* 81: 114-127. DOI: 10.1016/j.advwatres.2015.01.004.
- Daly ER, Fox GA, Fox AK. 2016. Correlating site-scale erodibility parameters from jet erosion tests to soil physical properties. *American Society of Agricultural and Biological Engineers, ASABE* 59(1): 115-128. DOI 10.13031/trans.59.11309.
- Debnath K, Nikora V, Aberle J, Westrich B, Muste M. 2007. Erosion of cohesive sediments: resuspension, bed load, and erosion patterns from field experiments. *J. Hydraul. Eng., ASCE* 133 (5): 508-520. DOI: 10.1061/(ASCE)0733-9429(2007)133:5(508).

- Debnath K, Chaudhuri S. 2010a. Bridge pier scour in clay-sand mixed sediments at near-threshold velocity for sand. *J. Hydraul. Eng.* 136 (9): 597-609.
- Debnath K, Chaudhuri S. 2010b. Laboratory experiments on local scour around cylinder for clay and clay-sand mixed beds. *Engineering Geology* 111: 51-61.
- Debnath K, Chaudhuri S. 2012. Local scour around noncircular piers in clay-sand cohesive sediment beds. *Eng. Geol.* 151(10): 1-14. DOI: 10.1016/j.enggeo.2012.09.013.
- Devi YS, Barbhuiya AK. 2017. Bridge pier scour in cohesive soil: a review. *Sadhana* 42 (10): 1803-1819. DOI: <https://doi.org/10.1007/s12046-017-0698-5>.
- Dickhudt PJ, Friedrichs CT, Sanford LP. 2011. Mud matrix solids fraction and bed erodibility in the York River Estuary, USA, and other Muddy Environments. *Continental Shelf Research* 31: S3-S13. DOI: 10.1016/j.csr.2010.02.008.
- Droppo IG, Exall K, Stafford K. 2008. Effects of chemical amendments on aquatic floc structure, settling and strength. *Water Research* 42(1-2): 169-179. DOI: 10.1016/j.watres.2007.06.054.
- Dunn IS. 1959. Tractive resistance of cohesive channels. *Journal of the Soil Mechanics and Foundations, ASCE* 85(SM3, Part 1): 1-24.
- Efron B, Hastie T, Johnstone I, Tibshirani R. 2004. Least angle regression. *Annals of Statistics* 32(2): 407-499
- Federal Highway Administration (FHWA) 2017. National bridge inventory. (<http://www.fhwa.dot.gov/bridge/nbi/ascii.cfm>) (last accessed on February 02, 2018)
- Fleming M, Neary V. 2004. Continuous hydrologic modeling study with the hydrologic modeling system. *ASCE Journal of Hydrologic Engineering* 9(3): 175-183
- Foth, HD. 1990. *Fundamentals of soil science*, 8th Edition. John Wiley & Sons, Canada
- Gerbersdorf SU, Jancke T, Westrich B. 2007. Sediment properties for assessing the erosion risk of contaminated riverine sites. *Journal of Soils and Sediments* 7(1): 25-35. DOI: 10.1065/jss2006.11.190.
- Gibson MM, Launder BE. 1978. Ground effects on pressure fluctuations in the atmospheric boundary layer. *J. Fluid Mech.* 86: 491-511.
- Gillott JE. 1987. *Clay in engineering geology*. Elsevier, Amsterdam.
- Golay F, Lachouette D, Bonelli S, Seppecher P. 2011. Numerical modelling of interfacial soil erosion with viscous incompressible flows. *Computer Methods in Applied Mechanics and Engineering* 200: 383-391. DOI: 10.1016/j.cma.2010.09.002.
- Grabowski RC, Droppo IG, Wharton G. 2011. Erodibility of cohesive sediment: The importance of sediment properties. *Earth Sci. Rev.* 105 (1): 101-120.
- Hanson GJ. 1990a. Surface erodibility of earthen channels at high stresses. I: Open channels testing. *Trans. ASAE* 33(1): 127-131.
- Hanson GJ. 1990b. Surface erodibility of earthen channels at high stresses. II: Developing an in-situ testing device. *Trans. ASAE* 33(1): 132-137.
- Hanson GJ, Simon A. 2001. Erodibility of cohesive streambeds in the loess area of the midwestern USA. *Hydrological Processes* 15: 23-28.
- Hanson GJ; Cook KR. 1997. Development of excess shear stress parameters for circular jet testing. *ASAE Paper No. 97-2227*, St. Joseph, MI, USA.
- Hanson GJ, Cook KR. 2004. Apparatus, test procedures, and analytical methods to measure soil erodibility in-situ. *Appl. Eng. Agric.* 20(4): 455-462.
- Hanson GJ, Robinson KM. 1993. The influence of soil moisture and compaction on spillway erosion. *Trans. ASAE* 36(5): 1349-1352.

- Hanson GJ, Robinson KM, Cook KR. 2002. Scour below an overfall: Part II. Prediction. *Trans. ASAE* 45(4): 957-964.
- Hickin EJ, Nanson GC. 1984. Lateral migration rates of river bends. *Journal of Hydraulic Engineering* 110(11):1557- 1567
- Holtz RD, Kovacs WD. 1981. An introduction to geotechnical engineering. Prentice Hall Inc., Englewood Cliffs, NJ, USA
- Hosny MM. 1995. Experimental study of local scour around circular bridge piers in cohesive soils. Ph.D. Dissertation, Civil Engineering Department, Colorado State University, Fort Collins, Colorado, USA
- Hydraulic Engineering Circular No. 18 (HEC-18) 2012. Evaluating scour at bridges. Fifth Edition, U.S Department of Transportation, Federal Highway Administration, Washington D.C.
- Jepsen R, Roberts J, Lick W. 1997. Effects of bulk density on sediment erosion rates. *Water Air Soil Pollution* 99: 21-31. DOI: <https://doi.org/10.1007/BF02406841>
- Johnson BD, Kranck K, Muschenheim DK. 1994. Physicochemical factors in particle aggregation. In: Wotton, R.S. (Ed.), *The biology of particles in aquatic systems*. Lewis, Boca Raton: 75-96
- Julian J, Torres R. 2006. Hydraulic erosion of cohesive riverbanks. *Geomorphology* 76(1): 193-206. DOI: 10.1016/j.geomorph.2005.11.003.
- Kamphuis JW, Hall KR. 1983. Cohesive material erosion by unidirectional current. *J. Hydraul. Eng.* 109: 39-62.
- Karamigolbaghi M, Ghaneizad SM, Atkinson JF, Bennett SJ, Wells RR. 2017. Critical assessment of jet erosion test methodologies for cohesive soil and sediment. *Geomorphology* 295: 529-536. DOI: <http://dx.doi.org/10.1016/j.geomorph.2017.08.005>.
- Karmaker T, Dutta S. 2011. Erodibility of fine soil from the composite river bank of Brahmaputra in India. *Hydrol. Process* 25: 104-111. DOI: 10.1002/hyp.7826.
- Keaton JR, Mishra SK, Clopper PE. 2012. Scour at bridge foundations on rock. National Cooperative Highway Research Program (NCHRP), Report 717, Transportation Research Board of National Academics, Washington, D.C.
- Keaton JR. 2013. Estimating erodible rock durability and geotechnical parameters for scour analysis. *Environmental & Engineering Geoscience* 19:319-343.
- Khanal A, Fox GA, Al-Madhhachi AT. 2016. Variability of erodibility parameters from laboratory mini jet erosion tests. *J. Hydrol. Eng.* 21(10). DOI: 10.1061/(ASCE)HE.1943-5548.0001404.
- Kirsten H. 1982. A classification system for excavating in natural materials, *Civil Engineering South Africa* 24:293-308.
- Kothyari UC, Kumar A, Jain RK. 2014. Influence of cohesion on river bed scour in wake region of piers. *J. Hydraul. Eng.* 14(1): 1-13.
- Kwak K. 2000. Prediction of scour depth versus time for bridge piers in cohesive soils in the case of multi-flood and layered soil systems. Ph.D. Dissertation, Texas A&M University, College Station, TX, USA.
- Lagasse PF, Schall JD, Johnson F, Richardson EV, Chang F. 1995. Stream stability at highway structures. Rep. No. FHWAIP-90-014 (HEC 20), Federal Highway Administration, Washington, D.C., USA.

- Langendoen EJ. 2000. CONCEPTS-Conservational channel evolution and pollutant transport system, Stream Corridor Version 1.0. U.S. Department of Agriculture, Agricultural Research Service, Oxford, MS, USA.
- Larsen EW, Fremier AK, Greco SE. 2006. Cumulative effective stream power and bank erosion on the Sacramento River, California, USA. *Journal of the American Water Resources Association* 42:1077-1097.
- Layzell AL, Mandel RD. 2014. An assessment of the erodibility of Holocene Lithounits comprising streambanks in northeastern Kansas, USA. *Geomorphology* 213: 116-127. <http://dx.doi.org/10.1016/j.geomorph.2014.01.003>.
- Leopold LB, Wolman MG, Miller JP. 1964. *Fluvial processes in geomorphology*. W. H. Freeman and Company, San Francisco, California, USA.
- Li Y. 2002. Bridge pier scour and contraction scour in cohesive soils on the basis of flume tests. Ph. D. Dissertation, Department of Civil Engineering, Texas A&M University, College Station, TX, USA.
- Lick W, McNeil J, Xu YJ, Taylor C. 1994. Measurements of the resuspension and erosion of sediments in rivers. Rep. Department of Mechanical and Environmental Engineering, University of California, Santa Barbara, CA, USA.
- Lick W, McNeil J. 2001. Effects of sediment bulk properties on erosion rates. *The science of the total environment*, Elsevier 266: 41-48.
- Lick W, Jin LJ, Gailani J. 2004. Initiation of movement of quartz particles. *J. Hydraul. Eng., ASCE* 130 (8): 755–761. DOI: 10.1061/(ASCE)0733-9429(2004)130:8(755).
- Lim SS. 2006. Experimental investigation of erosion in variable saturated clay soils. Ph.D. Dissertation, School of Civil and Environmental Engineering, The Univ. of New South Wales, Sydney, Australia.
- Liou, YD. 1970. Hydraulic erodibility of two pure clay systems. Ph.D. Dissertation, Colorado State University, Fort Collins, CO, USA.
- Lyle W, Smerdon ET. 1965. Relation of compaction and other soil properties to Eerosion resistance of soils. *Transactions of the American Society of Agricultural Engineers* 8(3): 419-422.
- Mahalder B; Schwartz JS; Palomino AM; Zirkle J. 2018a. Relationships between physical-geochemical soil properties and erodibility of streambanks among different physiographic provinces of Tennessee, USA. *Earth Surface Processes and Landforms* 43(2):401-416. DOI: 10.1002/esp.4252.
- Mahalder B, Schwartz JS, Palomino AM, Zirkle J. 2018b. Estimating erodibility parameters for streambanks with cohesive soils using the mini jet test device: A comparison of field and computational methods. *Water* 10(3), 304. DOI:10.3390/w10030304.
- Melville BM, Cheiw YM. 1999. Time scale for local scour at bridge piers. *J. Hydraul. Eng.* 125(1): 59-65. DOI: [https://doi.org/10.1061/\(ASCE\)0733-9429\(1999\)125:1\(59\)](https://doi.org/10.1061/(ASCE)0733-9429(1999)125:1(59)).
- Molinas A, Hosny MM. 1999. Experimental study on scour around circular piers in cohesive soil. Publication No. FHWA-RD- 99-186, Federal Highway Administration, U.S. Department of Transportation, McLean, VA, USA.
- McNeil J, Taylor C, Lick W. 1996. Measurements of erosion of undisturbed bottom sediments with depth. *J. Hydraul. Eng.* 122: 316-324. DOI: [https://doi.org/10.1061/\(ASCE\)0733-9429\(1996\)122:6\(316\)](https://doi.org/10.1061/(ASCE)0733-9429(1996)122:6(316)).
- Mehta AJ, Hayter EJ, Parker WR, Krone RB, Teeter AM. 1989. Cohesive sediment transport. I: Process description. *Journal of Hydraulic Engineering* 115:1076-1093.

- Mercier F, Bonelli S, Pinettes P, Golay F, Anselmet F et al. 2014. Comparison of CFD simulations with experimental jet erosion tests results. *J. Hydraul. Eng.* 140(5). DOI: 10.1061/(ASCE)HY.1943-7900.0000829, 04014006.
- Midgley TL, Fox GA, Wilson GV, Heeren DM, Langendoen E, Simon A. 2013. Streambank erosion and instability induced by seepage: In-situ constant-head experiments. *J. Hydrol. Eng.* 18(10): 1200-1210. DOI: 10.1061/(ASCE)HE.1943-5584.0000685.
- Miller RA. 1974. *The Geologic History of Tennessee: Tennessee Division of Geology, Bulletin 74.*
- Miller JH. 1991. Surficial geology of the Cane Creek Basin, Lauderdale County, Tennessee, U.S. Geological Survey, Water-Resources Investigation Report 90-4139, Nashville, TN, USA.
- Mitchell JK, Soga K. 2005. *Fundamentals of soil behavior.* 3rd Edition, John Wiley & Sons, Inc, Hoboken, New Jersey, USA.
- Molinas A, Jones S, Hosny M. 1999. Effects of cohesive material properties on local scour around piers. *Transportation Research Record*, 1690, Paper No. 99-1275.
- Moore JS. 1997. Field procedures for the head-cut erodibility index. *Transactions of the ASAE* 40:563-574. doi:10.13031/2013.21315.
- Mostafa TMS. 2003. Experimental modeling of local scour in cohesive soils. PhD Dissertation, Dept. of Civil and Environ. Eng., Univ. of South Carolina, Columbia, SC, USA.
- Mostafa TMS, Imran J, Chaudhry MH, Khan IB. 2008. Erosion resistance of cohesive soils. *J. Hydraul. Research* 46 (6): 777-787.
- Morgan RPC. 2005. *Soil erosion and conservation.* Blackwell, Oxford.
- National Engineering Handbook (NEH). 2011. Erodibility parameter selection for soil material horizons (surface detachment coefficient and headcut erodibility index).
- Neitsch SL, Arnold JG, Kiniry JR, Williams JR. 2011. Soil and water assessment tool theoretical documentation version 2009, Texas Water Resources Institute Technical Report No. 406, College Station, TX, USA.
- Nezu I, Nakagawa H. 1993. *Turbulence in open-channel flows.* Balkema, Rotterdam, The Netherlands.
- O'Brien RM. 2007. A Caution regarding rules of thumb for variance inflation factors. *Quality & Quantity*, Springer, 41:673–690. DOI 10.1007/s11135-006-9018-6
- Oh SJ. 2009. Experimental study of bridge scour in cohesive soil. Ph.D. Dissertation, Department of Civil Engineering, Texas A&M University, College Station, TX, USA
- Papanicolaou AN. 2001. Erosion of cohesive streambeds and banks, State Wash. Water Res. Cent. Rep. WRR-08, Washington. State University, Pullman, Washington, USA
- Paterson DM, Black KS. 1999. Water flow, sediment dynamics and benthic biology. *Adv. Ecological Res.* 29: 155-193.
- Perkins RG, Honeywill C, Consalvey M, Austin HA, Tolhurst TJ, Paterson DM. 2003. Changes in Microphytobenthic Chlorophyll a and EPS resulting from sediment compaction due to de-watering: opposing patterns in concentration and content. *Continental Shelf Research* 23: 575-586. [https://doi.org/10.1016/S0278-4343\(03\)00006-2](https://doi.org/10.1016/S0278-4343(03)00006-2)
- Perkins RG, Sun H, Watson J, Player MA, Paterson DM. 2004. In-line laser holography and video analysis of eroded flocs from engineered and estuarine sediments. *Environmental Science & Technology* 38: 4640-4648. DOI: 10.1021/es040011i
- Pierce CE, Gassman SL, Ray RP. 2011. Geotechnical materials database for embankment design and construction. Federal Highway Administration, Final Report. FHWA/SCDOT Report No. FHWA-SC-11-02

- Raudkivi AJ. 1990. Loose boundary hydraulics. 3rd edition, Pergamon Press, New York, USA.
- Ravisangar V, Sturm TW, Amirtharajah A. 2005. Influence of sediment structure on erosional strength and density of kaolinite sediment Beds. *J. Hydraul. Eng.-ASCE* 131(5): 356-365. DOI: 10.1061/(ASCE)0733-9429(2005)131:5(356)
- Regazzoni PL, Marot D. 2011. Investigation of interface erosion rate by jet erosion test and statistical analysis. *EJEC* 15:1167-1185. DOI: 10.3166/EJECE.15.1167-1185
- Roberts J, Jepsen R, Gotthard D, Lick W. 1998. Effects of particle size and bulk density on erosion of quartz particles. *J. Hydraul. Eng.-ASCE* 124(12): 1261-1267. DOI: [http://dx.doi.org/10.1061/\(ASCE\)0733-9429\(1998\)124:12\(1261\)](http://dx.doi.org/10.1061/(ASCE)0733-9429(1998)124:12(1261))
- Richardson EV, Davis SR. 2001. Evaluating scour at bridges. 4th Edition, U. S. Department of Transportation, Federal Highway Administration, Washington D.C.
- Safford JM. 1869. Geology of Tennessee, State of Tennessee, Nashville, USA.
- Sanford LP, Maa JPY. 2001. A unified erosion formulation for fine sediments. *Marine Geology* 179(1-2): 9-23. PII: S0025-3227(01)00201-8.
- Santamarina JC, Klein KA, Wang YH, Prencke E. 2002. Specific surface: Determination and relevance. *Can. Geotech. Journal* 39: 233-241. DOI: 10.1139/T01-077.
- Schwartz JS, Neff KJ, Dworak FJ, Woockman RR. 2015. Restoring riffle-pool structure in an incised, straightened urban stream channel using an ecohydraulic modeling approach. *Ecological Engineering* 78: 112-126. DOI: <http://dx.doi.org/10.1016/j.ecoleng.2014.06.002>.
- Shaikh A, Ruff JF, Wayne CA, Abt SA. 1988. Erosion rate of dispersive and nondispersive Clays. *J. Geotech. Engrg.* 114(5): 589-600.
- Shen HW, Schneider VR, Karaki S. 1969. Local scour around bridge piers. *Proc. ASCE* 95 (6): 1919-1940.
- Shirole AM, Holt RC. 1991. Planning for a comprehensive bridge safety assurance program. *Transp. Res. Rec.* 1290, Transportation Research Board, Washington, D.C.; 137-142.
- Simon A, Collison AJC. 2002. Quantifying the mechanical and hydrologic effects of vegetation on streambank stability. *Earth Surface Processes and Landforms* 27: 527-546.
- Simon A, Thomas RE, Klimetz L. 2010. Comparison and experiences with field techniques to measure critical shear stress and erodibility of cohesive deposits. In *Proceedings of the 2nd Joint Federal Interagency Conference on Sedimentation and Hydrologic Modeling*. U.S. Geological Survey: Reston, VA, USA.
- Simon A, Pollen-Bankhead N, Thomas RE. 2011. Development and application of a deterministic bank stability and toe erosion model for stream restoration. In: Simon, A., Bennett, S.J., Castro, J.M. (Eds.), *Stream Restoration in Dynamic Fluvial Systems*. American Geophysical Union, Washington, D.C., USA.
- Skempton AW. 1953. The colloidal activity of clays. *Proc., 3rd Int. Conf. of Soil Mechanics and Foundation Engineering* 1(1): 57-61.
- Sklar LS, Dietrich WE. 2004. A mechanistic model for river incision into bedrock by saltating bed load. *Water Resources Research* 40:W06301.
- Smerdon ET, Beasley RP. 1959. The tractive force theory applied to stability of open channels in cohesive sediments. University of Missouri, College of Agriculture, Agricultural Experiment Station, Columbia, Mo, USA.
- Smerdon ET, Beasley R. 1961. Critical tractive forces in cohesive Soil. *Agric. Eng.* 42(1): 26-29.
- Stein OR, Nett DD. 1997. Impinging jet calibration of excess shear sediment detachment parameters. *Trans. ASAE* 40(6): 1573-1580.

- Sutarto T, Papanicolaou AN, Wilson CG, Langendoen EJ. 2014. Stability analysis of semicohesive streambanks with CONCEPTS: Coupling field and laboratory investigations to quantify the onset of fluvial erosion and mass failure. *J. Hydraul. Eng.* 140(9). DOI: 10.1061/(ASCE)HY.1943-7900.0000899.
- Tan SK. 1983. Erosion of cohesive soils. PhD Thesis, Department of Civil Engineering, University of Auckland, New Zealand.
- Taylor C, Lick W. 1996. Erosion properties of reat Lakes sediments. Report, Department of Mechanical and Environmental Engineering, University of California, Santa Barbara, CA, USA.
- Thoman RW, Nieggoda SL. 2008. Determining erodibility, critical shear stress, and allowable discharge estimates for cohesive channels: Case study in the Powder River basin of Wyoming. *J. Hydraul. Eng.* 134 (12): 1677-1687.
- Thomsen L, Gust G. 2000. Sediment erosion thresholds and characteristics of resuspended aggregates on the western European continental margin. *Deep-Sea Research Part I-Oceanographic Research Papers* 47(10): 1881-1897.
- Ting FC, Briaud JL, Chen H, Gudavalli R, Perugu S, Wei G. 2001. Flume tests for scour in clay at circular piers. *Journal of Hydraulic Engineering* 127:969-978.
- TRB 2004. NCHRP Report 516. Pier and Contraction Scour in Cohesive Soils. Transportation Research Board, Washington D.C., USA.
- USACE. 1970. Laboratory soils testing. Engineer manual, EM1110-2-1906, Washington, D.C., USA.
- USDA-NRCS 1997. Field procedures guide for the head-cut erodibility index. Chapter 52, Part 628 Dams, 210-VI-NEH. Washington D.C.: USDA Natural Resources Conservation Service.
- USDA. 2011. Soil survey laboratory manual methods. Soil Survey Investigations Report No. 45, Version 2.0. US Department of Agriculture, Natural Resources Conservation Service, National Soil Survey Center: Lincoln, NE, USA.
- Utley B, Wynn TM. 2008. Cohesive soil erosion: Theory and Practice. World Environmental and Water Resources Congress: 1-10.
- Van den Berg JH. 1995. Prediction of alluvial channel pattern of perennial rivers. *Geomorphology* 12:259-279
- Van Ledden M, van Kesteren WGM, Winterwerp JC. 2004. A conceptual framework for the erosion behaviour of sand–mud mixtures. *Continental Shelf Research* 24(1): 1-11. DOI:10.1016/j.csr.2003.09.002
- Wardhana K, Hadipriono FC. 2003. Analysis of recent bridge failures in the United States. *Journal of Performance of Constructed Facilities* 17:144-150.
- Wibowo J, Yule D, Villanueva E, Temple D. 2005. Earth and rock surface spillway erosion risk assessment. The 40th US Symposium on Rock Mechanics (USRMS), American Rock Mechanics Association, Alaska, USA.
- William JW, Diehl, TH. 1993. Recent sedimentation and surface-water flow patterns on the flood plain of the North Fork Forked Deer River, Dyer County, Tennessee, U.S. Geological Survey, Water-Resources Investigations Report 92-4082, Nashville, TN, USA.
- Winterwerp JC, van Kesteren WGM. 2004. Introduction to the physics of cohesive sediment in the marine environment. Elsevier, Amsterdam, the Netherlands.
- Wischmeier WH, Mannering JV. 1969. Relation of soil properties to its erodibility. *Soil Sci. Soc. Am. Proc.* 33(1): 131-137.

- Wynn TM. 2004. The effects of vegetation on stream bank erosion. Ph.D. dissertation, Biological Systems Engineering, Virginia Polytechnic Institute and State University, Blacksburg, VA, USA.
- Wynn TM, Mostaghimi S. 2006. The effects of vegetation and soil type on streambank erosion, southwestern Virginia, USA. *Journal of the American Water Resources Association (AWARA)* 42(1): 69-82. DOI: 10.1111/j.1752-1688.2006.tb03824.x.
- Wynn TM, Henderson MB, Vaughan DH. 2008. Changes in streambank erodibility and critical shear stress due to subaerial processes along a headwater stream, southwestern Virginia, USA. *Geomorphology* 97: 260-273. DOI:10.1016/j.geomorph.2007.08.010.
- Wu NC. 2010. An exploratory data analysis of national bridge inventory. M.Sc. Thesis, Department of Civil Engineering, University of Virginia, USA.
- Yang CT. 1972. Unit stream power and sediment transport. *Journal of the Hydraulics Division* 98:1805-1826.
- Yang CT. 1973. Incipient motion and sediment transport. *Journal of the Hydraulics Division* 99:1679-1704.
- Zreik DA, Krishnappan BG, Germaine JT, Madsen OS, Ladd CC. 1998. Erosional and mechanical strengths of deposited cohesive sediments. *J. Hydraul. Eng.* 124(11): 1076-1085.

# Appendices

## **Appendix A: Published Journal Article:**

Mahalder, B., J.S. Schwartz, A.M. Palomino, and J. Zirkle. 2018. Estimating erodibility parameters for streambanks with cohesive soils using the mini jet test device: A comparison of field and computational methods. *Water*, 10, 304. DOI 10.3390/w10030304.

## **Appendix B: Journal Article Manuscript**

Mahalder, B., J.S. Schwartz, A.N. Papanicolaou, A.M. Palomino, and J. Zirkle. 2018. Comparison of erodibility parameters for cohesive streambank soils between an in-situ jet test device and laboratory conduit flume. *Journal of Hydraulics Engineering* (prepared for submission).

## **Appendix A: Published Journal Article:**

Mahalder, B., J.S. Schwartz, A.M. Palomino, and J. Zirkle. 2018. Estimating erodibility parameters for streambanks with cohesive soils using the mini jet test device: A comparison of field and computational methods. *Water*, 10, 304. DOI 10.3390/w10030304.

Article

# Estimating Erodibility Parameters for Streambanks with Cohesive Soils Using the Mini Jet Test Device: A Comparison of Field and Computational Methods

Badal Mahalder <sup>1</sup>, John S. Schwartz <sup>1,\*</sup>, Angelica M. Palomino <sup>1</sup> and Jon Zirkle <sup>2</sup>

<sup>1</sup> Department of Civil and Environmental Engineering, The University of Tennessee, Knoxville, TN 37996, USA; bmahalde@vols.utk.edu (B.M.); apalomin@utk.edu (A.M.P.)

<sup>2</sup> Tennessee Department of Transportation, Nashville, TN 37243, USA; Jon.Zirkle@tn.gov

\* Correspondence: jschwart@utk.edu; Tel.: +1-865-974-7721

Received: 28 January 2018; Accepted: 6 March 2018; Published: 11 March 2018

**Abstract:** The jet test device has been predominantly used for in situ critical shear stress ( $\tau_c$ ) and erodibility coefficient ( $k_d$ ) measurements of cohesive streambanks/beds using three analytical procedures: the Blaisdell method (BM), the iterative approach (IP), and the scour depth approach (SDP). Existing studies have reported that  $\tau_c$  and  $k_d$  estimates can be influenced by the computational procedure, time intervals for scour-hole depth measurements, and the pressure head selection. This study compared estimates of  $\tau_c$  and  $k_d$  among the three computational procedures using single and multiple pressure settings (SPS, MPS). A new method is introduced applying incrementally increasing pressure heads, hypothesizing depth-averaged erodibility parameters would be generated that better represent bank and fluvial erosion. Estimates of  $\tau_c$  applying the MPS-BM procedure were greater by 17% to 100% compared with SPS-BM procedures and  $k_d$  estimates were lower with less variability ( $\sigma = 3.54$ ) compared with other procedures from 126 jet tests among 21 Tennessee stream sites. This finding supports the hypothesis of increasing  $\tau_c$  and decreasing  $k_d$  with greater soil depths into the bank, suggesting the MPS-BM procedure can improve the estimation of  $\tau_c$  and  $k_d$  using the mini-jet test device. Overall, this study demonstrates the need to standardize field and computational procedures.

**Keywords:** fluvial erosion; streambank cohesive soils; critical shear stress; erodibility coefficient; jet test device; bank stability

## 1. Introduction

Concept development of a jet device for estimating erosion rates for cohesive soils was first introduced by Dunn [1], where critical shear stress ( $\tau_c$ ) and the erodibility coefficient ( $k_d$ ) are measured and used in the excess shear stress equation. The excess shear stress equation is expressed as:  $\varepsilon_T = k_d(\tau_b - \tau_c)^m$ , where  $\varepsilon_T$  is the erosion rate ( $\text{cm}\cdot\text{s}^{-1}$ ),  $k_d$  ( $\text{cm}^3\cdot\text{N}^{-1}\cdot\text{s}^{-1}$ ),  $\tau_c$  (Pa),  $\tau_b$  is the hydraulic boundary shear stress (Pa), and  $m$  is an empirical exponent [2–5]. In the 1990s, researchers with the US Department of Agriculture further developed the jet device consisting of a large submergence tank (test chamber) 30.0 cm in diameter and height [3,6,7]. They provided operational guidance for the in situ field data collection, in which depths of the scour hole formed by the impinging jet are measured over time. Commonly referred to as the “original” jet tester, it has been the dominant measurement tool for estimating in situ erodibility of cohesive streambank soils [6,7]. In the 2010s, the mini-jet test device was developed and first used by Simon et al. [8], where its submergence tank is 101.6 mm in diameter and 7.0 cm in height. Due to its smaller size, light weight, and the ease of field operation, the mini-jet device is more applicable for in situ testing on bed and bank surfaces. Al-Madhhachi et al. [9] compared

results from the original and mini-jet devices and found that  $k_d$  values were not significantly different, whereas  $\tau_c$  values were consistently lower from the mini-jet compared with the original jet tester.

Mini-jet operational guidance was provided by Al-Madhhachi et al. [9] where a constant pressure head setting with a pre-defined time interval were specified to measure the depth of the developing scour hole independent of soil type. However, their study noted that selection of the pressure head setting for a specific field test appeared to be dependent on soil type and the experience of the jet operator. Using the mini-jet device, Khanal et al. [10] recently investigated the influence of data collection time intervals and test termination times on erosion parameter estimations. They also suggested that an interactive effect of pressure head setting relative to the data collection intervals and length of the test may have influence on  $\tau_c$  and  $k_d$  estimations for different natural sediment types. It was hypothesized that inappropriate test selection of the pressure head setting could affect the  $\tau_c$  and  $k_d$  estimations significantly. Khanal et al. [10] identified the importance of the measurement time interval and pressure head selection; however, they did not report on the potential effect of changing soil properties with depth on  $\tau_c$  and  $k_d$  estimations. Differences in soil properties from the streambank surface inward into the bank material (subsurface) have the potential to influence the rate of scour hole development by the impinging jet. Therefore, critical research is needed to better understand how device operational procedures and streambank soil properties jointly affect the computation of erodibility parameters, and how operational procedures can be improved.

Many environmental factors affect streambank soil erodibility. It is well known that physical and geochemical properties of cohesive soils can affect erodibility, including bulk density, water content, dispersion ratio, percent clay and clay activity, plasticity index, organic matter content, pore water pH, and sodium adsorption ratio [2,11–16]. In general, cohesive soil properties consisting of clay, sand, silt, and gravel can be highly variable in natural riverine environments as a function of long-term geomorphic processes [17–19]. Mahalder et al. [16] found varying relationships to controlling erodibility parameters among different physiographic regions in Tennessee. Daly et al. [20] characterized variability of erodibility parameters within an Oklahoma watershed. At the local streambank scale, erodibility parameters varied among different surfaces vertically from the top of bank to the toe where an increase in bulk density and water content was observed, and thus, an increase in  $\tau_c$  apparently associated with soil consolidation [21–29]. Soil bulk density appears to also increase at a point on the bank inward from the surface into the bank due to subaerial processes, the wetting and drying action in association with seasonal climate variations, where erosion rates reduce consequently inward from the bank surface [18,24,30]. It is thought that any in situ soil test on the thin surficial layers will therefore substantially influence estimation of erodibility parameters compared with the deeper bank soil layers. Several studies reported that  $\tau_c$  of the upper surface (about 0–3 cm) is 3 to 5 times lower compared to underneath soil layers in both laboratory remolded and undisturbed soil samples [18,24,26]. The importance of bank point-scale variability is that it can affect the time-dependent measurements of scour hole depths during the jet device operation, particularly for the first few readings of a given test.

In order to improve operational procedures, the possible influence of soil property changes with depth of scour-hole development must be recognized, in addition to how data from the test measurements are used to compute  $\tau_c$  and  $k_d$  parameters. The computational procedure developed for the original jet device per Hanson and Cook [6] used the Blaisdell method (BM). More recent computational procedures have included the iterative principle (IP) described by Simon et al. [8] and the scour depth principle (SDP) described by Daly et al. [31]. Inconsistencies in  $\tau_c$  and  $k_d$  estimations have been reported using the same measured test data from the mini jet device [10,32,33]. Results from several studies have shown that the BM solution technique generally under-predicted  $\tau_c$  compared with the IP and SDP methods [8,20,31,32]. A limited number of study results using the IP and SDP solution methods showed very high  $k_d$  values corresponding to both higher and lower  $\tau_c$  values. In addition to the solution technique, inconsistencies in  $\tau_c$  and  $k_d$  estimations are likely due to interdependent factors of soil property changes, and highly complex hydrodynamics and turbulence

in the device test chamber as the scour hole shape develops [32,34–36]. Karamigolbaghi et al. [32] suggested that the head loss coefficient in the Blaisdell equation should be modified (BMM), accounting for jet confinement in the mini-jet device test chamber and its effect on scour hole development. Field observations reveal that depending on the soil type, soil physical conditions and resistance properties, and the jet characteristics, scour hole shape and formation alter with time and applied fluid forces. Similar observations were also reported by other studies [36–40]. These findings suggest that advances in the operational procedures for jet test devices need greater consideration of in situ soil properties, selection of appropriate test pressure head settings and measurement time intervals, and the computational methods for  $\tau_c$  and  $k_d$  estimation.

The objectives of this study were to: (1) investigate the influence of device pressure head selection on  $\tau_c$  estimates leading to development of an alternative field procedure using multiple pressure settings during a test, (2) compare differences in  $\tau_c$  and  $k_d$  estimations from three computational procedures, the BM, IP, and SDP for single pressure (SPS) and multiple pressure (MPS) field procedures, and (3) qualitatively describe differences in scour hole development and morphology per varying soil types and the resulting patterns for  $\tau_c$  and  $k_d$  versus jet device pressure setting. The rationale for investigating the influence of pressure setting is that it is hypothesized that jet procedures with a single pressure head may lead to erodibility parameter estimates heavily influenced by the surficial soil layer. Theoretically, scour hole depth changes over time during a jet test vary with soil cohesion, bulk density and/or other soil conditions, and those rate and field measurement differences ultimately influence estimations of  $\tau_c$  and  $k_d$  per computational method selected. If  $\tau_c$  and  $k_d$  parameters derived by the jet test device using a single pressure setting reflect the erodibility of surficial bank surface to a greater extent, when used in the excess shear equation they may over-predict streambank erosion rates. This research uniquely applies a multiple-pressure setting procedure to improve the mini-jet test device's field data collection and computational procedures for greater consistency in  $\tau_c$  and  $k_d$  estimations. Among research and practitioner river engineers there is a general understanding that erodibility measurements need to follow a standard procedure, and this study supports that effort.

## 2. Background for Jet Test Data Analysis

Estimating  $\tau_c$  and  $k_d$  from jet device test data has used the following computational procedures: BM [6,7], IP [8], and SDP [31]. These procedures are based on the theoretical understanding that shear stress can be computed from dispersion principles by a submerged fluid jet projected normal to an erodible surface developing a scour hole. Background on the computational procedures relevant to this study is described in this section. Hanson and Cook [6] developed an analytical procedure to calculate the erosion index parameter from jet test data based on jet diffusion principles developed by Stein and Nett [41]. This method was developed for the original submerged jet tester; however, the governing principles are consistent for both the original and mini-jet devices. The major assumption considered for this device was that the rate of scour depth or erosion rate ( $dJ/dt$ ) is a function of maximum stress at boundary. Therefore, the jet erosion rate equation was organized as [6,7]:

$$\frac{dJ}{dt} = k_d \left[ \frac{\tau_0 J_p^2}{J^2} - \tau_c \right], \text{ for } J \geq J_p. \quad (1)$$

where  $J$  is the scour depth (cm);  $J_p$  is the potential core length from jet origin (cm);  $k_d$  is the erodibility coefficient ( $\text{cm}^3 \cdot \text{N}^{-1} \cdot \text{s}^{-1}$ );  $\tau_0$  is the applied bottom shear stress (Pa); and  $\tau_c$  is the critical shear stress (Pa).

Based on soil type and conditions, the initial erosion rate may be substantial approaching zero asymptotically for the jet device [41]. The depth at which the applied shear stress on the soil surface does not produce any erosion ( $dJ/dt = 0$ ) is termed as the equilibrium scour depth ( $J_e$ ) and the shear stress to that depth is termed as  $\tau_c$ .

$$\tau_c = \tau_0 \left( \frac{J_p}{J_e} \right)^2 \quad (2)$$

where  $\tau_0 = C_f \rho_w U_0^2$  is the maximum shear stress due to the jet velocity at the nozzle (Pa);  $C_f = 0.00416$  is the friction coefficient;  $\rho_w$  is water density ( $\text{kg}\cdot\text{m}^{-3}$ );  $U_0 = C\sqrt{2gh}$  is the velocity of jet at orifice ( $\text{cm}\cdot\text{s}^{-1}$ );  $C$  is discharge coefficient;  $h$  is the applied head (cm) or pressure head;  $J_P = C_d d_0$ ;  $d_0$  is the nozzle diameter (cm); and  $C_d = 6.3$  is the diffusion constant. Writing a dimensionless form, Equations (1) and (2) were formed as follows [6]:

$$\frac{dJ^*}{dT^*} = \frac{(1 - J^{*2})}{J^{*2}} \quad (3)$$

where  $J^* = J/J_e$ ; and  $J_P^* = J_P/J_e$ . The dimensional time ( $T^*$ ) was also expressed as:

$$T^* = \frac{t}{T_r} \quad (4)$$

where  $t$  is the time of data measurement during the test; and  $T_r = J_e/k_d\tau_c$  is the reference time. Integrating Equation (3), the following form was developed [6]:

$$T^* - T_P^* = -J^* + 0.5 \ln\left(\frac{1+J^*}{1-J^*}\right) + J_P^* - 0.5 \ln\left(\frac{1+J_P^*}{1-J_P^*}\right) \quad (5)$$

Using Equations (3) to (5),  $\tau_c$  and  $k_d$  can be calculated using an Excel™ spreadsheet. However, Blaisdell et al. [42] showed that the time required to attain  $J_e$  is excessively high, hence, the calculation of  $\tau_c$  becomes impractical for efficient field testing. Therefore, they proposed a technique to calculate  $J_e$  by fitting scour depth data versus time as a hyperbolic function. The general form as proposed by Blaisdell et al. [42] of the equation was:

$$A = (f - f_0)^2 - x^2 \quad (6)$$

$$f = \log\left(\frac{J}{d_0}\right) - \log\left(\frac{U_0 t}{d_0}\right) \quad (7)$$

$$f_0 = \log\left(\frac{J_e}{d_0}\right) \quad (8)$$

$$x = \log\left(\frac{U_0 t}{d_0}\right) \quad (9)$$

The coefficients  $A$  and  $f_0$  can be determined using spreadsheet solver by fitting the scour depth data based on the plotting of  $f$  versus  $x$ , consequently,  $J_e$  was calculated  $J_e = d_0 10^{f_0}$ .

The IP and SDP approaches for estimating  $\tau_c$  and  $k_d$  are variations of the BM [20]. In the IP approach, initially  $\tau_c$  and  $k_d$  values are estimated from the Blaisdell solution based on  $T^*$  and  $J^*$  values. The erodibility parameters are then simultaneously solved in an iterative manner. The ultimate goal for this iterative solution method is to minimize the root-mean-square error between the measured and predicted time, where an upper bound of  $\tau_c$  is included to prevent the solution from exceeding the equilibrium scour depth. In the IP,  $\tau_c$  is a function of shear stress at the jet nozzle and maximum observed scour depth during jet test. Daly et al. [31] developed another spreadsheet routine that also solved for  $\tau_c$  and  $k_d$  iteratively, which is known as the SDP method. In this method, observed scour depth data from the jet test are fitted to the predicted scour depth data using the excess shear stress equation using initial guessed values of  $\tau_c$  and  $k_d$ . In this simultaneous solution method, by minimizing the sum of squared errors between measured and predicted scour depth data from the excess shear stress equation, final  $\tau_c$  and  $k_d$  values are estimated. Results of these recently developed solution techniques suggest a better fit with the measured scour depth data, though the reported  $k_d$  values were found to be much higher and unrealistic in some cases.

### 3. Materials and Methods

#### 3.1. Study Design

In order to meet the study objectives, two separate field operations were conducted for this study using the mini-jet test device. In the first field operation, the MPS approach was used at 21 sites across Tennessee from July 2014 through August 2015. The rationale for site selection was to obtain data across multiple physiographic regions [16], in which geographical details of these study sites are described below in Section 3.2. The second operation consisted of collecting scour hole depth measurements for a single pressure setting (SPS), and at the same site location collecting scour hole depth measurements using an alternative MPS approach. This comparative field operation was conducted during July 2017 on Gist Creek, Sevier County, Tennessee to provide sufficient justification for the MPS approach (Objective 1). Both field datasets applied the BM, IP, and SDP computational procedures in order to assess any differences between them (Objective 2). The Gist Creek dataset was collected after the main study which included the 21 statewide field sites to provide greater justification for applying the MPS procedure to improve the consistency of measured erodibility parameters. Field data collection and computational methods are described below in Section 3.3.

#### 3.2. Study Area

The Gist Creek study site is located in the Ridge and Valley Physiographic Province in eastern Tennessee (Figure 1). Gist Creek is a third order stream with a bank full width of 20 m. Five test locations including the upper and lower bank positions were investigated (designated as Loca.-I, -II, -III, -IV, and -V), totaling 10 tests per SPS and MPS field procedures.

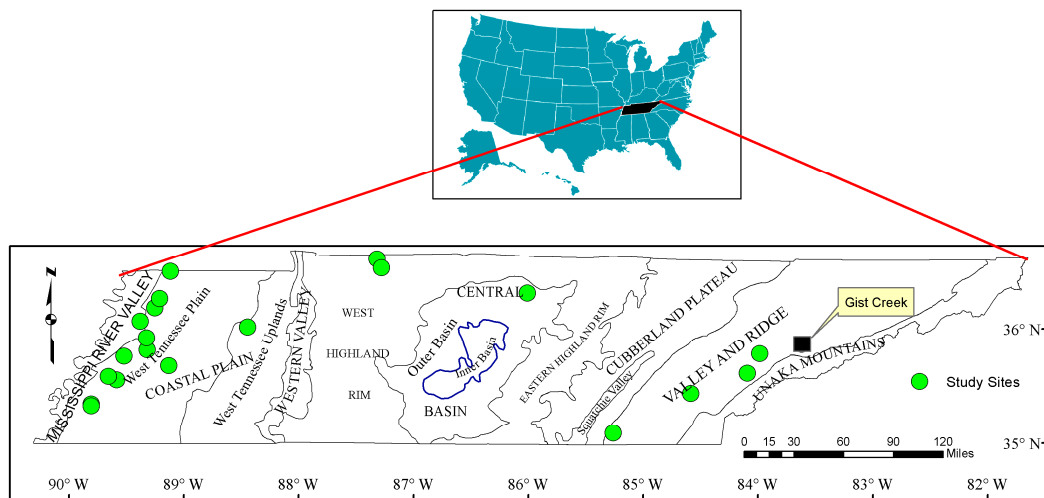


**Figure 1.** Study site locations using the mini-jet test device in Tennessee, where Gist Creek is shown as a black square and the sites used for the multiple-pressure test among the different physiographic provinces [43] are shown as green circles.

The field operation that used the MPS procedure for 21 sites was conducted across the state of Tennessee in four physiographic provinces: Valley and Ridge, Central Basin, West Highland Rim, and Coastal Plain, each with diverse geological settings with different dominant soil properties that govern estimates for the erodibility parameters [16]. Among these regions, five stream sites were located in the Valley and Ridge Physiographic Province, three sites in the West Highland Rim and the Central Basin, and 13 sites in the West Tennessee Plain and West Tennessee Uplands, sub-regions of the Coastal Plain physiographic province (Figure 1). The majority of the sites were from the western part of Tennessee,

which has predominantly cohesive (silt/clay) type materials. Mahalder et al. [16] have described the soil properties of each site in detail.

### 3.3. Field Data Collection and Computational Procedures

In general, site preparation for all mini-jet test locations consisted of taking care to maintain the ambient moisture content by avoiding days with rainfall. Test locations were visually selected so that soil was homogenous in character, and free from pebbles or rocks, vegetation, and root systems. Each test location was cleaned very gently using a shovel prior to conducting a test, and the bottom ring of the jet device was inserted into the soil using uniform pressure on the top of the bottom ring to minimize disturbances at the soil surface. After completing each test, two core samples near the test location were collected using a cylindrical coring device, which were analyzed in the University of Tennessee' Geotechnical Laboratory for bulk density, water content, and unconfined compressive strength (UCS). Approximately 1.4 kg of soil was also collected from the inside of the jet's bottom ring at each test location to measure selected physiochemical soil properties. Collectively, soil samples represented a wide variation in moisture content and bulk density associated with the diverse geological settings.

The jet operation procedure using the SPS follows the guidelines outlined by Hanson and Cook [7] and Al-Madhhachi et al. [9] with a slight modification, where scour-hole depth readings were measured at one-minute intervals. A centrifugal pump powered by a 2000-W portable generator provided water flow from the nearby stream through the jet device, and a constant pressure head was regulated by a ball valve and monitored by an inline pressure gage. The terminal test time was 46 min for a set pressure for the SPS method. These data were then used to estimate  $\tau_c$  and  $k_d$  by three computational methods: BM, SDP, and IP (Table 1).

The jet operation procedure using the MPS generally followed the field guidance by Hanson and Cook [7] and Al-Madhhachi et al. [9]; however, in the MPS procedure five different pressure settings were applied, starting from a lower to a higher pressure at each testing location. Selected pressures were adjusted based on testing location, soil type and condition, and test erosion rates. The applied pressure ranged from 4.14 kPa to 44.12 kPa. In some testing locations, the initial pressure was set as high as 27.58 kPa because lower pressure settings did not produce a scour hole due to the resistant soil erosion properties. For each pressure head setting, the test duration at each location was about 12–20 min, where three different time intervals were selected during the tests for the scour-hole depth measurements. The different time intervals during a MPS test were: (i) 30-s intervals for the first two readings, (ii) one-minute time intervals for 2–6 min, and (iii) two-minute time intervals for depth measurements until test termination. The applied pressure head was then increased to the next pressure increment after 12 min if the measured scour-hole depth difference between two consecutive readings was not more than one millimeter. If the difference between two consecutive scour-hole depth readings was greater than one millimeter, the test was continued for the next two-minute interval. These procedures were repeated for each incremental increased pressure head settings at the same test location. The total run time for a test at each location (applying all the five pressure heads) was about 60–100 min, depending on the progression of the scour depth. MPS mini-jet testing was conducted at upper, middle, and lower bank positions where possible for the 21 sites across Tennessee. These data were then used to estimate  $\tau_c$  and  $k_d$  by three computational methods: BM, SDP, and IP (Table 1).

The SPS procedure was exclusively used at the Gist Creek study site where the MPS procedure was concurrently conducted for a method comparison (Objective 1). For accomplishing this objective, ten tests were conducted, five per upper and lower bank locations (Table 2). For each of the upper bank test locations, five different pressures heads were applied they were: 11.72 kPa, 16.55 kPa, 20.68 kPa, 27.58 kPa, and 33.09 kPa. For the lower bank the selected pressures heads were: 13.79 kPa, 20.68 kPa, 27.58 kPa, 33.78 kPa, and 41.37 kPa. These pressure heads were also used incrementally for the MPS method by following similar procedures as discussed in the previous paragraph.

**Table 1.** Procedural summaries for field data collection and computation for erodibility parameters using the mini-jet device.

Procedures	Description/Working Principles
<i>Field Data Collection Procedures</i>	
Single Pressure Setting (SPS)	A single pressure setting is chosen in which scour depth readings are collected at pre-defined time intervals. Finally, equilibrium scour depth is assumed based on different computational methods (BM, SDP, and IP) and used in $\tau_c$ and $k_d$ calculation.
Multiple Pressure Settings (MPS)	Incrementally five different pressure heads are used at a test location starting from lower to higher. At each pressure head, test duration is about 12–20 min, where three different intervals are used for recording the scour depth readings.
<i>Computational Procedures</i>	
Blaisdell Method (BM)	The Blaisdell et al. [42] approach is used for equilibrium scour depth calculation and subsequently $\tau_c$ and $k_d$ are calculated [44].
Modified Blaisdell Method (BMM)	The Blaisdell et al. [42] approach is used for equilibrium scour depth calculation and subsequently $\tau_c$ and $k_d$ are calculated [44], however a head loss coefficient of 0.39 was applied as per Karamigolbaghi et al. [32] where 0.16 is typically used. The adjusted coefficient addresses the jet confinement in the mini-jet's submergence (tank) test chamber.
Scour Depth Principle (SDP)	Solved for $\tau_c$ and $k_d$ iteratively by plotting the original scour depth versus predicted scour depth using excess shear stress equation. In this simultaneous solution method, by minimizing the sum of squared errors between the measured scour data and the predicted scour depth data $\tau_c$ and $k_d$ values are estimated. Single pressure head is used for jet operation [31].
Iterative Principle (IP)	In the IP approach, $\tau_c$ and $k_d$ values are estimated from Blaisdell solution approach based on $T^*$ and $J^*$ values. Initial $\tau_c$ and $k_d$ values are estimated from Blaisdell method and simultaneously solved for erosion parameters iteratively by minimizing root-mean-square error between the measured and predicted time. In this method an upper limit is employed for the iteration of $\tau_c$ values and similar to the other two methods, the jet device is operated using a single pressure head [8].
<i>Computational Procedures for Erodibility Parameters Estimation</i>	
Multiple Pressure Settings using the BM (MPS-BM)	Solution approach follows the BM method for equilibrium scour depth prediction. However, MPS field data are used for the final $\tau_c$ and $k_d$ values estimation, where a spreadsheet is run separately using the scour depth readings for each applied pressure head. The estimated $\tau_c$ and $k_d$ values obtained from each pressure head and the corresponding scour depths data are then plotted on a normal graph against the corresponding pressure head. Finally, erodibility parameters at a test location are estimated based on the shape of plots (see Figure 2).
Multiple Pressure Settings using the SDP (MPS-SDP)	Solution approach follows the SDP method for equilibrium scour depth prediction using the MPS field procedures and data. A similar approach is followed for the final $\tau_c$ and $k_d$ values estimation as the MPS-BM method.
Multiple Pressure Settings using the IP (MPS-IP)	Solution approach follows the IP method for equilibrium scour depth prediction using the MPS field procedures and data. A similar approach is followed for the final $\tau_c$ and $k_d$ values estimation as the MPS-BM method.

**Table 2.** Mini-jet test conditions comparing single pressure setting (SPS) and multiple pressure settings (MPS) field data procedures at the Gist Creek study site, including soil properties among the five test locations per upper and lower bank areas.

Bank Position	Test Identifier	Test Location	Selected Pressure Head (kPa)	Test Duration (min)	Water Content (%)	Bulk Density (gm/cm <sup>3</sup> )
Upper Bank	SPS-1	I	11.72	46	17.73	1.77
	MPS-1		11.72–33.09	80	18.58	1.77
	SPS-2	II	16.55	46	21.20	1.79
	MPS-2		11.72–33.09	78	20.89	1.78
	SPS-3	III	20.68	46	19.42	1.78
	MPS-3		11.72–33.09	100	20.89	1.79
	SPS-4	IV	27.58	46	20.89	1.76
	MPS-4		11.72–33.09	100	21.12	1.78
	SPS-5	V	33.09	46	20.80	1.79
	MPS-5		11.72–33.09	100	21.85	1.78
Lower Bank	SPS-1	I	13.79	46	30.83	1.92
	MPS-1		13.79–41.37	80	31.83	1.90
	SPS-2	II	20.68	46	31.45	1.90
	MPS-2		13.79–41.37	80	32.14	1.90
	SPS-3	III	27.58	46	30.14	1.90
	MPS-3		13.79–41.37	90	29.54	1.90
	SPS-4	IV	33.78	46	29.51	1.92
	MPS-4		13.79–41.37	100	29.96	1.91
	SPS-5	V	41.37	46	31.28	1.90
	MPS-5		13.79–41.37	100	31.27	1.91

In the MPS procedure,  $\tau_c$  and  $k_d$  values were calculated individually for each pressure head setting and corresponding scour depth values. As summarized in Table 1, these data were used to estimate the erodibility parameters by the three computational methods: BM, SDP, and IP. Estimates for  $\tau_c$  and  $k_d$  using the BM was completed using a spreadsheet routine developed at the USDA National Sedimentation Laboratory. This spreadsheet routine was based on Hanson and Cook [6,7]. Erodibility parameters from the other two computational methods (SDP and IP) were also calculated using another spreadsheet provided per Daly et al. [31]. Therefore, using the MPS data and different computational procedures,  $\tau_c$  and  $k_d$  values were estimated and are denoted as: MPS-BM, MPS-SDP, and MPS-IP.

Per test pressure setting and associated individual computations of  $\tau_c$  and  $k_d$ , the erodibility parameters were plotted on normal graph paper. By doing so, three patterns were observed from these plots. Using selected data from the 21 stream sites across Tennessee, those patterns are demonstrated in Figure 2. The three distinct patterns were: (i) a concave-down shape (76 observations), (ii) a nearly linear pattern (20 observations), and (iii) scattered points (30 observations) using the MPS-BM method. For the concave-down shape, the critical shear stress ( $\tau_c$ ) was calculated by drawing an asymptotic line on the concave-down shaped curve (Figure 2a), and average values were taken for the scattered patterns. For the linearly increasing pattern, the maximum value was read from the plot as the  $\tau_c$  value. The majority of the tests demonstrated the concave-down shape. Similar procedures were followed for  $k_d$  value calculations. It is interesting to note that using MPS-SDP and MPS-IP methods, similar patterns were also observed. Though Figure 2 was provided in this paper only to demonstrate the computational procedures using MPS field collected data, these patterns appear to reflect a test response to the different soil properties. These patterns will be discussed further to supplement field observations related to dissimilarities in scour-hole development per different soil types (Objective 3). It is important to note that these plots in Figure 2 do not represent the same jet test data, rather the shapes are representative of different jet tests for the purpose of depicting the observed unique patterns.

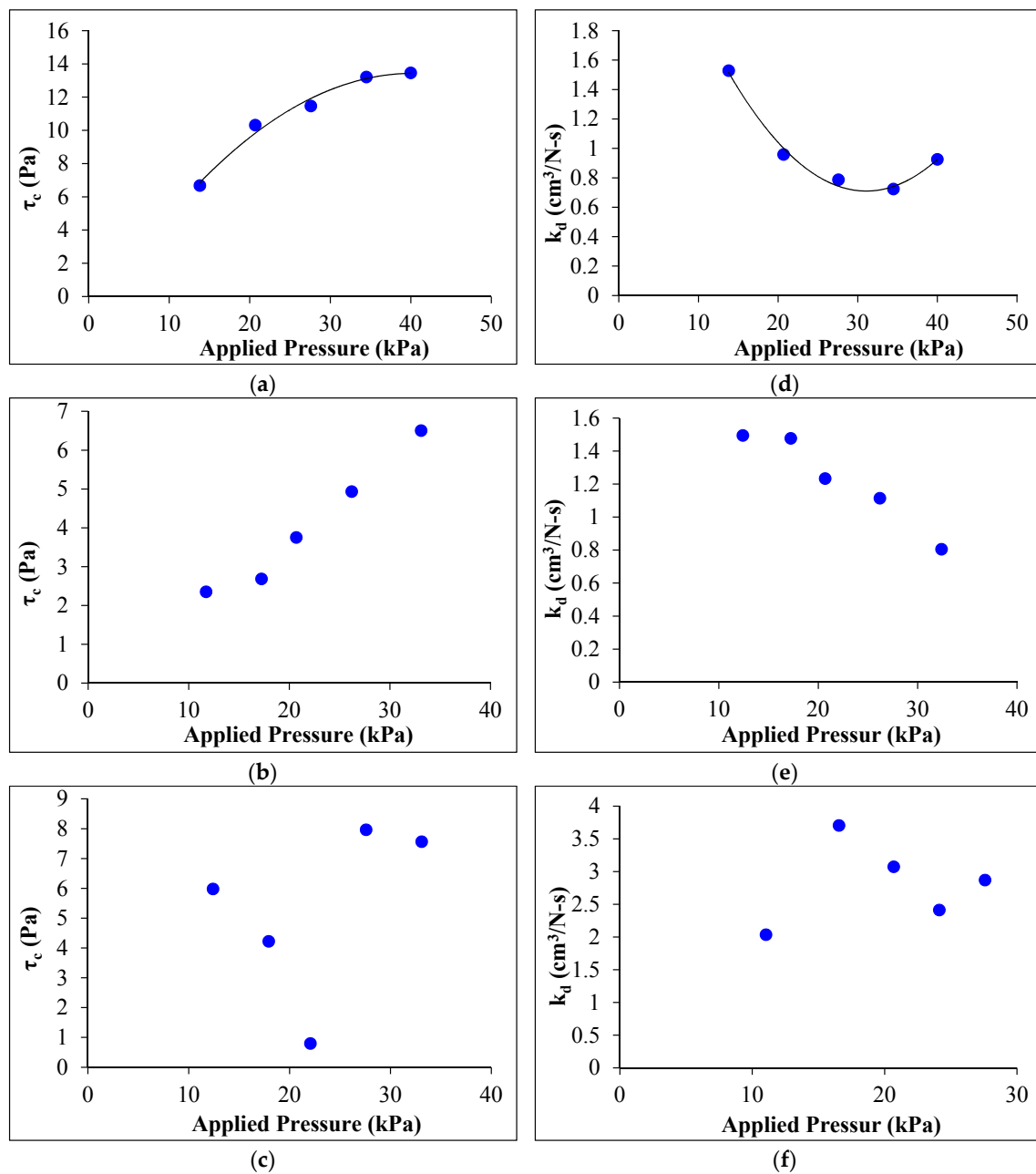


**Figure 2.** Response patterns of critical shear stress ( $\tau_c$ ) and erodibility coefficient ( $k_d$ ) to jet-test device pressure head setting. Data represented are identified for  $\tau_c$ : (a) concave-down shape, (b) linear, (c) scattered points and for  $k_d$ : (d) concave-up shape, (e) linear, and (f) scattered points.

## 4. Results and Discussion

### 4.1. Comparison of SPS and MPS Methods for Estimating Critical Shear Stress

Test locations on Gist Creek and jet device pressure settings for SPS and MPS methods are summarized in Table 2. Soil properties were generally consistent among the five test locations but differed between the upper and lower bank areas (Table 2). The soil of the upper bank was predominantly found as semi-cohesive with the  $D_{50}$  value ranging between 75  $\mu\text{m}$  to 95  $\mu\text{m}$  with clay content 15%, and the PI value was about 5%. Lower bank soil was found as cohesive, the  $D_{50}$  value was between 33  $\mu\text{m}$  to 40  $\mu\text{m}$ , clay content was 25%, and the PI value was 10%. Bulk density averaged 1.78  $\text{g}\cdot\text{cm}^{-3}$  for the upper bank and 1.91  $\text{g}\cdot\text{cm}^{-3}$  for the lower bank.

Using the SPS method, selection of pressure head influenced  $\tau_c$  estimates for different computational procedures for both lower and upper bank areas (Figure 3). BM results also found that estimated  $\tau_c$  values were significantly different from the SDP and IP methods over the range of applied test pressures for the lower bank ( $p = 0.008$ ), and upper bank ( $p < 0.001$ ). Lower banks soils were more cohesive with higher bulk densities than the upper bank locations, and as expected,  $\tau_c$  was greater. Regardless of soil type,  $\tau_c$  values were considerably higher at lower pressure heads. The computational method appears to have a greater effect on  $\tau_c$  estimates than individually per method, where for  $\tau_c$  on the lower bank area the SDP procedure was substantially greater than the BM and IP procedures. However, for the upper bank soils,  $\tau_c$  estimates were in similar ranges for the SDP and IP procedures.

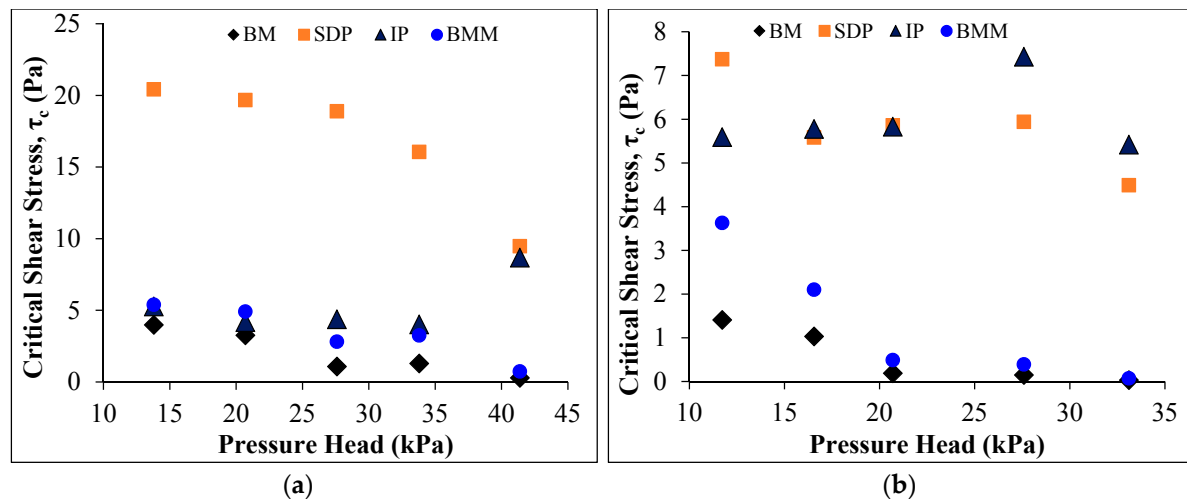


**Figure 3.** Using the SPS method, estimates of critical shear stress ( $\tau_c$ ) with different pressure heads are shown for the: (a) lower bank and (b) upper bank, based on the following computational procedures: BM = Blaisdell method, IP = iterative principle, SDP = scour depth principle, and BMM = modified Blaisdell method.

Karamigolbaghi et al. [32] reported that jet confinement could influence the jet test results and proposed a new value for the coefficient of  $C_f C_d^2$  as 0.39 instead of 0.16, which is also introduced in the jet test data analyses equations. Using this new coefficient, test data were also analyzed and termed as modified Blaisdell method (BMM). In Figure 3, the BMM was compared with the three methods (BM, SDP, and IP), which applied the original coefficient value of 0.16. The  $\tau_c$  estimates for BM and BMM procedures were similar among the pressure settings for the lower bank locations, which were more cohesive soils compared with the upper bank locations (Figure 3). Among the upper bank locations,  $\tau_c$  estimates using the BMM procedure were considerably higher than the BM procedure at the lower pressures (less than about 17 kPa). This result suggests pressure head setting and jet hydraulics affect  $\tau_c$  estimates to a greater extent, especially at lower pressure settings.

Using the MPS methods at the same Gist Creek test locations,  $\tau_c$  values were generally more consistent among the five locations using the MPS-BM procedures ( $\sigma = 0.36$  and 1.17 for lower and upper bank, respectively) compared with the MPS-SDP ( $\sigma = 0.91$ , and 5.51 for lower and upper bank, respectively) and MPS-IP ( $\sigma = 1.16$ , and 3.32 for lower and upper bank, respectively) procedures (Figure 4). Differences in estimated  $\tau_c$  values between the lower and upper banks align with other studies [21–23]. Relationships between  $\tau_c$  and corresponding pressure heads resulted in concave-down patterns (as demonstrated in Figure 2a) regardless of computational procedures. These findings also suggest that the  $\tau_c$  of the upper soil surface in both laboratory remolded and undisturbed soil samples could be lower compared to soil underneath the surface layer [18,24,26]. Therefore, using the SPS method, estimated  $\tau_c$  and  $k_d$  values likely represent that of the surficial soil layer, whereas the MPS method estimated  $\tau_c$  and  $k_d$  values represent depth-averaged parameters for the bank soil.

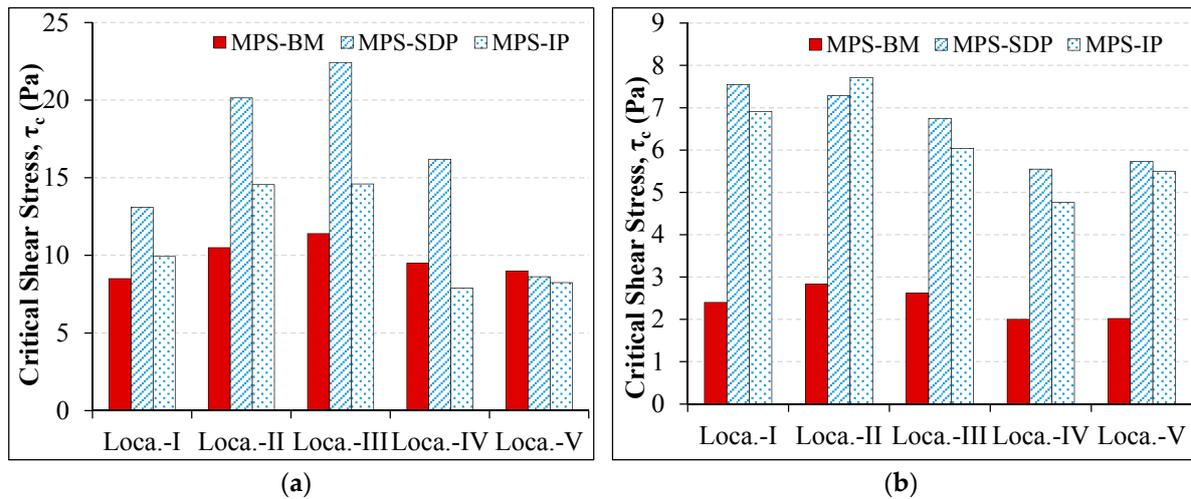


**Figure 4.** Based on the MPS method at the Gist Creek study site, critical shear stress ( $\tau_c$ ) estimates for the: (a) lower bank and (b) upper bank among the five test locations (Loca-1, -II, -III, -IV, and -V) and shown for the MPS-BM, MPS-IP, and MPS-SDP computational procedures.

Estimates for  $\tau_c$  using the BM and BMM procedures were also compared with the MPS-BM procedure (Figure 5). From these results, it was identified that pressure head selection could significantly influence  $\tau_c$  estimates regardless of the analysis method. However,  $\tau_c$  estimates using the MPS-BM procedure were generally more consistent among the five test locations, for both the upper and lower banks. This supports the hypothesis that pressure head selection could significantly affect the  $\tau_c$  estimation using the jet device, as was also observed by Khanal et al. [10].

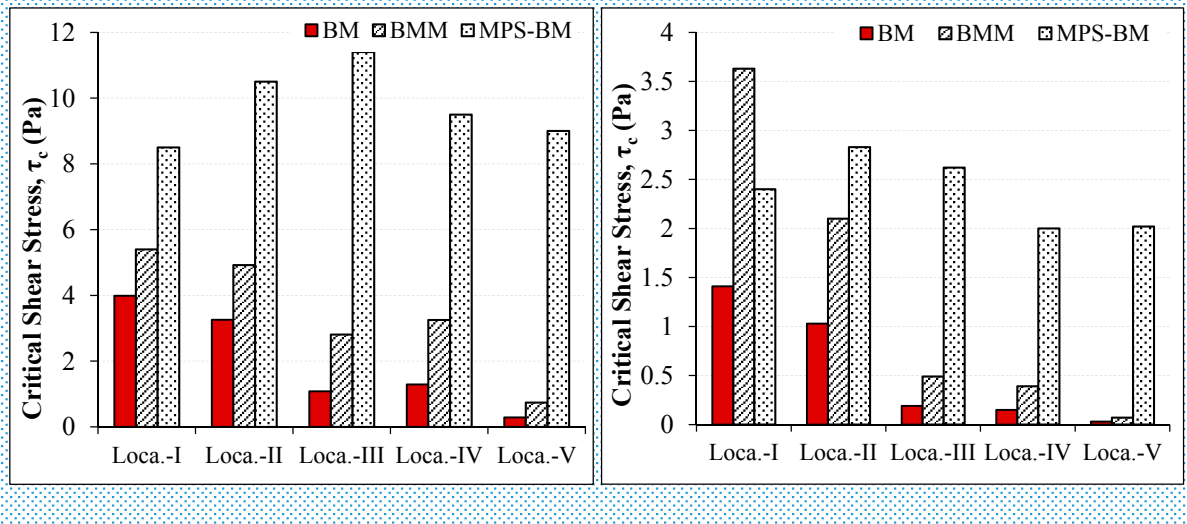


**Figure 5.** Estimates of critical shear stress ( $\tau_c$ ) at the five Gist Creek test locations for the: (a) lower bank and (b) upper bank area (Loca. -I, -II, -III, -IV, and -V). Computational methods: BM, BMM, and MPS-BM were compared.

The influence of the termination time interval on  $\tau_c$  and  $k_d$  estimations was investigated among the Gist Creek mini-jet test locations. Results from the data analyses found that if the test was terminated after 12–26 min, where the difference between two consecutive scour depth readings was less than 1 mm, estimated  $\tau_c$  and  $k_d$  values were similar with values from the full-length test. Therefore, in the new jet test operational protocol (MPS), a time interval of 12–20 min was selected for an applied pressure

head by observing the difference between two consecutive scour depth readings at the end of any test. As noted earlier, subaerial processes appear to decrease bulk density at the bank surface compared to soil into the bank. In the operational protocol for the original jet tester as outlined by Hanson and Cook [7] and Al-Madhhachi et al. [9], scour hole depth measurements are recorded at five-minute intervals. Using the MPS method developed for this study, it was observed that if we arbitrarily change the initial six readings inside the first five-minute time interval compared to the published interval for scour depth readings,  $\tau_c$  and  $k_d$  varied significantly. Results from this study indicate the initial and termination time intervals can substantially influence  $\tau_c$  and  $k_d$  estimates. Similar observations were also reported by Khanal et al. [10] but greater details are provided in this study.

#### 4.2. Comparison of MPS Method and Computational Procedures for Erodibility Parameters

Potential differences in  $\tau_c$  and  $k_d$  estimations from the newly developed MPS method were compared with the SPS method among the three computational procedures BM, IP, and SDP (Objective 2). Because no field tests were conducted using the SPS method among the 21 Tennessee sites, to compute  $\tau_c$  and  $k_d$  values per the SPS method scour depth readings corresponding to the first selected pressure head at each jet test were used and identified as: SPS-BM, SPS-IP, and SPS-SDP (Table 3).

**Table 3.** Statistical summary of erodibility parameters computed using different computational methods: SPS-BM, MPS-BM, SPS-SDP, MPS-SDP, SPS-IP, and MPS-IP (as defined in Table 1).

Methods	Critical Shear Stress, $\tau_c$ (Pa)				Erodibility Coefficient, $k_d$ (cm <sup>3</sup> /N·s)			
	Min	Max	Mean	Std. Dev	Min	Max	Mean	Std. Dev
Single Pressure Setting (SPS-BM)	0.00	12.43	2.48	2.25	0.53	24.28	3.84	3.84
Multiple Pressure Settings (MPS-BM)	0.09	26.80	5.13	3.82	0.56	24.28	3.26	3.54
Scour Depth Principle (SPS-SDP)	0.00	19.09	6.88	3.78	0.93	81.13	12.28	13.02
MPS using SDP method (MPS-SDP)	0.00	21.97	8.51	4.32	0.89	81.13	9.44	10.48
Iterative Principle (SPS-IP)	1.99	12.76	7.07	2.09	3.73	102.12	23.92	16.77
MPS using IP method (MPS-IP)	1.99	15.20	8.12	2.61	3.73	102.12	24.27	15.98

Among the 21 stream sites (126 jet tests), soil textures varied but generally were predominantly silty-loam and silty-clay-loam (Figure 1). Atterberg limit tests indicated the presence of cohesiveness in the soil samples since the PI values were between ~3 and 21. The LL and PL values were between 24% and 43%, and 17% and 31%, respectively. Some of the soil samples had a low PI (3.4–7.5), even though the material met the criteria for cohesive soils (minimum clay content of 5–10% by weight) as defined by Raudkivi [45] and Mitchell and Soga [46]. Bulk density of the tested soils was between 1.52 g·cm<sup>-3</sup> and 2.12 g·cm<sup>-3</sup>, and the  $D_{50}$  value was between 3.7  $\mu$ m and 40  $\mu$ m. Soil cohesion ranged from 8.55 kPa to 107.90 kPa. Details of other physical and geochemical properties of these soil samples were summarized in Mahalder et al. [16]. The relationship between  $\tau_c$  and  $k_d$  from the MPS-BM for the jet device dataset among the 21 Tennessee sites showed an inverse power relationship (Figure 6). The linear relationship between  $\tau_c$  and  $k_d$  is consistent with others [4,8,14], however the MPS result in this study scales higher for the erodibility parameters.

Mean  $\tau_c$  using the MPS-BM method was 5.13 Pa, over twice the mean of 2.48 Pa from the SPS-BM method (Table 3, Figure 7a). Estimates of  $\tau_c$  between the MPS-BM and SPS-BM methods were statistically different ( $p < 0.001$ , Mann-Whitney U test, SPSS- v.23.0). Mean  $k_d$  was 3.26 cm<sup>3</sup>·N<sup>-1</sup>·s<sup>-1</sup> using the MPS-BM method and 3.84 cm<sup>3</sup>·N<sup>-1</sup>·s<sup>-1</sup> from the SPS-BM method (Figure 7b); they were not significantly different ( $p = 0.116$ ). Similarly,  $\tau_c$  estimates from the MPS-BM procedure also compared with the SPS-SDP and SPS-IP procedures (Figure 7a). The mean  $\tau_c$  values using the MPS-BM method was found to be 5.13 Pa, and for the SPS-SDP and SPS-IP the mean values were found to be 6.88 Pa and 7.07 Pa, respectively. The median  $\tau_c$  using the MPS-BM method was statistically different from both the SPS-SDP and SPS-IP procedures ( $p < 0.001$ ). Estimated  $k_d$  values were significantly less for both the MPS-BM and SPS-BM procedures compared with the SPS-SDP and SPS-IP procedures (Table 3; Figure 7b). This result identified a major anomaly using these solution approaches where  $k_d$  values increased with increasing  $\tau_c$  values, and was similarly reported by Karamigolbaghi et al. [32]. It is

important to note that a wide range (about 1 to 3 orders of magnitude difference) in the estimated  $\tau_c$  and  $k_d$  values were observed among this dataset using different computational procedures.

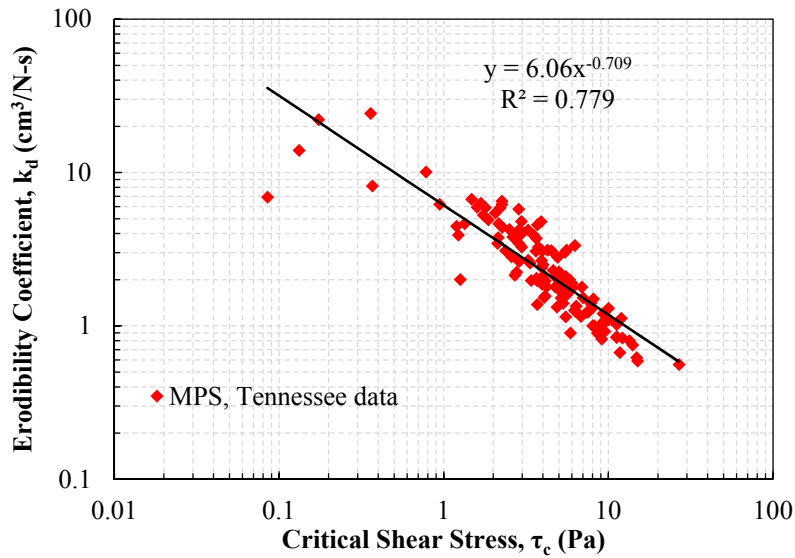


**Figure 6.** Relationship between critical shear stress ( $\tau_c$ ) and erodibility coefficient ( $k_d$ ) using the MPS method data from this study.

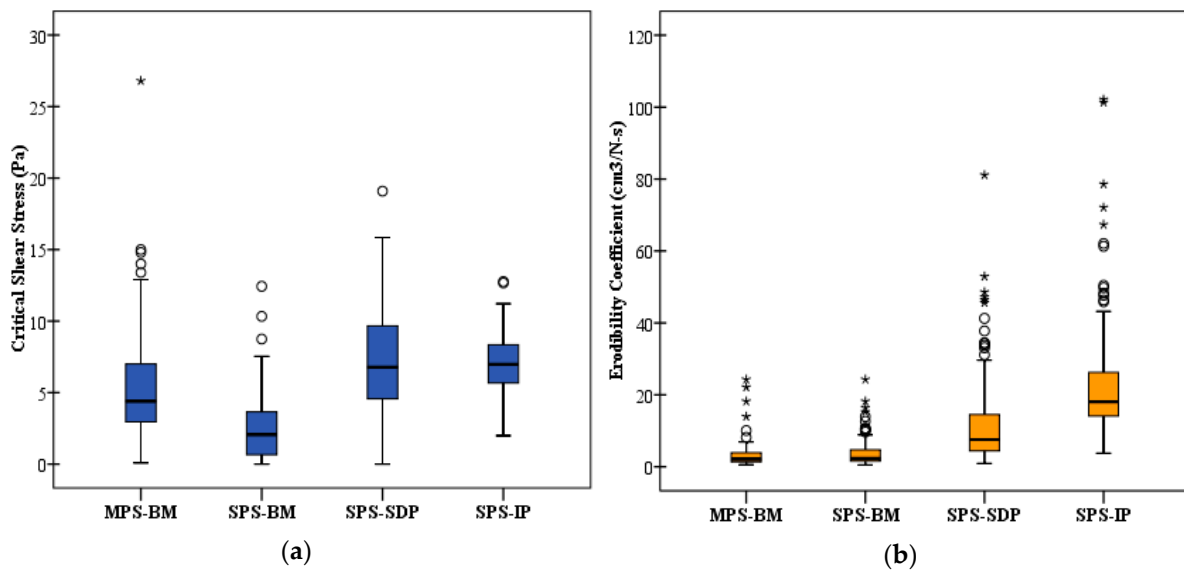


**Figure 7.** (a) Critical shear stress, and (b) erodibility coefficient using the field methods and computation procedures: MPS-BM, SPS-BM, SPS-SDP, and SPS-IP (as defined in Table 1).

Erodibility parameters estimated from the 126 jet test dataset using the MPS-BM, MPS-SDP, MPS-IP procedures were also compared (Figure 8). The mean  $\tau_c$  values were 8.51 Pa and 8.12 Pa, and mean  $k_d$  values were  $9.44 \text{ cm}^3 \cdot \text{N}^{-1} \cdot \text{s}^{-1}$  and  $24.27 \text{ cm}^3 \cdot \text{N}^{-1} \cdot \text{s}^{-1}$  for MPS-SDP and MPS-IP procedures, respectively. The erodibility parameters ( $\tau_c$  and  $k_d$ ) from the MPS-BM procedures were statistically different from the estimates using the MPS-SDP and MPS-IP procedures ( $p < 0.001$ , Mann-Whitney U test, SPSS v.23.0). Overall,  $\tau_c$  and  $k_d$  values were greater for both the MPS-SDP and MPS-IP procedures compared with SPS-SDP and SPS-IP. As defined in Figure 2, more discrete relationships between  $\tau_c$  and the corresponding pressure heads were observed with MPS-SDP (58 observations) and MPS-IP (42 observations) procedures. Also, based on field observations, discrete relationships between  $\tau_c$

and pressure head from the MPS method appeared to be dependent on the soil's physical properties. Therefore, these relationships for MPS-SDP and MPS-IP procedures deviated from the hypothesis that  $\tau_c$  increases with soil depth.

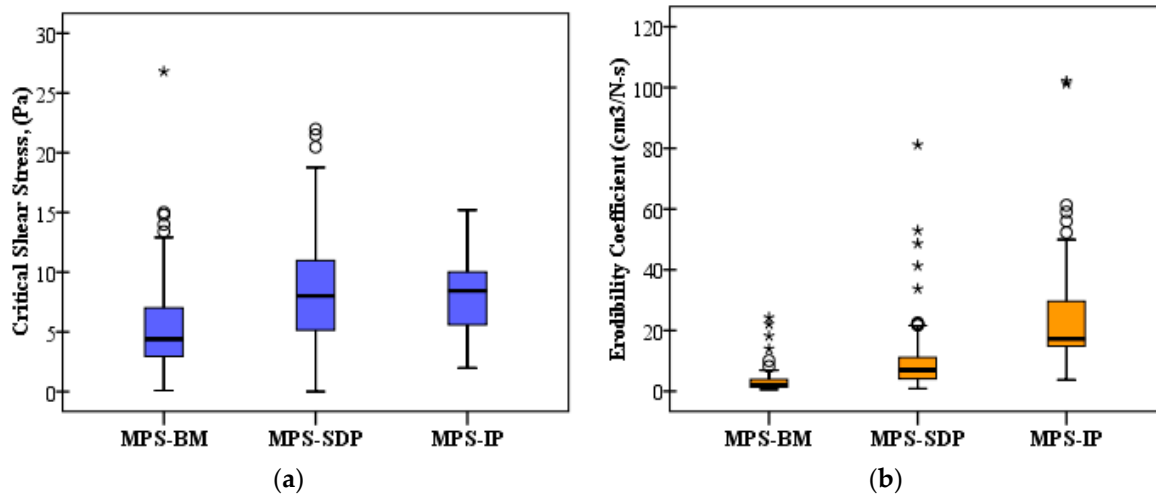


**Figure 8.** A comparison of (a) critical shear stress and (b) erodibility coefficient using the MPS method for the computational procedures: MPS-BM, MPS-SDP, and MPS-IP (as defined in Table 1).

Pairwise differences for  $\tau_c$  estimates between the MPS-BM and the other computational procedures were above and below a zero difference, though the median differences for these comparisons were negative except for the SPS-BM procedure (Figure 9a). The pairwise difference of  $\tau_c$  between the MPS-BM and SPS-BM procedures was positive with a range between 0.0 and 14.32 Pa, which indicates the MPS-BM procedure predicted 17% to 100% higher  $\tau_c$  values compared with the SPS-BM procedure. Of the 126 field tests only 29 resulted in positive  $\tau_c$  pairwise differences between MPS-BM and SPS-SDP, and SPS-IP procedures. When comparing the pairwise differences for  $\tau_c$  between MPS-BM and MPS-SDP, and MPS-IP procedures, only 13 and 18 observations were positive. The greater  $\tau_c$  values for the MPS method apparently accounts for the increased cohesive properties of soil as the scour hole develops during the field test.

Pairwise differences for  $k_d$  between MPS-BM and SPS-SDP, SPS-IP, MPS-SDP, and MPS-IP procedures were generally negative (Figure 9b). Therefore, both the SDP and IP procedures (using both the SPS and MPS methods) predicted much higher  $k_d$  values compared with the MPS-BM procedure. In general, these variations among all the procedures demonstrate how both field protocols and computational procedures greatly influence in situ  $\tau_c$  and  $k_d$  values. Using the published datasets from the Daly et al. [20,31] studies, a slight increase in  $\tau_c$  values were associated with significantly higher  $k_d$  values (Figure 10). Therefore, significantly higher erosion rates are expected using the linear erosion model with the SPS-SDP and SPS-IP computational results. Karamigolbaghi et al. [32] showed that the SPS-SDP and SPS-IP procedures predicted physically unrealistic erosion rates (negative erosion rate) using the Hanson and Cook [7] data. Likewise, the MPS-SDP and MPS-IP procedures did not physically improve the uncertainty associated with these two methods. Furthermore, this study found inconsistent  $k_d$  values using the SPS-SDP and SPS-IP procedures, which was also reported in previous studies [10,20,31].

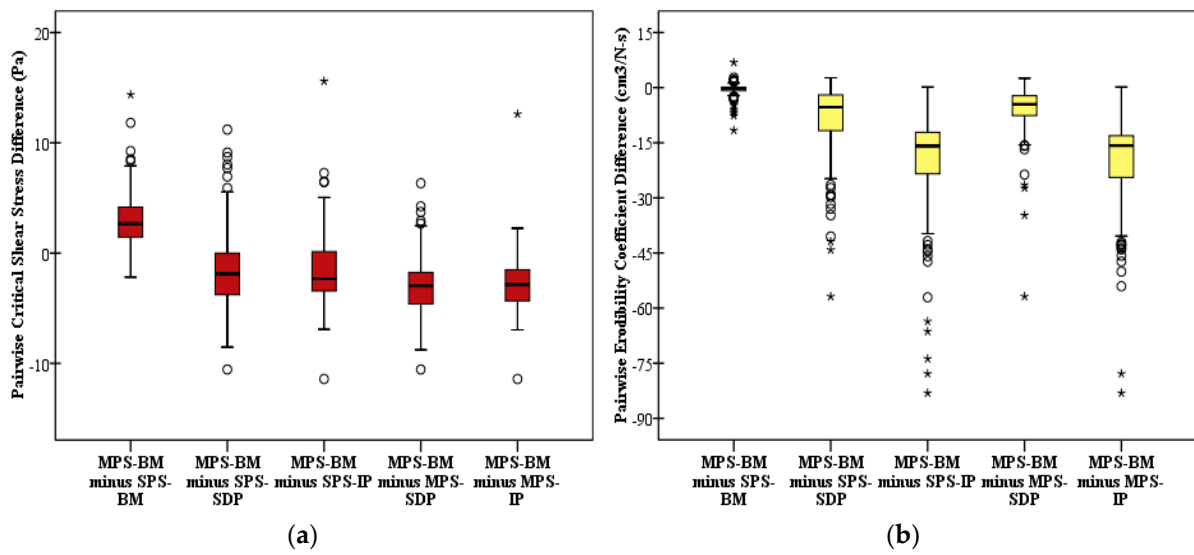


**Figure 9.** Pairwise differences between different solution techniques for: (a) critical shear stress ( $\tau_c$ ), and (b) erodibility coefficient ( $k_d$ ) estimations between: MPS-BM and SPS-BM; MPS-BM and SPS-SDP; MPS-BM and SPS-IP; MPS-BM and MPS-SDP; and MPS-BM and MPS-IP procedures.

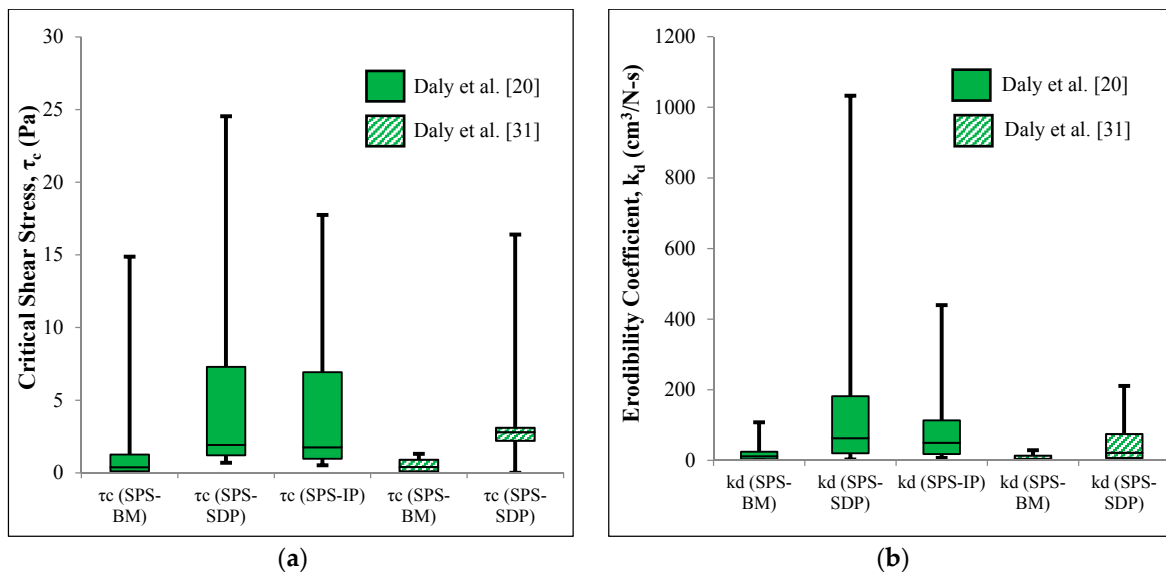


**Figure 10.** Comparison of (a) critical shear stress ( $\tau_c$ ) and (b) erodibility coefficient ( $k_d$ ) using the SPS-BM, SPS-SDP and SPS-IP methods based on data from Daly et al. [20,31].

Daly et al. [22] suggested that a reduction factor ( $\alpha$ ) in the excess shear stress equation to estimate erosion parameters using the SPS-SDP and SPS-IP computational procedures, could alleviate the problem to some extent, expressed as follows in Equation (10):

$$\varepsilon_T = k_d(\alpha \tau_b - \tau_c) = \alpha k_d \left( \tau_b - \frac{\tau_c}{\alpha} \right) \tag{10}$$

However, the acceptability of these two computational procedures may be limited if a reduction factor is required for erosion prediction, because it is understood that the reduction factor is site specific and also dependent on the expertise of the person who is operating the jet device in different regions and soil properties. Thus, further research is needed to address this issue using these two methods.

#### 4.3. Qualitative Observations in Scour-Hole Development and Morphology

Based on field observations, development and morphology of a scour hole subjected to jet hydraulic forces were dependent on several soil properties, which affected depth measurements over prescribed test time intervals. It has been demonstrated in this study how the time interval of scour-hole depth measurements, and the use of different computation procedures influence the estimation of the  $\tau_c$  and  $k_d$  parameters [10,21,31]. Thus, computed values of  $\tau_c$  and  $k_d$  are interdependent on soil properties, scour hole morphological development and depth measurements over time, and computational procedure using the depth measurements. As observed from this study, it was found that comparatively dry and loose soils (with higher  $D_{50}$ ) resulted in discrete patterns between pressure head settings and erodibility parameters (Figure 2c,f). By observing the position of the tested soil on the creek, it appeared that the soil formation age and cohesion had a substantial effect on the concave and linear increasing patterns (Figure 2a,b,d,e). It was also observed that a wider and shallower scour hole (Figure 11a) was observed for the concave and linear increasing patterns and a narrower deep scour hole (Figure 11b) was observed for the discrete pattern (Figure 2c,f). Nonlinear patterns appeared to occur as the scour depth increased with time and higher applied shear stress from increased device pressure (Figure 2a,d).



**Figure 11.** Photos of scour hole formation in different soil physical conditions (a) wide and shallower, and (b) narrow and deeper.

Khanal et al. [10] attempted to correlate erodibility parameters with applied pressure heads, though no specific patterns were reported in their study conducted on laboratory remolded soils and a limited number of tests utilizing only three pressure heads per test. The use of laboratory remolded soils limits the range of  $\tau_c$  and  $k_d$  estimates that can be obtained for multiple pressure settings which generated different response patterns based on soil conditions (as observed in Figure 2). In addition, remolded soils add to uncertainty in parameter estimation associated with whether adequate time for consolidation has occurred, which over time may affect soil cohesion. Khanal et al. [10] did observe that the initial time interval and the termination time interval significantly influenced the estimates for erodibility parameters based on soil properties. In this study, it was found that a change in an initial few scour depth data points (4–5 data points) significantly affected the computed erodibility parameter values. This observation suggests estimation of erodibility parameters with the jet device using a single pressure setting can be greatly influenced by soil properties at the test surface. Because the bulk density and cohesion of the soil strata generally increases with depth into the streambank, applying multiple pressure settings with the jet device can alleviate some of these issues with over-predicting  $\tau_c$

and  $k_d$  for streambanks with cohesive soil. In addition, for the dataset applied in this study, it appears that estimates of  $\tau_c$  and  $k_d$  using the MPS-BM procedure were comparatively more consistent with the SPS-SDP, MPS-SDP, SPS-IP and MPS-IP procedures.

## 5. Conclusions

This study investigated the effect of different pressure settings on the mini-jet device using three published computational procedures (BM, SDP, and IP) for estimating the  $\tau_c$  and  $k_d$  erodibility parameters, in which a unique MPS procedure was developed and tested. The effect of time interval selection for scour-hole depth measurements during an in situ test was also examined for the different field and computational procedures. The experimental study was based on the hypothesis that streambank soil cohesion and bulk density increases from the near surface into the bank, differing due to subaerial processes and other environmental factors, therefore  $\tau_c$  and  $k_d$  are affected as the jet device forms the scour hole at a test location. It was also hypothesized by incrementally increasing device pressure settings during the test that it would compensate for the assumed change in soil properties as the scour hole develops. Collectively from 21 streambank sites across different Tennessee physiographic regions (a dataset of 126 jet tests),  $\tau_c$  estimates applying the MPS-BM procedure were 17–100% greater than those applying the SPS-BM procedure, though the SPS-SDP, SPS-IP, MPS-SDP, and MPS-IP procedures generally estimated higher values. With  $k_d$  estimates, MPS-BM showed lower values and less variation ( $\sigma = 3.54$ ) in the dataset compared with the SPS-BM, SPS-SDP, SPS-IP, MPS-SDP, and MPS-IP procedures. These findings support the hypothesis of increasing  $\tau_c$  and decreasing erodibility as the soil depth increases for cohesive soils, whereas the SPS-SDP, MPS-SDP, SPS-IP, and MPS-IP procedures estimated results contradicted the hypothesis. The MPS-BM procedure generated more consistent results for  $\tau_c$  and  $k_d$  estimates (smaller ranges for the same applied dataset) compared with the SPS methods and the three computational procedures (BM, SDP, and IP).

It appears that the MPS field methodology provides an alternative to the reduction factor ( $\alpha$ ) suggested by others to be incorporated in the excess shear stress equation to address the over-prediction of soil erosion on streambanks when  $\tau_c$  and  $k_d$  estimates are used from the SPS method. The advantage of using the MPS is that  $\tau_c$  and  $k_d$  estimates are determined in situ whereas  $\alpha$  requires a known relationship as a function of soil properties. It was shown in this study, that relationships between applied device pressure, and  $\tau_c$  and  $k_d$  estimates were dependent on soil properties at the test location, which in turn affected the developmental morphology of the scour hole. Distinct patterns from these relationships were observed with different soil properties where it appears that with greater cohesion a concave-down to linear patterns were prominent in contrast to scattered patterns for less cohesive soils. This finding also suggests that the MPS method produces more consistent  $\tau_c$  and  $k_d$  estimates with more diverse soil properties.

Overall, it appears that the MPS method, in which incrementally increasing device pressure settings are applied for estimating  $\tau_c$  and  $k_d$  values, may better reflect fluvial erosion processes along a streambank/bed during a flood event. Consequently, average erodibility parameter values are represented rather than that of the surficial soil layer. The BM computational procedure appeared to generate more consistent estimates of  $\tau_c$  and  $k_d$  compared with the SDP and IP procedures, therefore the best results appear to be the MPS-BM procedure. More consistent procedures for estimating the erodibility parameters are a benefit to stream restoration practitioners improving on project designs that incorporate bank protection structures. Findings from this study suggest further research is needed to demonstrate its implications for improving the prediction of streambank erosion, in addition to an important and essential goal to standardize both field and computation methodologies.

**Acknowledgments:** This work was funded by Grant No. RES #2013-36 from the Tennessee Department of Transportation (TDOT). The authors would also like to thank Nancy Roberts for training and equipment support in the use of the Geotechnical Laboratory, Department of Civil and Environmental Engineering, the University of Tennessee, Knoxville. The authors would also like to thank Rob Thomas of USDA for sharing spreadsheets to analyze the jet-test device field data. Student field assistance was provided by Jordan Hicks and Zachariah Seiden.

**Author Contributions:** Badal Mahalder, the senior author generated the manuscript as part of his PhD dissertation, and co-authors John Schwartz, Angel Palomino, and Jon Zirkle supervised his research, in addition to direct text contributions to his study's manuscript.

**Conflicts of Interest:** The author declares no conflict of interest.

## References

- Dunn, I.S. Tractive Resistance of Cohesive Channels. *J. Soil Mech. Found.* **1959**, *85*, 1–24.
- Arulanandan, K.; Gillogley, E.; Tully, R. *Development of a Quantitative Method to Predict Critical Shear Stress and Rate of Erosion of Natural Undisturbed Cohesive Soils*; Waterways Experiment Station Technical Report, GL-80-5; USACE: Vicksburg, MS, USA, 1980.
- Hanson, G.J. Surface Erodibility of Earthen Channels at High Stresses. Part I-Open Channel Testing. *Trans. ASAE* **1990**, *33*, 127–131. [[CrossRef](#)]
- Hanson, G.J.; Simon, A. Erodibility of Cohesive Streambeds in the Loess Area of the Midwestern USA. *Hydrol. Process* **2001**, *15*, 23–28. [[CrossRef](#)]
- Sanford, L.P.; Maa, J.P.Y. A Unified Erosion Formulation for Fine Sediments. *Mar. Geol.* **2001**, *179*, 9–23. [[CrossRef](#)]
- Hanson, G.J.; Cook, K.R. Development of Excess Shear Stress Parameters for Circular Jet Testing. In *ASAE Paper No. 97-2227*; ASABE: St. Joseph, MI, USA, 1997.
- Hanson, G.J.; Cook, K.R. Apparatus, Test Procedures, and Analytical Methods to Measure Soil Erodibility in-situ. *Appl. Eng. Agric.* **2004**, *20*, 455–462. [[CrossRef](#)]
- Simon, A.; Thomas, R.E.; Klimetz, L. Comparison and Experiences with Field Techniques to Measure Critical Shear Stress and Erodibility of Cohesive Deposits. In Proceedings of the 2nd Joint Federal Interagency Conference on Sedimentation and Hydrologic Modeling, Las Vegas, NV, USA, 27 June–1 July 2010.
- Al-Madhhachi, A.T.; Hanson, G.J.; Fox, G.A.; Tyagi, A.K.; Bulut, R. Measuring Soil Erodibility Using a Laboratory “mini” JET. *Trans. ASABE* **2013**, *56*, 901–910.
- Khanal, A.; Fox, G.A.; Al-Madhhachi, A.T. Variability of Erodibility Parameters from Laboratory mini Jet Erosion Tests. *J. Hydrol. Eng.* **2016**, *21*. [[CrossRef](#)]
- Briaud, J.; Ting, F.; Chen, H.C.; Gudavilli, R.; Kwak, K.; Philogene, B.; Han, S.; Perugu, S.; Wei, G.; Nurtjahyo, P.; et al. *SRICOS: Prediction of Scour Rate at Bridge Piers*; Report 2937-1; Texas Transportation Institute, The Texas A&M University: College Station, TX, USA, 2001.
- Julian, J.; Torres, R. Hydraulic Erosion of Cohesive Riverbanks. *Geomorphology* **2006**, *76*, 193–206. [[CrossRef](#)]
- Wynn, T.M.; Mostaghimi, S. The Effects of Vegetation and Soil Type on Streambank Erosion, Southwestern Virginia, USA. *J. Am. Water Resour. Assoc. AWARA* **2006**, *42*, 69–82. [[CrossRef](#)]
- Thoman, R.W.; Niegoda, S.L. Determining Erodibility, Critical Shear Stress, and Allowable Discharge Estimates for Cohesive Channels; Case Study in the Powder River Basin of Wyoming. *J. Hydraul. Eng.* **2008**, *134*, 1677–1687. [[CrossRef](#)]
- Grabowski, R.C.; Droppo, I.G.; Wharton, G. Erodibility of Cohesive Sediment: The Importance of Sediment Properties. *Earth Sci. Rev.* **2011**, *105*, 101–120. [[CrossRef](#)]
- Mahalder, B.; Schwartz, J.S.; Palomino, A.M.; Zirkle, J. Relationships between physical-geochemical soil properties and erodibility of streambanks among different physiographic provinces of Tennessee, USA. *Earth Surf. Process. Landf.* **2017**. [[CrossRef](#)]
- Lick, W.; McNeil, J.; Xu, Y.J.; Taylor, C. *Measurements of the Resuspension and Erosion of Sediments in Rivers*; Department of Mechanical and Environmental Engineering, University of California: Santa Barbara, CA, USA, 1994.
- Zreik, D.A.; Krishnappan, B.G.; Germaine, J.T.; Madsen, O.S.; Ladd, C.C. Erosional and Mechanical Strengths of Deposited Cohesive Sediments. *J. Hydraul. Eng.* **1998**, *124*, 1076–1085. [[CrossRef](#)]
- Midgley, T.L.; Fox, G.A.; Wilson, G.V.; Heeren, D.M.; Langendoen, E.; Simon, A. Streambank Erosion and Instability Induced by Seepage: In-situ Constant-head Experiments. *J. Hydrol. Eng.* **2013**, *18*, 1200–1210. [[CrossRef](#)]
- Daly, E.R.; Fox, G.A.; Enlow, H.K.; Storm, D.E.; Hunt, S.L. Site-scale Variability of Streambank Fluvial Erodibility Parameters as Measured with a Jet Erosion Test. *J. Hydrol. Process.* **2015**, *29*, 5451–5464. [[CrossRef](#)]

21. Sutarto, T.; Papanicolaou, T.A.N.; Wilson, C.G.; Langendoen, E.J. Stability Analysis of Semicohesive Streambanks with CONCEPTS: Coupling Field and Laboratory Investigations to Quantify the Onset of Fluvial Erosion and Mass Failure. *J. Hydraul. Eng.* **2014**, *140*. [[CrossRef](#)]
22. Daly, E.R.; Miller, R.B.; Fox, G.A. Modelling Streambank Erosion and Failure along Protected and Unprotected Composite Streambanks. *Adv. Water Resour.* **2015**, *81*, 114–127. [[CrossRef](#)]
23. Daly, E.R.; Fox, G.A.; Fox, A.K. Correlating Site-scale Erodibility Parameters from Jet Erosion Tests to Soil Physical Properties. *Trans. ASABE* **2016**, *59*, 115–128. [[CrossRef](#)]
24. McNeil, J.; Taylor, C.; Lick, W. Measurements of Erosion of Undisturbed Bottom Sediments with Depth. *J. Hydraul. Eng.* **1996**, *122*, 316–324. [[CrossRef](#)]
25. Taylor, C.; Lick, W. *Erosion Properties of Great Lakes Sediments*; Department of Mechanical and Environmental Engineering, University of California: Santa Barbara, CA, USA, 1996.
26. Jepsen, R.; Roberts, J.; Lick, W. Effects of Bulk Density on Sediment Erosion Rates. *Water Air Soil Pollut.* **1997**, *99*, 21–31. [[CrossRef](#)]
27. Roberts, J.; Jepsen, R.; Gotthard, D.; Lick, W. Effects of Particle Size and Bulk Density on Erosion of Quartz Particles. *J. Hydraul. Eng.* **1998**, *124*, 1261–1267. [[CrossRef](#)]
28. Perkins, R.G.; Honeywill, C.; Consalvey, M.; Austin, H.A.; Tolhurst, T.J.; Paterson, D.M. Changes in Microphytobenthic Chlorophyll a and EPS Resulting from Sediment Compaction Due to de-watering: Opposing Patterns in Concentration and Content. *Cont. Shelf Res.* **2003**, *23*, 575–586. [[CrossRef](#)]
29. Perkins, R.G.; Sun, H.; Watson, J.; Player, M.A.; Paterson, D.M. In-line Laser Holography and Video Analysis of Eroded Flocs from Engineered and Estuarine Sediments. *Environ. Sci. Technol.* **2004**, *38*, 4640–4648. [[CrossRef](#)] [[PubMed](#)]
30. Lick, W.; McNeil, J. Effects of Sediment Bulk Properties on Erosion Rates. *Sci. Total Environ.* **2001**, *266*, 41–48. [[CrossRef](#)]
31. Daly, E.R.; Fox, G.A.; Al-Madhhachi, A.T.; Miller, R.B. A Scour Depth Approach for Deriving Erodibility Parameters from Jet Erosion Tests. *Trans. ASABE* **2013**, *56*, 1343–1351. [[CrossRef](#)]
32. Karamigolbaghi, M.; Ghaneezad, S.M.; Atkinson, J.F.; Bennett, S.J.; Wells, R.R. Critical Assessment of Jet Erosion Test Methodologies for Cohesive soil and Sediment. *Geomorphology* **2017**, *295*, 529–536. [[CrossRef](#)]
33. Mahalder, B.; Schwartz, J.S.; Papanicolaou, A.N.T.; Palomino, A.M.; Zirkle, J. Comparison of erodibility parameters for cohesive streambank soils between an in-situ jet test device and laboratory conduit flume. *J. Hydraul. Eng.* **2018**. (submitted).
34. Craft, T.; Graham, L.; Launder, B. Impinging Jet Studies for Turbulence Model Assessment—II. An Examination of the Performance of Four Turbulence Models. *Int. J. Heat Mass Transf.* **1993**, *36*, 2685–2697. [[CrossRef](#)]
35. Gibson, M.M.; Launder, B.E. Ground Effects on Pressure Fluctuations in the Atmospheric Boundary Layer. *J. Fluid Mech.* **1978**, *86*, 491–511. [[CrossRef](#)]
36. Mercier, F.; Bonelli, S.; Pinettes, P.; Golay, F.; Anselmet, F.; Philippe, P. Comparison of CFD simulations with experimental Jet Erosion Tests results. *J. Hydraul. Eng.* **2014**, *140*. [[CrossRef](#)]
37. Clark, L.A.; Wynn, T.M. Methods for Determining Streambank Critical Shear Stress and Soil Erodibility: Implications for Erosion Rate Predictions. *Trans. ASABE* **2007**, *50*, 95–106. [[CrossRef](#)]
38. Bonelli, S.; Brivois, O. The Scaling Law in the Hole Erosion Test with a Constant Pressure Drop. *Int. J. Numer. Anal. Methods Geomech.* **2008**, *32*, 1573–1595. [[CrossRef](#)]
39. Bonelli, S.; Golay, F.; Mercier, F. *On the Modelling of Interface Erosion*; Erosion of Geomaterials; Wiley/ISTE: Hoboken, NJ, USA, 2012; Chapter 6, pp. 187–222.
40. Golay, F.; Lachouette, D.; Bonelli, S.; Seppacher, P. Numerical Modelling of Interfacial Soil Erosion with Viscous Incompressible Flows. *Comput. Methods Appl. Mech. Eng.* **2011**, *200*, 383–391. [[CrossRef](#)]
41. Stein, O.R.; Nett, D.D. Impinging jet calibration of excess shear sediment detachment parameters. *Trans. ASAE* **1997**, *40*, 1573–1580. [[CrossRef](#)]
42. Blaisdell, F.W.; Clayton, L.A.; Hebaus, C.G. Ultimate Dimension of Local Scour. *J. Hydraul. Div.* **1981**, *107*, 327–337.
43. Miller, R.A. *The Geologic History of Tennessee*; Tennessee Division of Geology: Nashville, TN, USA, 1974; Volume 74.
44. Hanson, G.J.; Robinson, K.M.; Cook, K.R. Scour below an overfall: Part II. Prediction. *Trans. ASAE* **2002**, *45*, 957–964. [[CrossRef](#)]

45. Raudkivi, A.J. *Loose Boundary Hydraulics*, 3rd ed.; Pergamon Press: New York, NY, USA, 1990.
46. Mitchell, J.K.; Soga, K. *Fundamentals of Soil Behavior*, 3rd ed.; John Wiley & Sons, Inc.: Hoboken, NJ, USA, 2005.



© 2018 by the authors. Licensee MDPI, Basel, Switzerland. This article is an open access article distributed under the terms and conditions of the Creative Commons Attribution (CC BY) license (<http://creativecommons.org/licenses/by/4.0/>).

## **Appendix B: Journal Article Manuscript**

Mahalder, B., J.S. Schwartz, A.N. Papanicolaou, A.M. Palomino, and J. Zirkle. 2018.

Comparison of erodibility parameters for cohesive streambank soils between an in-situ jet test device and laboratory conduit flume. *Journal of Hydraulics Engineering* (prepared for submission).

# Comparison of erodibility parameters for cohesive streambank soils between an in-situ jet test device and laboratory conduit flume

Badal Mahalder, John S. Schwartz, A.N. Thanos Papanicolaou, Angelica M. Palomino, and Jon Zirkle

## ABSTRACT

Several methods have been developed to estimate erodibility parameters for cohesive streambanks, critical shear stress  $\tau_c$  and the erodibility coefficient  $k_d$ . This research compares estimates of these parameters between an in situ mini-jet device and a pressurized laboratory conduit flume. Operation of the mini-jet device applied a unique multiple pressure setting (MPS) procedure that accounts for the change in soil properties into the bank matrix from the surface. Both the mini-jet MPS approach and the conduit flume using the Sutarto et al. approach remove the effect of surface subaerial process on erodibility parameter estimations, and resulted in similar  $\tau_c$  and  $k_d$  estimates from the same bank soils. Estimates for  $\tau_c$  between the two devices were in general agreement compared to  $k_d$  especially for shear magnitudes greater than 5 Pa and consolidated soil with moisture contents greater than 20%. Erodibility estimates between devices differed likely due to the aggregate failure behavior of cohesive soils. Findings suggest  $\tau_c$  and  $k_d$  estimates are dependent on the device hydraulics, computational method, and soil properties.

**Keywords:** cohesive soil, erodibility, jet test device, conduit flume

## 1. INTRODUCTION

Erodibility parameters for cohesive soils, namely the critical shear stress ( $\tau_c$ ) and erodibility coefficient ( $k_d$ ), can range over orders of magnitude depending on the different measurement devices used in the analysis. These methods include the following: laboratory flume type tests (Briaud et al., 2001; Mostafa et al., 2008; Sutarto et al., 2014), laboratory hole erosion tests (Wan and Fell, 2004), in-situ direct measurements using submersible flumes (Amos et al., 1992; Houwing and van Rijn, 1998), rotating cylinder test (Moore and Masch, 1962; Arulanandan et al., 1973; Chapuis and Gatién, 1986), and jet test devices (Hanson, 1990; Hanson and Cook, 2004; Simon et al., 2010; Al-Madhhachi et al., 2013a). Each method has advantages and disadvantages related to its operational principles and analytical procedures for measuring  $\tau_c$  and  $k_d$  and estimating streambank erosion rates with applicability (Tolhurst et al., 2000; Aberle et al., 2003; Debnath et al., 2004; Debnath et al., 2007; Hobson, 2008; Weidner, 2012; Bones, 2014; Sutarto et al., 2014). However, a critical review is still needed to understand better the variability generated by these different devices and their inherent theoretical and operational principles.

A limited number of studies have compared erosion measurements using in-situ jet and flume devices in cohesive soil, though the main focus was to compare the  $k_d$  values (Hanson, 1990; Hanson and Cook, 2004; Hanson and Hunt, 2007; Al-Madhhachi et al., 2013b). Hanson (1990) related soil erodibility values at different water contents from both flume tests and in-situ jet tests assuming negligible  $\tau_c$  values. Similar to the Hanson (1990) study, assuming fixed  $\tau_c$  values, erosion rates were measured from the flume tests and the corresponding  $k_d$  values were compared to the jet test results considering the excess shear stress equation (Hanson and Cook, 2004; Hanson

and Hunt, 2007; Al-Maddhachi et al., 2013b). Soil samples in these studies consisted of different textures (e.g., silty clay, lean clay, or silty sand) and were compacted at different water contents. Yet, no direct comparisons between  $\tau_c$  and  $k_d$  values estimation have been reported using two independent devices to date in the literature. Several study results also identified that analytical solution methods can significantly influence the erodibility parameters estimated from jet test data (Daly et al., 2015; Khanal et al., 2016, Karamigolbaghi et al., 2017, Mahalder et al., 2018), although, an acceptable fit to the scour depth data from those solution methods were identified with a wide range in estimated  $\tau_c$  and  $k_d$  values. Currently, using linear excess shear stress principle, three analytical solution methods are available to predict  $\tau_c$  and  $k_d$  using jet test data: Blaisdell solution (BL) method, iterative solution (IP) method, and scour depth solution (SDP) method. Recently, Karamigolbaghi et al. (2017) showed that physically unrealistic values of erosion rates can be obtained from both the IP and SDP solution methods using the published data from the Hanson and Cook (2004) study.

Briaud et al. (2001) developed the erosion function apparatus (EFA) to assess soil erodibility to model scour around bridge piers using pressurized flow principles. In the EFA, a soil test sample is exposed to pressurized flow by controlling movement of the sample into the flow field from the apparatus bottom. However, the applied forces on the sample is both shear and drag where the drag force acts predominantly on the exposed soil sample protruded face consequently affecting the erosion rate. Papanicolaou (2001) and Papanicolaou et al. (2007) developed a field-laboratory testing protocol in which relatively undisturbed soil samples are collected from the field in a 30 cm by 10 cm open box and placed in a free-surface flume exposed to shear forces only. Similar to results found by Mallison (2008), an open channel flume limited the maximum applied shear that could be generated. Thus, Sutarto et al. (2014) developed a new pressurized flume to measure  $\tau_c$  and  $k_d$  integrating concepts from Briaud et al. (2001) and Papanicolaou et al. (2007). According to the working principle of this conduit flume, it is capable of applying a wide range of applied shear stresses parallel to the soil test surface compared to other devices such as the jet tester, annular flumes, EFA, and free-surface channels (Sutarto et al., 2014). The fact that the flow in the conduit is pressurized it allows the use of the flume on resistant soil surfaces where the applied shear stress values for erosion to occurs requires values up to nearly 60 Pa.

The arguments between laboratory flume and in-situ devices have been well documented in literature for  $\tau_c$  and  $k_d$  estimation in cohesive soils. It is well known that laboratory flume tests provide greater degree of control over the experimental conditions compared to in-situ field devices. However, it is understood that “undisturbed” soil sample collection is challenging since during sample collection and transport to the laboratory, soil microstructures can be altered significantly. In addition to this, other possible changes in soil physical properties (e.g., soil moisture) could significantly alter the erosion behavior of the collected soil samples compared to the source soil. In lieu, in-situ test devices preserve the original in-field conditions better (Houwing and van Rijn 1998; Hanson and Cook, 2004; Debnath et al., 2007), but it is difficult to maintain precision on specific controls during tests.

The objectives of this research were to compare estimates for erodibility parameters ( $\tau_c$  and  $k_d$ ) and quantify the variability between a pressurized conduit flume and a mini-jet device using the available jet operation and data analyses approaches. Device comparisons are discussed in terms of their fundamental theoretical and operational principles governing erosion. During each test, changes in the chemical composition of the sediment and water mix were also monitored for quantifying possible influence on inter-particle attraction forces in cohesive soils. This

comparative study provides context in which to evaluate results from previously published cohesive soil erosion studies thereby enhancing our ability to interpret data derived from these two measurement devices.

## 2. DEVICE DESCRIPTION

### 2.1 In-situ jet test device

The submerged jet device was developed for measuring soil erodibility parameters in-situ, but it can also be used in the laboratory (Hanson, 1990; Hanson and Cook, 1997; Hanson and Simon, 2001) based on Dunn (1959). The jet device has two models (i) the original jet (Hanson, 1990; Hanson and Cook, 1997; Hanson and Simon, 2001), and (ii) the mini jet (Simon et al., 2010; Al-Madhhachi et al., 2013a). The mini jet device is a scaled down version of the original jet device, and consists of a submergence tank with a water inlet nozzle and outlet port, an internal rotating plate, a pressure gage to determine the flow velocity, a valve, a depth gage, hoses and a base metal ring. A high-velocity jet of water is projected normal to the soil surface through a 3.18 mm diameter nozzle. The rotating plate prevents the water jet from impinging upon the soil surface at the test initiation and during the scour hole measurements at different time intervals. A water pump supplies water directly from the stream to the desired pressure heads by regulating the valve for conducting in-situ tests on stream bed or banks. During the tests, a water jet impacts the soil surface through the water and diffuses radially, which produces a shear stress on the soil surface to initiate scour. By recording the applied pressure during the test and the corresponding scour depth at different time intervals, an equilibrium scour depth is estimated and  $\tau_c$  and  $k_d$  can be calculated. The mini jet device is much smaller and lighter compared to the original jet device and easier to use both in the laboratory and in the field, this device is generally preferred over the original jet device and was used in this study.

### 2.2 Laboratory conduit flume

The laboratory conduit flume is a straight, recirculating, pressurized device with a useful length of 305 cm and a rectangular cross section of  $10 \times 5$  cm. A sample tray is placed 215 cm downstream from the flow entrance (Fig. 1) to ensure fully developed flow. A conical water storage tank is attached to the 7.5 hp variable-speed pump, which passes water through a 7.62-cm ID galvanized pipe into a  $50 \text{ cm}^2$  rectangular Plexiglas conduit. This flume has a wide range of operational flow rates from  $0.0025 \text{ m}^3 \text{ s}^{-1}$  to  $0.0157 \text{ m}^3 \text{ s}^{-1}$ , flow velocities ( $0.5\text{-}3.10 \text{ m s}^{-1}$ ), and the corresponding shear stresses (1-32 Pa) for testing different soil types (Sutarto et al., 2014).

Specific sample collection and flume operational protocols have been established for this flume (Sutarto et al., 2014). Relatively undisturbed soil samples are collected from the field and tested either in the field or in the laboratory. The sample tray location is over 40 times the height of the conduit from the upstream diffuser to ensure a fully developed boundary layer over the sediment sample (McNeil et al., 1996). Approaching the tray, the conduit bed and ceiling is covered with fine sand paper for replicating micro-roughness of soil surface. Soil samples in the tray can be adjusted using the jack screws underneath the tray for any necessary minor adjustments to ensure the flume bed and soil surface are at the same elevation.

### 3. METHODOLOGY

The rationale for this comparative study is thought to be dependent on understanding the working principles of these two devices, which have been reported in the following section. It has been identified that sample collection protocols for conduit flume could have critical influence on erodibility parameters estimation. Whereas, for jet device, operational and data analyses procedures were also found critical. All of these issues have been discussed in this section with detail methodological procedures, which have been followed for conducting this research study.

#### 3.1 Jet device hydraulic principles

Hanson and Cook (1997) developed an analytical procedure to calculate the erosion index parameter from jet test data based on the jet diffusion principles of Stein and Nett (1997). This method was developed for the original submerged jet test apparatus; however, the governing principles are consistent for both devices. The major assumption associated with this device is the rate of scour or the erosion rate ( $dJ/dt$ ) is a function of the maximum stress at the boundary. Therefore, the jet erosion rate equation expressed by Hanson and Cook (1997, 2004) is the following:

$$\frac{dJ}{dt} = k_d \left[ \frac{\tau_0 J_p^2}{J^2} - \tau_c \right], \text{ for } J \geq J_p \quad (1)$$

where  $J$  is the scour depth (cm);  $J_p$  is the potential core length from jet origin (cm);  $k_d$  is the erodibility coefficient ( $\text{cm}^3 \text{N}^{-1} \text{s}^{-1}$ );  $\tau_0$  is the applied bottom shear stress (Pa); and  $\tau_c$  is the critical shear stress (Pa).

Based on the soil type and water conditions, the initial erosion rate could be substantial and approaches zero asymptotically for the jet device (Stein and Nett, 1997). In addition, the depth at which the applied shear stress on the soil surface does not produce any erosion ( $dJ/dt = 0$ ) is termed as equilibrium scour depth ( $J_e$ ) and the shear to that depth is termed as  $\tau_c$ .

$$\tau_c = \tau_0 \left( \frac{J_p}{J_e} \right)^2 \quad (2)$$

where  $\tau_0 = C_f \rho_w U_0^2$  is the maximum shear stress due to the jet velocity at the nozzle (Pa);  $C_f = 0.00416$  is the friction coefficient;  $\rho_w$  is water density ( $\text{kg m}^{-3}$ );  $U_0 = C\sqrt{2gh}$  is the velocity of jet at orifice ( $\text{cm s}^{-1}$ );  $C$  is discharge coefficient;  $h$  is the applied pressure head (cm);  $J_p = C_d d_0$ ;  $d_0$  is the nozzle diameter (cm); and  $C_d = 6.3$  is the diffusion constant. Blaisdell et al. (1981) showed that the time required to attain  $J_e$  is excessively high, hence, the calculation of  $\tau_c$  can be problematic. Therefore, they proposed calculating  $J_e$  by fitting the scour depth data versus time as a hyperbolic function. This method is identified as BL in this article.

Two other solution techniques IP and SDP methods were reported recently based on linear excess shear stress equation (Simon et al., 2010; Daly et al., 2013) to estimate  $\tau_c$  and  $k_d$  values. In the IP approach, initial values of  $\tau_c$  and  $k_d$  are estimated from the BL method. Then, erosion parameters are iteratively and simultaneously solved by minimizing the root mean square error between the measured and estimated time. In the SDP approach, a generalized gradient reduction

method is used to reduce the sum-of-square errors between the measured and estimated scour depth using the excess shear stress equation. Daly et al. (2015) reported that the BL method under-predicts  $\tau_c$  and  $k_d$  compared to IP and SDP approaches. Therefore, the jet solution is dependent not only on operational protocol but also the solution approaches used for data analyses.

### 3.2 Conduit flume operational principle

In an open channel laboratory flume, the applied bed shear is calculated using  $\tau_b = \rho g h S$ , where  $\rho$  is the fluid density ( $\text{kg m}^{-3}$ ),  $g$  is the gravitational acceleration ( $\text{m s}^{-2}$ ),  $h$  is the flow depth (m), and  $S$  is the slope of the channel. However, the conduit flume is based on pressurized conduit flow and the Darcy-Weisbach equation can be used (Sutarto et al., 2014):

$$\tau_b = \frac{\rho U^2}{8} f \quad (3)$$

where  $U$  is the flow velocity ( $\text{m s}^{-1}$ ); and  $f$  is the Darcy-Weisbach friction factor calculated from Haaland (1983) equation:

$$\frac{1}{\sqrt{f}} = -1.8 \log \left[ \frac{6.9}{R_e} + \left( \frac{\varepsilon}{3.7d} \right)^{1.11} \right] \quad (4)$$

where  $\varepsilon$  is the wall relative roughness height; and  $R_e$  is the Reynolds Number ( $R_e = Ud/\nu$  with  $\nu$  being the kinematic viscosity of water and  $d$  is the effective diameter of the rectangular conduit calculated using hydraulic diameter ( $d_h$ ) (0.0667 m for this flume). White (2008) proposed  $d = 1.029*d_h$ , which was used for this flume's calculations. The corresponding erosion rate for each applied shear stress due to the flow was determined by the following equation as proposed by Sutarto et al. (2014):

$$E = \frac{\Delta C_{avg} Q}{A} \quad (5)$$

where  $\Delta C_{avg}$  is the average sediment concentration difference between two consecutive flows ( $\text{kg m}^{-3}$ );  $Q$  is the flow rate ( $\text{m}^3 \text{s}^{-1}$ ), and  $A$  is the surface area of the soil sample ( $\text{m}^2$ ). Equations 3-5 were used to compute applied shear stress and the corresponding erosion rate. Erosion rate was plotted against the applied shear stress on a normal graph, where  $\tau_c$  was identified as the y-intercept corresponding to zero erosion rate from the best fit line (Papanicolaou et al., 2007). From those plots, slope was also calculated for each sample to estimate the  $k_d$  value by considering linear erosion model.

### 3.3 Rationale for comparative study

Fluvial erosion, especially in cohesive soils, is complex where many process factors contribute to soil detachment over time leading to the difficulty in developing standard test measurements for  $\tau_c$  and  $k_d$  parameters. It is understood that selection of device to measure  $\tau_c$  in association with the data analyses protocols significantly affects estimating these parameters as discussed in the Introduction. In this study,  $\tau_c$  and  $k_d$  measurements obtained using both the mini-jet device and the pressurized conduit flume are compared. The working principles and operational protocols of these two devices are fundamentally different. Barring differences, these two devices

possess some unique attributes to assess erosion processes in the field and in the laboratory environment, and provide better insight to uncertainties associated with  $\tau_c$  and  $k_d$  measurements.

The jet device was developed based on the diffusion principle for calculating  $\tau_c$  values, which produces highly complex hydrodynamic forces and turbulences inside the submersible tank during development of the simple scour configuration (Craft et al., 1993; Mercier et al., 2014). Due to the flexibility associated to jet operation in the field, the ASTM Standard D5852 “Standard Test Method for Erodibility Determination of Soil in the Field or in the Laboratory by the Jet Index Method” was developed using the original jet device, which was withdrawn in 2016 with no complementary replacement. It is understood that the lack of a methodological replacement for the proposed ASTM standard is due to inconsistencies in both jet operation and analytical solution procedures among different soil types (Wahl, 2016).

With the unique nature of operation on literally any surface condition in a riverine environment, the jet device has become a popular tool to estimate erosion parameters in-situ. However, as noted earlier, several study findings reported that the jet test data analysis procedures could have significant influence on erosion rate estimation consequently three solution methods (BL, IP, and SDP) have been developed. Several studies reported that  $\tau_c$  values, estimated from the IP and SDP methods are greater than the BL estimated  $\tau_c$  values (Simon et al., 2010; Daly et al., 2013, 2015; Regazzoni and Marot, 2013; Karamigolbaghi et al., 2017). It is important to note that a single pressure head is used for jet operation following the guidelines as Hanson and Cook (2004) outlined. Recently, Khanal et al. (2016) identified the influence of data collection time interval and termination time interval on erosion parameters estimation, which were not considered in the standard jet operation protocol. They also identified the importance of pressure head selection for erosion parameters estimation during jet testing on different soil types, though they did not report that explicitly in their study.

In order to critically analyze the issues related to the jet operation and data analysis procedures, a comparative study is necessary to investigate whether the erodibility parameters estimated using the available jet operation protocols and solution methods are similar to those obtained using a more traditional laboratory flume. As reported earlier, in a conduit flume, a greater range of shear stresses can be applied to a soil sample parallel to the surface (similar to the natural flow condition). While the erosion rate is assumed linear for both the conduit flume and the jet device, greater control during the sample testing and the mode of stress applied to the sample surface can be advantageous when using the flume compared to the jet device. However, flume measurements are assumed to use relatively undisturbed samples, which may not be the case during field collection. Sample disturbance affects the estimation of the erodibility parameters. Considering all these aspects related to these two devices, and since no direct comparative study of erosion parameters estimation currently exists, the authors identified that a direct comparison between the results from these fundamentally different devices is critical to cohesive soil erosion studies.

### **3.4 Sites locations for soil collections**

In-situ mini-jet tests were conducted in the same locations from which soil samples were collected for the conduit flume experiments. The locations included the stream banks of Pond Creek, Coal Creek, Crooked Creek and Black Creek, all of which are in West Tennessee, USA (Fig. 2). These creeks are in Dyer County, Tipton County, Shelby County and Crockett County, respectively. In this study, the bank soils were classified as cohesive because greater than 94% of

the soil particles were finer than 0.074 mm (#200 sieve) and the clay content ranged between 18% and 39%.

The measurements and sample collection took place in November 2016. Soil samples were collected when local temperatures were about 16-20°C to avoid any freeze-thaw cycle effects. It is also important to note that during the sample collection, no significant change in soil moisture content was expected since the weather was dry. In this study, multiple pressure heads were used for jet testing instead of using a single pressure head. In a jet test location, pressure heads were increased from a lower head to higher (pressure head range was 12.40 kPa to 41.37 kPa). For each pressure head setting, the test duration at each location was about 12–20 min, using three different time intervals: (i) 30-s intervals for the first two readings, (ii) one-minute time intervals for 2–6 min, and (iii) two-minute time intervals for depth measurements until test termination. The applied pressure head was then increased after 12 min if the measured scour-hole depth difference between two consecutive readings was not more than one millimeter. If the difference between two consecutive scour-hole depth readings was greater than one millimeter, the test was continued for the next two-minute interval (Mahalder et al., 2018). A total of 26 in-situ jet tests were conducted and a corresponding number of relatively undisturbed soil samples were collected for the flume testing. Additional soil was also collected to measure soil physical properties including bulk density (BD), grain size distribution, moisture content (WC), Atterberg limits, and dispersion ratio (DR).

### **3.5 Soil sample collection**

Several studies have reported that with increasing bed slope,  $\tau_c$  decreased and the force balance for gravity with respect to slope complicates erosion estimates (Luque and Beek, 1976; Whitehouse and Hardisty, 1988; Chiew and Parker, 1994; Dey et al., 1999; Dey, 2003). Therefore, in this study, jet tests were conducted on relatively horizontal plane on bank/bed and soil samples were collected from those locations for conduit flume tests to negate the effects of gravity in erosion parameters estimation. Soil sample collections for the conduit flume were modified from the protocols as described in Sutarto et al. (2014) to further reduce disturbances from placing the collected sample in the flume's testing tray. A metal frame matching the dimensions of the sample tray was used (Fig. 3). Two polymer filler end caps were also manufactured to fill the gaps at the testing tray ends. Roughness at the top surface of these polymer end caps was similar to course sand paper. The surficial area of a test soil sample inside the rectangular box was 0.0254 m<sup>2</sup>.

After finishing each jet test, the rectangular frame was driven into the ground close to the jet test location using uniform pressure at the top of the rectangular box (Fig. 4). The top soil surface was kept undisturbed to capture the natural soil formation to replicate the exact roughness conditions for erosion process. The four sides of the frame were then carefully excavated using a long tapping knife. The soil underneath the box was cut using a wire saw with extreme care to avoid any possible disturbances. The frame with the soil sample was then removed from the ground and immediately wrapped with plastic wrap and aluminum foil paper to avoid any moisture loss from the soil surface and stored in a cooler. After finishing the sample collections, coolers containing soil samples were stored in a climate controlled room to avoid further moisture loss from the soil sample before starting the flume tests.

### **3.6 Soil sample testing in laboratory conduit flume**

Before starting a sample test, the conical storage tank and the flume pipes were filled and flushed several times to remove any deposits from the flume conduit and pipes. After cleaning the

conduit flume system, the testing tray was removed and soil sample was placed into it. The tray was remounted in the flume with the same orientation as in the channel. Two filler end caps were also inserted at the upstream and downstream side of sample box as discussed in the previous section. The conical storage tank and flume were then filled again slowly using tap water. The pump was started at a very low frequency to remove all the air bubbles from the conduit flume without triggering the onset of erosion. The initial flow rate was adjusted by the variable speed frequency control to set levels corresponding to increasing applied shear stress. The flume was kept at the same applied shear for about 10 minutes allowing the flow to stabilize after the increase. After 10 minutes, two 1-L water-eroded sediment samples were drawn from the conduit flume using four Tygon tubes downstream side of the sample testing tray (Sutarto et al., 2014). When the sediment-water samples were collected, the flow rate was increased to the next test level. Five to six flow rates were applied for each soil sample test in the conduit flume.

Inter-particle forces in cohesive soils are dependent not only on the physical properties of the soil but on the exposed environmental conditions such as pore water chemistry, flowing water chemistry, and physical conditions. In the jet test, water is pumped from the creek and subsequently passed through the outlet from the submersible tank. Therefore, it is expected that only minor changes in chemical compositions would occur to the running water during the test. On the contrary, in conduit flume since it is a recirculating system, the water chemistry could alter considerably when compared to that of the stream water and consequently affect the erosional behavior of the tested cohesive soils. Henceforth, some chemical properties of the sediment-water mix were measured and the variations were observed during the sample testing as discussed in the Methodology. In the conduit flume, since tap water was used the properties of the tap water were also measured along with the stream water used for the jet test. The cation concentrations (CC), water pH (pH), and the electric conductivity (EC) of flume water were measured to detect changes during the experiments. Water pH and EC were measured using an automated titration system (Mantech PC-Titrate® system) and the CC was measured by ion chromatography (IC) using Dionex 2100/1100 dual column system with background suppression following standard methods (Eaton et al., 2005). The chemical compositions were measured at the beginning and end of each test. These measurements were compared to the stream water used in the jet device.

Suspended sediment concentrations in the sediment-water samples were measured through filtration using pre-weighed glass microfiber filters with 0.75  $\mu\text{m}$  pore opening. Filter papers with soil particles were oven-dried at 60<sup>0</sup>C for about 48 hrs until a constant weight was observed. Average suspended sediment concentrations ( $C_{avg}$ ) were computed for the paired set of bottles collected for each flow rate. Using flow rate readings, applied shear stresses on the soil surface were calculated as described in the previous section. For calculating  $\tau_c$ , erosion rate (E) was plotted against the applied shear stress ( $\tau_b$ ) on a normal graph paper.  $\tau_b$  and E were calculated using Equations 10-12. From these plots,  $\tau_c$  was estimated as the shear stress corresponding to E = 0 by drawing a best fitted line through the data points for a soil sample (Sutarto et al., 2014). In this study, filtered water samples were also preserved for future chemical analysis to observe the possible chemical composition changes in the tested water during sample testing. It was hypothesized that a possible chemical composition changes in the sample water could affect erosion behavior of the test soils.

### 3.7 Data analysis

Mini-jet test data analysis was conducted using the MPS method as described by Mahalder et al. (2018). Mahalder et al. (2018) identified that pressure head selection could have significantly

influence the erodibility parameters estimation using a single pressure head. In the MPS method, scour depth data corresponding to the applied pressure head was analyzed individually by applying BL solution procedures and  $\tau_c$  and  $k_d$  values were estimated. These estimated  $\tau_c$  and  $k_d$  values were then plotted on a normal graph against the corresponding pressure head. Finally,  $\tau_c$  and  $k_d$  values for a specific test location were calculated from the shape of the plots. The MPS method is new for jet operation and data analysis, so the authors of this article suggest the readers to review the MPS method in detail as reported by Mahalder et al. (2018) for further clarification. Erosion parameters were also calculated by using the BL approach and the newly developed IP and SDP methods with the single pressure head (traditional jet operation protocol), where the initial pressure head at each test location and the corresponding scour depths data were taken for the analyses. The analyses were conducted using a spreadsheet developed by Daly et al. (2013, *personal communication*).

Statistical differences for  $\tau_c$  between the results from these two devices were compared using mean separation ANOVA. Statistical correlations between the conduit flume tests data and jet tests data (using all the four solution techniques) for  $\tau_c$  was developed. Similar to the  $\tau_c$ , statistical correlation for  $k_d$  was also developed. Changes in the water chemistry during soil tests were investigated from the water chemistry analyses. Statistical analyses were conducted with SPSS v.23.0.

## 4. RESULTS

### 4.1 Critical shear stress measurement

For this comparative study, mini-jet test data were analyzed using four different methods as discussed above. Jet test results using the MPS method showed  $\tau_c$  ranged between 0.09 Pa to 23.50 Pa. Data range from the other three methods were found as follows: 0.013 Pa to 14.97 Pa; 0 Pa to 25.38 Pa; and 5.08 Pa to 20.68 Pa for BL, SDP and IP methods, respectively. Data collected for the conduit flume tests included the specific flow rates, which correspond to the applied shear stresses, and SSCs and were utilized to compute  $C_{avg}$  and erosion rates (Table 1). Table 1 represents example calculations for four test runs with the conduit flume. Results from the conduit flume tests showed that  $\tau_c$  ranged between 1.75 Pa to 20.50 Pa. Four representative plots for  $\tau_c$  calculation among 26 samples tested are presented in Fig. 5. In these plots, the y-intercept corresponding to  $E = 0$  was identified as the  $\tau_c$  for a soil sample. Results from the jet tests using the above mentioned four methods and the conduit flume are presented in Table 2.

### 4.2 Statistical data analysis

Measured  $\tau_c$  values using the jet device and the conduit flume were compared using a mean separation ANOVA test to identify possible differences in mean values among these results ( $n = 26$ ). The mean value of  $\tau_c$  were found 8.44 Pa from conduit flume test, 9.58 Pa from in-situ jet test (MPS), 6.79 Pa for the BL, 9.72 Pa for the IP, and 13.11 Pa for the SDP methods, respectively [Fig. 6(a)]. It was also found that the SDP method results showed wide variation in the predicted  $\tau_c$  values ( $\sigma = 8.27$ ) and the IP method showed the least variation ( $\sigma = 3.65$ ) in the dataset. The mean separation ANOVA analysis showed that mean values among these five analyses methods were statistically different for an  $\alpha$  of 0.05 ( $p = 0.013$ ). The Tukey HSD comparison methods showed that the statistical differences among the mean values were found between conduit flume and SDP methods ( $p = 0.035$ ), and between BL and SDP methods ( $p = 0.001$ ). Similar to  $\tau_c$ , SDP

method predicted  $k_d$  values showed wide variation ( $\sigma = 8.92$ ) in the dataset. Mean values of  $k_d$  were found to vary widely among these five methods as:  $2.99 \text{ cm}^3 \text{ N}^{-1} \text{ s}^{-1}$  ( $\sigma = 2.63$ ),  $1.80 \text{ cm}^3 \text{ N}^{-1} \text{ s}^{-1}$  ( $\sigma = 2.62$ ),  $1.97 \text{ cm}^3 \text{ N}^{-1} \text{ s}^{-1}$  ( $\sigma = 2.81$ ),  $7.15 \text{ cm}^3 \text{ N}^{-1} \text{ s}^{-1}$  ( $\sigma = 8.92$ ), and  $13.94 \text{ cm}^3 \text{ N}^{-1} \text{ s}^{-1}$  ( $\sigma = 7.13$ ) for conduit flume, MPS, BL, SDP, and IP method, respectively [Fig. 6(b)]. The mean separation ANOVA analysis also showed that  $k_d$  values were statistically different for an  $\alpha$  of 0.05 ( $p < 0.001$ ) among these methods. The IP method estimated mean  $k_d$  value was statistically different when compared to the mean from other four methods ( $p < 0.001$ ). Statistical differences for mean values between MPS and SDP ( $p = 0.008$ ), BL and SDP ( $p = 0.008$ ) were also observed using Tukey HSD comparison methods.

**Table 1.** Experimental conditions from the conduit flume test for four example samples and the corresponding parameter calculations.

Sample identifier	$Q$ (gpm)	$Q \times 10^3$ (m <sup>3</sup> /s)	$U$ (m/s)	$R_{def}$	$\tau_w$ (Pa)	$u_*$ (m/s)	$C_{avg} \times 10^2$ (kg/m <sup>3</sup> )	$\Delta C_{avg} \times 10^2$ (kg/m <sup>3</sup> )	$E \times 10^3$ (kg/m <sup>2</sup> /s)
<b>COCRSP-2</b>	93	5.86	1.17	79743	4.73	0.069	0.33	0.33	0.77
	128	8.08	1.62	109754	8.84	0.094	3.40	3.07	9.74
	154	9.72	1.94	132048	12.71	0.113	6.93	3.52	13.44
	185	11.67	2.33	158629	18.23	0.135	18.01	11.08	50.79
	203	12.81	2.56	174063	21.90	0.148	41.98	23.97	120.57
<b>COCRSP-3</b>	136	8.58	1.72	116614	9.95	0.010	1.36	1.36	4.60
	156	9.84	1.97	133763	13.03	0.114	3.36	2.00	7.61
	180	11.36	2.27	154342	17.28	0.131	9.00	5.64	25.16
	205	12.93	2.59	175778	22.33	0.149	15.32	6.32	32.11
	223	14.07	2.81	191212	26.37	0.162	25.15	9.82	54.27
<b>COCRSP-7</b>	126	7.95	1.59	108039	8.57	0.093	3.48	3.48	10.86
	145	9.15	1.83	124331	11.29	0.106	12.93	9.45	33.95
	167	10.54	2.11	143195	14.90	0.122	20.94	8.01	33.13
	189	11.92	2.38	162059	19.02	0.138	34.65	13.71	64.24
	207	13.06	2.61	177493	22.76	0.151	53.80	19.15	98.19
<b>CRCRSP-5</b>	170	10.72	2.15	145767	15.40	0.124	0.38	0.38	1.47
	186	11.74	2.35	159486	18.43	0.136	1.82	1.44	6.64
	206	12.99	2.60	176635	22.56	0.150	4.45	2.63	13.41
	221	13.94	2.79	189497	25.91	0.161	6.54	2.09	11.45
	232	14.63	2.93	198929	28.51	0.169	11.88	5.34	30.69

**Table 2.** Estimated critical shear stress ( $\tau_c$ ) using jet test and conduit flume test for four West Tennessee study sites.

Study Site Creek Name	Sample identifier	Critical shear stress, $\tau_c$ (Pa)				
		Conduit flume test	Jet test (MPS)	Jet test (BL)	Jet test (IP)	Jet test (SDP)
<b>Coal Creek</b>	COCRSP-1	12.4	11.90	5.60	6.39	0.00
	COCRSP-2	8.20	7.74	5.02	6.67	21.50
	COCRSP-3	9.50	4.95	4.05	6.69	15.56
	COCRSP-4	4.20	4.90	6.00	6.16	4.01
	COCRSP-5	4.82	4.08	8.90	8.26	20.61
	COCRSP-6	11.50	4.53	6.23	6.32	13.19
	COCRSP-7	7.50	7.74	6.22	6.12	0.00
<b>Crooked Creek</b>	CRCRSP-1	8.17	1.90	0.06	8.82	2.40
	CRCRSP-2	13.90	11.10	10.47	8.57	16.92
	CRCRSP-3	7.90	9.00	10.18	9.95	16.80
	CRCRSP-4	5.00	7.76	1.63	11.60	13.32
	CRCRSP-5	16.90	17.90	11.96	11.48	18.65
	CRCRSP-6	13.20	12.22	8.43	8.56	14.36
	CRCRSP-7	5.00	11.03	6.54	8.91	15.62
<b>Pond Creek</b>	POCRSP-1	1.75	6.00	4.08	8.26	9.47
	POCRSP-2	15.20	15.20	8.10	6.54	19.21
	POCRSP-3	20.50	23.50	14.46	13.91	25.38
	POCRSP-4	4.00	0.09	0.01	5.08	3.59
	POCRSP-5	1.80	7.10	0.95	11.27	10.03
	POCRSP-6	3.20	4.50	1.45	12.09	0.20
<b>Black Creek</b>	BLCRSP-1	3.00	8.50	10.05	14.42	23.85
	BLCRSP-2	15.90	22.20	13.88	13.90	19.27
	BLCRSP-3	6.40	14.97	14.97	14.95	25.31
	BLCRSP-4	2.00	3.21	0.35	20.68	0.00
	BLCRSP-5	1.75	8.51	8.11	9.78	18.52
	BLCRSP-6	14.50	18.50	8.76	7.23	13.14

In Fig. 7, linear prediction models for  $\tau_c$  using the conduit flume results as the dependent variable and the jet test results using the MPS as independent variable showed that the correlation value was 0.58 and adjusted  $R^2$  value of 0.56 ( $p < 0.001$ ). Similar significant results with the BL method showed  $R^2$  value was 0.35 and adjusted  $R^2$  value was 0.32 [Figs. 7(a and b)].

Data normality was checked by plotting the residuals, which showed normal distribution in the dataset. However, using both the SDP ( $p = 0.08$ ) and IP ( $p = 0.60$ ) methods the correlations were not statistically significant as  $R^2$  values were found 0.12 for SDP and 0.01 for IP, respectively [Figs. 7(c and d)]. It is also important to note that the SDP method predicted  $\tau_c$  values were consistently higher with some exceptions, whereas the IP method predicted values showed mixed results. Similar linear prediction models for the  $k_d$  values were also developed in this study as mentioned in the Methodology. Correlation value was found 0.42 ( $p < 0.001$ ) between the conduit flume and the MPS method data and the  $R^2$  value was 0.32 using BL method data [Figs. 8(a and

b)]. However, similar to  $\tau_c$  results, correlations for  $k_d$  values using both the SDP and IP showed very low  $R^2$  values [Figs. 8(c and d)]. It was also found that both the SDP and IP methods predicted  $k_d$  values were consistently higher with some exception compared to the flume data.

### 4.3 Properties of soil samples and water chemistry during experiments

The soil samples tested in this study were silty-clay-loams and clay-loams. Greater than 94% of the grains passed through a #200 sieve (opening 0.074 mm). BD ranged between 1.65 g cm<sup>-3</sup> to 2.25 g cm<sup>-3</sup> and the median grain size ( $D_{50}$ ) was between 7.0  $\mu$ m to 22  $\mu$ m. Results also showed that DR range was between 0.22 and 0.55, and the clay content ranged between 18% and 39% for the soil samples. Details of other soil physical properties are presented in Table 3.

**Table 3.** Physical properties of test soil samples from West Tennessee.

Properties	Minimum	Maximum	Mean	Standard Dev.
<b>Bulk density, BD (g cm<sup>-3</sup>)</b>	1.65	2.25	1.97	0.14
<b>D<sub>50</sub> (<math>\mu</math>m)</b>	7.00	22.00	13.76	3.31
<b>Liquid Limits, LL (%)</b>	24.10	40.60	32.54	4.34
<b>Plastic Limit, PL (%)</b>	17.80	25.60	21.88	2.33
<b>Plasticity Index, PI (%)</b>	5.60	19.97	10.65	3.63
<b>Water Content, WC (%)</b>	17.60	33.25	24.22	4.06
<b>Dispersion Ratio, DR</b>	0.22	0.55	0.33	0.08
<b>Clay Content, Clay (%)</b>	18.00	39.00	25.58	5.31
<b>Clay Activity, CA</b>	0.31	0.56	0.41	0.06
<b>% Passing # 200 sieve, Pass200</b>	93.00	98.00	96.15	1.32

The changes in the physical and chemical compositions of the water during conduit flume experiments were found relatively low (Table 4). Overall the EC values were found increasing but the pH values were almost similar. The SAR values increased from 0.43% to 9.40% and the KIF values increased from 0.07% to 17.15%. In this study, water sample testing showed that the Na<sup>+</sup> ion concentration ranged between 10.53 mg/L and 16.44 mg/L, and the concentration of K<sup>+</sup> ion ranged between 1.67 mg/L to 2.38 mg/L after the first flow rate. Overall an increasing trend was observed for Na<sup>+</sup>, K<sup>+</sup>, Ca<sup>2+</sup> and Mg<sup>2+</sup> ionic concentrations though variations were relatively low (Table 4).

## 5. DISCUSSION

Several research studies have focused on improving methods for estimating  $\tau_c$  and  $k_d$  with the in-situ jet tests and laboratory flumes being the predominant methods applied. In-situ methods can better represent the actual stream conditions because the soil is undisturbed prior to testing; however, a hydraulic jet is applied normal to the erodible surface with shear stress derived by diffusion relationships. During the impingement, the nature of the force exerted transitions from

normal to shear as the scour evolves (Ghaneezad, 2016). In contrast, the pressurized conduit flume creates a shear stress exerted atop of the erodible surface representing closely the shearing action exerted to the soil surface by the flow in field conditions along a bank/bed profile; however, care should be given, as is the case here, with the improvements made in the Sutarto et al. (2014) approach that there is minimal soil sample disturbances. Therefore, the device dependent variability in  $\tau_c$  and  $k_d$  are expected since the stress distribution procedures and the erosion mechanism are different in these two devices.

**Table 4.** Range variation of water chemistry during the conduit flume tests.

Parameters	Range after first operated flow rate	Range after final operated flow rate	Range in percentage change
Na <sup>+</sup> (mg/L)	10.53 – 16.44	11.67 – 17.05	0.14% – 13.97%
K <sup>+</sup> (mg/L)	1.67 – 2.38	1.70 – 2.76	0.93% – 30.51%
Ca <sup>2+</sup> (mg/L)	16.70 – 27.46	18.77 – 29.20	0.69% – 25.36%
Mg <sup>2+</sup> (mg/L)	5.06 – 7.76	5.26 – 8.09	0.14% – 19.61%
SAR	3.12 – 3.96	3.31 – 4.01	0.07% – 17.16%
KIF	0.34 – 0.42	0.33 – 0.46	0.43% – 9.40%
Conductivity, EC (μS/cm)	189.8 – 282.98	201.56 – 297.29	0% – 3.77%
pH	7.71 – 8.10	7.75 – 8.12	0% – 22.86%

In general, results from our study indicated that  $\tau_c$  estimates compared better between devices than  $k_d$ , in general [Figs. (6-8)]. Depending on the jet test analyses methods, MPS method estimated erodibility parameters from this device were more closely correlated with the conduit flume. It is hypothesized that since both the conduit flume test and the MPS methods test hydraulics better replicate each other, better correlation could have found. In addition, when either the MPS or the BL data analysis approach are used, erodibility parameters were comparable from a broad perspective, though differences were observed and provided valuable insight to erosion behavior of cohesive soils and the testing methods.

Median  $\tau_c$  values for the conduit flume, MPS and BL jet test methods including all tests ranged from 0 Pa to 25.38 Pa [Fig. 6(a)]. The  $\tau_c$  correlations less than 5 Pa were highly variable between the conduit flume and the jet test MPS and BL methods, though significant linear relations were observed for  $\tau_c$  for the entire testing range (Fig. 7). This suggests that for lower strength samples mostly operational differences drove the identified differences. It is also possible that the choice of  $J_p$  is quite sensitive for weaker soils. Above 5 Pa, the MPS jet test method correlated the best with the conduit flume results thereby suggesting that stronger samples exhibit less variability than the weaker ones and operational differences of the two methods get masked (i.e., in this case the choice of  $J_p$  is less sensitive). Study results also showed that at lower WC (usually stronger soils as WC is inversely related to strength), jet test data showed higher  $\tau_c$  values compared to the conduit flume results using the MPS, BL, IP, and SDP method represented as small circles in the graph (Fig. 7). It is interesting to note that comparable results from these two devices were identified especially for consolidated cohesive soils with relatively higher moisture content (> 20%). However, for relatively dry soils, statistically non-significant correlation was identified due to the challenges associated with the sample collection. Based on field observations, it was hypothesized that during sample collection, micro-cracks developed around the edges of the

sample collecting rectangular boxes. The weakened soil may have eroded more quickly from those areas during the conduit flume tests, resulting in lower  $\tau_c$  values.

Results also showed that estimating  $k_d$  values was challenging since lower correlations were found from these two devices using any jet test solution method (Fig. 8). Similar findings have also been reported in several studies using jet test data (Hanson and Simon, 2001, Simon et al., 2010; Daly et al., 2015; Mahalder et al., 2018). Findings for  $k_d$  values using jet device showed this parameter was greater than the estimates from the conduit flume (Fig. 8). However, the MPS and the BL analysis methods for the jet test data were better correlated than the SDP and IP methods. Regardless of any methods, the range of  $k_d$  values from this study was found between 0.30 to 40.98  $\text{cm}^3 \text{N}^{-1} \text{s}^{-1}$ . Similar to other studies (Hanson and Simon, 2001; Wynn and Mostaghimi, 2006; Simon et al., 2010; Daly et al., 2015), inverse power law relationships with  $\tau_c$  and  $k_d$  were identified using both the conduit flume and jet test data (Fig. 9). Relationship from the SDP method was not developed due to the presence of zero values in the calculated  $\tau_c$  values. In order to assess better the comparison between the jet test device and the conduit flume in terms of erodibility estimates, this study design would have to be expanded where local bank erosion rates at the sample site are surveyed.

In this study, tested soil samples had similar physical characteristics. By the definition of Raudkivi (1990), tested soil samples were cohesive also since clay percentage was greater than 18% by weight and high PI values (Table 3). The studied stream sites were from the Coastal Plain physiographic province with Neogene and Quaternary rock system, deposited from both marine and non-marine sand, silt and clay with sand dominant (Miller, 1974). Mahalder et al. (2017) identified that in cohesive soils,  $\tau_c$  predictive equations differed among different geology and reported multiple predictive equations. These studied stream sites were among one of those reported groups, where Pass200, WC, CA, BD and organic content (OC) were found the most significant soil properties among others to predict  $\tau_c$ . Though, limited soil physical properties (Table 3) were measured for this case, similar correlation patterns to  $\tau_c$  were identified. Clay%, CA, BD and Pass200 showed positive correlation to  $\tau_c$  considering the results obtained from both the conduit flume and the jet test device (using all the four available methods). However, WC did not show any specific correlation to  $\tau_c$ , which was thought to be influencing the erosion pattern for some of the soil samples as discussed in the earlier section, resulting the variation in the erosion parameters ( $\tau_c$  and  $k_d$ ) estimation.

Both the physical, geochemical, and biological properties can significantly affect the erosional behavior of cohesive soils due to the inter-particle attraction forces (Grabowski et al., 2011). In this study, the physical and biological properties of tested soil samples were similar. Therefore, the change in water chemistry was measured during sample testing, which can significantly affect the erosional behavior in cohesive soils. With the conduit flume, the water supply is external to instream conditions; therefore, in this study the possible influences on erosion rates or erodibility parameters were explored. Analyses of sediment-water mix samples showed the pH value changed between 0% to 22.86% and EC ranged between 0% and 3.77% for the flowing water during the sample testing (Table 4). Erosion of cohesive sediments can be differed in different clay minerals in varying pH and ionic concentrations (Liou, 1970). The relationship between  $\tau_c$  and soil pore water pH shows that with increasing pH, the concentration of  $\text{H}^+$  ions decreases, resulting in an increase in the double layer thickness. Consequently, a greater repulsive force was expected in the soil particles (Winterwerp and van Kesteren, 2004). However, Ravisangar et al. (2005) suggested that at low ionic concentration (lower EC value) erosion rate is higher at higher pH and vice-versa

at low pH. They also reported that at higher ionic concentration, pH had no effect on erosion behavior in cohesive sediments. In this study, since both the pH and EC values changed during sample testing in the conduit flume, the effect on erosion behavior is further needed to be studied.

Influence of clay minerals and pore fluid conditions also affect the erosion behavior of cohesive soils. Using different clay minerals and pore fluid conditions, Liou (1970) reported a positive correlation between SAR and  $\tau_c$ . The influence of SAR on the repulsive forces is positively correlated; consequently influence the erosion potential for cohesive soils based on clay mineral (Liou, 1970; Alizadeh, 1974; Arulanandan, 1975). It was also reported that KIF and  $\tau_c$  are negatively correlated. Soils with higher KIF values were typically friable and eroded away easily and a negative correlation is expected (Wynn and Mostaghimi, 2006). During the samples testing in the conduit flume, the SAR values changed from 0.07% to 17.16% and the changes in KIF values were ranged 0.43% to 9.40%. Results from this study showed that water chemistry did change during the test; however, the influence on erosion was not clear. An experimental study design with different flume water chemistries would have to be implemented for better understanding the influence on erosion processes.

Erosion patterns and scour hole development in cohesive soils using a jet device is also dependent on soil physical properties (Mahalder et al., 2018). Mahalder et al. (2018) identified that soils with relatively lower moisture content and lower cohesion showed narrower and deeper scour holes, and for moderately moist consolidated soils with higher cohesion showed shallower and wider scour holes. For the later case, it was hypothesized that layer by layer removal of soil aggregates from the underneath soil column could be prominent as shear forces above the critical are being applied on the soil surface. From field observations and during the sample testing in the conduit flume, comparable incidents were observed to support this hypothesis (Fig. 10). Therefore, during conduit flume testing, aggregate removal was found prominent for some soil samples. At lower flow rates, those aggregates were found to be unbroken and moving as bedload following both the rolling and saltation movements. Consequently, non-uniform sediment concentrations in the conduit flume may have occurred as those aggregates could have been broken at higher flow rates during the latter stage of the test. These circumstances may have influenced some results as the erosion rate was found to be very high for some intermediate flow rates, influencing the correlations for predicting  $\tau_c$  and  $k_d$  values. This observation might be a future research topic for estimating erodibility parameters using the conduit flume especially for consolidated cohesive soils. Similar scenarios were also observed for jet device at higher pressure heads as the broken soil layers underneath the water jet were found stagnant. However, the depth gage attached to the jet device did not record any changes in the erosion depth though the soil was already broken. In association with the data analyses procedures, this issue must be addressed for the jet device in future to erosion parameters prediction in-situ for cohesive soils.

Findings from this study and field observations also identified that the differences among different devices are not only dependent on the working principles of these devices but the type of soil samples being tested. Working with naturally formed soils, it is always expected a wide variation of heterogeneity in the soil layers affecting the erodibility parameters. Using the jet device, since these parameters are being obtained from a point, it requires multiple tests to obtain an average value. In addition to the jet test data analyses procedures, the jet operation protocol was found another source of possible variation in the correlation.

The conduit flume was a more controlled device for predicting erodibility parameters. However, the assumption of uniform sediment concentration across the conduit may not be always

correct depending on soil types. It is also important to mention that the applied shear stress calculation procedures during testing might not be always accurate with higher sediment concentration in the flowing water and irregular soil surface due to erosion during testing. These issues are thought to be important and need to be addressed in addition to the sample collection protocol for the conduit flume.

## 6. CONCLUSIONS

Device dependent variability for erosion parameters ( $\tau_c$  and  $k_d$ ) prediction was studied using a laboratory device: the pressurized conduit flume, and an in-situ device: the submersible mini-jet. Statistically significant correlations for results from conduit flume tests and jet tests data were identified for both the  $\tau_c$  and  $k_d$  values. However, key findings from this study suggests that the operational and data analyses procedures in jet tests were persuasive for these correlations since results from the MPS method showed higher  $R^2$  values for both  $\tau_c$  ( $R^2 = 0.58$ ) and  $k_d$  ( $R^2 = 0.42$ ) values. The variations in  $k_d$  estimations were substantial using both these two devices regardless of the data analyses procedures. It is also clear that soil type and soil moisture content has significant impact on the sample collection, which evidently influenced the  $\tau_c$  and  $k_d$  values estimation using the conduit flume tests. Similar scenarios were observed for jet device, where soil heterogeneity may have affected the results since the jet is impacting at a point. Form the test hydraulics perspective it is also though that conduit flume and MPS method are similar in nature, which may have influenced the better comparable erodibility parameters as observed in this study.

**Acknowledgement:** This research was funded by Grant No. RES#2013-36 from the Tennessee Department of Transportation (TDOT). The authors would also like to thank Robert Thomas of USDA for sharing spreadsheets to analyze the jet-test device field data. Construction of the mini-jet device and conduit flume test chamber was completed by Ken Thomas and Larry Roberts at the University of Tennessee Civil Engineering Machine Shop. Dr. Chris Wilson has shown the first author the operation of the conduit flume. Student field assistance was provided by Mollika Roy.

## 7. REFERENCES

- Aberle, J., Nikora, V., McLean, S., Doscher, C., McEwan, I., Green, M., Goring, D., and Walsh, J. (2003). "Straight Benthic Flow-Through Flume for In Situ Measurement of Cohesive Sediment Dynamics." *J. Hydraul. Eng.*, 129 (1), 63-67.
- Alizadeh, A. (1974). "Amount and Type of Clay and Pore fluid Influences on the Critical Shear Stress and Swelling of Cohesive Sediments." Ph.D. Dissertation, University of California, Davis, CA, USA.
- Al-Madhhachi, A. T., Hanson, G. J., Fox, G. A., Tyagi, A. K., and Bulut, R. (2013a). "Measuring Soil Erodibility Using a Laboratory "mini" JET." *Trans. ASABE*, 56 (3), 901-910.
- Al-Madhhachi, A. T., Hanson, G. J., Fox, G. A., Tyagi, A. K., and Bulut, R. (2013b). "Deriving Parameters of a Fundamental Detachment Model for Cohesive Soils from Flume and Jet Erosion Tests." *Trans. ASABE*, 56 (2), 489-504.

- Amos, C. L., Grant, J., Daborn, G. R., and Black, K. (1992). "Sea Carousel - a Benthic Annular Flume." *Estuarine, Coastal and Shelf Science*, 34, 557-577.
- Arulanandan, K. (1975). "Fundamental Aspects of Erosion of Cohesive Sediments." *Journal of Hydraulics Division*, 101(HY5), 635-639.
- Arulanandan, K., Sargunam, A., Loganathan, P., and Krone, R. B. (1973). "Application of Chemical and Electrical Parameters to Prediction of Erodibility." *Soil erosion: Causes and mechanisms; prevention and control*, Special Rep. 135, Highway Research Board, Washington, D.C., 42-51.
- Blaisdell F. W., Clayton L. A., and Hebaus C. G. (1981). "Ultimate Dimension of Local Scour.: *Journal of Hydraulics Division*, 107 (3), 327-337.
- Bones, E. J. (2014). "Predicting Critical Shear Stress and Soil Erodibility Classes Using Soil Properties." M.Sc. Thesis, Georgia Institute of Technology, GA, USA.
- Briaud, J., Ting, F., Chen, H. C., Gudavilli, R., Kwak, K., Philogene, B., Han, S., Perugu, S., Wei, G., Nurtjahyo, P., Cao, Y., and Li, Y. (2001). "SRICOS: Prediction of Scour Rate at Bridge Piers." Report 2937-1, Texas Transportation Institute, The Texas A&M University, College Station, Texas, USA.
- Chapuis, R. P., and Gatien, T. (1986). "An Improved Rotating Cylinder Technique for Quantitative Measurements of the Scour Resistance of Clays." *Can. Geotech. J.*, 23, 83-87.
- Chiew, Y. M., and Parker, G. (1994). "Incipient Sediment Motion on Non-Horizontal Slopes." *J. Hydra. Res.*, 32(5), 649-660.
- Craft, T., Graham, L., and Launder, B. (1993). "Impinging Jet Studies for Turbulence Model Assessment – II. An Examination of the Performance of Four Turbulence Models." *Int. J. Heat Mass Transfer*, 36(10), 2685-2697.
- Daly, E. R., Fox, G. A., Al-Madhhachi, A. T., and Miller, R. B. (2013). "A Scour Depth Approach for Deriving Erodibility Parameters from Jet Erosion Tests." *Trans. ASABE*, 56(6), 1343–1351.
- Daly E. R., Fox G. A., Enlow H. K., Storm D. E., and Hunt S. L. (2015). "Site-scale Variability of Streambank Fluvial Erodibility Parameters as Measured with a Jet Erosion Test." *J. Hydrological Process*, 29, 5451-5464.
- Debnath, K., Nikora, V., and Grace, C. (2004). "Erosion of Cohesive Sediments in Canterbury Streams." *The Water Balance, Book of Abstracts of the New Zealand Hydrological Society Symp.*, Queenstown, New Zealand, 67-68.
- Debnath, K., Nikora, V., Aberle, J., Westrich, B., and Muste, M. (2007). "Erosion of Cohesive Sediments: Resuspension, Bed Load, and Erosion Patterns from Field Experiments." *J. Hydraul. Eng.*, 133 (5), 508-520.
- Dey, S., Dey Sarker, H. K., and Debnath, K. (1999). "Sediment Threshold Under Stream Flow on Horizontal and Sloping Beds." *J. Eng. Mech.*, 125(5), 545-553.
- Dey, S. (2003). "Threshold of Sediment Motion on Combined Transverse and Longitudinal Sloping Beds." *J. of Hydraulic Research*, 41(4), 405-415. DOI: 10.1080/00221680309499985.

- Eaton, A. D., Clesceri, L. S., Rice, E. W., and Greenburg, A. E. (2005). "Standard Methods for the Examination of Water and Wastewater." AWWA, WEF, American Public Health Association, Washington, D.C., USA.
- Dunn, I. S. (1959). "Tractive Resistance of Cohesive Channels. Journal of the Soil Mechanics and Foundations." ASCE, 85(SM3, Part 1), 1-24.
- Ghaneizad, S. M. (2016). "Impinging Jets in a Confined Environment: Application for Soil Erosion." Ph. D. Dissertation, Department of Civil, Structural and Environmental Engineering, State University of New York, Buffalo, NY, USA.
- Gibson, M. M., and Launder, B. E. (1978). "Ground Effects on Pressure Fluctuations in the Atmospheric Boundary Layer." J. Fluid Mech., 86, 491-511.
- Grabowski, R. C., Droppo, I. G., and Wharton, G. (2011). "Erodibility of Cohesive Sediment: The Importance of Sediment Properties." Earth Sci. Rev. 105 (1), 101-120.
- Haaland, S. E. (1983). "Simple and Explicit Formulas for the Friction Factor in Turbulent Pipe Flow." J. Fluids Eng., 105(1), 89-90.
- Hanson, G. J. (1990). "Surface Erodibility of Earthen Channels at High Stresses: II. Developing an in situ Testing Device." Trans., ASAE, 33(1), 132-137.
- Hanson, G. J., and Simon, A. (2001). "Erodibility of Cohesive Streambeds in the Loess Area of the Midwestern USA." Hydrological Processes, 15, 23-38.
- Hanson, G. J., and Cook, K. R. (1997). "Development of Excess Shear Stress Parameters for Circular Jet Testing." ASAE Paper No. 972227. St. Joseph, Michigan, USA.
- Hanson G. J., and Cook K. R. (2004). "Apparatus, Test Procedures, and Analytical Methods to Measure Soil Erodibility in-situ." Appl. Eng. Agric., 20 (4), 455-462.
- Hanson, G. J., and Hunt, S. L. (2007). "Lessons Learned Using Laboratory Jet Method to Measure Soil Erodibility of Compaction Soils." Applied Eng. in Agric. 23 (3), 305-312.
- Hobson, P. M. (2008). "Rheologic and Flume Erosion Characteristics of Georgia Sediments from Bridge Foundations." M.Sc. Thesis, Georgia Institute of Technology, GA, USA.
- Houwing, E. J., and van Rijn, L. C. (1998). "In Situ Erosion Flume (ISEF): Determination of Bed-shear Stress and Erosion of a Kaolinite Bed." Journal of Sea Research, 39, 243-253.
- Karamigolbaghi, M, Ghaneizad, S. M., Atkinson, J. F., Bennett, S. J., and Wells, R. R. (2017). "Critical Assessment of Jet Erosion Test Methodologies for Cohesive soil and Sediment." Geomorphology, 295, 529-536. DOI: <http://dx.doi.org/10.1016/j.geomorph.2017.08.005>
- Khanal, A., Fox, G. A., and Al-Madhhachi, A. T. (2016). "Variability of Erodibility Parameters from Laboratory mini Jet Erosion Tests." J. Hydro. Eng., 21(10). DOI:10.1061/(ASCE)HE.1943-5548.0001404
- Liou, Y. D. (1970). "Hydraulic Erodibility of Two Pure Clay Systems." Ph.D. Dissertation, Colorado State University, Fort Collins, CO, USA.
- Luque, R. F., and van Beek, R. (1976). "Erosion and Transport of Bed-Load Sediment." J. Hydr. Res., 14(2), 127-144.

- Mahalder B., Schwartz J. S., Palomino A. M., and Zirkle, J. (2017). "Relationships between physical-geochemical soil properties and erodibility of streambanks among different physiographic provinces of Tennessee, USA." *Earth Surface Processes and Landforms*. DOI: 10.1002/esp.4252
- Mahalder B., Schwartz J. S., Palomino A. M., and Zirkle, J. (2018). "Estimating erodibility parameters for streambanks with cohesive soils using the mini jet test device: A comparison of field and computational methods." *Water* 10(3), 304. DOI: 10.3390/w10030304
- Mallison, T. (2008). "Comparing in-situ submerged jet test device and laboratory flume methods to estimate erosional properties of cohesive soils for stream bank stability models." M.Sc. Thesis, University of Tennessee, Knoxville, TN, USA.
- McNeil, J., Taylor, C., and Lick, W. (1996). "Measurement of Erosion of Undisturbed Bottom Sediments with Depth." *J. Hydraul. Eng.*, 122(6), 316-324. DOI: [http://dx.doi.org/10.1061/\(ASCE\)0733-9429\(1996\)122:6\(316\)](http://dx.doi.org/10.1061/(ASCE)0733-9429(1996)122:6(316))
- Mercier, F., Bonelli, S., Pinettes, P., Golay, F., and Anselmet, F. et al. (2014). "Comparison of CFD simulations with experimental Jet Erosion Tests results." *J. Hydraul. Eng.*, 140(5). DOI: 10.1061/(ASCE)HY.1943-7900.0000829, 04014006
- Miller, R. A. (1974). "The Geologic History of Tennessee." Tennessee Division of Geology, Bulletin 74.
- Moore, W. L., and Masch, Jr., F. D. (1962). "Experiments on the Scour Resistance of Cohesive Sediments." *J. Geophys. Res.*, 67(4), 1437-1449.
- Mostafa, T. M. S., Imran, J., Chaudhry, M. H., and Khan, I. B. (2008). "Erosion Resistance of Cohesive Soils." *Journal of Hydraulic Research*, 46 (6), 777-787.
- Papanicolaou, A. N. (2001). "Erosion of Cohesive Streambeds and Banks." State of Washington Water Res. Cent. Rep. WRR-08, Washington. State University, Pullman, Washington.
- Papanicolaou, A. N., Elhakeem, M., and Hilldale, R. (2007). "Secondary Current Effects on Cohesive River Bank Erosion." *Water Resour. Res.*, 43 (12).
- Raudkivi, A. J. (1990). *Loose Boundary Hydraulics*. 3rd edition, Pergamon Press, New York, USA.
- Ravisangar, V., Sturm, T. W., and Amirtharajah, A. (2005). "Influence of Sediment Structure on Erosional Strength and Density of Kaolinite Sediment Beds." *J. Hydraul. Eng.*, 131 (5), 356-365.
- Regazzoni, P. L., and Marot, D. (2013). "A comparative Analysis of Interface Erosion Tests." *Nat Hazards*, 67, 937-950.
- Simon, A., Thomas, R. E., and Klimetz, L. (2010). "Comparison and Experiences with Field Techniques to Measure Critical Shear Stress and Erodibility of Cohesive Deposits." In Proc. 2nd Joint Federal Interagency Conference. Reston, VA, USA.
- Stein, O. R., and Nett, D. D. Nett. (1997). "Impinging Jet Calibration of Excess Shear Sediment Detachment Parameters." *Trans. ASAE*, 40(6), 1573-1580.
- Sutarto, T., Papanicolaou, T. A. N., Wilson, C. G., and Langendoen, E. J. (2014). "Stability Analysis of Semicohesive Streambanks with CONCEPTS: Coupling Field and Laboratory

- Investigations to Quantify the Onset of Fluvial Erosion and Mass Failure.” *J. Hydraul. Eng.*, 140(9). DOI: 10.1061/(ASCE)HY.1943-7900.0000899
- Tolhurst, T. J., Black, K. S., Paterson, D. M., Mitchener, H. J., Termaat, G. R., and Shayler, S. A. (2000). “A Comparison and Measurement Standardisation of Four in situ Devices for Determining the Erosion Shear Stress of Intertidal Sediments.” *Continental Shelf Research*, 20, 1397-1418.
- Wahl, T. L. (2016). “The Submerged Jet Erosion Test: Past-Present-Future.” *USSD International Symposium on the Mechanics of Internal Erosion for Dams and Levees*, Salt Lake City, UT, USA.
- Wan, C. F., and Fell, R. (2004). “Investigation of Rate of Erosion of Soils in Embankment Dams.” *J Geotech. Geoenviron. Eng.*, 130(4), 373-380.
- Weidner, K. L. (2012). “Evaluation of the Jet Test Method for determining the erosional properties of Cohesive Soils: A Numerical Approach.” M.Sc. Thesis, Department of Civil Engineering, Virginia Polytechnic Institute and State University, Blacksburg, VA, USA.
- White, F. M. (2008). *Fluid Mechanics*. 6th Ed., McGraw-Hill, New York, USA.
- Whitehouse, R. J. S., and Hardisty, J. (1988). “Experimental Assessment of Two Theories for the Effect of Bed Slope on the Threshold of Bed-Load Transport.” *Mar. Geol.*, 79, 135-139.
- Winterwerp, J. C., and van Kesteren, W. G. M. (2004). *Introduction to the Physics of Cohesive Sediment in the Marine Environment*. Elsevier, Amsterdam, The Netherlands.
- Wynn, T. M., and Mostaghimi, S. (2006). “The Effects of Vegetation and Soil Type on Streambank Erosion, Southwestern Virginia, USA.” *Journal of the American Water Resources Association (AWARA)*, 42(1), 69-82.

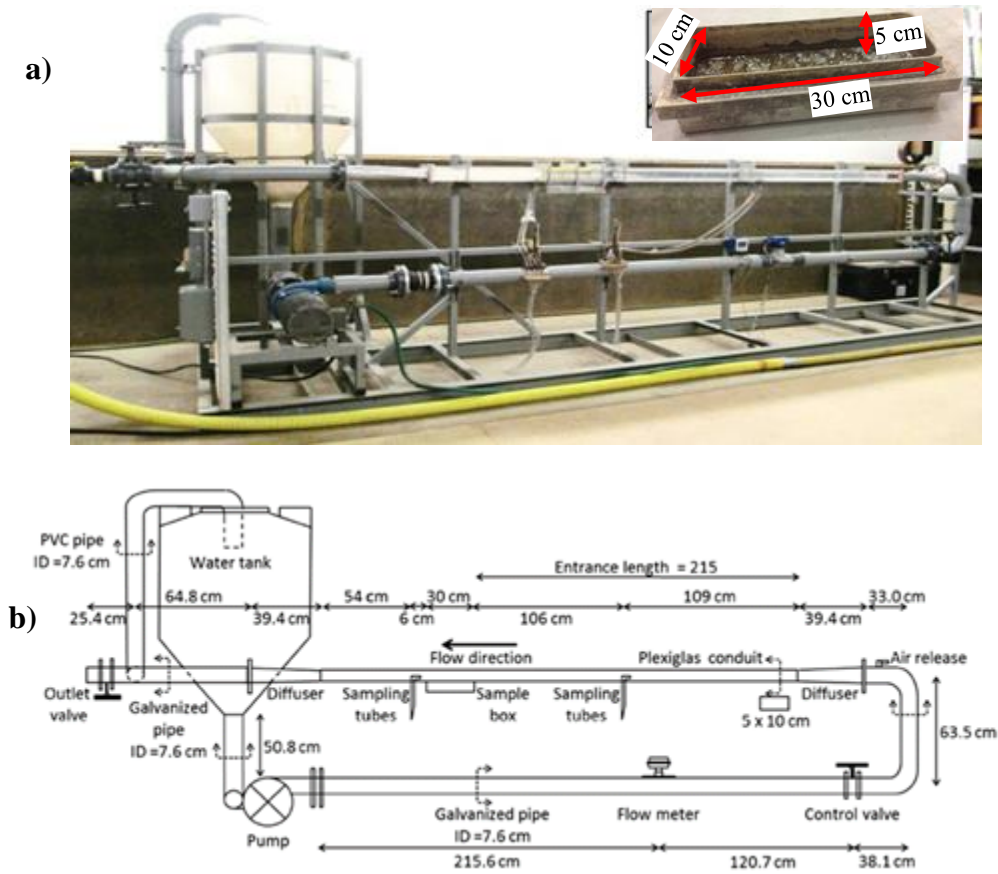


**Fig. 1.** Conduit flume showing: a) photo of flume with testing box, and b) details of flume dimensions (Sutarto et al., 2014).

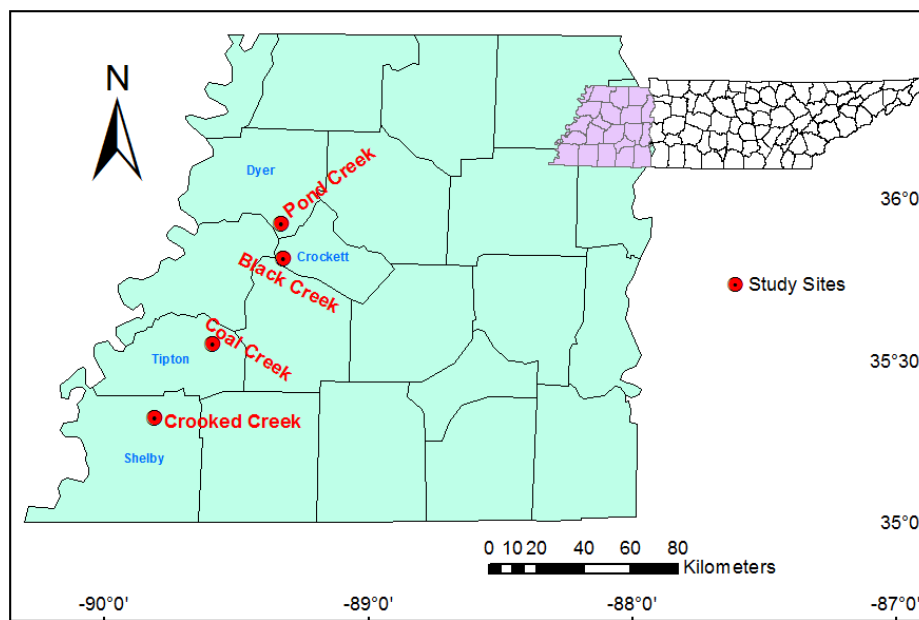


**Fig. 2.** Study area with in-situ jet testing and soil collection locations in West Tennessee.

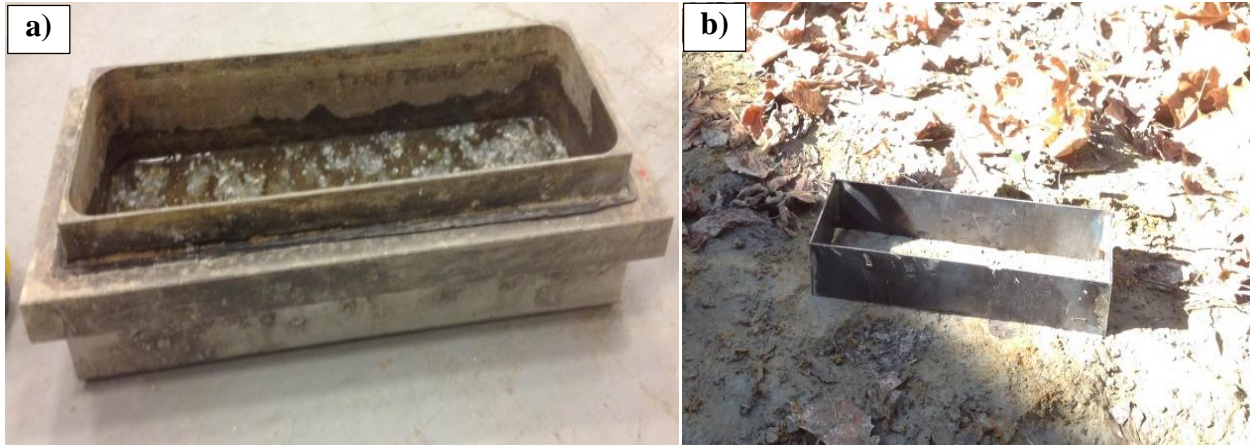


**Fig. 3.** For use the laboratory conduit flume photos show: a) the testing tray and b) the rectangular metal box to field collect soil samples.



**Fig. 4.** In-situ mini-jet testing and sample collection at the Black Creek site.

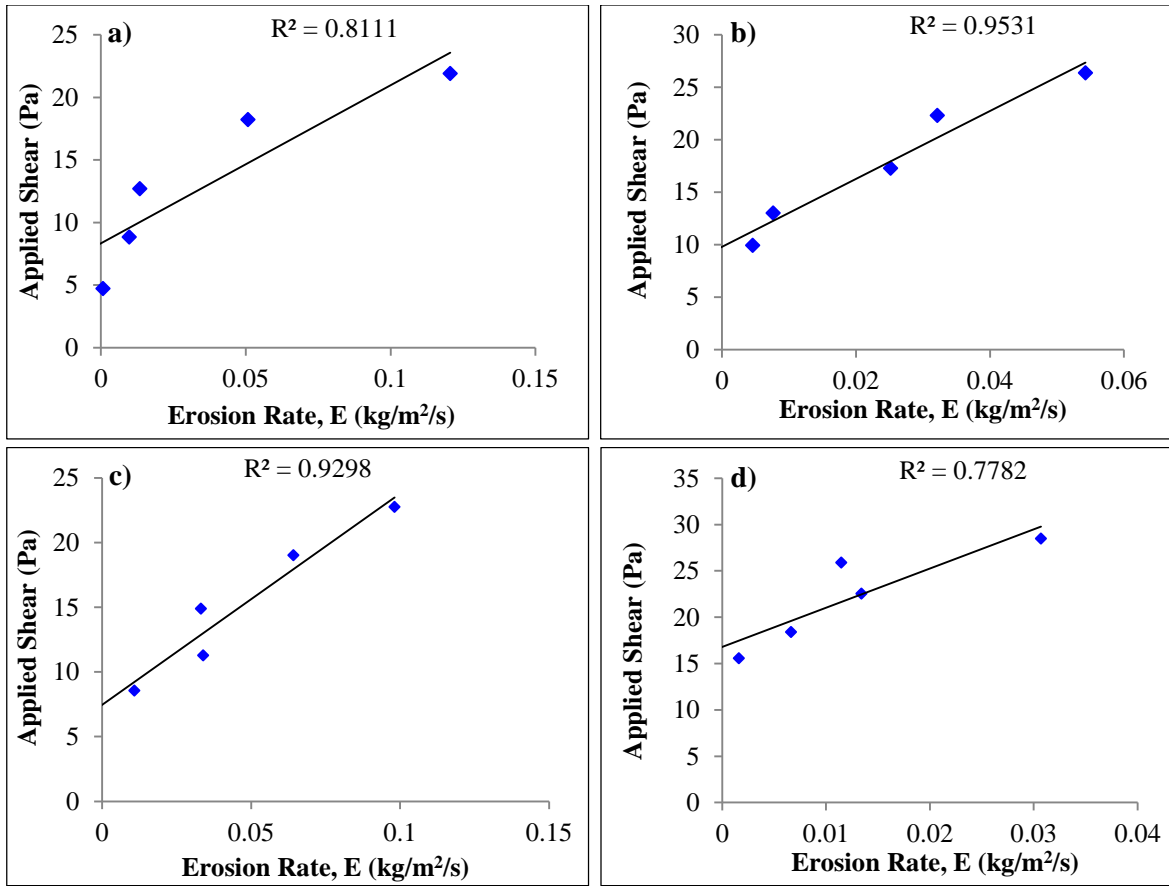


**Fig. 5.** Conduit flume test results from four samples as presented in Table 1; the  $\tau_c$  is determined as the y-intercept where  $E = 0$ . These plots represent the sample identifier: a) COCRSP-2, b) COCRSP-3, c) COCRSP-7, and d) CRCRSP-5.

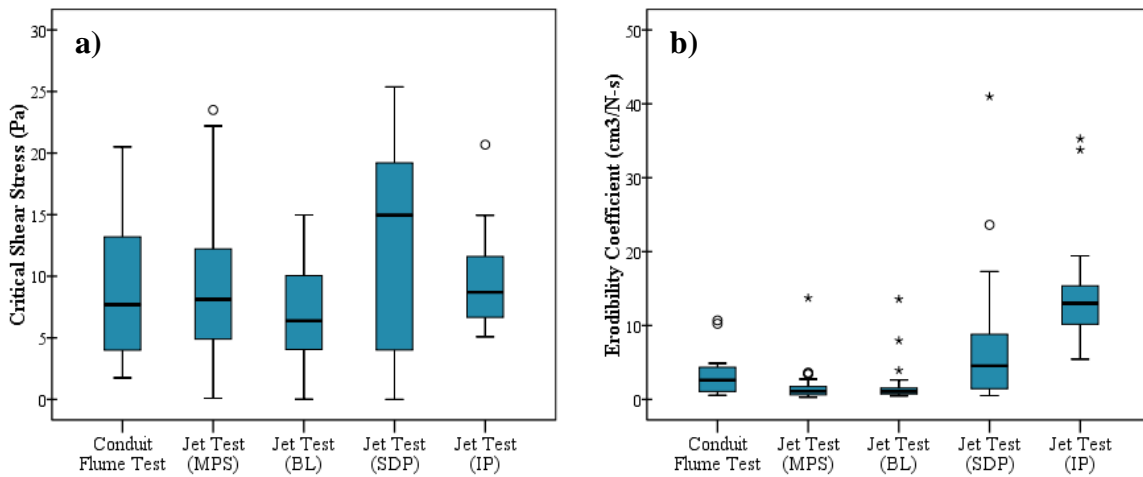


**Fig. 6.** a) Critical shear stress ( $\tau_c$ ), and b) erodibility coefficient ( $k_d$ ) comparisons using conduit flume test and jet test results.

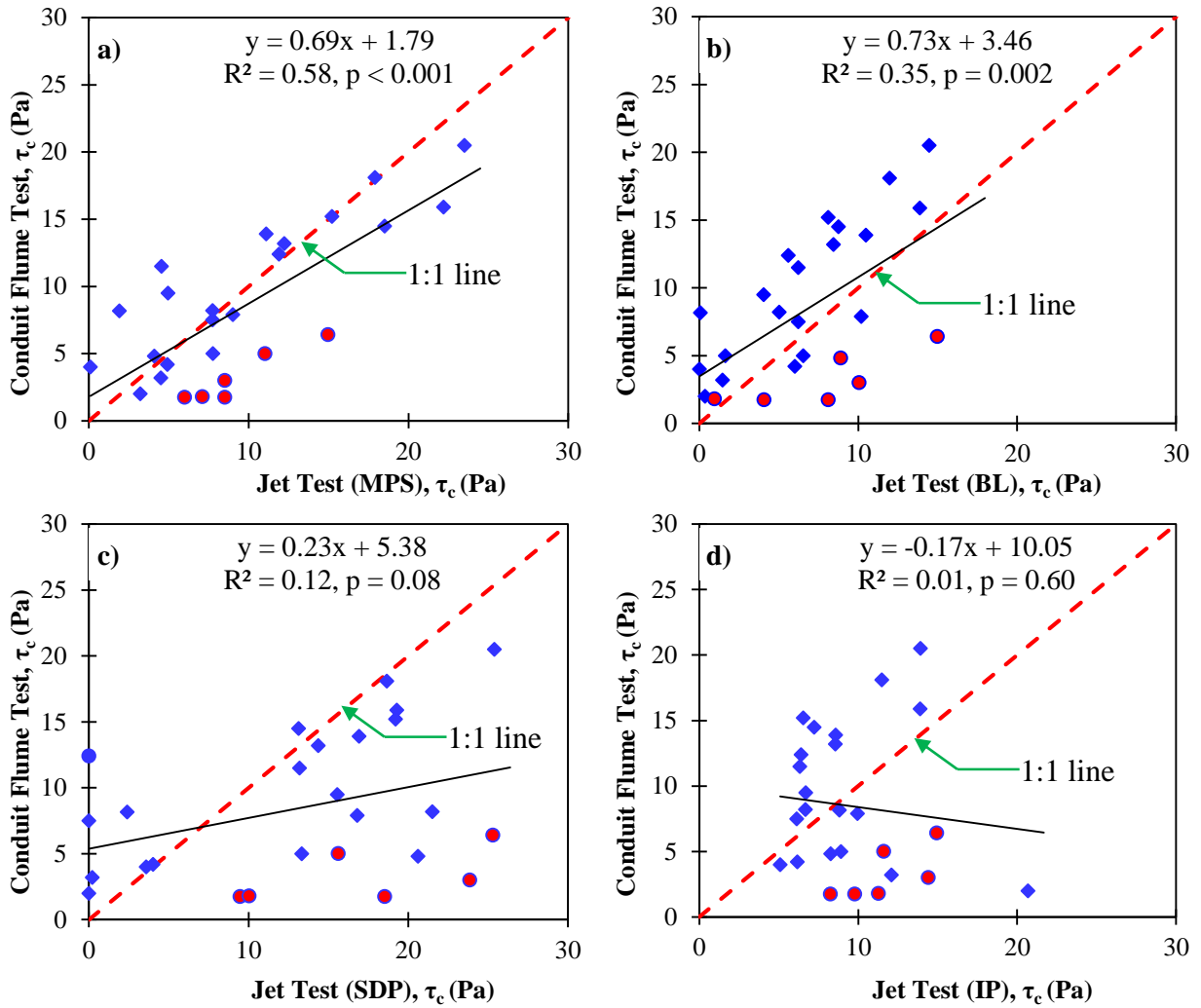


**Fig. 7.** Critical shear stress comparison with conduit flume test results: a) using multiple pressure settings (MPS), b) using Blaisdell method (BL), c) using scour depth principle (SDP), and d) using iterative principle (IP). Red circles in a) indicate the samples with WC < 18.5%.

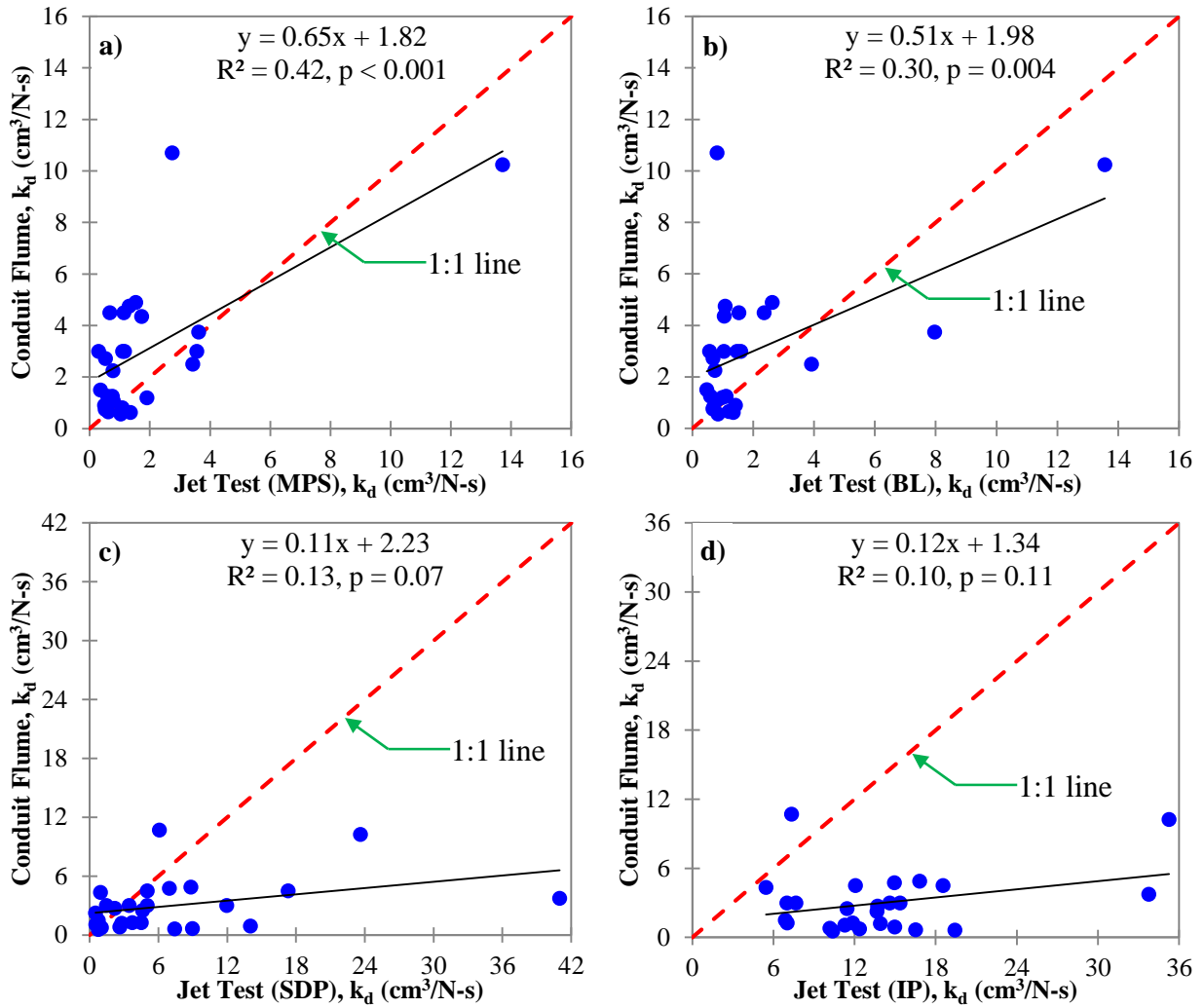


**Fig. 8.** Erodibility coefficient comparison with conduit flume test results: a) using multiple pressure settings (MPS), b) using Blaisdell method (BL), c) using scour depth principle (SDP), and d) using iterative principle (IP).

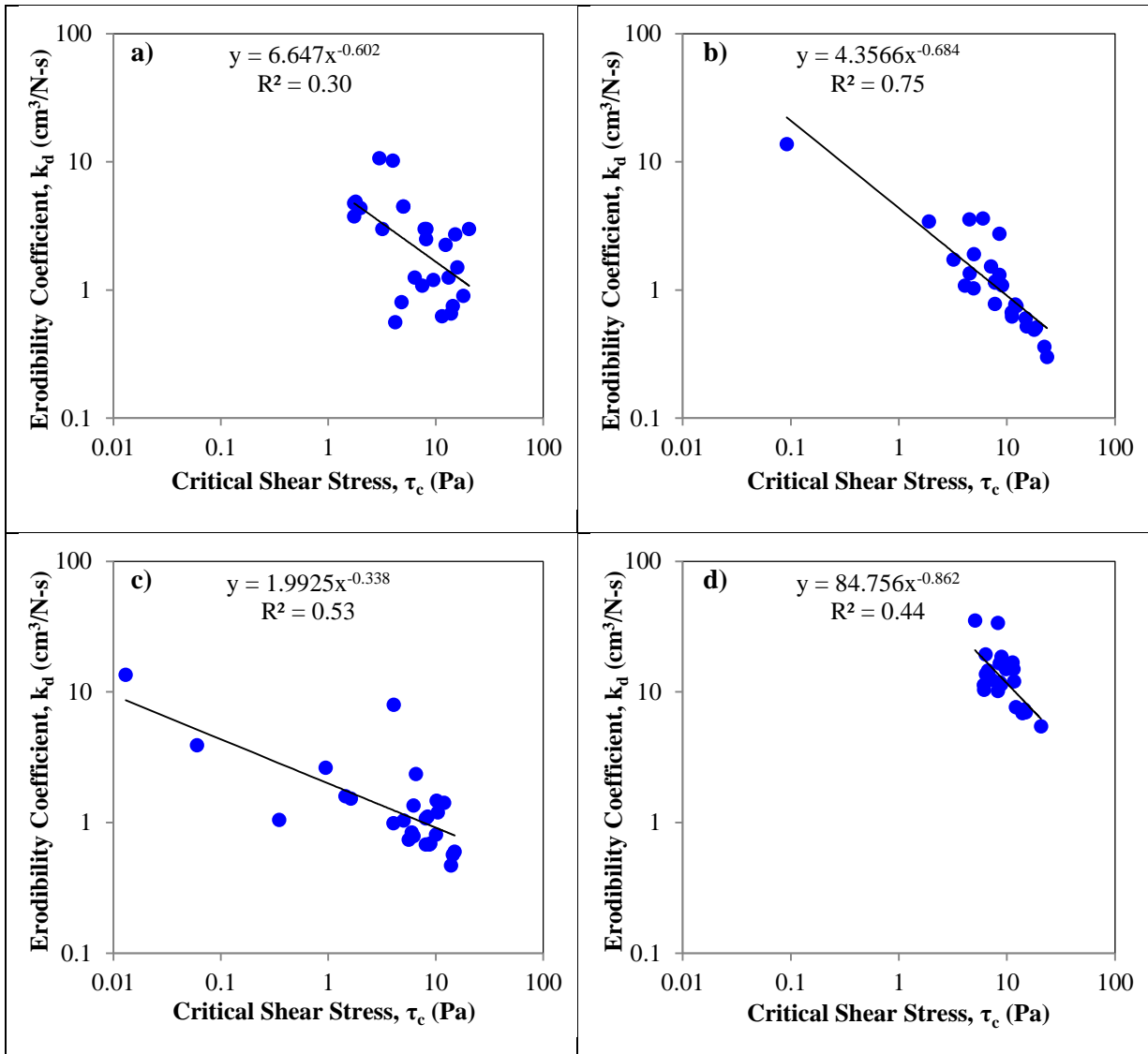


**Fig. 9.** Relationship between critical shear stress ( $\tau_c$ ) and erodibility coefficient ( $k_d$ ): a) conduit flume, b) jet test (MPS), c) jet test (BL), and d) jet test (IP).

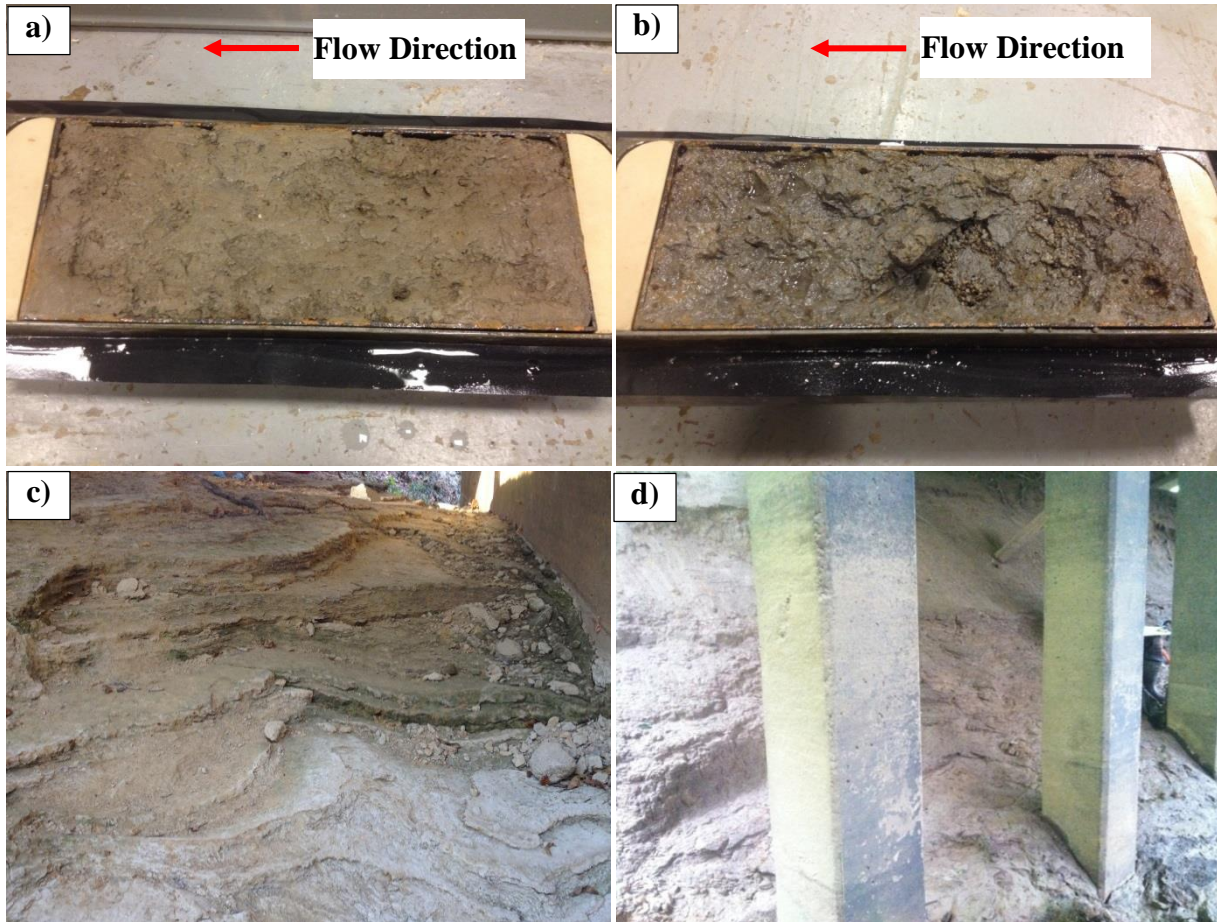


**Fig. 10.** Erosion pattern of tested soil sample in conduit flume: a) before test, b) after test, erosion pattern from field observations: c) at bottom of creek, and d) around structures.